DESIGN SUPPORT FOR MOTION CONTROL SYSTEMS

— A MECHATRONIC APPROACH —

PROEFSCHRIFT

ter verkrijging van
de graad van doctor aan de Universiteit Twente,
op gezag van de rector magnificus,
prof. dr. F.A. van Vught,
volgens besluit van het College voor Promoties
in het openbaar te verdedigen
op vrijdag 25 februari 2000 te 16.45 uur

door

Hendrik Jan Coelingh

geboren op 14 maart 1971
te Hengelo

Dit proefschrift is goedgekeurd door
prof. dr. ir. J. van Amerongen, promotor
prof. dr. ir. M.P. Koster, promotor
dr. ir. T.J.A. de Vries, assistent-promotor.

to Moniek

This dissertation has been completed in partial fulfillment of the requirements of the Dutch Institute of Systems and Control DISC for graduate study.

ISBN 90-36514118

Printed by Drukkerij Twente Hengelo B.V.

Cover design: Moniek van Rosse

Summary

This thesis discusses the development of design support for motion control systems, using a mechatronic design approach. The placement module of the Philips Fast Component Mounter (FCM), an industrial pick-and-place machine, is used as a running example.

To fully exploit the advantages of mechatronic design, tuning a ready-for-use controller is not sufficient. Rather, an elaborate and complex trajectory for the design of a control system has to be followed to obtain a deep understanding of the design problem. By providing high-quality design support the amount of knowledge about the design problem early in the design process will increase. This is important, as at these moments there is still considerable design freedom. Consequently, better founded design decisions can be made and the development time decreases.

Two distinct stages of mechatronic control system design are addressed: conceptual design and detailed design.

For conceptual design an assessment method is formulated that supports the design of a feasible reference path generator, control system and electromechanical plant with appropriate sensor locations, in an integrated way. This method is based on a classification of standard transfer functions, plant models and closed-loop systems. The assessment method can be applied in several ways, depending on the available knowledge about the design problem. Together with dedicated computer support, the assessment method quickly provides insight in the design problem and feasible goals and required design efforts can be estimated at an early stage.

For detailed design, a transparent and structured design method is proposed, in order to meet the more or less conflicting requirements for a controlled system, in terms of performance, stability, disturbance attenuation and robustness. A standard control configuration is used that involves a feedback component, a disturbance observer, a feedforward component and a reference path generator. Starting from a successful conceptual design, the structured design method supports the (evolutionary) design of motion control systems, by providing relevant design procedures and computer support. It enables the design of control systems,

which are successful in practice, with fairly simple means, in relatively short time and simultaneously with the design of the plant.

In a mechatronic design process, physically motivated plant models are generally used to describe the dynamic behavior of the electromechanical plant. The physical parameter values in such a model are often only known within bounds. Computer support, based on Quantitative Feedback Theory (QFT), has been developed for the design of control systems which assure that the motion specifications are met, despite this uncertainty. A review on dealing with physical parameters in QFT is presented, as well as a procedure that converts point-to-point motion specifications into appropriate frequency-domain specifications. The resulting design support gives a clear view upon the influence of physical parameter uncertainty on the design of the closed-loop system.

By means of practical application to the placement module of the FCM, we illustrate the design support presented in this thesis. We mainly focus on evaluation of the design enhancement and not on maximization of the performance of the controlled system.

The design support presented in this thesis helps the designer to more easily gain insight in the design problem, without requiring advanced control engineering skills, while indicating whether performance and robustness demands of the final design are being satisfied. An important consequence is that the required overall development time decreases.

Samenvatting

Dit proefschrift behandelt de ontwikkeling van ontwerpgereedschappen voor bewegingsregelingen voor elektromechanische systemen, waarbij gebruik wordt gemaakt van een mechatronische ontwerpaanpak. De plaatsingsmodule van de Philips Fast Component Mounter (FCM), een industriële *pick-and-place* machine, wordt als lopend voorbeeld gebruikt.

Om de voordelen van de mechatronische ontwerpaanpak volledig te benutten, kan niet volstaan worden met het inregelen van een bestaand regelsysteem, maar moet een uitgebreid traject voor het ontwerpen van een regelsysteem worden gevolgd om een diep inzicht in het ontwerpprobleem te verkrijgen. Door het aanbieden van goede ontwerpondersteuning, kan de kennis van het ontwerpprobleem vroeg in the ontwerp proces, vergroot worden. Dit is belangrijk want op dat moment is er nog aanzienlijke ontwerpvrijheid. Het gevolg is dat beter gefundeerde ontwerpkeuzes gemaakt kunnen worden en dat de ontwikkeltijd af neemt.

Twee verschillende ontwerpstadia worden besproken: het conceptuele en het gedetailleerde ontwerpstadium.

Voor het conceptueel ontwerp is een methode geformuleerd die het geïntegreerd ontwerpen van de referentiepadgenerator, het regelsysteem en het elektromechanische proces inclusief sensor locatie, ondersteund. Deze methode is gebaseerd op een classificatie van standaard overdrachtsfuncties, proces modellen en gesloten-lus systemen. De methode kan op verschillende manieren worden toegepast, afhankelijk van de beschikbare kennis over het ontwerpprobleem. In combinatie met de specifieke computerondersteuning verschaft de methode inzicht in het ontwerpprobleem en kunnen realistische doelen en de benodigde inspanning vroeg in het ontwerpproces ingeschat worden.

Voor het gedetailleerde ontwerp wordt een transparante en gestructureerde ontwerp methode voorgesteld, om de min of meer tegenstrijdige eisen van een geregeld systeem te behalen. Deze eisen zijn gesteld in termen van prestatie, stabiliteit, verstoringsonderdrukking en robuustheid. Een standaard regelaarconfiguratie wordt gebruikt, die bestaat uit een terugkoppeling, een vooruitkoppeling, een verstoringschatter en een referentiepadgenerator. Uitgaande van een succesvol conceptueel ontwerp ondersteunt de gestructureerde ontwerpmethode het

(evolutionair) ontwerpen van bewegingsregelingen, door het aanbieden van relevante frequentiedomein georiënteerde ontwerpprocedures en computer-ondersteuning. Het maakt het ontwerpen van regelsystemen mogelijk, die succesvol zijn in de praktijk, met tamelijk eenvoudige middelen, in een relatief korte tijd en simultaan met het procesontwerp.

In een mechatronisch ontwerpproces worden in het algemeen fysisch gemotiveerde modellen gebruikt om het dynamische gedrag van het elektromechanische proces te beschrijven. De waarden van de fysische parameters in deze modellen zijn vaak alleen bekend binnen bepaalde grenzen. Computerondersteuning, gebaseerd op Quantitative Feedback Theory (QFT), is ontwikkeld voor het ontwerpen van regelsystemen die er voor zogren dat de bewegingsspecificatie gehaald wordt ondanks deze onzekerheid. Een overzicht van het gebruik van fysische parameters in QFT wordt gepresenteerd, evenals een procedure die bewegingsspecificaties omzet in geschikte frequentiedomein eisen. De resulterende ontwerpondersteuning geeft een helder beeld van de invloed van fysische parameter onzekerheid op het ontwerp van het gesloten-lus systeem.

Door middel van een praktische toepassing op de plaatsingsmodule van de FCM, illustreren we de ontwerpondersteuning uit dit proefschrift. We richten ons met name op de evaluatie van de ondersteuning en niet op het maximaliseren van de prestatie van het geregelde systeem.

De ontwerpondersteuning uit dit proefschrift helpt de ontwerper om op eenvoudige wijze inzicht in het ontwerpprobleem te verkrijgen, zonder vergaande regeltechnische vaardigheden te verlangen, terwijl wordt aangegeven of de prestatie- en robuustheideisen van het uiteindelijke ontwerp gehaald kunnen worden. Een belangrijke gevolg is dat de vereiste ontwikkelingstijd korter zal zijn.

List of symbols and abbreviations

Symbol	Meaning	Unit
c	stiffness (translation)	$[\mathrm{N} \cdot \mathrm{m}^{-1}]$
d	damping (translation)	$[\mathrm{N} \cdot \mathrm{s} \cdot \mathrm{m}^{-1}]$
e_0	maximum positional error	[m]
g	stability margin in s-plane	
h_m	motion distance	[m]
i	transformation ratio	
j	$\sqrt{-1}$	
k	stiffness (rotation)	$[\mathrm{N} \cdot \mathrm{m} \cdot \mathrm{rad}^{-1}]$
k_d	gain in velocity loop	$[\mathrm{N} \cdot \mathrm{m}^{-1} \cdot \mathrm{s}]$
k_m	motor constant	$[\mathrm{N} \cdot \mathrm{m} \cdot \mathrm{A}^{-1}]$
k_p	gain in position loop	$[\mathrm{N} \cdot \mathrm{m}^{-1}]$
m	mass	[kg]
$n(t)$	measurement noise	
$p\,(s, q\,)$	polynomial with physical parameters	
q	(vector of) physical parameter(s)	
$r(t)$	reference path	[m]
s	Laplace operator	
s_l	low-frequency disturbance suppression	
t	time	[s]
t_m	motion time	[s]
$u(t)$	control signal, *i.e.* plant input	
$u_\mathrm{c}(t)$	control signal from $\mathcal{C}$	
$u_\mathrm{f}(t)$	forcing function or control signal from $\mathcal{F}$	
$v(t)$	measured velocity	$[\mathrm{m} \cdot \mathrm{s}^{-1}]$
$w(t)$	disturbance signal	
$\hat{w}(t)$	estimated disturbance signal	
$x(t)$	state (vector)	
$\hat{x}(t)$	estimated state (vector)	

$x_{\mathrm{o}}(t)$	observer state (vector)	
$x_w(t)$	state (vector) of disturbance model	
x_0	initial state	
$y(t)$	measured (position) output	[m]
$z(t)$	output (position) to be controlled	[m]
A	system matrix	
A_w	system matrix of disturbance model	
B	input matrix	
C	output matrix	
C_w	output matrix of disturbance model	
$C(s)$	feedback compensator transfer function	
D	throughput matrix	
E	observer transfer matrix	
E_0	relative maximum positional error	
F	(input) force	[N]
$F(s)$	prefilter transfer function	
G	relative stability margin in s-plane	
$H(s)$	command response or closed-loop transfer function	
I	unit matrix	
J	inertia	$[\mathrm{kg} \cdot \mathrm{m}^2]$
K	proportional gain	
L	observer gain matrix	
L_{D}	observer gain matrix for disturbance model	
L_{P}	observer gain matrix for plant model	
$L(s)$	loop transfer function	
$L_0(s)$	nominal loop transfer function	
M_{S}	peak of the sensitivity function	
$P(s)$	plant transfer function	
$P(s,q)$	plant transfer function with physical parameter uncertainty	
$P_0(s)$	nominal plant transfer function	
Q	Q-box	
$S(s)$	sensitivity function	
$S_{\mathrm{o}}(s)$	observer sensitivity function	
$S_{\mathrm{u}}(s)$	input sensitivity function	
T	torque	$[\mathrm{N} \cdot \mathrm{m}]$
$T(s)$	complementary sensitivity function	
$T_{\mathrm{o}}(s)$	observer complementary sensitivity function	

$\mathcal{C}$	control system or feedback component	
$\mathcal{D}\left(j\omega_i, Q\right)$	denominator template	
$\mathcal{F}$	feedforward component or prefilter	
$\mathcal{F}_{\mathbb{C}}\left(j\omega_i, Q\right)$	value set	
$\mathcal{F}_{\mathrm{N}}\left(j\omega_i, Q\right)$	template	
$\mathcal{H}_{\mathrm{spec}}$	frequency tolerance band	
$\mathcal{N}\left(j\omega_i, Q\right)$	numerator template	
$\mathcal{O}$	disturbance observer	
$\mathcal{P}$	physical (electromechanical) plant	
$\mathcal{P}_{\mathrm{m}}\left(s, Q\right)$	mixed uncertainty model	
$\mathcal{P}_{\mathrm{p}}\left(s, Q\right)$	parametric plant family	
$\mathcal{R}$	reference path generator	
$\mathcal{T}_{\mathrm{spec}}$	thumbprint specification	
$\mathcal{W}$	set of waveform structured signals	
α	absolute damping	
$\alpha(\omega)$	lower-bound on frequency tolerance band	
β	tameness factor	
$\beta(\omega)$	upper-bound on frequency tolerance band	
ε	performance constant for second-degree reference path	
γ	performance constant for third-degree reference path	
ϕ_{m}	phase margin	
φ	motor angle	[rad]
ρ	frequency ratio	
τ	periodic ratio	
τ_{d}	derivative time constant	
τ_{h}	high-frequency roll-off time constant	
τ_{i}	integral time constant	
$\upsilon_i(t)$	i-th elementary waveform function	
ω	frequency	$[\mathrm{rad} \cdot \mathrm{s}^{-1}]$
ω_{ar}	anti-resonance frequency	$[\mathrm{rad} \cdot \mathrm{s}^{-1}]$
ω_{b}	bandwidth	$[\mathrm{rad} \cdot \mathrm{s}^{-1}]$
ω_{c}	gain cross-over frequency	$[\mathrm{rad} \cdot \mathrm{s}^{-1}]$
ω_{d}	velocity loop quantity	
ω_{l}	upper limit of low-frequency disturbance	$[\mathrm{rad} \cdot \mathrm{s}^{-1}]$
ω_{peak}	frequency of the peak of the sensitivity function	$[\mathrm{rad} \cdot \mathrm{s}^{-1}]$
ω_{p}	position loop quantity	
ω_{r}	resonance frequency	$[\mathrm{rad} \cdot \mathrm{s}^{-1}]$

ω_σ	frequency for observer poles	$[\mathrm{rad} \cdot \mathrm{s}^{-1}]$
ζ	relative damping	
Δ	unstructured uncertainty	
$\Upsilon_i(s)$	Laplace transform of i-th elementary waveform function	
Ω	frequency space	
Ω_p	optimal dimensionless controller settings for position loop	
Ω_d	optimal dimensionless controller settings for velocity loop	
$\mathbb{C}$	complex plane	
$\Im$	imaginary part	
$\Re$	real part	
AR	anti-resonance - resonance	
COM	center of mass	
D	double integrator	
FCM	Fast Component Mounter	
N	non-minimum phase	
PCB	Printed Circuit Board	
PM	Placement Module	
QFT	Quantitative Feedback Theory	
R	resonance	
RA	resonance - anti-resonance	

Table of contents

1 Introduction

1.1 Products involving motion control

In modern society, an increasing number of products is in operation that relies on automatic control of motion. This motion may be the primary function of the product, such as in cruise control of cars, but more often it is a precondition for the functionality of a product. This can be seen in consumer products such as compact-disc players, videocassette recorders and cameras, as well as in professional products such as assembly machines. These products all have moving parts that require high-performance automatic control; see *e.g.* (Steinbuch and Norg, 1998). When the functionality of a product relies on accurate motions, then motion control is a crucial issue in the design of that product.

Global market developments show a continuous demand for new, cost-effective, high-quality products. Simultaneously, the market fosters the need to develop these products at a very rapid and accelerating pace. These trends have consequences for the design of both products and production machines, because there is less time to design and manufacture higher-quality products, at lower costs. Technological advances *and* enhancement of the design process are required to fulfill these needs.

As an illustration we consider current developments in electronics. Technological advances lead to larger variations in the size of electronic components and to components with more pins. As a consequence, the requirements for assembly machines for printed circuit boards (PCB's) are changing. Assembly operations must be performed more flexibly, faster and with higher accuracy. An example of the current state of the art is the Fast Component Mounter (FCM) of Philips (Philips, 2000). Flexibility is obtained by enabling in-flight component centering and fault detection by means of a laser alignment system. This machine is capable of placing 60,000 components per hour, under nominal conditions. The FCM comprises a series of up to 16 servo-controlled pick-and-place robots, the so-called Placement Modules or PM modules. In figure 1.1 a schematic diagram of the motion in y-direction of the PM module is shown. A more elaborate description of the FCM is given in appendix A.

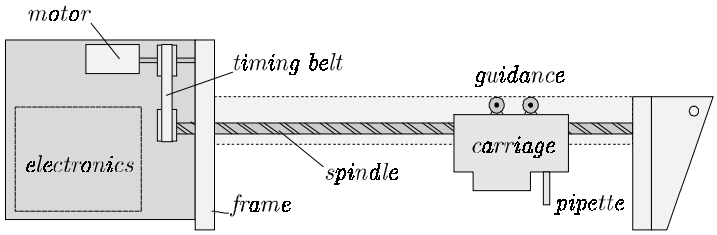

FIGURE 1.1 *Schematic diagram of a placement module of the FCM*

Control aspects within the integrated design of this type of electromechanical motion systems are subject of this thesis. While focusing on the role these aspects play or should play in the design process, support is developed to enhance the design.

Section 1.2 describes the scope of research; topics that are discussed are control engineering, mechatronic design, motion control in the mechatronic design process and the use of design tools. In section 1.3 the aim of research is defined and section 1.4 finally gives an outline of the contents of this thesis.

1.2 Scope of research

1.2.1 Control engineering

From the desired functionality of a product, several tasks can be deduced for the design of a technical (sub) system. The objective of *control engineering* is to obtain a certain dynamic behavior that allows the system to actually perform these tasks in an optimal way. In case of the PM module of an FCM, the functionality is to mount electronic components on a PCB. The main task of this module can be characterized as moving the pipette along the spindle from one position to another, within a certain time and with certain accuracy (figure 1.1), *i.e.* to perform a point-to-point motion.

Controlled systems are generally represented by a block diagram as in figure 1.2, where the following elements can be distinguished:

- The *plant* $\mathcal{P}$ is the system to be controlled. It has inputs u, outputs z that have to be controlled and measured outputs y.
- The *reference path generator* $\mathcal{R}$ produces a reference signal r that indicates the desired behavior for the output z of $\mathcal{P}$.

- The *control system* $\mathcal{C}$ uses the reference signal r of $\mathcal{R}$ and measurement y of $\mathcal{P}$ to generate a control signal u to manipulate the output z of $\mathcal{P}$.

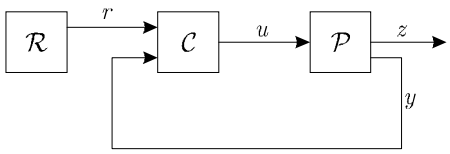

FIGURE 1.2 *Block diagram of a controlled system*

Once the task has been determined and some knowledge about $\mathcal{P}$ is available, one can start with the design of the control system. In case the designer lacks thorough knowledge and experience of specific problems in this problem domain, two possible design trajectories exist:

1. *Short trajectory.* A ready-for-use controller is applied, which is tuned for the particular problem; see *e.g.* (Åström and Hägglund, 1995).
2. *Elaborate trajectory.* A custom-made controller is obtained through an iterative design process that involves problem specification, modeling, identification, linearization, controller design, simulation, evaluation and implementation.

The controller obtained by the short trajectory generally gives worse performance, but the development time is relatively short. The elaborate trajectory can lead to far better solutions, but only if the designer has the skills to gain a *deep understanding of the problem.* The consequence for the design process is that the elaborate design trajectory causes a longer development time. Not all designers will have sufficient skills, therefore Graebe stated an open challenge in the field of high-performance robust control, *i.e.* "*decreasing the control engineering skills required of a designer*" (Graebe, 1999). From this perspective, we will take a closer look at each of the individual steps in the elaborate trajectory:

Problem specification. The task for the (control) system often has to be transformed into specifications that can be handled by available design methods. Tasks are often indicated in space and time, *e.g.* the point-to-point motion for the PM module of the FCM. A design method such as optimal control requires specifications to be expressed in terms of an appropriate cost criterion. It is not straightforward to find a criterion that will indeed be adequate for the task.

Modeling the plant. Controllers are generally designed on basis of a dynamic model of the plant. Different analytical modeling techniques can be used for obtaining a plant model, depending on the design stage, the design knowledge, the desired model or the type of plant. Examples of techniques that are used for modeling mechanical plants are finite element methods (Zienkiewicz, 1971; Cook, 1974) and

multi-body systems (Wittenburg, 1977; Kane and Levinson, 1985; Jonker, 1988). Bond graphs (Paynter, 1975; Cellier, 1991) are both a modeling technique as well as a representation that is suited well for systems involving different physical domains. Other useful representations are equations, block diagrams and iconic diagrams.

Identification. In addition to analytical modeling, an analytical plant model can be obtained or verified by experimental modeling. In this case a finite number of data is extracted from the physical plant. Consecutively, several techniques are available, in both time and frequency domain, to identify models from these data. Identification techniques can also be used to estimate parameter values of the analytical model on the basis of measured data (Söderström and Stoica, 1989; Ljung, 1999).

Linearization and *reduction.* The resulting plant model often is too complex, *i.e.*, it may contain nonlinearities and higher-order terms that initially do not have to be considered for control system design. To obtain a suitable plant model, linearization (Kailath, 1980) can be applied and consecutively the resulting linear model can be reduced to an appropriate order (Decoster and van Cauwenberghe, 1976a; Decoster and van Cauwenberghe, 1976b; Wortelboer, 1994). This allows the application of analytical design methods for linear systems.

Controller design. Once specifications and a suitable plant model are obtained, the actual design of the control system can start. There are many methods for control system design (Levine, 1996). Which of the methods is preferable depends on the specifications, the plant model and the knowledge and experience of the designer.

Simulation and *evaluation.* To predict the behavior of the controlled system, simulations are performed with both the linear reduced-order model and with the full-order, nonlinear model. Using simulation results, frequency responses and other tools, the design of the controller is evaluated. Depending on the outcome, iterations will take place or the controller will be implemented.

Implementation. Once the design of the controller has been evaluated successfully, the control system can be implemented. In mechatronic systems the control system is generally implemented as a computer algorithm.

Remark 1.1

The implementation of the controller in a computer results in the interconnection of a continuous-time system with a discrete-time system. Due to sampling and quantization, this may have consequences for the dynamic behavior of the total system (Åström and Wittenmark, 1997). However, in this thesis we will only consider continuous-time controllers, which is justified when the discrete-time controller is implemented appropriately.

1.2.2 Mechatronic design

Before a new system is ready for production, decisions have been made on how the system will function, what its components are, how its components will be produced and assembled, and many more. These decisions are part of the design process (Ullman, 1997). In the design process we distinguish the following steps:

1. *User specifications.* Give a rough description of the functions and properties of the product.
2. *Technical specifications.* Translate the user specifications into quantified technical terms and split up the overall functionality in subfunctions.
3. *Conceptual design.* Generate concepts that are to perform the different subfunctions and make a selection based on rough evaluations.
4. *Detailed design.* Generate physical embodiments of the selected concepts and make a rough selection, based on ample evaluation.
5. *Evaluation.* Perform thorough analysis of the selected concepts and designs and make a definitive solution.
6. *Documentation.* Make the complete documentation needed for the manufacturer of the prototype.
7. *α-test.* Manufacture and test each subsystem.
8. *β-test.* Assemble and test the complete system.

De Vries (1994) proposed a *model of designing*, in order to explain the applicability of design support on the basis of characteristic features of the design process and to predict what kind of support would increase chances for successful completion of the design process. Three characteristics of design were identified as crucial (De Vries, 1994):

- design is context dependent.
- design problems are ill-structured and incomplete.
- design involves a time-constrained initiation of change.

Therefore, we will view design as a *contextually situated evolutionary process*. This concerns the product being designed as well as the knowledge about the design problem.

The design and development activities in the design process are related to the field of *systems engineering*. This is not an engineering discipline in the same context as for example electrical and mechanical engineering, but it can be considered as "a process employed in the evolution from the point when a need is identified through the production and/or construction and ultimate deployment of that system for consumer use" (Blanchard and Fabrycky, 1990). This was recognized as essential in product or system design, because the engineering specialists in the underlying disciplines were not capable of considering the system as a whole. An important characteristic of systems engineering is that an *integrated approach* is employed to the design of the system as a whole. The purpose is to achieve a design that

optimally uses the design freedom in all underlying disciplines. A desired functionality can be implemented in one or another physical domain or an imperfection in one part of the system can be compensated for by another part.

Generally, complex design problems are solved by separation into partial subproblems. Hence, one uses the fact that complex problems, like designing, are "ill-structured in the large, but well structured in the small" (Simon, 1973). Complex ill-structured design problems are split into small well-structured problems, to which local problems solvers are applied. However, the application of an integrated design approach complicates the design process, as domain specific subproblems should be solved by taking into account the consequences of a solution in other domains or by finding alternative solutions in other domains (figure 1.3). As these choices may have major consequences for the design, it is wise to make these choices early in the design process. Therefore, "the conceptual design task is of crucial importance when using an integrated problem solving approach" (De Vries, 1994).

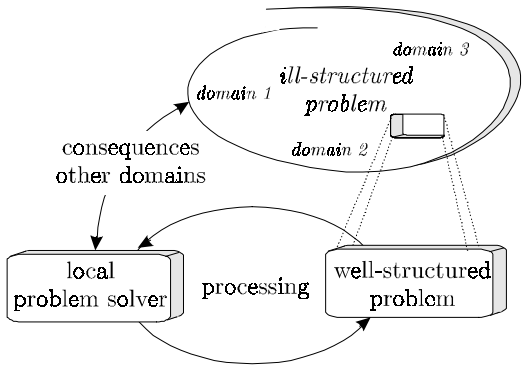

FIGURE 1.3 *Schematic structure of solving ill-structured problems (adapted from (Simon, 1973))*

In this thesis, the design of controlled electromechanical systems is considered. The application of an integrated approach to this multidisciplinary field is referred to as mechatronics. Mechatronics is defined in various ways; two useful definitions are:

Definition 1.1a Mechatronics

Mechatronics is a technology which combines mechanics with electronics and information technology to form both functional interaction and spatial integration in components, modules, products and systems (Buur, 1990).

Definition 1.1b Mechatronics

> *Mechatronics is a synergistic combination of precision mechanical engineering, electronic control and systems thinking in the design of products and manufacturing processes (IRDAC, 1986).*

The first definition stresses the fact that mechatronics considers functional interaction and spatial integration of subsystems. The second definition indicates that mechatronics is not a conventional engineering discipline or a technology, but a design approach. A more restrictive description, which is however suitable for our present concerns, is that "mechatronics encompasses the knowledge base and the technologies required for the flexible generation of controlled motion" (Van Brussel, 1996).

Mechatronics considers the design of controlled electromechanical systems as a whole, instead of a subsequent design of domain specific subsystems. Classical design patterns started with the design of the mechanical subsystem, followed by the design of electronics and finally the design of the controller. In order to obtain functional interaction and spatial integration, subsystem designs need to overlap, and hence simultaneous involvement of several disciplines needs to be realized in a coordinated way. Or, as Isermann (1996) states: "simultaneous engineering has to take place". The design process of controlled electromechanical systems with a mechatronic design approach is therefore generally more complex, but leads to systems with a superior price-performance ratio. Other credits that are claimed by mechatronic design are that it leads to more flexibility, higher performance, higher reliability and that it often opens up a new dimension to the product's operation (Hewit and Bouazza-Marouf, 1996). The application of mechatronics can even lead to the design of products that would have been impossible without this interdisciplinary and synergistic approach (Van Amerongen, 1998).

The complexity of today's products is often such that generally a team of people from diverse areas of expertise is required to transform an idea into a product (Ullman, 1997). Mechatronic design is teamwork; the specialists from the underlying disciplines that work in this design team must have the ability to look beyond the design problem within their own field, in order to profit from the advantages of mechatronics design.

1.2.3 Motion control in the mechatronic design process

This research is focused on a particular class of mechatronic systems:

Definition 1.2 Electromechanical motion system

> *An electromechanical motion system is an electrically actuated mechanical plant that requires the control of the position of the end-effector (figure 1.4).*

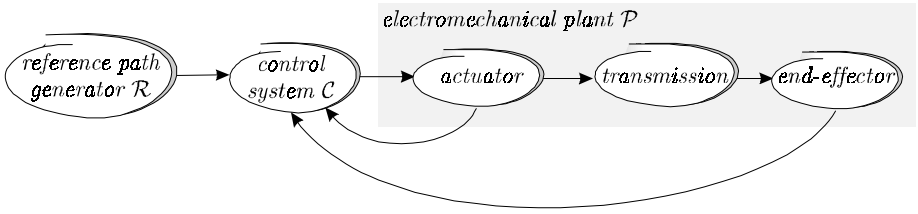

FIGURE 1.4 *Electromechanical motion system*

Characteristics of this class are that a path generator indicates a reference path for the end-effector. The actuator drives the end-effector through a transmission. The controller processes information from the (position) sensors that are generally located at the actuator and/or the end-effector, such that the desired behavior of the position of the end-effector is obtained.

Within this restricted class of electromechanical motion systems, we define motion control in a mechatronics sense:

Definition 1.3 Motion Control

Motion control is that part of the mechatronic design process that is concerned with the design and implementation of the control system $\mathcal{C}$ and the reference path generator $\mathcal{R}$ for the position of the end-effector of electromechanical motion systems.

Control engineering, as one of the underlying disciplines of mechatronics, is concerned with the improvement of the dynamic behavior of complex technical systems conform the requirements. It is directed towards synthesis, using methods, techniques and tools from systems engineering and several other disciplines. Control theory is concerned with obtaining fundamental knowledge, by taking an abstract perspective, such that it provides a profound mathematical basis for practical application.

McClamroch (1998) assessed the conflict between the abstract perspective of control theory and the application perspective of control engineering: "The former views a control system in terms of abstract input-output equations or state equations and poses control questions in abstract terms. The latter takes a more concrete view and attempts to make use of the special physical features of such systems, both in forming control problems and in designing controllers. The control design approach associated with the former view attempts to formulate a standard mathematical problem that captures the important control design objectives. The latter view makes use of prior knowledge and experience with similar operational control systems together with extensive trail and error; moreover it often views

control design as only a part of the larger issue of system design." The last statement corresponds with our view of mechatronic control system design.

In (Åström and Wittenmark, 1997) this conflict is described as "reconcile the large-scale, fuzzy, real problem with the simple well-defined problems that control theory can handle". This problem can be found in many engineering disciplines, but "control engineering is a field where a comparatively sophisticated theory is needed to understand problems" (Åström and Wittenmark, 1997).

The best approach is an integration of both perspectives. The abstract perspective of control theory offers many formalisms, methods and techniques for solving general (complex) control problems, while the physics-based application perspective of control engineering can exploit the context of the total system. McClamroch (1998) asserts that more attention needs to be given to achieving true integration of both perspectives.

When we want to achieve this integration of perspectives, a deep understanding of the practical design problem is required, in order to formulate the problem in abstract terms that control theory can handle. This deep understanding is also required to fully exploit the advantages of mechatronic design. Therefore, the elaborate trajectory for control system design has to be followed (section 1.2.1). Ideally, this is done during the design of the overall system, *i.e.* during mechatronic design. However, this trajectory can also be followed to improve the performance and robustness properties of an existing electromechanical system.

1.2.4 Design tools

The rapid technological developments and the continuing need for reduced time-to-market of new products demand more and more advanced design tools. Design tools are instruments that support parts of the design process and may exist in the form of methods, techniques and software. Successful application of mechatronic control system design requires proper design tools to handle complexity and to support the elaborate design trajectory.

Control theory provides a wide variety of methods for the design of controllers. Most of these methods are developed from a mathematical perspective and consider the plant as unalterable. Examples of these design methods are optimal control (Anderson and Moore, 1971; Kwakernaak and Sivan, 1972), Quantitative Feedback Theory (Horowitz, 1982; D'Azzo and Houpis, 1995; Houpis and Rasmussen, 1999) and H_∞ control theory (Doyle *et al.*, 1989; Kwakernaak, 1993; Zhou *et al.*, 1996).

There are only a few methods for the design of controllers for electromechanical motion systems that do look upon the design problem from a mechatronic

perspective. These methods simultaneously consider the design of the controller and the plant. Examples can be found in (Groenhuis, 1991; Rankers, 1997; Koster *et al.*, 1999). However, these methods do not consider all aspects of control system design and are generally not sufficient on their own to obtain high performance.

For the design of modern control systems, the use of computer tools is indispensable. Such tools facilitate (automated) manipulations of the proposed design, allow to record and browse through relevant knowledge and experience, and document the process (Van Amerongen *et al.*, 2000). In the control community, Matlab and Simulink (MathWorks, 2000) are widespread tools for modeling, controller design, identification and controller realization. These tools do not provide specific support for problems of mechatronic control system design. "Because mechatronic design is a relatively young area, the level of support is below that of the individual domains that can be found in mechatronic systems" (Breunese, 1996).

It is our belief that design tools that are currently available can be enhanced to better support mechatronic design of control systems for electromechanical motion systems.

1.3 Problem statement and approach

Section 1.1 signaled an increasing need for electromechanical motion systems with higher performance and good reliability that are developed within shorter time. These demands can be partially met by the application of a mechatronic design approach, but at the cost of a more complex design process (section 1.2.2). Within this design process more attention needs to be given to achieving true integration of the abstract perspective of control theory and the physics-based application perspective of control engineering; moreover, the design of the control system should be considered as a part of the design of the system as a whole (section 1.2.3). To fully exploit the advantages of mechatronic design and of integration of perspectives, an elaborate and complex trajectory for the design of a control system has to be followed to obtain a deep understanding of the design problem (section 1.2.1 and 1.2.3). These requirements confirm the need for enhancement of existing design tools, in order to better support the design of control systems for electromechanical motion systems (section 1.2.4).

By contemplating the issues mentioned above, we define the aim of this research as:

Aim of Research

Enhance (mechatronic) design of control systems for electromechanical motion systems, such that insight in the design problem is obtained more easily, the control engineering skills required of the designer decrease and performance and robustness properties of the final design improve. As a result, the required development time should decrease.

Figure 1.5 reflects the design paradox of Ullman (1997) and visualizes our aim of research. Design enhancement should increase the amount of knowledge about the design problem early in the design process, when there is still considerable design freedom. Consequently, better founded design decisions can be made and the development time decreases.

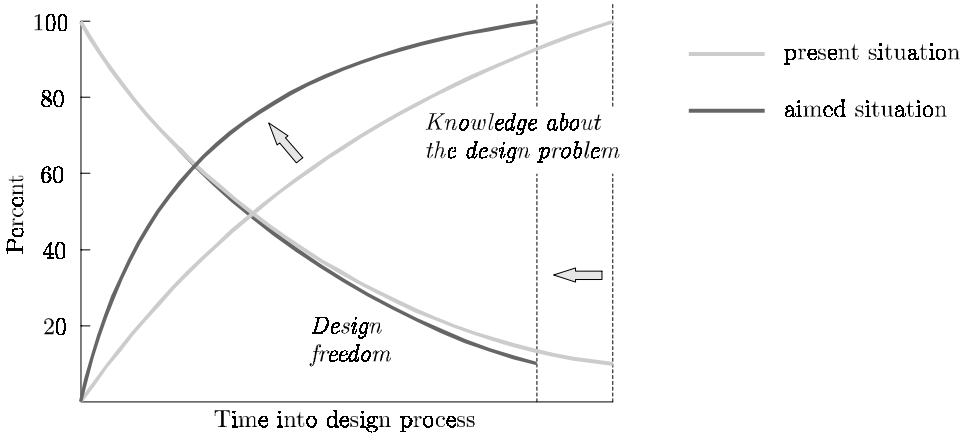

FIGURE 1.5 *Objectives of design enhancement*

From the model of designing De Vries (1994) identified three ways to enhance designing:

1. formalize design knowledge.
2. automate activities on the basis of formalized design knowledge.
3. incorporate formalized knowledge and automated activities in computer-based systems that are helpful in design practice.

We will use this approach in order to reach our aim of research. We will address two distinct stages in the design process, *i.e.* conceptual design and detailed design, as these stages concern design problems with different characteristics, designers work in different ways and different kinds of design support are required. In order to evaluate the (automated) design enhancement, we will consider the design of a control system for the PM module of the FCM as a practical application.

1.4 Outline of thesis

In chapter 2 we will address *conceptual design*. First, we shortly describe the specific problems in this design stage. Standard situations will be classified in different forms. An existing design method, appropriate for a restricted class of systems, is modified such that it is applicable to other classes as well. Finally, the modified design method is used to develop computer-based support, which includes design automatons for model simplification and model reduction.

In chapter 3 a framework for the *detailed design* of motion controllers is proposed. This framework will guide the designer from the conceptual design towards a final design in a structured way. Gradually, more disturbances, uncertainties and nonlinearities are incorporated in the plant model while the control system is extended with appropriate functionality. For the control system we use a standard configuration that contains a reference path generator, a feedback component, a feedforward component and a disturbance observer. Computer support for detailed design is provided as a 20-sim library (Controllab Products, 2000) containing standard templates and components for control system design.

During detailed design, one may have to deal with physically motivated plant models that contain *uncertain physical parameters*. In chapter 4 we argue that Quantitative Feedback Theory (Horowitz, 1982) is an appropriate controller design method in these situations. However, before being able to apply QFT, the designer has to construct uncertainty regions in the Nichols chart (templates) and has to convert time-domain specifications into the frequency domain. These are not straightforward tasks. In chapter 4 we will review several template construction methods and we will formulate a procedure to convert the specifications. The result will be an automated design tool, which uses 20-sim (Controllab Products, 2000) and the Matlab QFT toolbox (Borghesani *et al.*, 1994), that supports the design of a control system, given time-domain performance specifications and a plant model with uncertain physical parameters.

Chapter 5 discusses the practical *application* of the proposed design enhancement. We present a design of the control system of the PM module of the FCM, which has been introduced in this chapter.

In chapter 6 the design enhancement and experimental results are discussed. Finally the conclusions are drawn.

2 Conceptual design

2.1 Introduction

In section 1.2.2, we indicated that the conceptual design stage is crucial during mechatronic design of electromechanical motion systems, as the functional interaction over problem domains and the spatial integration of subsystems are best determined early in the design process. When we reconsider typical choices made by the designers of the FCM, we see that they have not chosen for a machine that employs a single high-performance pick-and-place robot with a working area corresponding to the maximum dimensions of a PCB. Rather, a machine with multiple pick-and-place modules was designed that operates on a narrow strip of the surface of a PCB at a relatively low speed. This minimizes wear and assures that positioning accuracy can be attained more easily. This choice is typical for the conceptual design stage and it has major consequences for the remainder of the design process, including the design of the control system.

We define the conceptual design problem of controlled electromechanical motion systems as:

Definition 2.1 Conceptual design problem

> *Obtain a feasible design for the path generator, control system and electromechanical plant with appropriate sensor locations, in an integrated way.*

When we want to achieve this aim, we encounter two major difficulties: control theory requires definitive specifications and a definitive model of the electromechanical plant, although both are not available. We will provide a solution to these problems by formalizing design knowledge in four steps:

1. Formulate time-domain task specifications.
2. Classify standard electromechanical plants.
3. Characterize plant dynamics.
4. Characterize closed-loop dynamics.

Before we address these steps, we consider plant models that are typically used during conceptual design. According to Oelen (1995) these models should:
- be simple and of low order;
- have a small number of parameters,

such that the model of the controlled system provides:
- reliable estimates of the dominant dynamic behavior;
- reliable estimates of the attainable bandwidth of the controlled system.

Plant models should preferably be linear, unless their principle of operation depends on their nonlinearity. The advantage of these simple models is that these can be more easily interpreted by the designer and, additionally, plant properties can more easily be related to properties of other subsystems. Rankers (1997) states that "if simulations, based on an elementary model of the product, show that the specifications are not met, then chances are extremely small that the final product will perform according to specifications".

The class of electromechanical motion systems (definition 1.2) considered here requires positioning of an end-effector. The simplest representation of the dynamic behavior of these systems is a second-order model, *i.e.* a moving mass with an applied force (figure 2.1a). When we also incorporate the fact that the plant has limited stiffness and we consider a lumped parameter approach, then we obtain a fourth-order model that takes into account the dominant compliance, *e.g.* figure 2.1b.

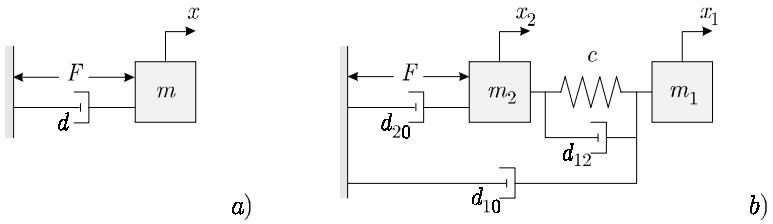

FIGURE 2.1 *Iconic diagram of common plant models*
a) moving-mass system
b) mass-spring-mass system

Definition 2.2 Fourth-order model

A fourth-order model is a lumped parameter representation of the dominant dynamic behavior of electromechanical motion systems, in which only the rigid-body mode and the lowest mode of vibration are taken into account.

The mass-spring-mass system with an applied force of figure 2.1b indicates a common fourth-order model. In section 2.2.2 an overview will be given of all standard fourth-order models within the class of electromechanical motion systems.

Statement 2.1 The use of fourth-order plant models

For conceptual design of controllers for electromechanical motion systems, fourth-order plant models are most suited, as these models are simple and of low order, have a small number of parameters, and yet competently describe the performance-limiting factor. Therefore, they are a good basis to provide reliable estimates of the dominant dynamic behavior and the attainable closed-loop bandwidth.

During model building, one generally comes up with a plant model that is not a standard fourth-order model. It will consist of interconnected component models, such as models of actuators, transmissions and guidances. As a result, the plant model will be of higher order and it will contain transmission ratios and therefore many parameters. This can be seen in the plant model of the PM module of the FCM. This model is built from several component models, as shown in the bond graph model of figure 2.2. The component models of the transmission (belt drive) and the spindle have a finite stiffness and include a transmission ratio. The model of the frame contains a finite stiffness as well, thus the plant model has an order higher than four, contains two transmissions and many parameters (refer chapter 5).

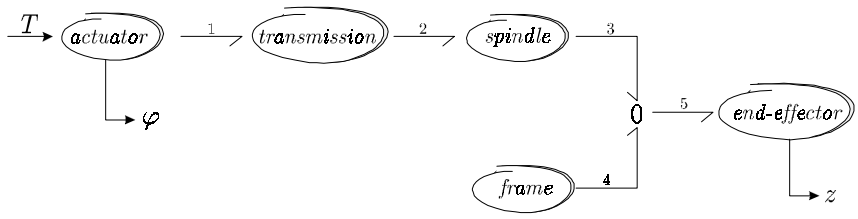

FIGURE 2.2 *Bond graph model of the placement module*

If possible, this model has to be converted to a standard fourth-order model, since we are only interested in the rigid-body mode and the lowest mode of vibration. Therefore, model simplification and model reduction techniques have to be applied. Model simplification will simplify the representation of the model without changing the contents of the underlying mathematical descriptions. Typical actions that are performed during simplification are the removal of dependent elements and the application of transformation rules. Model reduction techniques will change both the representation and the contents of the plant models. A typical action is the removal of higher-order effects. When a plant can be represented by a fourth-order model, then application of model simplification and reduction techniques should result in a plant model in a standard form. The parameters in this transformed

model should be a combination of the parameters of the original model, in order to be able to relate the results of the design methods to the initial plant model.

Statement 2.2 Model simplification and reduction

During conceptual design, model simplification and model reduction techniques should preserve the relations between the parameters of the transformed model and the parameters of the original model, in order to relate individual component characteristics to the dominant plant behavior and vice versa.

When a fourth-order model competently represents a plant, the controlled system can be designed in an integrated way. *I.e.*, the interaction between the control system, the electromechanical plant and the path generator can be taken into account explicitly during the design process. An example of a method featuring this, referred to as *the assessment method*, has been developed by Groenhuis (1991).

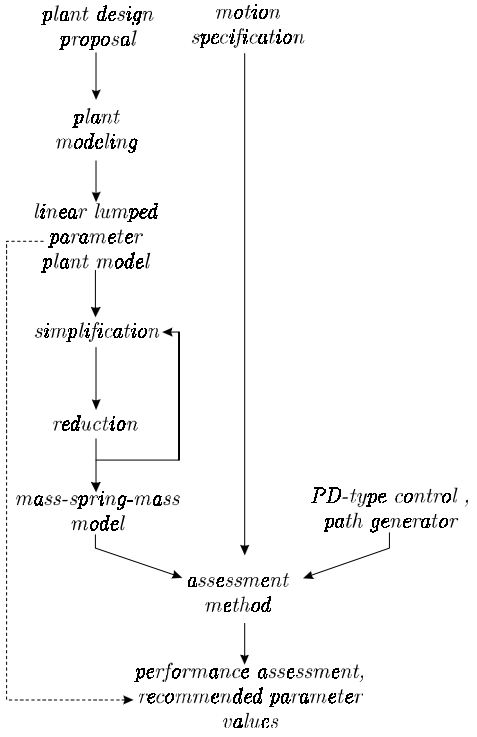

FIGURE 2.3 *Conceptual design procedure*

In figure 2.3 the overall procedure for conceptual design of electromechanical motion systems, according to the assessment method, is indicated. The problems in this design procedure, which will be addressed in this chapter, are that:

- the assessment method of Groenhuis (1991) is only applicable for one class of fourth-order electromechanical motion systems;
- the design steps simplification, model reduction and assessment are laborious, error prone and time consuming.

Therefore, in this chapter we present:

- a generalization of the assessment method;
- an (automated) algorithm for model simplification;
- an (automated) algorithm for model reduction;
- computer-based support for performance assessment,

whereby extending and enhancing the design procedure of figure 2.3.

The classification of standard electromechanical plants and characterization of plant dynamics are described in section 2.2. Section 2.3 describes a generalization of the assessment method and a characterization of closed-loop dynamics, such that the assessment method can be applied to all standard plants. In literature, several techniques for model simplification and model reduction have been described. However, most do not comply with statement 2.2 or are not described in a way suited for automation. In section 2.4 and 2.5 algorithms for respectively automated model simplification and automated model reduction are formulated that do fulfill these requirements. Section 2.6 discusses the development of a computer tool to support the assessment method. Finally, in section 2.7 the conclusions are presented.

This chapter is an extended and revised version of previous publications: (Coelingh *et al.*, 1997b), (Coelingh *et al.*, 1997c), (Coelingh *et al.*, 1998) and (Van Amerongen *et al.*, 2000).

2.2 Fourth-order plant models

2.2.1 Basic characteristics of fourth-order transfer functions

When designing control systems on the basis of a fourth-order plant model, we consider the plant transfer functions from the input force F to both the measured position y, which is used for feedback, and to the position to be controlled z. In the moving mass model of figure 2.1a the position to be controlled is identical to the measured position. In the fourth-order model of figure 2.1b two positions x_1 and x_2,

and their corresponding velocities, can be measured and fed back. Depending on which position is measured ($y = x_1$ or $y = x_2$), a different plant transfer function $P(s)$ will result. The denominator polynomial of the transfer function $P(s)$, *i.e.* the characteristic polynomial, is always the same for a particular dynamic system. The numerator polynomial in the different transfer functions depends on which position is considered. In (Miu, 1991) it is described how the numerator of a transfer function of a control systems with mechanical flexibilities depends on the location of the actuator and the sensor. In this section, we will discuss five types of transfer functions at an abstract level. These five types characterize all transfer functions of standard fourth-order models. This characterization originates from (Koster *et al.*, 1999) and (Rankers, 1997), but here a different notation is used (Van Dijk, 1999) and an additional transfer function type is included. The transfer function $P(s)$ is the transfer function from the input force ($u = F$) to a position (x_1 or x_2) in which mechanical damping is neglected. In general, damping does not dominate the dynamics of the mechanism and it unnecessarily complicates the considerations that follow here.

Remark 2.1

During conceptual design of control systems, we do not explicitly consider the influence of friction. Mechanical friction is difficult to estimate and highly nonlinear (Armstrong-Hélouvry et al., 1994); it should preferably be minimized by means of proper mechanical design. In any way, it will usually be impossible to anticipate friction characteristics of a plant during the conceptual design stage.

Miu (1993) shows how a zero pair moves along the imaginary axis for different locations of the sensor. We will use this phenomenon, which is referred to as *migration of zeros*, to characterize different types of plant transfer functions. We consider the location of the complex conjugate zero pair in the s-plane with respect to the complex conjugate pole pair. We will refer to these pairs as the *anti-resonance frequency* respectively the *resonance frequency* of a plant transfer function.

Type AR: Anti-resonance - Resonance
The type AR transfer function is:

$$P_{\mathrm{AR}}(s) = \frac{1}{ms^2} \cdot \frac{s^2 + \omega_{\mathrm{ar}}^2}{s^2 + \omega_{\mathrm{r}}^2} \cdot \frac{\omega_{\mathrm{r}}^2}{\omega_{\mathrm{ar}}^2}, \quad \omega_{\mathrm{ar}} < \omega_{\mathrm{r}} \tag{2.1}$$

where the mass m is the *total mass* to be moved, ω_{ar} is the anti-resonance frequency and ω_{r} is the resonance frequency. The Bode diagram and the pole-zero map in the s-plane are shown in figure 2.4. Note that the anti-resonance frequency of a type AR transfer function is smaller than the resonance frequency; *i.e.* the zero pair, located on the imaginary axis, is closer to the origin than the pole pair.

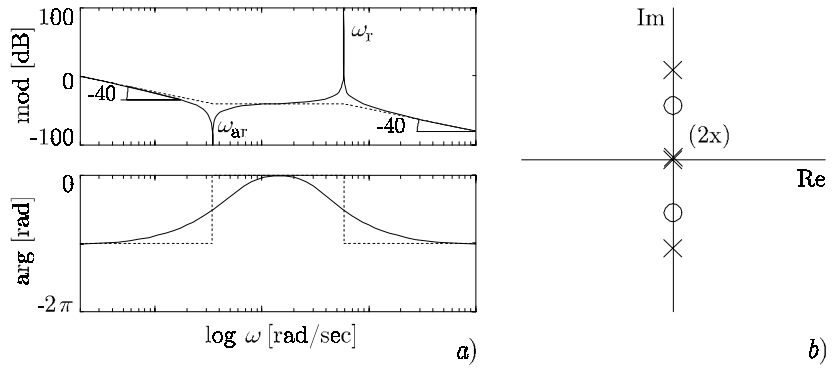

FIGURE 2.4 *Bode diagram and pole-zero map of a type AR transfer function*

The low-frequency behavior (LF) resembles that of a double integrator:

$$P_{\mathrm{AR}}(j\omega)_{\mathrm{LF}} \approx \frac{1}{m(j\omega)^2} \tag{2.2}$$

with a slope -40 dB per decade and a phase of $-\pi$ radians. In the middle-frequency (MF) region, *i.e.* frequencies between the anti-resonance and resonance frequency, the system behaves like a constant gain:

$$P_{\mathrm{AR}}(j\omega)_{\mathrm{MF}} \approx \frac{(j\omega)^2}{m(j\omega)^2\,\omega_{\mathrm{ar}}^2} = \frac{1}{m\omega_{\mathrm{ar}}^2} \tag{2.3}$$

This also means that at the anti-resonance frequency, the phase shifts from $-\pi$ to 0 radians. For frequencies larger than the resonance frequency, we see the high-frequency behavior (HF):

$$P_{\mathrm{AR}}(j\omega)_{\mathrm{HF}} \approx \frac{(j\omega)^2\,\omega_{\mathrm{r}}^2}{m(j\omega)^2\,(j\omega)^2\,\omega_{\mathrm{ar}}^2} = \frac{\omega_{\mathrm{r}}^2}{m(j\omega)^2\,\omega_{\mathrm{ar}}^2} \tag{2.4}$$

The amplitude characteristic for higher frequencies rolls off with a slope of -40 dB per decade and the phase shifts back to $-\pi$ radians.

Type D: Double integrator
The type D transfer function is given by (2.1) with $\omega_{\mathrm{ar}} = \omega_{\mathrm{r}}$, such that it can be rewritten as:

$$P_{\mathrm{D}}(s) = \frac{1}{ms^2} \tag{2.5}$$

where m is the total mass to be moved. It seems that we actually have to do with a second-order transfer function that physically is related to a mass with an applied force. However, the denominator polynomial is of second order because the

numerator polynomial apparently has two roots that are identical to two roots of the denominator polynomial, *i.e.*, pole-zero cancellation occurs. This can be clearly seen in the pole-zero map of figure 2.5. The corresponding Bode diagram shows a constant slope of -40 dB per decade, while the phase is $-\pi$ radians.

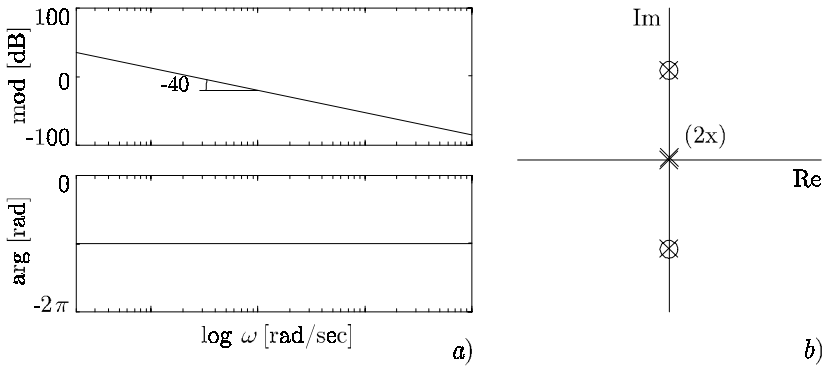

FIGURE 2.5 *Bode diagram and pole-zero map of a type D transfer function*

Type RA: Resonance - Anti-resonance
This type is comparable to the type AR transfer function, but differs because for the type RA system the resonance frequency is smaller than the anti-resonance frequency. The transfer function of a type RA transfer function is:

$$P_{\mathrm{RA}}(s) = \frac{1}{ms^2} \cdot \frac{s^2 + \omega_{\mathrm{ar}}^2}{s^2 + \omega_{\mathrm{r}}^2} \cdot \frac{\omega_{\mathrm{r}}^2}{\omega_{\mathrm{ar}}^2}, \quad \omega_{\mathrm{ar}} > \omega_{\mathrm{r}} \tag{2.6}$$

In the s-plane this type is characterized by a zero pair on the imaginary axis that is located further away from the origin than the resonance pole pair. The Bode diagram and the pole-zero map are shown in figure 2.6.

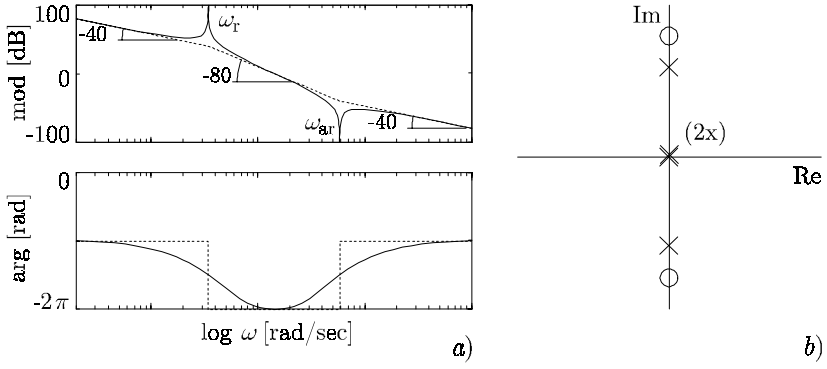

FIGURE 2.6 *Bode diagram and pole-zero map of a type RA transfer function*

The low-frequency behavior of this transfer function can be approximated by:

$$P_{\mathrm{RA}}(j\omega)_{\mathrm{LF}} \approx \frac{1}{m(j\omega)^2} \tag{2.7}$$

with a slope of -40 dB per decade and a phase of $-\pi$ radians. The middle-frequency behavior, between the resonance and anti-resonance frequency, is characterized by:

$$P_{\mathrm{RA}}(j\omega)_{\mathrm{MF}} \approx \frac{\omega_{\mathrm{r}}^2}{m(j\omega)^2(j\omega)^2} \tag{2.8}$$

The slope is now -80 dB per decade and the phase shifts to -2π radians. The high-frequency behavior follows from:

$$P_{\mathrm{RA}}(j\omega)_{\mathrm{HF}} \approx \frac{(j\omega)^2\omega_{\mathrm{r}}^2}{m(j\omega)^2(j\omega)^2\omega_{\mathrm{ar}}^2} = \frac{\omega_{\mathrm{r}}^2}{m(j\omega)^2\omega_{\mathrm{ar}}^2} \tag{2.9}$$

where the phase shifts back to $-\pi$ radians.

Type R: Resonance
The type R transfer function is:

$$P_{\mathrm{R}}(s) = \frac{1}{ms^2} \cdot \frac{\omega_{\mathrm{r}}^2}{s^2 + \omega_{\mathrm{r}}^2} \tag{2.10}$$

This transfer function type has no zero pair (or rather, a zero pair at a frequency outside the frequency range of interest) and thus no anti-resonance frequency. The Bode diagram and corresponding pole-zero map are shown in figure 2.7.

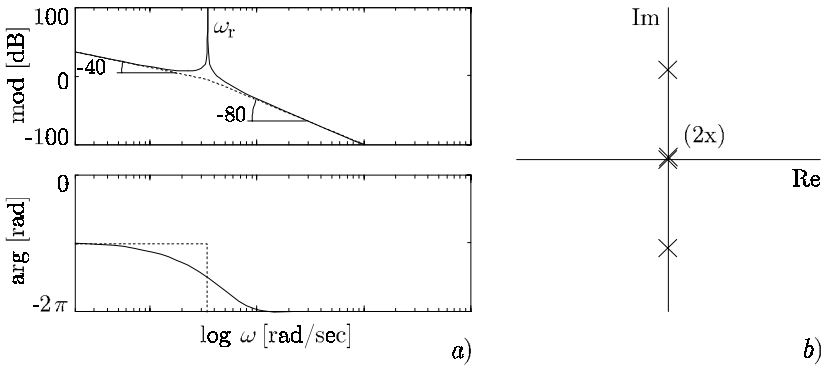

FIGURE 2.7 *Bode diagram and pole-zero map of a type R transfer function*

For the lower frequencies (LF), much smaller than ω_{r}, this system behaves like a double integrator:

$$P_{\mathrm{R}}(j\omega)_{\mathrm{LF}} \approx \frac{1}{m(j\omega)^2} \tag{2.11}$$

with a phase equal to $-\pi$ radians. At the resonance frequency ω_{r} the response will go to infinity and the phase will rapidly change to -2π radians. For frequencies higher than the resonance frequency (HF) the amplitude characteristic rolls off with a slope of -80 dB per decade:

$$P_{\mathrm{R}}(j\omega)_{\mathrm{HF}} \approx \frac{\omega_{\mathrm{ar}}^2}{m(j\omega)^2(j\omega)^2} \tag{2.12}$$

Type N: Non-minimum phase
The transfer function of a type N system is:

$$P_{\mathrm{N}}(s) = \frac{1}{ms^2} \cdot \frac{s^2 - \omega_{\mathrm{ar}}^2}{s^2 + \omega_{\mathrm{r}}^2} \cdot \frac{\omega_{\mathrm{r}}^2}{-\omega_{\mathrm{ar}}^2} \tag{2.13}$$

This type is characterized by a zero at $s = \pm\,\omega_{\mathrm{ar}}$ (figure 2.8). Because of the zero in the right-half plane this type is referred to as non-minimum phase. The Bode diagram is also shown in figure 2.8.

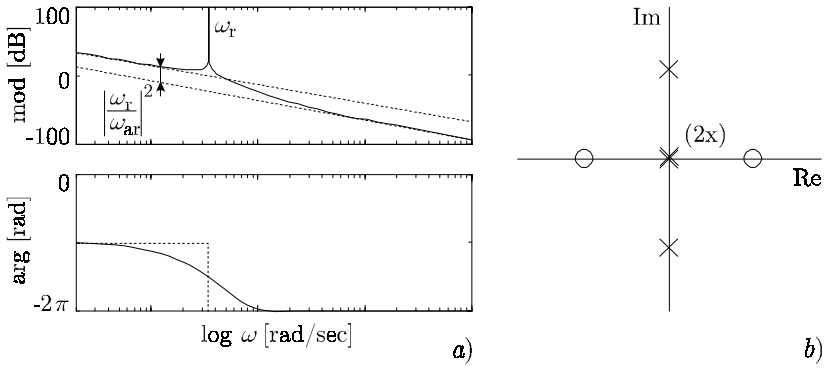

FIGURE 2.8 *Bode diagram and pole-zero map of a type N transfer function*

For lower frequencies (LF), *i.e.* below ω_{r}, this system behaves like a double integrator:

$$P_{\mathrm{N}}(j\omega)_{\mathrm{LF}} \approx \frac{1}{m(j\omega)^2} \tag{2.14}$$

with a phase equal to $-\pi$ radians. At the resonance frequency ω_{r} the phase will change to -2π radians. For frequencies above the resonance frequency (HF) the amplitude characteristic rolls off with a slope of -40 dB per decade:

$$P_{\mathrm{N}}(j\omega)_{\mathrm{HF}} \approx \frac{1}{m(j\omega)^2} \cdot \frac{\omega_{\mathrm{r}}^2}{-\omega_{\mathrm{ar}}^2} \tag{2.15}$$

Depending on the relative size of ω_{r} and ω_{ar} three different situations can occur:
- When ω_{r} is smaller than ω_{ar}, the high-frequency asymptote is located below the low-frequency asymptote, as in figure 2.8.
- When ω_{r} equals ω_{ar}, the high-frequency asymptote equals the low-frequency asymptote.
- When ω_{r} is larger than ω_{ar}, the high-frequency asymptote is located above the low-frequency asymptote.

2.2.2 Classes of electromechanical motion systems

The basic transfer functions listed above can be used to describe four classes of electromechanical motion systems. The plant models describing these classes are referred to as *standard (fourth-order) plant models*. The classes are characterized by the mechanical subsystem that contains the dominant stiffness. We distinguish (Koster *et al.*, 1999):
1. The flexible mechanism
2. The flexible frame
3. The flexible actuator suspension
4. The flexible guidance

We will indicate how the dynamic behavior of these systems is described by the basic transfer functions. For each class, more than one transfer function can be obtained, depending on the location of the sensor. Note that for a particular plant, the denominator, and therefore the resonance frequency ω_{r}, as well as the total mass to be moved m, are unique. The anti-resonance frequency ω_{ar} varies with the location of the sensor.

The flexible mechanism
When the dominant stiffness c is located in the mechanism, the system can be described by the mass-spring-mass model of figure 2.9.

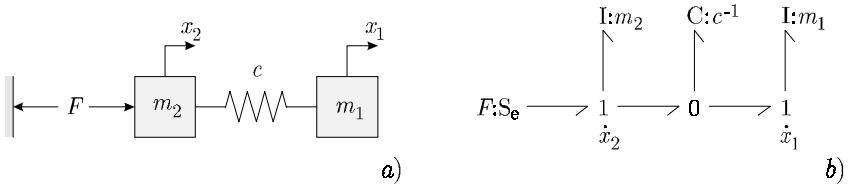

FIGURE 2.9 *Iconic diagram a) and bond graph b) of the flexible mechanism*

The input force ($u = F$) acts on the motor mass m_2 at position x_2. The position of the end-effector mass m_1 is x_1, which is also the position to be controlled z. When we measure the position of the actuator ($y = x_2$), we obtain a transfer function of type AR. The parameters in this transfer function are the total mass m, the anti-resonance frequency ω_{ar} and the resonance frequency ω_r. The expressions for these parameters, in case of a flexible mechanism, are:

$$m = m_1 + m_2 \tag{2.16}$$

$$\omega_{ar} = \sqrt{\frac{c}{m_1}} \tag{2.17}$$

$$\omega_r = \sqrt{\frac{c}{m_1} + \frac{c}{m_2}} \tag{2.18}$$

The transfer function from the input force to the position of the end-effector ($y = x_1$) is of type R. The expressions for the relevant parameters are as in (2.16) and (2.18).

The flexible frame
The model of figure 2.10 describes the situation where the dominant stiffness c is located in the supporting frame. The mass of the frame is m_2 at position x_2. The mass m_1 is a rigid body containing, amongst others, the mass of the actuator and the end-effector. The position of this rigid body x_1 is the position to be controlled z. This position can be measured with respect to the frame or with respect to the fixed world, resulting in a different type of transfer function.

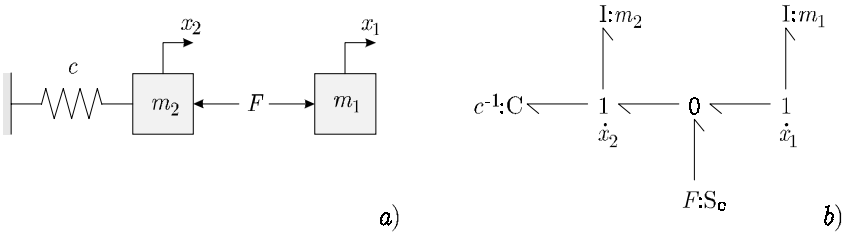

FIGURE 2.10 *Iconic diagram a) and bond graph b) of the flexible frame*

The transfer function from the input force ($u = F$) to the position measurement with respect to the frame ($y = x_1 - x_2$) is of type AR. The expression for the parameters m, ω_{ar} and ω_r of the type AR transfer function, in case of the flexible frame, are:

$$m = m_1 \tag{2.19}$$

$$\omega_{\mathrm{ar}} = \sqrt{\frac{c}{m_1 + m_2}} \tag{2.20}$$

$$\omega_{\mathrm{r}} = \sqrt{\frac{c}{m_2}} \tag{2.21}$$

When the end-effector position is measured with respect to the fixed world ($y = x_1$), we obtain a transfer function of type D. The single parameter in this transfer function is m (2.19). The resonance frequency ω_{r} is cancelled by an anti-resonance frequency of equal magnitude, according to (2.21).

The flexible actuator suspension
The model of figure 2.11 represents a system consisting of a rotating actuator with a transmission that is contained in a flexible suspension. Linear movements of the end-effector m_1 are a combination of movements due to actuator rotations and suspension vibrations. The actuator, with an applied torque T, has an inertia J. Together with the transmission i it is placed in a suspension with mass m_2 and stiffness c. The velocity of the end-effector m_1 is the addition of the velocity of the suspension and the transformed angular velocity of the actuator. In figure 2.11 it is shown how the torque T, the actuator position φ and the actuator inertia J have been transformed.

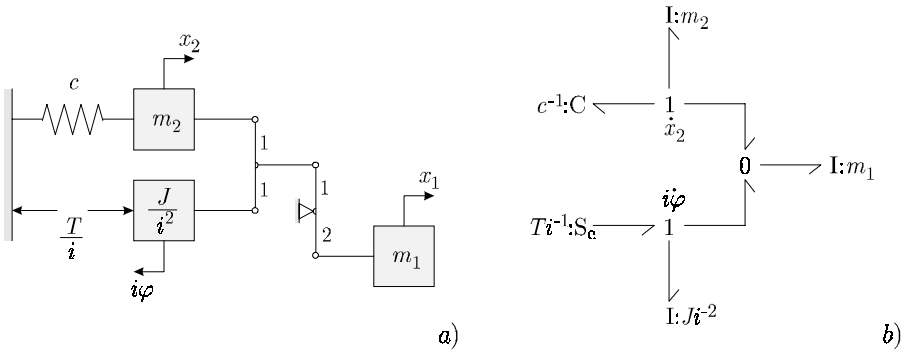

FIGURE 2.11 *Iconic diagram a) and bond graph b) of the flexible suspension*

The transfer function from the input force ($u = T/i$) to the position of the actuator ($y = i\varphi$) is of type AR. The expressions for parameters in the type AR transfer function of the flexible actuator suspension are:

$$m = \frac{J}{i^2} + m_1 \tag{2.22}$$

$$\omega_{\mathrm{ar}} = \sqrt{\frac{c}{m_1 + m_2}} \tag{2.23}$$

$$\omega_{\mathrm{r}} = \sqrt{\frac{\left(J + i^2 m_1\right)c}{J\left(m_1 + m_2\right) + i^2 m_1 m_2}} \tag{2.24}$$

When the position of the end-effector is measured ($y = x_1$), a type RA transfer function is obtained. The expression for the anti-resonance frequency ω_{ar} is:

$$\omega_{\mathrm{ar}} = \sqrt{\frac{c}{m_2}} \tag{2.25}$$

Remark 2.2

In (Miu, 1991) a physical interpretation of transfer function zeros for simple control systems with mechanical flexibilities is described. It is shown that whereas the poles are the resonances of a flexible structure, the zeros are the resonances of a constrained substructure. In case of the flexible mechanism, flexible frame and flexible suspension, the anti-resonance frequency can be looked upon as the resonance frequency of the system in case the actuator is blocked, i.e. constrained.

The flexible guidance
The final class is characterized by a flexibility in the guiding system. In figure 2.12 the dynamics of this class are illustrated. Due to an input force ($u = F$) the mass m will move in the x-direction. Additionally, F will excite a rocking mode around the center of mass (COM), due to the flexibility c. The inertia of the guided system is denoted by J.

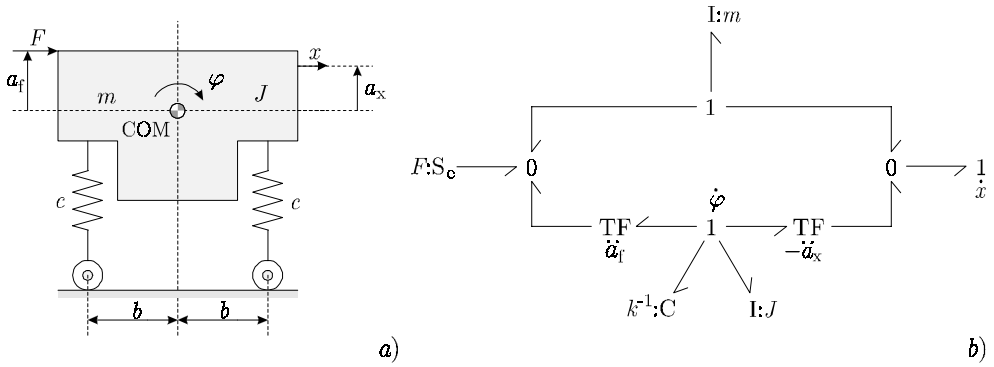

FIGURE 2.12 *Sketch a) and bond graph model b) of the flexible guidance*

The type of transfer function from the input force ($u = F$) to the measured position ($y = x$) depends on geometrical properties: the distances a_{f} and a_{x}. The expressions for parameters in the transfer function are:

$$\omega_{\mathrm{ar}} = \sqrt{\frac{k}{J + m a_{\mathrm{f}} a_{\mathrm{x}}}} \tag{2.26}$$

$$\omega_{\mathrm{r}} = \sqrt{\frac{k}{J}} \tag{2.27}$$

where,

$$k = 2cb^2 \tag{2.28}$$

We can distinguish five situations:

1. When F and x are at the same side of the COM ($a_{\mathrm{x}} > 0$ and $a_{\mathrm{f}} > 0$ or $a_{\mathrm{x}} < 0$ and $a_{\mathrm{f}} < 0$) we obtain a type AR transfer function, because $\omega_{\mathrm{ar}} < \omega_{\mathrm{r}}$.
2. When either F or x are exactly located at the COM ($a_{\mathrm{x}} = 0$ or $a_{\mathrm{f}} = 0$), we obtain a type D transfer function, as ω_{ar} equals ω_{r}. Note that $a_{\mathrm{x}} = 0$ or $a_{\mathrm{f}} = 0$ are two different situations, where the rocking mode of the plant is unobservable respectively uncontrollable.
3. When F and x are at different sides of the COM ($a_{\mathrm{x}} > 0$ and $a_{\mathrm{f}} < 0$) or ($a_{\mathrm{x}} < 0$ and $a_{\mathrm{f}} > 0$) we obtain a type RA transfer function, under the condition that $J + m\, a_{\mathrm{x}}\, a_{\mathrm{f}} > 0$.
4. When F and x are at different sides of the COM and $J + m\, a_{\mathrm{x}}\, a_{\mathrm{f}} = 0$ we obtain an R type transfer function, as ω_{ar} is located at infinity.
5. When F and x are at different sides of the COM and $J + m\, a_{\mathrm{x}}\, a_{\mathrm{f}} < 0$ we obtain an N type transfer function, as ω_{ar} is complex.

2.3 Assessment method

In (Groenhuis, 1991) as well as in (Koster *et al.*, 1999) formalized design knowledge has been described for the design of electromechanical transient systems, for which the dominant stiffness is located in the mechanism, *i.e.* figure 2.9. A design procedure has been formulated that aims for the minimization of the positional error of the end-effector after a change in the reference path (point-to-point motion). The plant model is fourth order, but only two states are measured for control, *i.e.* a position and a velocity, such that only the rigid-body mode of the plant is controlled. The design procedure can be applied in several ways, thus advocating a true mechatronic design approach. An advantage of this method is

that little information about the plant is needed, while a reliable estimation of the worst case performance can be obtained. We will extend this method such that it is applicable to all classes of electromechanical motion systems presented in section 2.2.2. Therefore, we will first determine the dimensionless parameters that allow us to describe general plant transfer functions independent of particular problem settings. A similar approach has been presented in (Åström *et al.*, 1992) for process control. Next, closed-loop characteristics are classified and optimal dimensionless controller settings are obtained, as well as relations between dominant plant characteristics, performance and reference path characteristics. Finally, the assessment method is described in the form of a design procedure.

2.3.1 Dimensionless parameters and closed-loop characteristics

Before we can consider the closed-loop transfer function, we have to make a choice for the control system $\mathcal{C}$. We have chosen a PD-type control system that implements a proportional action k_p on a positional error and a proportional action k_d on a measured velocity v. The positional error is obtained as the difference between a measured position y and the reference path r. The variable to be controlled is the position of the end-effector z. This general closed-loop transient system is shown in figure 2.13.

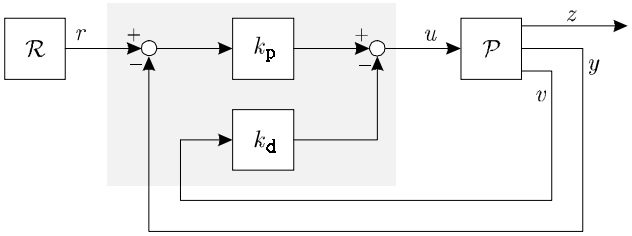

FIGURE 2.13 *General closed-loop transient system*

Remark 2.3

The basic characterization of fourth-order transfer functions of section 2.2.1 holds for transfer functions from input force to position. This characterization can also be applied to transfer functions from input force to velocity, when the term s^2 in the denominator is replaced by the term s.

Remark 2.4

For each class of electromechanical motion systems a position and velocity can be measured at either the end-effector or the actuator, possibly with respect to the frame. Alternatively, the designer can opt for measuring the position of the end-effector and the velocity of the actuator.

We will introduce some (dimensionless) quantities that allow us to draw general conclusions for controlled fourth-order systems. First we define two loop quantities: the position loop quantity ω_{p} and the velocity loop quantity ω_{d}:

$$\omega_{\mathrm{p}} = \sqrt{\frac{k_{\mathrm{p}}}{m}} \tag{2.29}$$

$$\omega_{\mathrm{d}} = \frac{k_{\mathrm{d}}}{m} \tag{2.30}$$

where m is the total mass to be moved.

An important dimensionless quantity, which is related to the plant, is the *frequency ratio* ρ:

$$\rho = \left(\frac{\omega_{\mathrm{ar}}}{\omega_{\mathrm{r}}}\right)^2 \tag{2.31}$$

This ratio relates the resonance frequency of a plant to the anti-resonance frequency.

So far, the plant transfer functions have been described without mechanical damping, as damping is not of importance for conceptual design of the controlled system. However, during the simulations we will implicitly use a small amount of damping. The polynomials of the basic fourth-order transfer functions consist of a combination of the terms, of which the following will be extended with an amount of damping, as shown here:

$$\begin{aligned} s^2 \quad &\rightarrow \quad s(s+\alpha) \\ s^2 + \omega_{\mathrm{r}}^2 \quad &\rightarrow \quad s^2 + 2\zeta_{\mathrm{r}}\omega_{\mathrm{r}}s + \omega_{\mathrm{r}}^2 \\ s^2 + \omega_{\mathrm{ar}}^2 \quad &\rightarrow \quad s^2 + 2\zeta_{\mathrm{ar}}\omega_{\mathrm{ar}}s + \omega_{\mathrm{ar}}^2 \end{aligned}$$

The *dimensionless controller settings* Ω_{p} and Ω_{d} relate the loop quantities ω_{p} and ω_{d} to the anti-resonance frequency of the plant. These settings can be considered the dimensionless versions of the proportional actions k_{p} and k_{d}.

$$\omega_{\mathrm{p}} = \Omega_{\mathrm{p}} \cdot \omega_{\mathrm{ar}} \tag{2.32}$$

$$\omega_{\mathrm{d}} = \Omega_{\mathrm{d}} \cdot \omega_{\mathrm{ar}} \tag{2.33}$$

The reference path is assumed to be a smooth spline function. The smoothness is determined by a degree. If the reference path is of degree 2, it involves two pieces of second-order polynomials. If it is of degree 3, it involves three pieces of third-order polynomials. The reference path specifies, in terms of the position of the end-

effector, a distance h_m that has to be covered within a motion time t_m. The control goal is to guarantee an upper bound e_0 on the absolute value of the positional error of the end-effector after the reference path has reached the end point (figure 2.14).

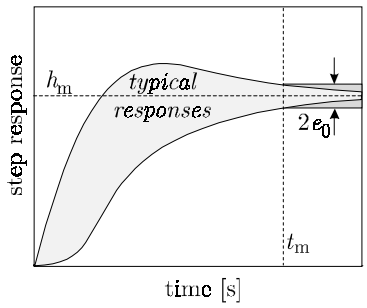

FIGURE 2.14 *Reference path and typical responses*

The maximum relative positional error E_0 is defined as the ratio between the positional error e_0 and the motion distance h_m:

$$E_0 = \frac{e_0}{h_m} \tag{2.34}$$

A crucial dimensionless quantity is the periodic ratio τ that relates the anti-resonance frequency of the plant and the motion time t_m:

$$\tau = \frac{2\pi}{\omega_{ar} t_m} \tag{2.35}$$

We will now discuss the closed-loop transfer functions $H(s)$, *i.e.* the transfer functions from the reference path r to the measured position y, when using a control system as in figure 2.13. The transfer function $H(s)$ is also referred to as the command response. We use the classification of plant models and plant transfer functions discussed in the previous section, as well as the dimensionless quantities introduced above. So far we obtained:

- a classification into four electromechanical motion systems.
- a characterization of five plant transfer functions, *i.e.* transfer function *types*.

For each class a minimum of three sensor combinations and thus three closed-loop configurations are relevant:

1. position and velocity measurement at the actuator;
2. position and velocity measurement at the end-effector;
3. position measurement at the end-effector and velocity measurement at the actuator.

where position and velocity may be measured with respect to the fixed world or another reference, *e.g.* the machine frame. The dimensionless quantities are used to characterize these closed-loop dynamics in general terms. When we combine this with the transfer function *types* (section 2.2.1), we can describe closed-loop dynamics in general terms, independent of a particular *class* (section 2.2.2). We will refer to these closed-loop transfer functions as *concepts*.

Concept AR: Anti-resonance - Resonance
When both the open-loop transfer function from input force F to the measured position y and to the measured velocity v are characterized by type AR, then the closed-loop transfer function is called concept AR. This concept is applicable when the actuator position and velocity of, for example, the flexible mechanism or the flexible actuator suspension are measured (section 2.2.2). The closed-loop transfer function $H(s)$ from reference path r to the measured position y is:

$$H_{\mathrm{AR}}(s) = \frac{\left(s^2 + \omega_{\mathrm{ar}}^2\right)k_{\mathrm{p}}\omega_{\mathrm{r}}^2}{m\omega_{\mathrm{ar}}^2 s^4 + k_{\mathrm{d}}\omega_{\mathrm{r}}^2 s^3 + \left(k_{\mathrm{p}} + \omega_{\mathrm{ar}}^2 m\right)\omega_{\mathrm{r}}^2 s^2 + \omega_{\mathrm{ar}}^2 k_{\mathrm{d}}\omega_{\mathrm{r}}^2 s + \omega_{\mathrm{ar}}^2\omega_{\mathrm{r}}^2 k_{\mathrm{p}}} \tag{2.36}$$

Dividing the numerator and denominator by the total mass to be moved, *i.e.* m, and substituting (2.34) and (2.35), results in the dimensionless transfer function:

$$H_{\mathrm{AR}}(s) = \frac{\left(s^2 + \omega_{\mathrm{ar}}^2\right)\omega_{\mathrm{p}}^2\omega_{\mathrm{r}}^2}{\omega_{\mathrm{ar}}^2 s^4 + \omega_{\mathrm{d}}\omega_{\mathrm{r}}^2 s^3 + \left(\omega_{\mathrm{p}}^2 + \omega_{\mathrm{ar}}^2\right)\omega_{\mathrm{r}}^2 s^2 + \omega_{\mathrm{ar}}^2\omega_{\mathrm{d}}\omega_{\mathrm{r}}^2 s + \omega_{\mathrm{ar}}^2\omega_{\mathrm{p}}^2\omega_{\mathrm{r}}^2} \tag{2.37}$$

When we introduce (dimensionless) damping to the type AR plant transfer function, we obtain:

$$P_{\mathrm{AR,d}}(s) = \frac{1}{ms\left(s+\alpha\right)} \cdot \frac{s^2 + 2\zeta_{\mathrm{ar}}\omega_{\mathrm{ar}}s + \omega_{\mathrm{ar}}^2}{s^2 + 2\zeta_{\mathrm{r}}\omega_{\mathrm{r}}s + \omega_{\mathrm{r}}^2} \cdot \frac{\omega_{\mathrm{r}}^2}{\omega_{\mathrm{ar}}^2} \tag{2.38}$$

Here, ζ_{ar} is the relative damping of the zero pair and the subscript d indicates that damping is included in the transfer function. The closed-loop transfer function is now described by:

$$H_{\mathrm{AR,d}}(s) = \frac{b_2 s^2 + b_1 s + b_0}{a_4 s^4 + a_3 s^3 + a_2 s^2 + a_1 s + a_0} \tag{2.39}$$

The coefficients in this transfer function with, respectively without damping, are:

$$
\begin{aligned}
b_2 &= \omega_{\mathrm{p}}^2\omega_{\mathrm{r}}^2 & b_2 &= \omega_{\mathrm{p}}^2\omega_{\mathrm{r}}^2\\
b_1 &= 2\zeta_{\mathrm{ar}}\omega_{\mathrm{ar}}\omega_{\mathrm{p}}^2\omega_{\mathrm{r}}^2 & b_1 &= 0\\
b_0 &= \omega_{\mathrm{ar}}^2\omega_{\mathrm{p}}^2\omega_{\mathrm{r}}^2 & b_0 &= \omega_{\mathrm{ar}}^2\omega_{\mathrm{p}}^2\omega_{\mathrm{r}}^2\\
a_4 &= \omega_{\mathrm{ar}}^2 & a_4 &= \omega_{\mathrm{ar}}^2\\
a_3 &= (2\zeta_{\mathrm{r}}\omega_{\mathrm{r}} + \alpha)\omega_{\mathrm{ar}}^2 + \omega_{\mathrm{d}}\omega_{\mathrm{r}}^2 & a_3 &= \omega_{\mathrm{d}}\omega_{\mathrm{r}}^2\\
a_2 &= \left(2\alpha\zeta_{\mathrm{r}}\omega_{\mathrm{r}} + \omega_{\mathrm{r}}^2\right)\omega_{\mathrm{ar}}^2 + \left(\omega_{\mathrm{p}}^2 + 2\zeta_{\mathrm{ar}}\omega_{\mathrm{ar}}\omega_{\mathrm{d}}\right)\omega_{\mathrm{r}}^2 & a_2 &= \left(\omega_{\mathrm{ar}}^2 + \omega_{\mathrm{p}}^2\right)\omega_{\mathrm{r}}^2\\
a_1 &= \left(\alpha + \omega_{\mathrm{d}}\right)\omega_{\mathrm{ar}}^2\omega_{\mathrm{r}}^2 + 2\zeta_{\mathrm{ar}}\omega_{\mathrm{ar}}\omega_{\mathrm{p}}^2\omega_{\mathrm{r}}^2 & a_1 &= \omega_{\mathrm{d}}\omega_{\mathrm{ar}}^2\omega_{\mathrm{r}}^2\\
a_0 &= \omega_{\mathrm{ar}}^2\omega_{\mathrm{p}}^2\omega_{\mathrm{r}}^2 & a_0 &= \omega_{\mathrm{ar}}^2\omega_{\mathrm{p}}^2\omega_{\mathrm{r}}^2
\end{aligned}
\tag{2.40}
$$

Concept D: Double integrator
When both open-loop transfer functions (from force F to the measured position y and to the measured velocity v) are of type D, then the closed-loop transfer function is called concept D. When we introduce damping in the type D transfer function we obtain:

$$P_{\mathrm{D}}(s) = \frac{1}{ms(s+\alpha)} \tag{2.41}$$

where α is the absolute damping of the real pole. The resulting closed-loop transfer function from reference path r to the measured position y, with damping, is:

$$H_{\mathrm{D,d}}(s) = \frac{\omega_{\mathrm{p}}^2}{s^2 + \left(\alpha + \omega_{\mathrm{d}}\right)s + \omega_{\mathrm{p}}^2} \tag{2.42}$$

Remark 2.5

It can be shown that a plant characterized by this transfer function is not observable and/or not controllable. When the location of actuators and sensors is considered, this has to be taken into account. One can also take advantage of this property, in order to avoid excitation of the resonance frequencies.

Concept RA: Resonance - Anti-resonance
When both open-loop transfer functions are of type RA, then the closed-loop transfer function is referred to as concept RA. The expression for the transfer function of concept RA is identical to the expressions for the concept AR transfer function, *i.e.* (2.39) and (2.40). The difference is that the anti-resonance frequency is larger than the resonance frequency in case of concept RA.

Concept R: Resonance
When both open-loop transfer functions are of type R, then the closed-loop transfer function is referred to as concept R. When we introduce damping in the type R plant transfer function we obtain:

$$P_{\mathrm{R,d}}(s) = \frac{1}{ms(s+\alpha)} \cdot \frac{\omega_{\mathrm{r}}^2}{s^2 + 2\zeta_{\mathrm{r}}\omega_{\mathrm{r}}s + \omega_{\mathrm{r}}^2} \tag{2.43}$$

Here, ζ_{r} is the relative damping of the pole pair and α is the absolute damping of the real pole. The corresponding closed-loop transfer function is described by:

$$H_{\mathrm{R,d}}(s) = \frac{b_0}{a_4 s^4 + a_3 s^3 + a_2 s^2 + a_1 s + a_0} \tag{2.44}$$

The coefficients in this function, with respectively without damping, are:

$$\begin{aligned} b_0 &= \omega_{\mathrm{p}}^2\omega_{\mathrm{r}}^2 & b_0 &= \omega_{\mathrm{p}}^2\omega_{\mathrm{r}}^2 \\ a_4 &= 1 & a_4 &= 1 \\ a_3 &= 2\zeta_{\mathrm{r}}\omega_{\mathrm{r}} + \alpha & a_3 &= \alpha \\ a_2 &= 2\alpha\zeta_{\mathrm{r}}\omega_{\mathrm{r}} + \omega_{\mathrm{r}}^2 & a_2 &= \omega_{\mathrm{r}}^2 \\ a_1 &= \left(\alpha + \omega_{\mathrm{d}}\right)\omega_{\mathrm{r}}^2 & a_1 &= \omega_{\mathrm{d}}\omega_{\mathrm{r}}^2 \\ a_0 &= \omega_{\mathrm{p}}^2\omega_{\mathrm{r}}^2 & a_0 &= \omega_{\mathrm{p}}^2\omega_{\mathrm{r}}^2 \end{aligned} \tag{2.45}$$

Concept N: Non-minimum phase
A concept N transfer function occurs when both open-loop transfer functions are of type N, *i.e.* are non-minimum phase. The expression for the closed-loop transfer function is similar as for concept AR and RA, *i.e.* (2.39) and (2.40), with $-\omega_{\mathrm{ar}}^2$ substituted for ω_{ar}^2 and the relative damping ζ_{ar} equal to zero.

So far, we have discussed concepts where the position and velocity are measured at the same location. Now, we will discuss concepts where the velocity is measured at the actuator and the position at the end-effector. In terms of the basic transfer functions this means that the transfer function from the input force F to the measured velocity v is always of type AR and the transfer function from input force F to the measured position y may be of type D, RA, R or N (refer section 2.2.2).

Concept AR-R
When the open-loop transfer function from the input force F to the measured position y is of type R and from the input force F to the measured velocity v is of type AR, we obtain concept AR-R. This, for example, occurs when we measure the actuator velocity and end-effector position of the flexible mechanism. We will

derive the closed-loop transfer function $H(s)$ from the reference path r to the measured position y, using the block diagram of figure 2.15.

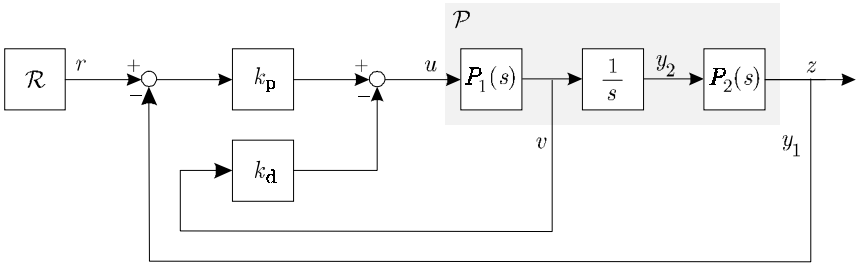

FIGURE 2.15 *Construction of closed-loop transfer function when using two sensors*

We first close only the velocity loop of figure 2.15, with $P_1(s)$ a type AR transfer function from the input force ($u = F$) to the measured velocity v. The resulting closed-loop transfer function from the reference path r to the velocity v is:

$$H_1(s) = \frac{V}{R} = \frac{\left(s^2 + \omega_\mathrm{ar}^2\right)\omega_\mathrm{r}^2}{m\omega_\mathrm{ar}^2 s^3 + k_\mathrm{d}\omega_\mathrm{r}^2 s^2 + m\omega_\mathrm{ar}^2\omega_\mathrm{r}^2 s + \omega_\mathrm{ar}^2 k_\mathrm{d}\omega_\mathrm{r}^2} \tag{2.46}$$

Consecutively, we integrate the measured velocity v, which gives position y_2, which generally is the motor position. We replace the numerator of the resulting transfer function with the numerator of the transfer function from input force F to the measured position y_1, *i.e.* replace the type AR numerator with the type R numerator:

$$\begin{aligned} H_2(s) &= H_1(s) \cdot \frac{1}{s} \cdot P_2(s) = H_1(s) \cdot \frac{1}{s} \cdot \frac{\omega_\mathrm{ar}^2}{\left(s^2 + \omega_\mathrm{ar}^2\right)} \cdot 1 \\ &= \frac{\omega_\mathrm{ar}^2\omega_\mathrm{r}^2}{s\left(\omega_\mathrm{ar}^2 s^3 + \omega_\mathrm{d}\omega_\mathrm{r}^2 s^2 + \omega_\mathrm{ar}^2\omega_\mathrm{r}^2 s + \omega_\mathrm{ar}^2\omega_\mathrm{d}\omega_\mathrm{r}^2\right)} \end{aligned} \tag{2.47}$$

Note that in (2.47) we divide by the type AR numerator and we multiply with the type R numerator, which equals 1. Finally, we close the position loop of figure 2.15, resulting in the closed-loop transfer function $H(s)$ from reference path r to the measured position y. Similarly as before, we substitute the dimensionless quantities and we introduce (dimensionless) damping, such that we obtain:

$$H_{\text{AR-R,d}}(s) = \frac{b_0}{a_4 s^4 + a_3 s^3 + a_2 s^2 + a_1 s + a_0} \tag{2.48}$$

The coefficients in this function, with respectively without damping, are:

$$
\begin{aligned}
b_0 &= \omega_{\mathrm{ar}}^2\omega_{\mathrm{p}}^2\omega_{\mathrm{r}}^2 & b_0 &= \omega_{\mathrm{ar}}^2\omega_{\mathrm{p}}^2\omega_{\mathrm{r}}^2\\
a_4 &= \omega_{\mathrm{ar}}^2 & a_4 &= \omega_{\mathrm{ar}}^2\\
a_3 &= \big(2\xi_{\mathrm{r}}\omega_{\mathrm{r}} + \alpha\big)\omega_{\mathrm{ar}}^2 + \omega_{\mathrm{d}}\omega_{\mathrm{r}}^2 & a_3 &= \omega_{\mathrm{d}}\omega_{\mathrm{r}}^2\\
a_2 &= \big(2\alpha\xi_{\mathrm{r}}\omega_{\mathrm{r}} + \omega_{\mathrm{r}}^2\big)\omega_{\mathrm{ar}}^2 + 2\xi_{\mathrm{ar}}\omega_{\mathrm{ar}}\omega_{\mathrm{d}}\omega_{\mathrm{r}}^2 & a_2 &= \omega_{\mathrm{r}}^2\omega_{\mathrm{ar}}^2\\
a_1 &= \big(\alpha + \omega_{\mathrm{d}}\big)\omega_{\mathrm{ar}}^2\omega_{\mathrm{r}}^2 & a_1 &= \omega_{\mathrm{d}}\omega_{\mathrm{ar}}^2\omega_{\mathrm{r}}^2\\
a_0 &= \omega_{\mathrm{ar}}^2\omega_{\mathrm{p}}^2\omega_{\mathrm{r}}^2 & a_0 &= \omega_{\mathrm{ar}}^2\omega_{\mathrm{p}}^2\omega_{\mathrm{r}}^2
\end{aligned}
\tag{2.49}
$$

Concept AR-D

When the open-loop transfer function from the input force F to the measured position y is of type D and from F to the measured velocity v is of type AR, we obtain concept *AR-D*. The transfer function is derived in a similar way as for concept *AR-R*. The transfer function $H_1(s)$ from r to v is identical to (2.46). The type AR numerator is now replaced with a type D numerator, similar as in (2.47), but with:

$$
P_2(s) = \frac{\omega_{\mathrm{ar}}^2}{\big(s^2 + \omega_{\mathrm{ar}}^2\big)} \cdot \frac{\big(s^2 + \omega_{\mathrm{r}}^2\big)}{\omega_{\mathrm{r}}^2}
\tag{2.50}
$$

Subsequently closing the position loop gives the closed-loop transfer function $H(s)$ for concept *AR-D*:

$$
H_{\text{AR-D,d}}(s) = \frac{b_2 s^2 + b_1 s + b_0}{a_4 s^4 + a_3 s^3 + a_2 s^2 + a_1 s + a_0}
\tag{2.51}
$$

The coefficients in this function, with respectively without damping, are:

$$
\begin{aligned}
b_2 &= \omega_{\mathrm{p}}^2\omega_{\mathrm{ar}}^2 & b_2 &= \omega_{\mathrm{p}}^2\omega_{\mathrm{ar}}^2\\
b_1 &= 2\zeta_{\mathrm{r}}\omega_{\mathrm{r}}\omega_{\mathrm{p}}^2\omega_{\mathrm{ar}}^2 & b_1 &= 0\\
b_0 &= \omega_{\mathrm{r}}^2\omega_{\mathrm{p}}^2\omega_{\mathrm{ar}}^2 & b_0 &= \omega_{\mathrm{r}}^2\omega_{\mathrm{p}}^2\omega_{\mathrm{ar}}^2\\
a_4 &= \omega_{\mathrm{ar}}^2 & a_4 &= \omega_{\mathrm{ar}}^2\\
a_3 &= \big(2\zeta_{\mathrm{r}}\omega_{\mathrm{r}} + \alpha\big)\omega_{\mathrm{ar}}^2 + \omega_{\mathrm{d}}\omega_{\mathrm{r}}^2 & a_3 &= \omega_{\mathrm{d}}\omega_{\mathrm{r}}^2\\
a_2 &= \big(2\alpha\zeta_{\mathrm{r}}\omega_{\mathrm{r}} + \omega_{\mathrm{r}}^2 + \omega_{\mathrm{p}}^2\big)\omega_{\mathrm{ar}}^2 + 2\zeta_{\mathrm{ar}}\omega_{\mathrm{ar}}\omega_{\mathrm{d}}\omega_{\mathrm{r}}^2 & a_2 &= \big(\omega_{\mathrm{r}}^2 + \omega_{\mathrm{p}}^2\big)\omega_{\mathrm{ar}}^2\\
a_1 &= \big(\alpha + \omega_{\mathrm{d}}\big)\omega_{\mathrm{ar}}^2\omega_{\mathrm{r}}^2 + 2\zeta_{\mathrm{r}}\omega_{\mathrm{r}}\omega_{\mathrm{p}}^2\omega_{\mathrm{ar}}^2 & a_1 &= \omega_{\mathrm{d}}\omega_{\mathrm{ar}}^2\omega_{\mathrm{r}}^2\\
a_0 &= \omega_{\mathrm{r}}^2\omega_{\mathrm{p}}^2\omega_{\mathrm{ar}}^2 & a_0 &= \omega_{\mathrm{r}}^2\omega_{\mathrm{p}}^2\omega_{\mathrm{ar}}^2
\end{aligned}
\tag{2.52}
$$

Concept AR-RA
When the open-loop transfer function from the input force F to the measured position y is of type RA and from F to the measured velocity v is of type AR, then the closed-loop transfer function is referred to as concept AR-RA. This transfer function is obtained in a similar way as above, but with:

$$P_2(s) = \frac{\omega_{\mathrm{ar}}^2}{\left(s^2 + \omega_{\mathrm{ar}}^2\right)} \cdot \frac{\left(s^2 + \omega_{\mathrm{ar}*}^2\right)}{\omega_{\mathrm{ar}*}^2} \tag{2.53}$$

where $\omega_{\mathrm{ar}*}$ indicates the anti-resonance frequency of the type RA transfer function, which is larger than ω_{r}, and ω_{ar} is the anti-resonance frequency of the type AR transfer, which is smaller than ω_{r}. The closed-loop transfer function $H(s)$ for concept AR-RA is:

$$H_{\mathrm{AR\text{-}RA,d}}(s) = \frac{b_2 s^2 + b_1 s + b_0}{a_4 s^4 + a_3 s^3 + a_2 s^2 + a_1 s + a_0} \tag{2.54}$$

$$\begin{aligned}
b_2 &= \omega_{\mathrm{p}}^2\omega_{\mathrm{ar}}^2\omega_{\mathrm{r}}^2 & b_2 &= \omega_{\mathrm{p}}^2\omega_{\mathrm{ar}}^2\omega_{\mathrm{r}}^2 \\
b_0 &= 2\zeta_{\mathrm{ar}*}\omega_{\mathrm{ar}*}\omega_{\mathrm{p}}^2\omega_{\mathrm{ar}}^2\omega_{\mathrm{r}}^2 & b_0 &= 0 \\
b_0 &= \omega_{\mathrm{ar}*}^2\omega_{\mathrm{p}}^2\omega_{\mathrm{ar}}^2\omega_{\mathrm{r}}^2 & b_0 &= \omega_{\mathrm{ar}*}^2\omega_{\mathrm{p}}^2\omega_{\mathrm{ar}}^2\omega_{\mathrm{r}}^2 \\
a_4 &= \omega_{\mathrm{ar}}^2\omega_{\mathrm{ar}*}^2 & a_4 &= \omega_{\mathrm{ar}}^2\omega_{\mathrm{ar}*}^2 \\
a_3 &= (2\zeta_{\mathrm{r}}\omega_{\mathrm{r}} + \alpha)\omega_{\mathrm{ar}}^2\omega_{\mathrm{ar}*}^2 + \omega_{\mathrm{d}}\omega_{\mathrm{ar}*}^2\omega_{\mathrm{r}}^2 & a_3 &= \omega_{\mathrm{d}}\omega_{\mathrm{ar}*}^2\omega_{\mathrm{r}}^2 \\
a_2 &= \left(2\alpha\zeta_{\mathrm{r}}\omega_{\mathrm{r}} + \omega_{\mathrm{r}}^2\right)\omega_{\mathrm{ar}}^2\omega_{\mathrm{ar}*}^2 + & a_2 &= \left(\omega_{\mathrm{ar}*}^2 + \omega_{\mathrm{p}}^2\right)\omega_{\mathrm{ar}}^2\omega_{\mathrm{r}}^2 \\
&\quad \omega_{\mathrm{p}}^2\omega_{\mathrm{ar}}^2\omega_{\mathrm{r}}^2 + 2\zeta_{\mathrm{ar}}\omega_{\mathrm{ar}}\omega_{\mathrm{d}}\omega_{\mathrm{ar}*}^2\omega_{\mathrm{r}}^2 & & \\
a_1 &= \left(\alpha + \omega_{\mathrm{d}}\right)\omega_{\mathrm{ar}}^2\omega_{\mathrm{ar}*}^2\omega_{\mathrm{r}}^2 + 2\zeta_{\mathrm{ar}*}\omega_{\mathrm{ar}*}\omega_{\mathrm{p}}^2\omega_{\mathrm{ar}}^2\omega_{\mathrm{r}}^2 & a_1 &= \omega_{\mathrm{d}}\omega_{\mathrm{ar}}^2\omega_{\mathrm{ar}*}^2\omega_{\mathrm{r}}^2 \\
a_0 &= \omega_{\mathrm{ar}*}^2\omega_{\mathrm{p}}^2\omega_{\mathrm{ar}}^2\omega_{\mathrm{r}}^2 & a_0 &= \omega_{\mathrm{ar}*}^2\omega_{\mathrm{p}}^2\omega_{\mathrm{ar}}^2\omega_{\mathrm{r}}^2
\end{aligned} \tag{2.55}$$

Concept AR-N
When the open-loop transfer function from F to the measured position y is of type N and from F to the measured velocity v is of type AR, the closed-loop transfer function is referred to as concept AR-N. The transfer function is similar to concept AR-RA according (2.54) and (2.55), with the relative damping ζ_{ar} equal to zero and $\omega_{\mathrm{ar}*}^2$ substituted by $-\omega_{\mathrm{ar}*}^2$.

For each class of electromechanical motion systems of section 2.2.2 we will now summarize the concepts that can be applied. For the first three classes this is straightforward as for each class we can distinguish three concepts, as indicated in

table 2.1, table 2.2 and table 2.3, that correspond to the three possible combinations of sensor locations.

Measurement: y, v	Concept
$x_1, \dot{x}_1$	R
$x_2, \dot{x}_2$	AR
$x_1, \dot{x}_2$	AR-R

TABLE 2.1 *Concepts for the flexible mechanism*

Measurement: y, v	Concept
$x_1, \dot{x}_1$	D
$x_1 - x_2, \dot{x}_1 - \dot{x}_2$	AR
$x_1, \dot{x}_1 - \dot{x}_2$	AR-D

TABLE 2.2 *Concepts for the flexible frame*

Measurement: y, v	Concept
$x_1, \dot{x}_1$	RA
$i\varphi, i\dot{\varphi}$	AR
$x_1, i\dot{\varphi}$	AR-RA

TABLE 2.3 *Concepts for the flexible suspension*

For the flexible guidance (section 2.2.2, figure 2.12) it is more complicated to indicate the applicable concepts. In the left two columns of table 2.4, we indicate the concepts for the situations where the position y and velocity v are measured at the same location, *i.e.* at a_x. At the right two columns we assume that the velocity is measured at the location where the force excites the system, *i.e.* at a_f, and the position is measured at a_x.

Measurement: y, v	Concept	Measurement: y, v	Concept
$x_{a_x}, \dot{x}_{a_x}$ $a_x > 0$ and $a_f > 0$ $a_x < 0$ and $a_f < 0$	*AR*	$x_{a_x}, \dot{x}_{a_f}$ $a_x > 0$ and $a_f > 0$ $a_x < 0$ and $a_f < 0$	*AR*
$x_{a_x}, \dot{x}_{a_x}$ $a_x = 0$ or $a_f = 0$	*D*	$x_{a_x}, \dot{x}_{a_f}$ $a_x = 0$	*AR-D*
$x_{a_x}, \dot{x}_{a_x}$ $a_x > 0$ and $a_f < 0$ $a_x < 0$ and $a_f > 0$ $J + ma_x a_f > 0$	*RA*	$x_{a_x}, \dot{x}_{a_f}$ $a_x > 0$ and $a_f < 0$ $a_x < 0$ and $a_f > 0$ $J + ma_x a_f > 0$	*AR-RA*
$x_{a_x}, \dot{x}_{a_x}$ $a_x > 0$ and $a_f < 0$ $a_x < 0$ and $a_f > 0$ $J + ma_x a_f = 0$	*R*	$x_{a_x}, \dot{x}_{a_f}$ $a_x > 0$ and $a_f < 0$ $a_x < 0$ and $a_f > 0$ $J + ma_x a_f = 0$	*AR-R*
$x_{a_x}, \dot{x}_{a_x}$ $a_x > 0$ and $a_f < 0$ $a_x < 0$ and $a_f > 0$ $J + ma_x a_f < 0$	*N*	$x_{a_x}, \dot{x}_{a_f}$ $a_x > 0$ and $a_f < 0$ $a_x < 0$ and $a_f > 0$ $J + ma_x a_f < 0$	*AR-N*

TABLE 2.4 *Concepts for the flexible guidance*

2.3.2 Dimensionless optimal controller settings

By performing numerous simulations with the dimensionless closed-loop transfer functions $H(s)$, *feasible* dimensionless controller settings for the different concepts can be obtained (Groenhuis, 1991). Different values for the dimensionless controller settings Ω_p and Ω_d result in different values for the loop quantities ω_p and ω_d and in turn result in different closed-loop transfer functions $H(s)$. For all these transfer functions, the positional error is determined, for identical reference paths. The feasible settings are defined as those values that result in a sufficiently small positional error with a sufficiently large *stability margin*. This stability margin

defines a forbidden region between $-g$ and 0 in the s-plane, for the poles of the closed-loop system $H(s)$. The dimensionless version of this margin is defined as:

$$G = \frac{g}{\omega_{\text{ar}}} \tag{2.56}$$

A sufficient stability margin is considered to be attained for $G = 0.2$. The *optimal dimensionless controller settings* are defined as those settings that result in the smallest positional error with a sufficient stability margin, for different values of the frequency ratio.

Remark 3.6

When we determine the feasible dimensionless controller settings, we implicitly assume that the settings that lead to a minimal error of the measured position y, also lead to a minimal error of the end-effector position z.

Concept AR
In figure 2.16 three charts are shown with feasible regions for different frequency ratios.

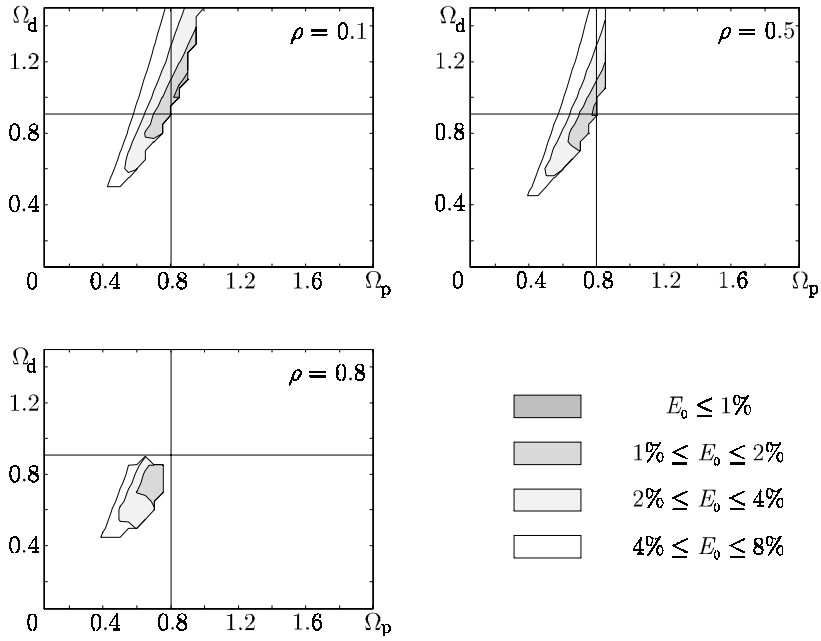

FIGURE 2.16 *Regions with feasible dimensionless parameters for concept AR with* $\rho = 0.1$, $\rho = 0.5$ *and* $\rho = 0.8$

These regions indicate values of Ω_p and Ω_d that result in a relative positional error E_0 smaller than 0.01, 0.02, 0.04 and 0.08, while meeting the stability margin (2.56). The difference between these charts is the value for the frequency ratio ρ that is used: 0.1, 0.5 respectively 0.8. The values for the damping used in the simulations are similar as the values used in (Groenhuis, 1991) and reflect practical settings: $\alpha = 0.01 \cdot \omega_r$, $\zeta_r = 0.15$ and $\zeta_{ar} = 0.06$. During all simulations discussed in this section we use a second-degree reference path with a motion time t_m of 1 [s] and a periodic time constant τ of 0.4.

From these three charts we select the optimal dimensionless controller settings for concept AR as $\Omega_p = 0.8$ and $\Omega_d = 0.9$, which are indicated in figure 2.16 by means of a cross hair. The cross hair cannot be located exactly in the regions with minimal error for all values for the frequency ratio ρ, rather an acceptable location as close as possible to these regions has been selected.

Concept D
For concept D similar simulations are performed, with the single damping parameter α equal to $0.01 \cdot \omega_r$. The response of this concept is independent of the frequency ratio ρ, therefore only a single chart is shown in figure 2.17. The optimal dimensionless controller settings for concept D have been selected as $\Omega_p = 0.9$ and $\Omega_d = 0.9$, as indicated by the cross hair in figure 2.17.

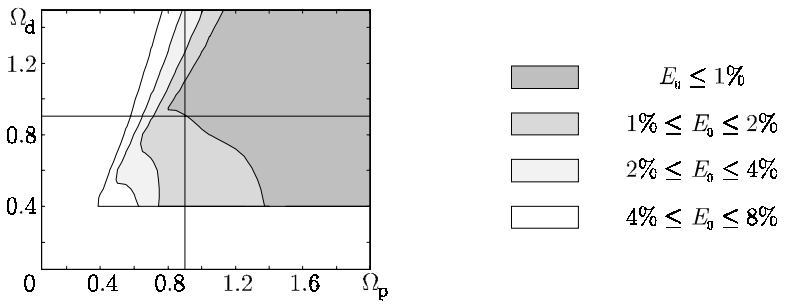

FIGURE 2.17 *Regions with feasible dimensionless parameters for concept D*

Concept RA
For the concept RA transfer function no feasible dimensionless quantities exist, as the required stability margin (2.56) cannot be met. This can be illustrated by means of the root-loci of figure 2.18.

The root-locus for the concept RA transfer function shows, unlike the concept AR root-locus, that the closed-loop poles can never be shifted further into the left half plane than the location of the zero pair. As the zeros do not meet the stability margin (2.56), the closed-loop poles of the concept RA transfer function will not meet this margin either.

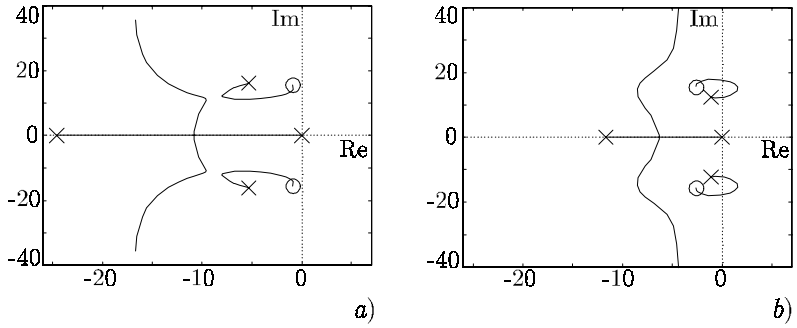

FIGURE 2.18 *Root-loci for a) concept AR and b) concept RA transfer functions*

Remark 2.7

The closed-loop systems discussed in this section contain an inner and an outer loop. However, a root-locus can only be drawn for a single loop. When we construct a root-locus, we construct it with a closed velocity loop. The actual locus now depends on the controller setting Ω_d*. In figure 2.18 the velocity loop is closed with* $\Omega_d = 0.9$*.*

Concept R
The feasible dimensionless controller settings for concept R are shown in figure 2.19 for a frequency ratio ρ of 0.1. The values for the damping parameters used in the simulations are: $\alpha = 0.01 \cdot \omega_r$ and $\zeta_r = 0.15$. The optimal dimensionless controller settings for concept R have been selected as $\Omega_p = 1.4$ and $\Omega_d = 0.45$. These are indicated in figure 2.19 by means of the cross hair.

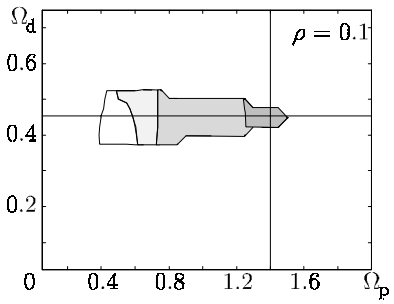

FIGURE 2.19 *Regions with feasible dimensionless parameters for concept R.*

Concept N
For concept N a similar phenomenon occurs as for concept RA. The stability margin (2.56) cannot be met and therefore, no feasible dimensionless controller settings exist. In figure 2.20 the root locus is drawn with $\Omega_d = 0.1$.

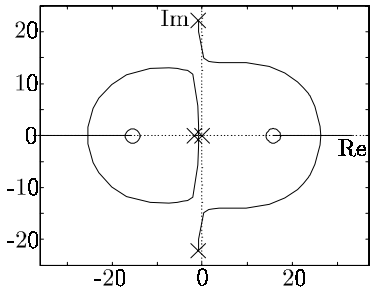

FIGURE 2.20 *Root locus of concept N*

The complex pole pair immediately enters the right half plane and the system becomes unstable. For larger values of Ω_d the complex pole pair is already located in the right half plane and the system is always unstable.

Concept AR-D
The feasible dimensionless controller settings for concept *AR-D* are shown in figure 2.21 for three different values of the frequency ratio ρ: 0.1, 0.5 and 0.75.

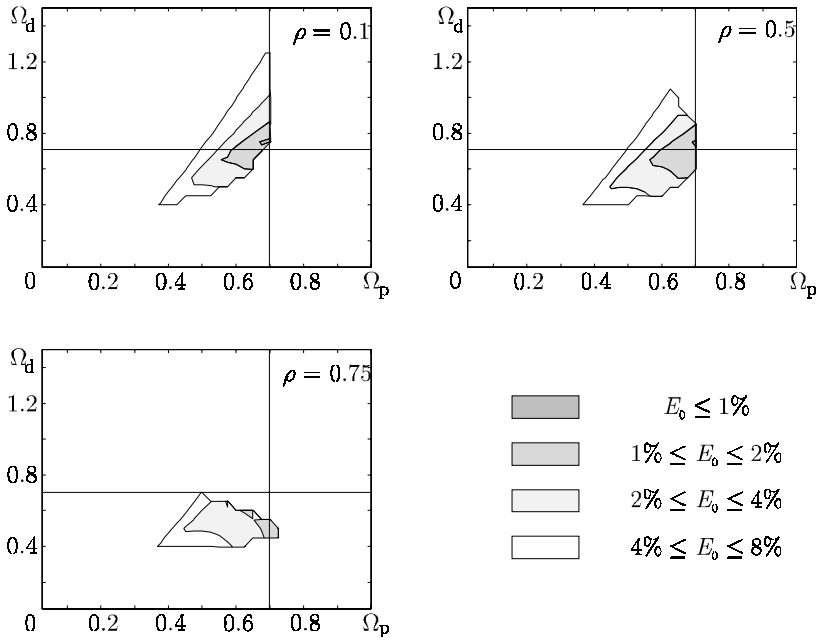

FIGURE 2.21 *Regions with feasible dimensionless parameters for concept AR-D with* $\rho = 0.1$, $\rho = 0.5$ *and* $\rho = 0.75$

The optimal dimensionless controller settings are $\Omega_p = 0.7$ and $\Omega_d = 0.7$.

Concept AR-RA
For concept *AR-RA* we have to consider two different frequency ratios, as we consider two different anti-resonance frequencies, *i.e.* ω_{ar} and ω_{ar^*}. The frequency ratio for ω_{ar^*} is defined similarly as (2.31):

$$\rho^* = \left(\frac{\omega_{ar^*}}{\omega_r}\right)^2 \tag{2.57}$$

The feasible controller settings are now determined for different combinations of two frequency ratios.

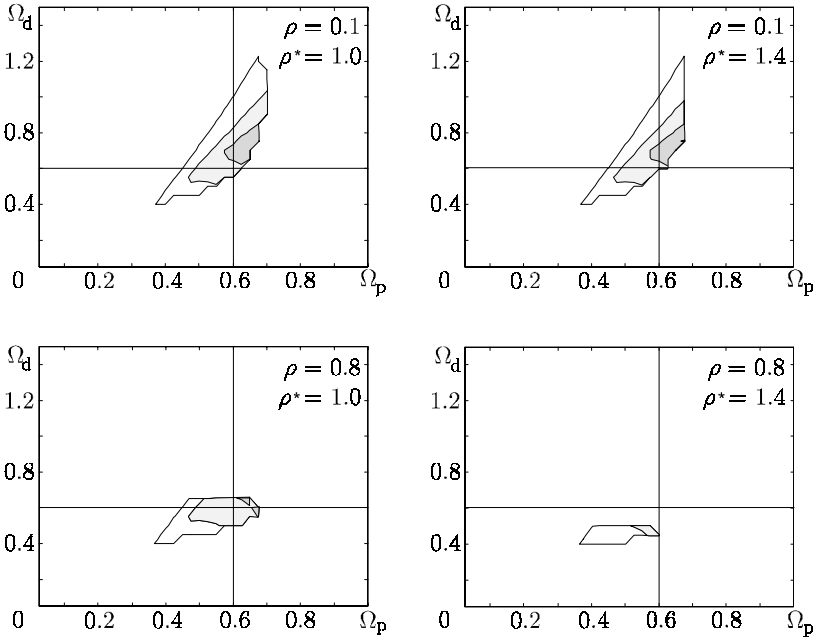

FIGURE 2.22 *Regions with feasible dimensionless parameters for concept AR-RA*

The optimal dimensionless controller settings are $\Omega_p = 0.6$ and $\Omega_d = 0.6$.

Concept AR-R
The feasible dimensionless controller settings for concept *AR-R* are shown in figure 2.23 for two different values of the frequency ratio ρ: 0.1 and 0.5. The selected optimal dimensionless controller settings are $\Omega_p = 0.6$ and $\Omega_d = 0.7$.

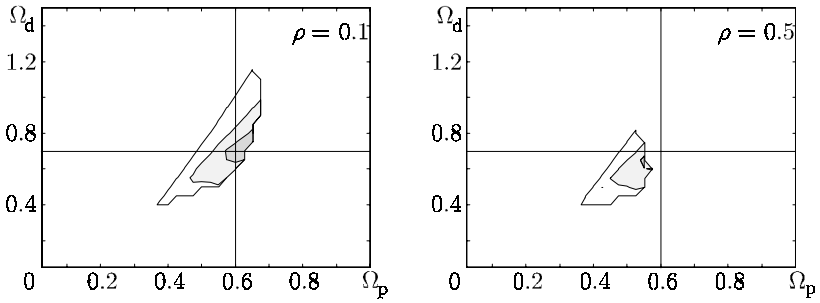

FIGURE 2.23 *Regions with feasible dimensionless parameters for concept AR-R with* $\rho = 0.1$ *and* $\rho = 0.5$

Concept AR-N

Similarly as for concept *AR-RA*, we have to consider two different frequency ratios for concept *AR-N*. A difference is that the frequency ratio ρ^* can now be smaller than 1, as the real zeros can be located closer to the origin than the complex pole pair. For different combinations of the frequency ratios we determine the feasible dimensionless controller settings.

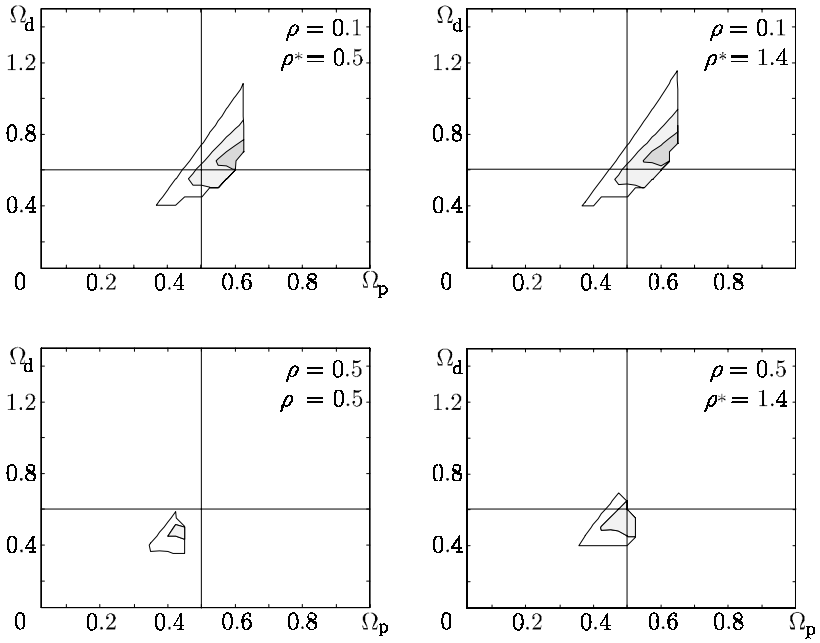

FIGURE 2.24 *Regions with feasible dimensionless parameters for concept AR-N*

The selected optimal dimensionless controller settings are $\Omega_p = 0.5$ and $\Omega_d = 0.6$.

In table 2.5 the conditions on the frequency ratios and the optimal dimensionless controller settings for all concepts are summarized.

Concept	Condition	Optimal setting	
		Ω_p	Ω_d
AR	$0.1 < \rho < 0.8$	0.8	0.9
D	-	0.9	0.9
RA	-	-	-
R	$0.1 < \rho < 0.12$	1.4	0.45
N	-	-	-
AR-D	$0.1 < \rho < 0.75$	0.7	0.7
AR-RA	$0.1 < \rho < 0.8$ $1.0 < \rho^* < 1.4$	0.6	0.6
AR-R	$0.1 < \rho < 0.5$	0.6	0.7
AR-N	$0.1 < \rho < 0.5$ $0.5 < \rho^* < 1.4$	0.5	0.6

TABLE 2.5 *Optimal dimensionless controller settings*

2.3.3 Dimensionless problem-plant relation

Using the dimensionless quantities and the optimal dimensionless controller settings, we can determine a relation between the specification, *i.e.* the desired motion of the end-effector, and the plant, which is independent of the particular problem setting. This relation is expressed in terms of the maximum relative positional error E_0 and the periodic ratio τ. We consider the dimensionless closed-loop transfer functions, *i.e.* the concepts described in the previous section, with the optimal dimensionless quantities of table 2.5. In numerous simulations the periodic ratio τ is varied, by applying different second-degree reference paths to the (optimal) closed-loop transfer functions. For all values of τ the relative positional error is calculated. The upper bound for second-degree reference paths can be expressed as (Groenhuis, 1991):

$$E_0 = \varepsilon \cdot \tau^2 \tag{2.58}$$

where ε is a constant that depends on the particular concept that is considered. We mainly consider the situations where the relative positional error is smaller than 1%, as this is generally required by modern electromechanical motion systems.

Concept AR
The relation between the relative positional error E_0 and the periodic ratio τ for concept AR is calculated for three different values of the frequency ratio ρ: 0.1, 0.5 and 0.8. During all simulations discussed in this section we use an anti-resonance frequency ω_{ar} of 1 [rad/s]. The values for the (dimensionless) damping used in each concept equal those of the previous section. In figure 2.25 the results of the simulations with a second-degree reference path are shown. The straight line indicates the estimated upper bound of the positional error. For $\tau < 0.4$ the constant ε in the expression for the upper bound (2.58) for concept AR equals 0.09.

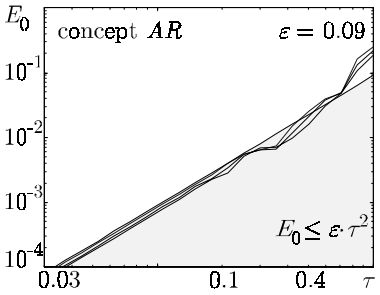

FIGURE 2.25 *The relative positional error as a function of the periodic ratio τ for concept AR and second-degree reference paths, using $\rho = 0.1$, $\rho = 0.5$ and $\rho = 0.8$*

Concept D
The relation between the relative positional error E_0 and the periodic ratio τ for concept D is shown in figure 2.26a. The constant ε in the expressions for the upper bounds of concept D equals 0.07.

Concept R
The results for concept R are shown in figure 2.26b for two values of the frequency ratio ρ: 0.1 and 0.12. The upper bound for a second-degree reference path is characterized by $\varepsilon = 0.06$.

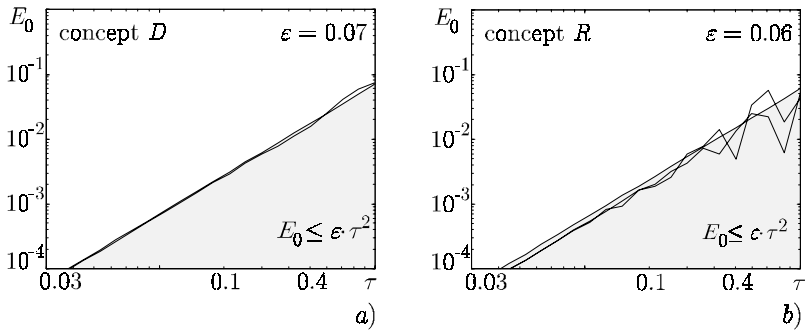

FIGURE 2.26 *The relative positional error as a function of the periodic ratio τ for a) concept D and for b) concept R using $\rho = 0.1$ and $\rho = 0.12$*

Concept AR-D

For concept *AR-D* simulations have been performed for a frequency ratio ρ of 0.1, 0.5 and 0.75. The results are shown in figure 2.27a. The upper bound for a second-degree reference path is characterized by $\varepsilon = 0.11$.

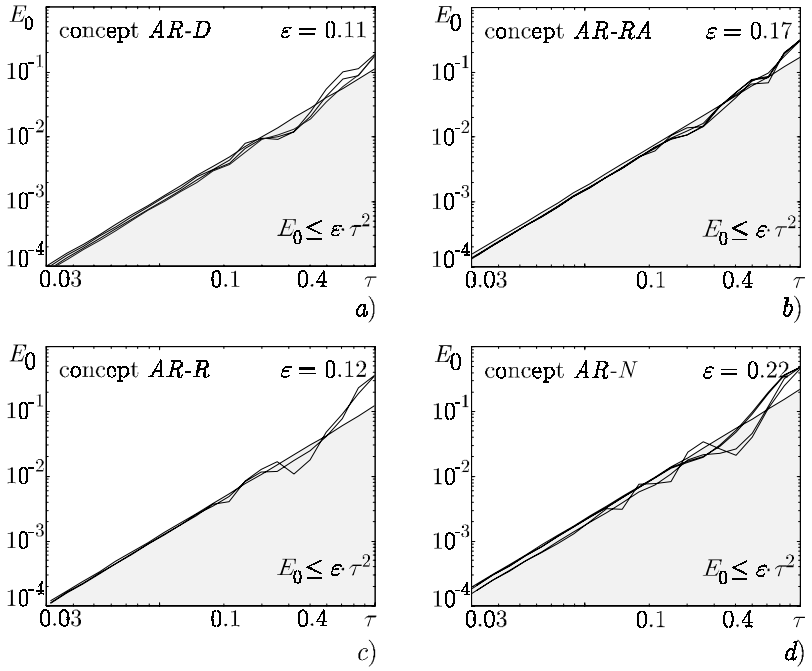

FIGURE 2.27 *The relative positional error as a function of the periodic ratio τ for a) concept AR-D, b) concept AR-RA, c) concept AR-R and d) concept AR-N.*

Concept AR-RA
The results for concept *AR-RA* are shown in figure 2.27b, for four different combinations of the two frequency ratios. The first frequency ratio ρ equals 0.1 or 0.8 and the second ratio ρ^* equals 1 or 1.4. The upper bound for a second-degree reference path is characterized by $\varepsilon = 0.17$.

Concept AR-R
For concept *AR-R* simulations are performed for a frequency ratio ρ of 0.1 and 0.5. The results are shown in figure 2.27c. The upper bound for a second-degree reference path is characterized by $\varepsilon = 0.12$.

Concept AR-N
Finally, the results for concept *AR-N* are shown in figure 2.27d, for four different combinations of the two frequency ratios. The first frequency ratio ρ equals 0.1 or 0.5 and the second ratio ρ^* equals 0.5 or 1.4. The upper bound for a second-degree reference path is characterized by $\varepsilon = 0.22$.

Instead of using a second-degree reference path, the designer may choose a third-degree reference path, *i.e.* a reference path with limited jerk. When the same simulations as above are performed, an upper bound for third-degree reference paths can also be determined. The upper bound is characterized by:

$$E_0 = \gamma \cdot \tau^3 \tag{2.59}$$

In table 2.6 the dimensionless problem-plant relations for all concepts are summarized for both second- and third-degree reference paths.

Concept	Condition	Performance constants	
		ε	γ
AR	$0.1 < \rho < 0.8$	0.09	0.35
D	-	0.07	0.21
R	$0.1 < \rho < 0.12$	0.06	0.06
AR-D	$0.1 < \rho < 0.75$	0.11	0.33
AR-RA	$0.1 < \rho < 0.8$ $1.0 < \rho^* < 1.4$	0.17	0.60
AR-R	$0.1 < \rho < 0.5$	0.12	0.40
AR-N	$0.1 < \rho < 0.5$ $0.5 < \rho^* < 1.4$	0.22	0.60

TABLE 2.6 *Dimensionless problem-plant relations*

2.3.4 Application of assessment method

So far, we have determined (dimensionless) relations between the attainable performance, the reference path and the plant, which are independent of the particular problem setting. Together with the optimal dimensionless controller settings, we use these relations to formulate an assessment method that can be used in various ways, depending upon the specific design context. The three crucial design parameters are the periodic ratio τ, the anti-resonance frequency ω_{ar} and the relative servo error E_0. Once two of these three design parameters are chosen, the third will follow automatically. If the frequency ratio ρ lies between it's lower and upper bound given in table 2.5, the optimal controller settings can be found, such that the controlled system fulfills all specifications. This is visualized in figure 2.28.

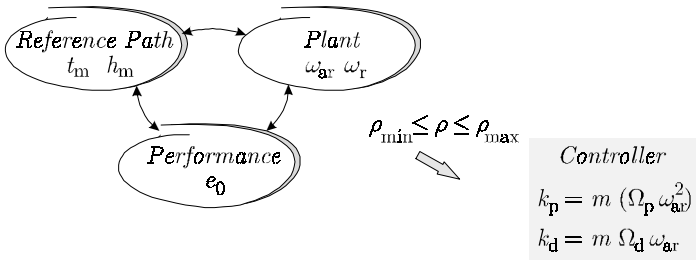

FIGURE 2.28 *Application of assessment method*

Design procedure 2.1 Assessment method

1. *Determine the class of electromechanical motion systems that is at hand.*
2. *Determine the concept that is at hand, by looking at the location of the position and velocity sensor. Refer to table 2.5 to verify whether optimal dimensionless controller settings can validly be applied.*
3. *Depending on the situation perform one of the following three alternatives:*
   a) When the reference path and the desired performance are fixed, calculate the periodic ratio τ, using table 2.6 and:

   $$\tau = \sqrt{\frac{E_0}{\varepsilon}} \quad \text{or} \quad \tau = \sqrt[3]{\frac{E_0}{\gamma}}$$

   Determine the minimum required anti-resonance frequency of the plant with:

   $$\omega_{\mathrm{ar,\,req}} = \frac{2\pi}{\tau t_{\mathrm{m}}}$$

This value can be used to calculate the required (dominant) stiffness of a particular plant, as well as the resonance frequency ω_r, in case the mass distribution is assumed to be fixed.

b) When the reference path and the anti-resonance frequency of the plant are known, calculate τ according to:

$$\tau = \frac{2\pi}{\omega_{ar}\, t_m}$$

and determine the attainable performance, using table 2.6 and:

$$E_0 = \varepsilon \cdot \tau^2 \;\; or \;\; E_0 = \gamma \cdot \tau^3$$

c) When the desired performance and the anti-resonance frequency of the plant are known, calculate τ as a function of the motion distance h_m using table 2.6 and:

$$\tau = \sqrt{\frac{e_0}{\varepsilon \cdot h_m}} \;\text{ or }\; \tau = \sqrt[3]{\frac{e_0}{\gamma \cdot h_m}}$$

Next, determine the reference path, by finding a trade-off between the motion distance h_m and the motion time t_m that fulfills the equality:

$$\sqrt{\frac{e_0}{\varepsilon \cdot h_m}} = \frac{2\pi}{\omega_{ar} t_m}$$

4. When the frequency ratio ρ fulfills the requirements of table 2.5, the control system for a particular problem setting and a particular controller configuration can be implemented by:

$$k_p = m \cdot (\Omega_p \cdot \omega_{ar})^2 \text{ and } k_d = m \cdot \Omega_d \cdot \omega_{ar}$$

2.4 Model simplification algorithm

2.4.1 The need for simplification

Component-based modeling is a convenient way for the designer to build a model of the dynamic behavior of an electromechanical plant. This can be done efficiently when a library of reusable component models is provided (Breunese *et al.*, 1998). However, connecting standard component models will generally result in a plant model that it is difficult to analyze and comprehend, due to a high order, dependency among elements and a redundant structure. In the final model, only

the phenomena relevant for the problem addressed should be included. Therefore, systematic methods must be employed to remove superfluous modeling elements and structure (Rinderle and Subramaniam, 1991). We will use bond graphs to describe the plant models, because simplification rules have been formally described and bond graphs are applicable in any energetic domain.

Simplification will transform the representation of the model without changing the contents of the underlying mathematical descriptions. In order to avoid laborious and error prone model simplification, automation is preferred, which requires that all simplification rules have to be described explicitly and ordered appropriately. During simplification, the relations between the parameters of the simplified and the original plant model have to be preserved (statement 2.2).

The algorithm that will be described is only applicable to a particular class of bond graph models (Van Lochem, 1997), *i.e.* models that are tree-like compositions of linear single-port elements, junctions, sources and non-modulated transmissions. This class does not contain bond loops as in figure 2.29, because transmissions cannot be removed from these loops.

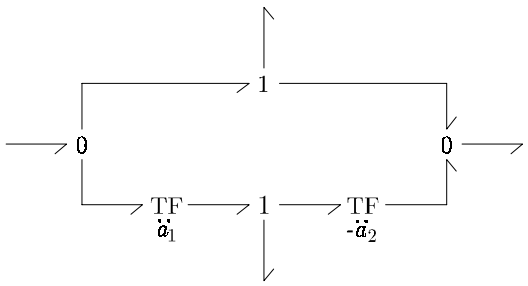

FIGURE 2.29 *Transmission in bond graph loop*

Generally, the models of the electromechanical motion systems considered in this thesis comply with these criteria. Exceptions are those models than contain a flexible guidance, as discussed in section 2.2.2.

Definition 2.3 Model simplification problem

Given a bond graph model of an electromechanical plant that complies with the criteria mentioned above, automatically simplify this model to a model without transmissions, dissipative elements and dependent storage elements, and without redundancy in the junction structure.

2.4.2 Bond graph simplification rules

Before the simplification algorithm will be described, some well-known simplification rules for model transformations will be summarized, as these play a special role in this context. For other bond graph simplifications rules we refer to (Breedveld and van Amerongen, 1994).

Transmissions
The two types of transmissions that are considered are the transformer (*TF*) and the gyrator (*GY*). A transmission can be eliminated from a model by joining it with a storage element or a source. Some examples are shown in figure 2.30. The parameter value and the type of storage element may change due to this simplification, as well as the source type and its modulation factor. The factor k indicates the transformation ratio of a variable of a particular bond graph element. Initially this factor equals one, but due to transformations of an element this factor will be changed.

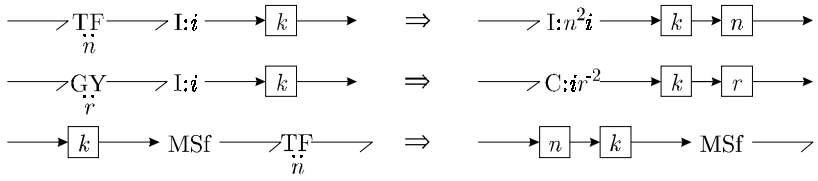

FIGURE 2.30 *Elimination of transmissions*

Two transmissions connected by one bond can be replaced by one transmission (Breedveld, 1984b). This simplification is carried out by first determining the type of the new transmission and calculating the new expression for the parameter value. Next, one transmission is eliminated and the other is replaced by the new transmission. The four possible combinations are shown in figure 2.31.

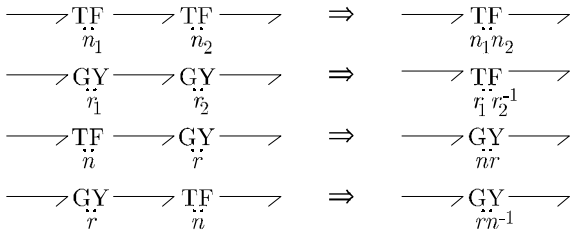

FIGURE 2.31 *Joining of transmissions*

Finally, transmissions can be propagated across junctions (Breedveld, 1984a), as shown in figure 2.32.

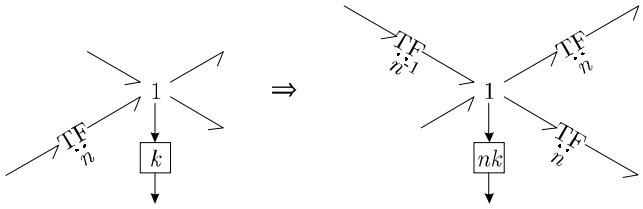

FIGURE 2.32 *Propagation of a transmission*

2.4.3 The simplification algorithm

These simplification rules will now be captured in an algorithm that fulfills the requirements of statement 2.2. The algorithm has been implemented in the mechatronic design environment 20-sim (Controllab Products, 2000). Bond graph storage elements, junctions and sources are extended with a special factor k, already introduced in the previous section. Storage elements and junctions contain a signal port through which a variable can be obtained for purposes of display or control. From a 1-junction the flow signal can be obtained, from a 0-junction the effort signal and from a storage element the state. Modulated sources contain a signal port through which a signal can be provided that modulates a flow or an effort. Both types of signals will be multiplied with the factor k that initially equals 1.

When transmissions are propagated through the model, signals and parameters will be transformed. When for example the motor inertia is transformed, the motor velocity is probably transformed as well, thus creating a virtual motor velocity. The factor k of the 1-junction representing the motor velocity will be *divided* by the transformation factor. The actual motor velocity can thus be obtained by multiplying the virtual motor velocity with the new value of the factor k. In this way the simplified model can be related to the original model. Original input and output variables will be preserved, such that a controller designed for the simplified model can be connected to the original model without alterations.

As design specifications are generally given in terms of the position of the end-effector, it is convenient to use the coordinates of the end-effector as a reference in the simplified plant model. Therefore, transmissions will be propagated away from this reference point. Use is being made of an existing propagation machine (Breunese, 1996).

After application of the algorithm to models of electromechanical motion systems, it should be possible to compare the relevance of masses and stiffnesses, as these are expressed in unambiguous coordinates. The designer can for example determine

that a particular stiffness is very large with respect to other stiffnesses and therefore not relevant for the dominant dynamic behavior.

When we remind remark 2.1 and the assessment method described in the previous section, we note that friction and damping are not considered. Therefore, the simplification incorporates the removal of dissipative elements. The consecutive steps of the algorithm are described below.

Design procedure 2.2 Simplification algorithm

1. *Remove dissipative elements.*
2. *Determine the direction of propagation for the transmissions, away from the end-effector, and assign this direction to all bonds.*
3. *Simplify the junction structure by removal of dangling junctions, joining of neighboring junctions and elimination of double differences.*
4. *Eliminate dependent storage elements.*
5. *Join neighboring transmissions.*
6. *Join transmissions with neighboring storage elements and sources.*
7. *Propagate transmissions through the graph according to the indicated direction of propagation.*
8. *Repeat the steps 3 to 7 until no action can be performed in anymore.*

The bond graph model has now either been simplified according the requirements of statement 2.2, or the bond graph model is not a member of the class of models considered here.

2.5 Model reduction algorithm

The simplified model of the electromechanical plant is generally not in the form of a standard plant model required by the assessment method. A standard fourth-order model only contains the lowest mode of vibration, while a simplified model may contain several modes as it may be of higher order. To convert a simplified model to the standard form, a model reduction method is required. In literature, various systematical methods for model reduction have been described. A common method used for mechanical systems is modal truncation (Skelton and Hughes, 1980; Rankers, 1997). When a state-space system is written in Jordan form, the states can be ordered such that the eigenvalues are located on the diagonal of the system matrix in increasing order, *i.e.* from the lowest to the highest vibration

mode. When the model is truncated, only the higher modes are removed. The advantage is that the poles of the reduced model are a subset of the poles of the original model. A comparison between different reduction methods is presented in (Decoster and van Cauwenberghe, 1976a; Decoster and van Cauwenberghe, 1976b) and (Wortelboer, 1994).

Isaksson and Graebe (1993) state that good control requires a model that approximates the magnitude of the frequency response of the plant $P(j\omega)$, starting at lower frequencies and continuing to the highest possible bandwidth. In our situation we want to reduce the model before applying the assessment method. The appeal of the assessment method lies in its simplicity and its mechatronic character. Therefore, an explicit requirement of a model reduction method is that it preserves the physical interpretation of the model.

Definition 2.4 Model reduction problem

Given a successfully simplified bond graph model of an electromechanical motion system, automatically reduce this model to a standard plant, while preserving physical interpretation and maintaining the possibility to apply the controller that has been designed for the reduced model, to the original model.

2.5.1 Model reduction for assessment method

There are two physical properties of a plant model that have to be preserved after model reduction:

1. *The total mass that has to be moved.* This can be seen from the expression for the controller settings (design procedure 2.1), where both controller parameters in the position and the velocity loop are proportional with the total mass. If the total mass is changed, the values for the controller settings will be different and, as a consequence, the controller applied to the original model or the real-world plant will not work according to expectation.
2. *The location of the stiffness that results in the lowest mode of vibration.* When this location is preserved, it can be determined to which class of electromechanical motion systems the plant belongs. As a result, the types of transfer function from input force F to motor position and end-effector position are known. When the outcome of the assessment method is that a desired performance cannot be met with a certain model, the location of the stiffness gives an indication for the mechanical subsystem(s) that should be altered.

Existing reduction methods result in mathematical models, in which the physical interpretation of the lowest vibration mode is lost (property 2). Therefore, we present a simple reduction method that fulfills these criteria.

For model reduction, we consider the transfer function from the input force to the position of the motor, when appropriate with respect to the frame. This transfer function $P(s)$ always consists of a series of anti-resonance resonance pairs, independent of the type of standard plant that will result. The advantage is that the reduced transfer function is always of type AR. The frequency response $P(j\omega)$ can be automatically calculated from a bond graph model. Next, it has to be determined which stiffness in the physical model results in the lowest mode of vibration. Once the dominant stiffness is determined, the other stiffnesses can be removed from the model and the model can be simplified, using the algorithm from section 2.4.3. The result will be a plant model in one of the standard forms of section 2.2.2.

This simple reduction method will be illustrated by means of the bond graph model of figure 2.33 that represents a general electromechanical motion system. Four different situations will be considered, each with the dominant stiffness located in a different mechanical subsystem.

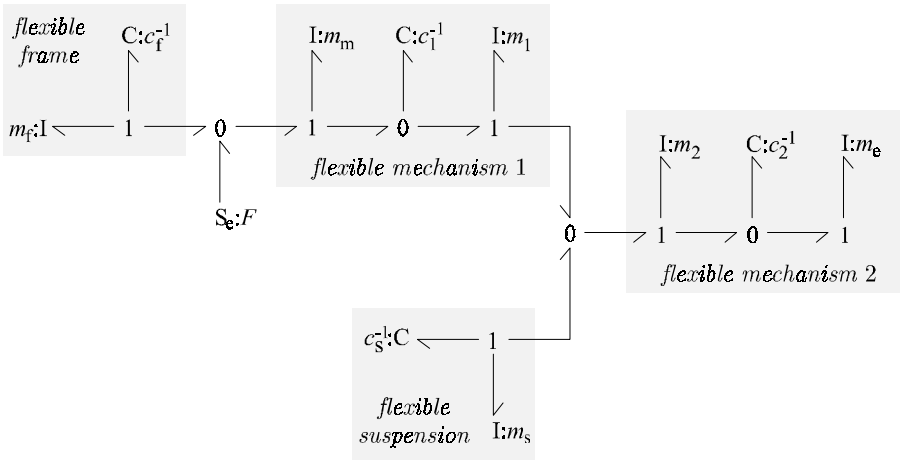

FIGURE 2.33 *Generalized higher-order motion system*

The values of the masses are $m_f = 10$ [kg], $m_m = 1$ [kg], $m_1 = 1$ [kg], $m_2 = 2$ [kg], $m_s = 10$ [kg] and $m_e = 2$ [kg]. In table 2.7 four situations are presented. The columns indicate the resulting standard plant. For each situation the values of the stiffnesses in the model are given, as well as the dominant (anti-) resonance frequencies for the original and reduced model. The dominant stiffness in each situation is underlined. Next, the positional error for the original and reduced model are given. The errors correspond to a second-degree reference path with $t_m = 1$ [s] and $h_m = 1$ [m].

		Flexible frame	Flexible mechanism 1	Flexible mechanism 2	Flexible actuator suspension
c_f	[N/m]	$\underline{1.0 \cdot 10^6}$	$2.0 \cdot 10^7$	$2.0 \cdot 10^7$	$2.0 \cdot 10^7$
c_s	[N/m]	$5.0 \cdot 10^6$	$5.0 \cdot 10^6$	$5.0 \cdot 10^6$	$\underline{1.25 \cdot 10^6}$
c_1	[N/m]	$5.0 \cdot 10^6$	$\underline{2.5 \cdot 10^5}$	$5.0 \cdot 10^6$	$5.0 \cdot 10^6$
c_2	[N/m]	$5.0 \cdot 10^5$	$5.0 \cdot 10^5$	$\underline{1.25 \cdot 10^5}$	$5.0 \cdot 10^5$
original model					
ω_{ar}	[rad/s]	254	271	341	304
ω_r	[rad/s]	316	425	392	333
e_0	[m]	$6.64 \cdot 10^{-5}$	$1.01 \cdot 10^{-4}$	$5.15 \cdot 10^{-6}$	$3.8 \cdot 10^{-5}$
reduced model					
ω_{ar}	[rad/s]	250	250	353	310
ω_r	[rad/s]	316	433	387	330
e_0	[m]	$5.69 \cdot 10^{-5}$	$0.90 \cdot 10^{-4}$	$4.50 \cdot 10^{-6}$	$3.2 \cdot 10^{-5}$

TABLE 2.7 *Result of model reduction*

It can be seen that the (anti-) resonance frequency of the original and the reduced model correspond reasonably well. This also holds for the positional error obtained with the reduced model in comparison to the error obtained with the original model.

Remark 2.8

Model reduction to fourth order has to be performed with care in case the second mode of vibration is situated close to the first mode, as this may result in an unstable closed-loop system. A factor 3 is generally sufficient for the relative distance between these modes. When this factor is smaller, the second vibration mode should have sufficient physical damping.

2.5.2 The reduction algorithm

The approach described in the previous sub-section is summarized in a step-wise procedure:

Design procedure 2.3 Model reduction

This procedure is applicable to models that have been simplified by design procedure 2.2.

1. *Determine the two lowest modes of vibration in the transfer function from the input force to the position of the actuator.*
2. *Check whether the second mode of vibration is situated closer to the first mode than a factor 3. If so, give a warning.*
3. *Determine which stiffness in the model results in the lowest mode of vibration.*
4. *Determine in which mechanical subsystem this dominant stiffness is located.*
5. *Remove all other stiffnesses from the model and simplify the model.*
6. *Determine which class of electromechanical motion system is at hand.*

2.6 Automated performance assessment

The assessment method can be applied in several ways, as indicated by design procedure 2.1 and figure 2.28. This flexibility is both an advantage and a disadvantage of the method. It allows for a true mechatronic design approach, but it does not provide transparent insight in the dependencies between different design parameters. However, these dependencies are a key factor for successful application of the method. By means of computer-based support this problem can be overcome, when it is focused on the implementation of the relations between different design parameters. A change in one design parameter should immediately be reflected in other design parameters. If for example a smaller positional error is required, then either a larger motion time t_{m}, or an increase of the dominant stiffness of the plant should be presented as solutions.

2.6.1 Constraints satisfaction

Dependencies can be compared quite natural to *constraints*. Ullman (1997) describes a possible view upon the design process as: "when a new problem is begun, the design requirements effectively *constrain* the possible solutions to a subset of all possible product designs". The assessment method indicates that the relative positional error E_0 and motion time t_{m} constrain the dominant stiffness of

the plant (possible product designs). Besides design requirements, laws of nature also constrain possible designs.

In object-oriented programming constraints are considered to be functional relationships between entities of an object model (Rumbaugh *et al.*, 1991). These relationships must be maintained during the design process, such that a change in one property results in a corresponding change in dependent properties of other objects. This process is called *propagation*. Implementation of the dependencies in computer support can actually be done by such constraints. Technical details about these constraints and propagation are explained in (De Vries *et al.*, 1997).

As propagation will at any time satisfy the dependencies between reference path, plant and performance, an appropriate controller can always be determined, under the condition that the frequency ratio lies between its lower and upper bound (figure 2.28). The exact values of the controller settings depend on properties of the plant, such as the total mass to be moved and the lowest mode of vibration. Relations between plant and controller can also be implemented by means of constraints, such that a valid controller and thus a controlled-system that fulfills all specifications always exist, although the plant may obtain unrealistic parameter values.

As the constraints can be solved in several directions, the causal relations between constraint variables are not fixed. Therefore, bi-directional arrows between constraints and constraint variables are used here after. Blocks, which contain the equation the constraint is based on, represent constraints. The following objects can be recognized in the design process of electromechanical motion systems that have properties that play a role in the constraint system:

Plant
Design parameters related to the plant are the total mass m, the anti-resonance frequency ω_{ar}, the resonance frequency ω_r and the frequency ratio ρ. These depend on physical properties of the plant, *i.e.* the mass contribution and the dominant stiffness. This dependency is different for each class of motion systems, as indicated in section 2.2.2. Design parameters and physical parameters are implemented as constraint variables. The relations between these constraint variables have to be maintained during the design process and will therefore be implemented by constraints. If, for example in the flexible mechanism, a larger end-effector mass occurs due to a change in the specifications, this will be propagated to either a higher stiffness or a lower anti-resonance frequency, such as in figure 2.34.

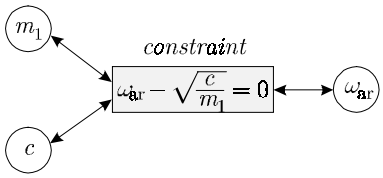

FIGURE 2.34 *Example of plant constraint*

Specifications and performance
The specifications consist of the parameters for the motion time t_m and for the motion distance h_m. The absolute maximal positional error e_0 can be considered as a part of the specifications and of the performance, as it is a predicted value. The main dependencies between plant, reference path and performance (figure 2.28) can be implemented by only two constraints, as the third dependency is redundant. In figure 2.35 an illustration of the working principle of these two main constraints is given. It indicates how a change of the motion time t_m or anti-resonance frequency ω_{ar} may affect the maximal relative positional error E_0, when using a second-degree reference path.

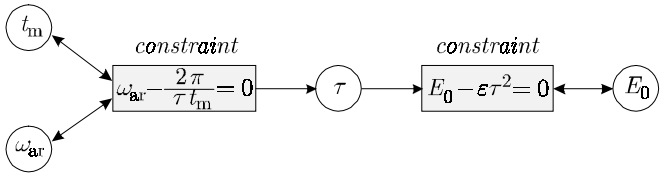

FIGURE 2.35 *Main constraints in the assessment method*

Controller
The two parameters of the controller can at any time be determined on basis of the dimensionless quantities and the plant parameters. Constraints can be made using the equations for the proportional action in the position loop k_p and the velocity loop k_d. The dimensionless controller setting have a fixed value for a particular concept and the other variables are already existing in the constraint system.

2.6.2 Computer support

The mechatronic design environment 20-sim (Controllab Products, 2000) supports conceptual mechatronic design from a modeling perspective. The assessment method is implemented as a design tool in the 20-sim environment, using a centralized propagation technique and a constraint solver as described in (De Vries *et al.*, 1997).

Model of the system under design
The underlying plant model of the design tool is a linear fourth-order state-space description. The elements of the matrices depend on the physical parameters in the plant model. The constraint variables can be considered "pointers" to these parameters in the state-space description. If a constraint variable changes, the state-space description is automatically updated. Also a model of the reference path generator and the controller exist that have a similar connection to the constraint variables describing these phenomena. At any stage in the design process the underlying models correspond to the situation in the constraint system, such that a valid mathematical description of all sub-systems of the design exists.

Representation of design parameters
To provide better "look and feel", the design parameters are presented together with a corresponding representation. The plant model of a flexible mechanism with the physical parameters motor mass, end-effector mass and dominant stiffness are shown together with an iconic diagram in figure 2.36.

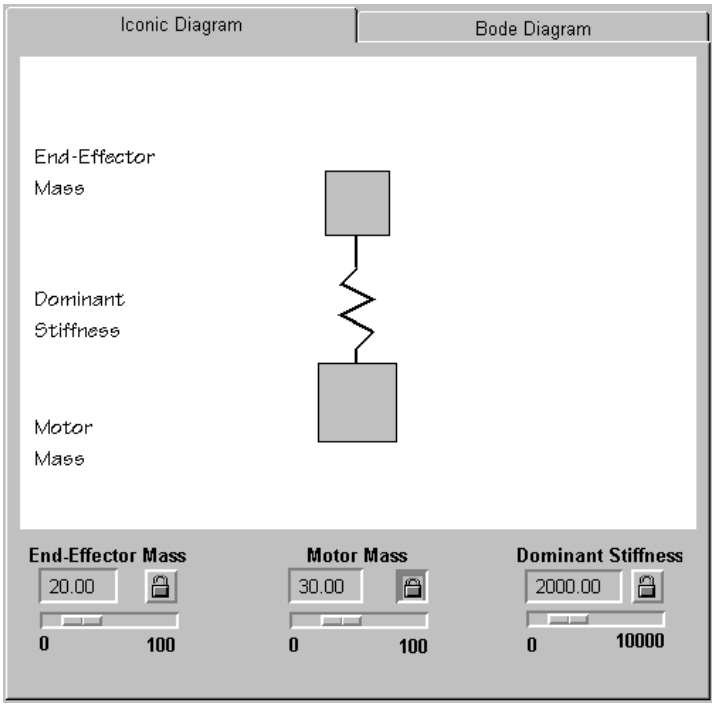

FIGURE 2.36 *Iconic diagram with corresponding design parameters*

A physical parameter is related to its representation by a constraint, such that a larger mass results in a larger mass icon. Similarly, an increase in the dominant

stiffness will result in a smaller stiffness icon. The iconic diagram will provide the designer with a feeling of the behavior of the system to be controlled. Looking at an iconic diagram with for example a large end-effector mass and a small stiffness intuitively shows that it is difficult to control fast motions of the end-effector.

Multiple view is offered on the system under design. The lowest vibration mode and the frequency ratio are shown in a Bode diagram of the open-loop system. A closed-loop Bode diagram shows the attainable bandwidth ω_b. The reference path and an indication of the response are shown in a time plot. The design parameters related to this diagram are the motion time, motion distance and the absolute positional error. Again the representation is related to the values of the underlying design parameters by means of constraints.

Functionality
There exist many dependencies in the systems that are all implemented by means of constraints. A change of one parameter can result in a change of many other parameters. Therefore, the possibility to fix a design parameter is provided by a "lock" as indicated in figure 2.36. Once a design parameter has a desired value it can be fixed, such that the constraint system cannot change it anymore.

Remark 2.9

A prototype of the design tool has been realized for the flexible mechanism.

2.7 Conclusions

The aim of conceptual design is to obtain a feasible design for the reference path generator, control system and electromechanical plant with appropriate sensor locations, in an integrated way. For transient systems, *i.e.* positioning systems, this has been worked out.

First we described standard problems, by means of a classification of four electromechanical motion systems. These *classes* use standard fourth-order plant transfer functions, which are referred to as *types*. Dimensionless quantities are used to characterize closed-loop behavior, *i.e.* reference path generator, controller and plant. Again several standard closed-loop transfer functions have been defined, which are referred to as *concepts*.

For these standard problems we have determined standard solutions. Relations between the dimensionless quantities of the reference path, controller and plant have been obtained heuristically by means of numerous simulations. These relations

can now be used in an *assessment method*, which considers functional interaction between domain specific subsystems and considers consequences of solutions and alternative solutions in other domains.

Interactive computer-based support is developed for conceptual design of electromechanical motion systems, using constraints, such that it:

- supports the complete conceptual design stage;
- supplies design automatons for fast and correct model simplification and order reduction, while maintaining physical plant parameter interpretation;
- provides transparency in the relations between different design parameters;
- supports application of the assessment method in an explorational design mode, as local design goals can easily be changed, while information after a change is preserved;
- puts emphasis on the interpretation of the results instead of the application of procedures.

The principal benefits of the assessment method and the computer support are that they quickly provide insight in the design problem and that feasible goals and required design efforts can be estimated at an early stage.

3 Detailed design

3.1 Introduction

After conceptual design, the design process will proceed towards a design proposal that is to be the guideline for prototyping. The character of the design problem at hand will gradually change. During detailed design, we need to incorporate the fact that "the real underlying problem in engineering control system design invariably involves the on-line feedback control of an uncertain, usually nonlinear, physical process. ... The engineer usually likes to work with, and benefits from, a systematic approach to the design problem; such systematic approaches are often the outcome of past design experience" (Athans, 1971). The systematic design approach should contain a well-balanced trade-off between the theoretical need for generality and the practical quest for domain specific solutions (Konda *et al.*, 1992).

Taking into account these considerations, we will develop a transparent and structured design method for electromechanical motion systems, using the outcome of past design experience. Problems that such a design method should address are that:

1. the plant model is only partially known;
2. control theory is method-oriented and not problem-oriented;
3. the control system evolves with the plant model.

Ad 1
After conceptual design, the design proposal will contain a simple model of the electromechanical plant. When the design process is continued, modeling and experimentation is used to gain more insight in the structure and properties of this subsystem. Phenomena will be incorporated in the plant model, which did not appear in the simple models of conceptual design, such as nonlinear friction and disturbances. Gradually, the plant models will evolve towards more detailed models, such that they better represent the real-world behavior.

Remark 3.1

We assume that a complete realized plant is not yet available due to the mechatronic design approach, thus no information can be obtained through measurements and system identification.

Several models of the electromechanical plant may be used that suit different purposes, such as (Oelen, 1995):

- Determination of the control system, *i.e.* determination of the controller structure and choice of parameters. These models should give a good approximation of the dominant properties of the system to be controlled.
- Evaluation of the control system. Effects present in the real plant should be present in the model. However, the predictions of the momentaneous values of the variables in the model do not need to match the exact value of the corresponding variables of the real plant, *i.e.* the model should provide qualitative accuracy. *E.g.*, if the plant has high-frequency poles, then these should be incorporated in the model, but the damping of these high-frequency vibrations does not have to match the damping of the corresponding vibrations in the real plant.
- Incorporation in the control system. A plant model may be incorporated in the control system, such as in observers, feedforward components or linearizing feedback. In these models a trade-off has to be made between computational cost and quantitative accuracy.

Ad 2
The *technical specification* for a controlled electromechanical motion system will contain a description of the task it has to perform. This task is generally specified in terms of time and space. During conceptual design we partially dealt with this problem, as the assessment method can directly deal with the task description. Most controller design methods used in detailed design require *design specifications* for performance, stability, disturbance attenuation and robustness, which generally have to be expressed in abstract terms, such as cost criteria, desired frequency responses, weighting functions or desired locations of the closed-loop poles. The designer somehow has to convert the task description into an appropriate design specification, something that is not always straightforward.

During modeling of electromechanical plants, several unfavorable effects will be incorporated that have to be dealt with by the control system. Examples are friction, geometric nonlinearities, uncertain physical parameters and actuator saturation. However, controller design methods often cannot deal with these problems explicitly. This is due to the fact that control theory is method-oriented, while the designer works problem-oriented. Design methods can cope with plant problems that are defined in more abstract terms, such as unstructured uncertainty and input disturbance. Again the designer is forced to convert the descriptions. "The success of the design process often hinges on the capability of the engineer to

understand the physics of the problem and his ability to translate physical requirements and constraints into mathematical language" (Athans, 1971). This process is referred to as *modeling the disturbances* (Steinbuch and Norg, 1998).

Ad 3
It has been mentioned that plant models evolve during the design process. In an integrated design approach like mechatronics, it is required that the controlled system is evaluated as a whole. Thus the control system will need to evolve along with the plant model. The controller proposed during conceptual design has to be evaluated and possibly modified at several occasions. Ideally, this is done in close relation with the physics of the plant model, such that the influence of the control system can be related to the properties of the plant, *i.e.*, the mechatronic approach can be maintained.

Considering the problems summarized above, we define the detailed design problem as:

Definition 3.1 Detailed design problem

Formulate a transparent and structured design method that, given a successful conceptual design, supports the (evolutionary) design of a control system that achieves:
- *performance*
- *robust stability*
- *disturbance attenuation*
- *robustness for model uncertainties,*

while assuring that these are maintained when the design is materialized.

During conceptual design, several design proposals will generally have been evaluated and those that promise to be successful will be taken into the detailed design stage. During detailed design, we assume several properties of the electromechanical plant to be unalterable, *i.e.*:
- task specifications
- location of the sensor(s)
- approximate location of the lowest mode of vibration

Also the reference path, *e.g.* second- or third-degree path, chosen during conceptual design, will generally be unaltered. However, in some situations an exception will be made, as discussed in section 3.4.

In section 3.2 we will discuss an existing design philosophy and we will explain how it can be used to come to a structured design method. We will introduce a control configuration that we will use throughout this chapter. In section 3.3 we will derive a design procedure for the feedback component in this configuration. Some design issues for the so-called open-loop forcing function, the feedforward component and

reference path generator are discussed in section 3.4. A design procedure for the disturbance observer in the control configuration is derived in section 3.5. To support the structured design method, we provide a library of components and templates in the mechatronic design environment 20-sim. The ideas behind this library are described in section 3.6. Finally, in section 3.7, we evaluate the structured design method and we draw conclusions.

3.2 Controller design philosophy

The detailed design problem (definition 3.1) makes clear that a control system has to achieve several objectives. We will discuss the design of a control system that is built from a combination of different components. However, the actual design of these components is not straightforward, as they cannot be designed independently. In order to properly deal with this, we need to take a closer look at the interaction of the components. A similar problem, in the use of Linear-Quadratic-Gaussian (LQG) control, motivated Athans (1971) to describe a design philosophy, consisting of three basic steps:

1. Deterministic ideal response analysis and design.
2. Stochastic estimation analysis and design.
3. Stochastic feedback control system design.

This philosophy has been rewritten and extended with new insights in classical control theory by De Roover (1997). We will use this philosophy to come to a structured design procedure for detailed control system design.

3.2.1 Controller design philosophy

First we will summarize the design philosophy formulated by De Roover (1997). Here, we will omit the first step, *i.e.* modeling the plant, the disturbances and the specifications, as we focus on control system design. In section 3.5 we come back to the issue of disturbance modeling. Modeling the specifications is discussed in chapter 2 and in section 4.5.

Deterministic ideal response synthesis

Consider the case that there are no disturbances acting on the plant and that there are no model uncertainties. When the plant model is a lumped LTI system, it can be described as:

$$\mathcal{P}_{\text{id}}: \quad \begin{aligned} \dot{x}(t) &= Ax(t) + Bu(t), \quad x(0) = x_0 \\ y(t) &= Cx(t) + Du(t) \end{aligned} \tag{3.1}$$

The model $\mathcal{P}_{\text{id}}$ uniquely describes how the states $x(t)$ and the output $y(t)$ respond to any input $u(t)$. We assume that the task of the controlled system is described by an ideal deterministic output time function $y_{\text{id}}(t)$. The goal is to determine the ideal deterministic input time function, denoted $u_{\text{id}}(t)$, which results in the ideal deterministic state trajectory $x_{\text{id}}(t)$ and thus in the desired ideal deterministic output time function $y_{\text{id}}(t)$. The term *ideal* means "in the best possible way", *i.e.* the ideal output $y_{\text{id}}(t)$ should be a *realistic* output motion and not a hypothetical output motion. The computed ideal responses should incorporate any available knowledge of the performance limiting properties of the physical plant, *e.g.* dynamic effects or actuator saturation.

Robust regulation and nominal tracking

Once the ideal responses are known, we consider the actual plant $\mathcal{P}$, where we have to deal with disturbance w and model uncertainties. The actual output of this plant will deviate from the ideal one. This deviation is:

$$\delta y(t) = y(t) - y_{\text{id}}(t) \tag{3.2}$$

When the actual output has to follow the ideal output as close as possible, a control correction $\delta u(t)$ is needed in addition to the ideal input $u_{\text{id}}(t)$, in order to compensate for this deviation:

$$u(t) = u_{\text{id}}(t) + \delta u(t) \tag{3.3}$$

The computation of $\delta u(t)$ on basis of the measured deviation $\delta y(t)$ is referred to as *robust regulation*, as the output is regulated around its ideal value. The dynamic system that performs this regulation is the feedback compensator $\mathcal{C}$, for which three tasks have been identified:

- stabilization of the control system;
- suppression of disturbance signals;
- reduction of the effects of model uncertainty.

By separating the controller in a deterministic ideal part and an uncertain part, tracking ideal time functions is separated from robust regulation. The interconnection of the two is shown in figure 3.1. Exact tracking is only obtained in the nominal case where the actual plant $\mathcal{P}$ equals the ideal plant $\mathcal{P}_{\text{id}}$, therefore *nominal tracking* is achieved.

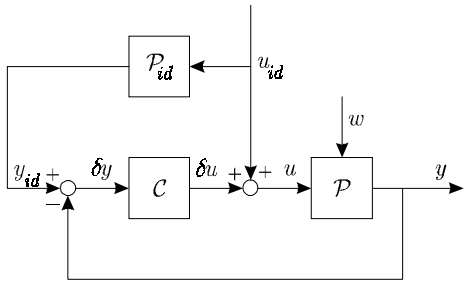

FIGURE 3.1 *Interconnection of deterministic ideal time functions with robust feedback compensator (De Roover, 1997).*

Robust asymptotic tracking

Under special conditions, not only robust regulation and nominal tracking can be achieved, but also robust asymptotic tracking. Three possible situations have been identified:

1. $\mathcal{P} = \mathcal{P}_{\text{id}}$, and $w \in \mathcal{W}$
2. $\mathcal{P} \neq \mathcal{P}_{\text{id}}$, and u_{id}, $y_{\text{id}} \in \mathcal{W}$
3. $\mathcal{P} \neq \mathcal{P}_{\text{id}}$, and $w = 0$.

where $\mathcal{W}$ is the set of waveform structured signals (appendix B). The second condition in situations 1 and 2 means that the disturbance respectively ideal input and output can be described by (semi) deterministic signals (Johnson, 1976). In these situations, robust tracking can be achieved when an *internal model* of the signal generating system is incorporated in the feedback compensator $\mathcal{C}$. An example is the disturbance observer (Johnson, 1971), which will be discussed in section 3.5. In situation 3, robust tracking can be achieved by incorporating the model uncertainty into the design of the ideal deterministic inputs and outputs. For details of this situation we refer to (De Roover, 1997).

Controller components

In literature the two-degrees-of-freedom (2-DOF) controller, *e.g.* figure 3.2, is well known. The name originates from the freedom to process the reference signal r and the feedback signal y independently. It seems that this controller configuration has three degrees-of-freedom, *i.e.* $\mathcal{R}$, $\mathcal{C}$ and $\mathcal{F}$. But there are at most two independent parts in the control signal u, namely a part independent of the measured output y and a variable dependent of the measured output y (De Roover, 1997). However, given a compensator $\mathcal{C}$, one can choose different combinations of $\mathcal{R}$ and $\mathcal{F}$ that result in the same output y. This can be exploited so as to facilitate the design of the components $\mathcal{R}$ and $\mathcal{F}$. Instead of degrees-of-freedom, we will therefore refer to the number of controller components (CC). The control system of figure 3.2, for example, is a 3-CC controller.

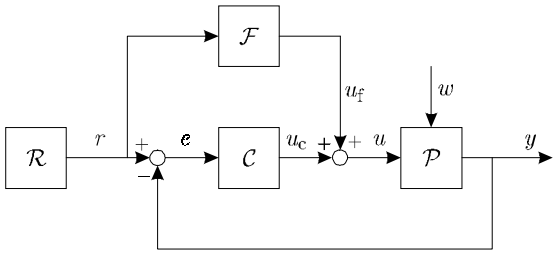

FIGURE 3.2 *General 2-DOF or 3-CC servo system*

Controller design framework
Based on the previously described design philosophy De Roover (1997) proposed the following control design framework:

1. Model the plant and the disturbance signals w as extensively as necessary to achieve the desired (high) performance;
2. Given a (nominal) model of the plant, design a deterministic force input signal u_f that drives the output of this plant model y along a desired trajectory, such that both the force input and the desired trajectory optimally satisfy the desires of the user;
3. Given a (nominal) model of the plant, design a feedback compensator that achieves (robust) regulation, *i.e.* attenuation of disturbances and robustness against parameter variations and unmodeled dynamics;
4. Implement 2. and 3. in the 3-CC nominal tracking scheme of figure 3.2;
5. If the force input u_f and reference trajectory r can be modeled as persistent signals, robust asymptotic tracking can be achieved by extending the controller with an internal model of these signals.

3.2.2 Towards a structured design method for mechatronic control systems

The design philosophy and controller design framework outlined above are not readily applicable in the mechatronic design process, for two reasons:

1. *starting point.* The first step of the framework is to model the plant, disturbances and specifications as extensively as needed. However, in section 3.1 we argued that during detailed design the plant model is only partially known and that this model will only gradually evolve to a description that competently represents the real-world system.
2. *objective.* The design philosophy is developed with the aim to describe how the three design variables ($\mathcal{R}$, $\mathcal{C}$ and $\mathcal{F}$) should be combined such that the performance of the controlled system is *maximized* (De Roover, 1997). This implies that the most advanced design tools are to be used, with the possible consequence of a complex control system and a complex design process. However, in many designs, the designer will not have to obtain maximum

performance, especially not at the cost of a complex control system. Often, a designer will be satisfied when the performance is satisfactorily within a specific context, *i.e.* when it is *good enough*.

We will therefore develop a structured design method for mechatronic control system design, using the basic ideas of the presented philosophy, but sometimes with different implementations. The structured design method will use a particular control configuration.

Definition 3.2 Control configuration

The control configuration is the decomposition of the overall control system into a set of components with predetermined interactions.

Roughly four types of components will be distinguished (figure 3.3):

1. The *reference path generator* $\mathcal{R}$ that generates the reference path r.
2. The *feedback component* $\mathcal{C}$ that uses the reference path r and the measured output y, to generate a control signal u_c.
3. The *feedforward component* $\mathcal{F}$ that has the reference path r as input and generates a forcing function u_f.
4. The *disturbance observer* $\mathcal{O}$ that uses the control signal u and the measured output y to estimate the states of the plant and the disturbance model, in order to estimate and compensate the input disturbance w acting on the plant.

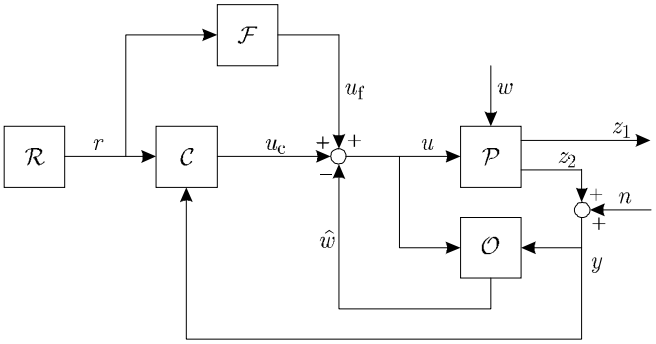

FIGURE 3.3 *Control configuration used in structured design method*

Reference path generator $\mathcal{R}$

The design philosophy makes clear that a choice of reference path r is part of the design of the control system. The reference path will approximately indicate the desired motion for the end-effector, but the actual signal should be chosen in harmony with the other components of the control system and the electromechanical plant.

Feedback component $\mathcal{C}$
The most important component of the control configuration in figure 3.3 is the feedback component. In some cases, all four objectives (refer definition 3.1) can be achieved by only a reference path generator and a feedback component, *i.e.* a 2-CC controller. However, this is generally not possible or desirable, as it is difficult to design such a component meeting multiple objectives. For a stable closed-loop system, we can state that the output y of a controlled system has to follow the reference path r with a small error e and has to reject disturbances w, despite model uncertainties. It is well known that this can theoretically be achieved by a feedback component $\mathcal{C}$ with large gain. However, in practice this will not work, as a large gain can make the system unstable and it increases the cost of feedback.

Statement 3.1 Cost of feedback

The cost of feedback is an indication for the pitfalls of feedback. An appropriate measure for the cost of feedback is the feedback gain, as large feedback gains:
1. *will result in a large control signal u; this requires large power, an expensive actuator and the electromechanical plant has to deal with large inputs;*
2. *cause measurement (or sensor) noise n to affect the system output z unattenuated.*

Feedforward controller $\mathcal{F}$
According to the design philosophy, the main function of the feedforward component $\mathcal{F}$ is to generate the forcing function u_{f}, which results in nominal tracking. Addition of a feedforward component to a 2-CC controller may improve performance, without affecting the stability, disturbance attenuation and robustness properties. Similar as for the feedback component, the feedforward component should be designed such that the plant input u will not become "unpleasant", *i.e.*, the cost of feedforward should also be limited. *E.g.*, large or fast-changing inputs have to be avoided. The design of this component is shortly discussed in section 3.4.

Disturbance observer $\mathcal{O}$
The main function of the disturbance observer $\mathcal{O}$ is to attenuate disturbances acting on the plant. Under special conditions, this observer can be designed independent of the feedback component. Disturbance observer design is discussed in section 3.5.

The functions of the control system can thus be distributed over different components in the control configuration. This may be used to simplify the design and the design process. We start with a 2-CC configuration containing $\mathcal{R}$ and $\mathcal{C}$. We will only add a feedforward component $\mathcal{F}$ or a disturbance observer $\mathcal{O}$ when necessary.

An initial 2-CC configuration is obtained during conceptual design, were we mainly focussed on performance and robust stability. We will shortly reflect upon the assessment method, presented in the previous chapter, in the light of the design philosophy and design framework described above. During assessment, we only used simple plant models, due to limited knowledge of the plant. Therefore, only parts of step 2 and 3 of the design framework, *i.e.* design of an ideal input and robust regulation, were relevant. The assessment method is consistent with these steps:

- *Ideal deterministic response synthesis.* In the assessment method, we do not use a forcing function u_f in order to obtain an ideal deterministic input u_{id}. The consequence is that errors between the output y and its ideal value y_{id} are not only caused by disturbances and modeling errors anymore. Errors also originate from the fact that plant dynamics are implicitly ignored. In the 2-CC configuration, we only generate a plant input u when an error has occurred, *i.e.* a difference between the ideal output y_{id} and the output y. This error also occurs under nominal conditions, *i.e.* when we would exactly know the dynamics of the plant and no disturbances are present. In terms of the design philosophy we can state that during conceptual design we have chosen the reference path r equal to the ideal output y_{id}. Within the assessment method the reference path can be chosen such that it represents a *realistic* output motion. A second-degree reference path, for example, can be constructed from a maximum acceleration and velocity, thus incorporating physical limitations of the amplifier, actuator or mechanical subsystem. The assessment method can also be applied such that it proposes a second-degree reference path with certain maximum acceleration and velocity. This proposal incorporates knowledge of dynamical effects of the plant that limit the performance. The values of the maximum acceleration and velocity can now be used to select an appropriate amplifier and actuator.
- *Robust regulation and nominal tracking.* The feedback component acts upon the error between the reference path r and the measured output y. When we consider the control system used in conceptual design, we see that the measured output consists of two components, *i.e.* a measured position and a measured velocity. The measured position is compared to the reference path. The measured velocity is implicitly compared to zero, *i.e.*, it is assumed that the ideal velocity time function is zero. For servo systems, which also have to track the reference path for $t \in [0, t_m]$, this makes no sense. For transient systems performing point-to-point motions, the ideal velocity in the time interval of interest ($t \geq t_m$) is indeed zero. The measured position does not necessarily correspond to the position to be controlled z. In these cases, the reference path indicates an ideal time function for the measured position and it is assumed that the position to be controlled will automatically follow.

As long as the extensions of the plant model are indeed extensions and not significant modifications, the results of the assessment method are valid and should

be reused during detailed design. This holds for the reference path generator, the control system as well as the plant.

3.3 Feedback component

3.3.1 PID controller structure

In this section, we will discuss the design of PID feedback components that can be integrated in the control configuration of figure 3.3. We will use PID control, as this contains the primary actions that are generally required for control of electromechanical motion systems. Furthermore, industrial applications commonly use these fixed-order motion controllers. If the requirements cannot be met, the PID can easily be extended by means of, for example, loop shaping (see chapter 4) or by addition of a notch filter. These extensions require an initial feedback controller, for which the PID discussed in this section forms a good starting point.

A PID has three parameters, corresponding to: the proportional, integral and derivative action. Roughly, it can be stated that these actions all have their own function. The proportional action primarily provides a desired bandwidth, the derivative action primarily ensures stability and the integral action provides extra gain at low frequencies, in order to suppress low-frequency disturbances. Because the controller also acts on measurement noise n, it is necessary to reduce the feedback gain at high frequencies. This can be achieved by means of a roll-off filter. The design of this filter will be integrated in the design procedure.

In chapter 2 we discussed feedback components $\mathcal{C}$ for electromechanical motion systems that use the reference path, a measured position and a measured velocity as inputs. Depending on the *concept*, the position and velocity were measured at different locations in the plant. Three different combinations were considered, where position and velocity were measured with respect to the fixed world or another reference, *e.g.* the machine frame. These combinations are:

1. position and velocity measurement at the actuator;
2. position and velocity measurement at the end-effector;
3. position measurement at the end-effector and velocity measurement at the actuator.

In this section we will not use actual velocity measurements, but rather construct a velocity signal from a position signal using a tame derivative action. The reason is that commonly position sensors are used. The consequence is that one position sensor is required in combinations 1 and 2 and two position sensors are required in combination 3. We distinguish two different PID configurations:

1. The *PID compensator*, which generates a control signal u, using an error, *i.e.* the difference between the reference path r and a measured position y, as inputs (figure 3.4a). This compensator can only be applied in combinations 1 and 2.
2. The *PID controller*, which generates a control signal u, using the reference path r and two measured positions (y_1, y_2) as inputs (figure 3.4b). The inputs y_1 and y_2 may be chosen identical. The essential difference is that the derivative action does not operate on r. The controller can be applied in all three combinations.

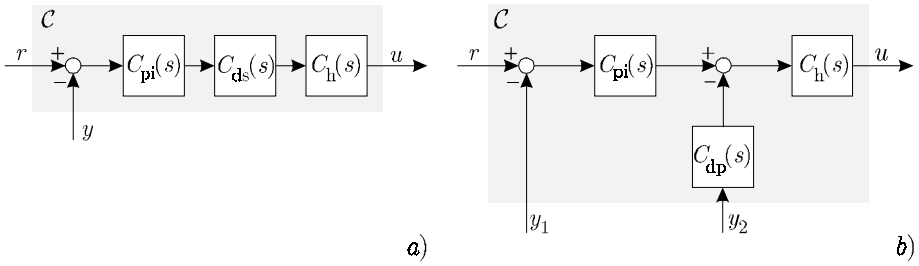

FIGURE 3.4 *a) PID compensator and b) PID controller configuration*

The transfer function of the PID compensator in series form with a second-order roll-off filter is described by:

$$\begin{aligned} C_{\mathrm{pi}}(s) &= K \cdot \frac{\tau_{\mathrm{i}} s + 1}{\tau_{\mathrm{i}} s} \\ C_{\mathrm{ds}}(s) &= \frac{\tau_{\mathrm{d}} s + 1}{\tau_{\mathrm{d}} \beta s + 1} \\ C_{\mathrm{h}}(s) &= \frac{1}{\tau_{\mathrm{h}} s + 1} \end{aligned} \tag{3.4}$$

such that

$$C(s) = C_{\mathrm{pi}}(s) \cdot C_{\mathrm{ds}}(s) \cdot C_{\mathrm{h}}(s) = K \cdot \left(\frac{\tau_{\mathrm{i}} s + 1}{\tau_{\mathrm{i}} s} \right) \cdot \left(\frac{\tau_{\mathrm{d}} s + 1}{\tau_{\mathrm{d}} \beta s + 1} \right) \cdot \left(\frac{1}{\tau_{\mathrm{h}} s + 1} \right) \tag{3.5}$$

where K denotes the proportional gain, τ_{i} the integral time constant, τ_{d} the derivative time constant and τ_{h} the high-frequency roll-off time constant. The tameness factor β is chosen such that the derivative action is effective over a limited frequency range only. In order to have a derivative effect, β is chosen smaller than 1.

An asymptotic Bode plot of the PID compensator is shown in figure 3.5. The tameness factor β determines the magnitude of the phase lead that will maximally

occur. When β becomes larger and gets closer to 1, $1/\tau_{\mathrm{d}}$ and $1/\beta\tau_{\mathrm{d}}$ will move towards each other, such that the phase-lead effect will be reduced.

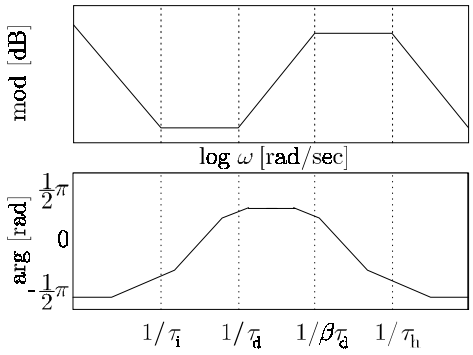

FIGURE 3.5 *Asymptotic Bode plot of the PID compensator*

The PID controller, as indicated in figure 3.4b, is described by three separate transfer functions. The proportional and integral action $C_{\mathrm{pi}}(s)$, as well as the roll-off filter $C_{\mathrm{h}}(s)$ are given in (3.4). The (parallel) derivative action is described by:

$$C_{\mathrm{dp}}(s) = K \cdot \frac{\tau_{\mathrm{d}} s}{\tau_{\mathrm{d}} \beta s + 1} \tag{3.6}$$

The measurement y_2 entering the derivative action $C_{\mathrm{dp}}(s)$ can either be the actuator position or the end-effector position, depending on the concept that is considered. The meaning of the parameters in (3.6) is the same as in (3.5).

We define the problem we address in this section as:

Definition 3.3 PID design problem

Given a standard fourth-order plant model, design a PID controller or PID compensator, which:

1. *achieves sufficiently high bandwidth ω_{b};*
2. *gives sufficient suppression of low-frequency disturbances;*
3. *ensures a maximum peak-value of the magnitude of the sensitivity function;*
4. *uses limited control energy.*

The bandwidth is defined as:

Definition 3.4 Bandwidth ω_{b}

The bandwidth ω_{b} is the frequency for which $|1 - T(j\omega)|$ first crosses the 0 dB-line from below.

where $T(j\omega)$ is the complementary sensitivity function. When a compensator is used, this implies the more common definition of bandwidth, *i.e.* the frequency where the sensitivity function $S(j\omega)$ first crosses the 0 dB-line from below, see *e.g.* (Skogestad and Postlethwaite, 1996). However, this is not true for the controller configuration, as the sum of the sensitivity and complementary sensitivity function do not equal 1. The bandwidth ω_b defined above provides a good indication for the closed-loop performance and is applicable for both configurations.

Before we actually derive a design procedure, we will shortly describe the relation between the PID design addressed in this chapter and assessment method of chapter 2.

After successful application of the assessment method, a proposal for a controlled system is available, including a sensible reference path, an indication of the lowest mode of vibration of the plant and the sensor locations. Unlike during conceptual design, we will consider these properties of the system design to be unalterable at this stage. For the values of the proportional actions in the controller, merely a sensible indication is given. After more extensive modeling of the dynamic behavior of the plant, the controller should be reconsidered. Now, not only performance plays a role, but also additional aspects such as the stability margin, disturbance attenuation and the cost of feedback. The design procedure discussed here is more appropriate for this purpose, as the specifications are stated in terms of the sensitivity function, *i.e.* frequency-domain design, and the controller includes an integral action. One major benefit of frequency domain design is the close link to experimental information that can be obtained by measuring the frequency response. However, it is desirable to reuse the controller settings proposed in the conceptual design. We will show that it is wise to use the *bandwidth* ω_b of the conceptual design as the starting point of the PID design.

3.3.2 PID design for second-order plants

Firstly, we consider the design of PID compensators (figure 3.4a) with a roll-off filter, as described in (De Roover, 1997). We use this systematic approach to PID design, as it tailored to electromechanical motion systems and it provides the designer with more insight in design trade-offs than tuning rules, such as in *e.g.* (Rankers, 1997). Secondly, we make some modifications to this approach. Finally, we formulate a design procedure, which starts from frequency-domain specifications and a second-order plant model, *i.e.* a moving mass model:

$$P(s) = \frac{1}{ms^2} \tag{3.7}$$

with m denoting the total mass to be moved.

The specification used in the design procedure of De Roover (1997) are:

1. sufficiently high bandwidth ω_b.
2. sufficient suppression of low-frequency vibrations: $|S(j\omega)| < s_l$ for $\omega < \omega_l$.
3. maximum peak-value of the sensitivity magnitude: $|S(j\omega)| < M_S$.
4. limited control energy.

where the sensitivity function, with PID *compensator* $C(s)$ according (3.5), is given by:

$$S(s) = \frac{1}{1 + P(s)C(s)} \tag{3.8}$$

and the peak of the sensitivity function is defined as:

Definition 3.5 Peak of the sensitivity function M_S

The peak of the sensitivity function M_S is:

$$M_S = \max_{\omega} |S(j\omega)| \triangleq |S(j\omega)|_\infty$$

The sensitivity function is a suitable means to specify the functionality of a feedback component (refer section 3.2.1). Requirements 1 and 2 correspond to the function of disturbance suppression, while requirement 3 corresponds to the functions stability and robustness. Requirement 4 is used to find the best of all candidates, *i.e.* the one with the smallest cost of feedback. When the control configuration consists of only a feedback compensator and a reference path generator, *i.e.* a 2-CC control system, the PID compensator also has to provide performance. This can be specified by means of the bandwidth ω_b.

All specifications are now expressed in terms of the sensitivity function. However, a disadvantage of using the sensitivity function is that it is very insensitive to a major cost of feedback: the effects of measurement noise n (Horowitz, 1991). Therefore, we always need to inspect the complementary sensitivity function $T(s)$ after the design of the feedback component.

PID compensator

For the PID compensator we consider the peak of the sensitivity function M_S in more detail. A typical open-loop Nyquist plot of the loop transfer function $L(j\omega) = P(j\omega)C(j\omega)$ is shown in figure 3.6a, where $P(j\omega)$ and $C(j\omega)$ are derived from (3.7) respectively (3.5).

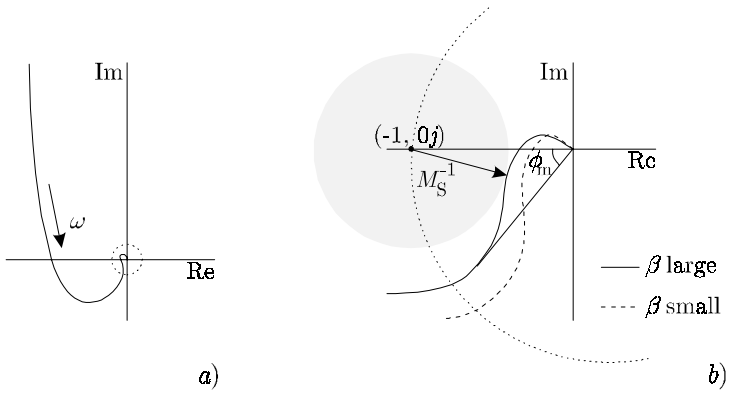

FIGURE 3.6 *a) Nyquist plot of $L(j\omega)$ b) Sensitivity function peak reduction*

A close-up of the loop transfer function of the PID controlled moving-mass system around the point $(-1,\, 0j)$ is shown in figure 3.6b. The maximum phase lead of the PID compensator is less than 90° and should occur at about the phase margin. It can be seen that when the phase lead at the phase margin increases, the graph is pushed away from the point $(-1,\, 0j)$. The same will happen at the frequency where $|S(j\omega)| = M_S$. Hence, there is a close relation between the maximum peak of the sensitivity function M_S and the phase margin ϕ_m. For a given M_S it is guaranteed that (Skogestad and Postlethwaite, 1996):

$$\phi_m \geq 2\arcsin\left(\frac{1}{2M_S}\right) \tag{3.9}$$

Thus, to allow a certain maximum on the sensitivity function, a minimum phase margin has to be guaranteed.

$$M_S \leq \left(2\sin\left(\frac{\phi_m}{2}\right)\right)^{-1} \tag{3.10}$$

Note that this is a necessary and not a sufficient condition. As the phase change caused by the plant $P(j\omega)$, (3.7), is always −180°, the minimum required phase lead of the PID compensator ϕ_c corresponds to the required phase margin ϕ_m. The magnitude of this phase lead is determined solely by the tameness factor β:

extra phase lead ϕ_c	tameness factor β
0°	1
55°	0.1
78°	0.01

TABLE 3.1 *Relation between extra phase lead and tameness factor β*

Not only the amount of phase lead is important, but also the frequency at which it occurs. It is desirable to put the maximum phase lead at the frequency where the sensitivity function peaks ω_{peak}. This ensures that M_S is small enough, using minimum phase lead ϕ_c. The smaller this phase lead, the smaller the gain at that and higher frequencies, which corresponds to the requirement of limited control energy. The relation between the required bandwidth ω_b and the frequency at the peak of the sensitivity function has been stated as: "For good designs, this frequency ω_{peak} is approximately two times the bandwidth" (De Roover, 1997). The compensator parameter τ_d determines at which frequency the phase lead ϕ_c occurs, *i.e.* in the middle between $1/\tau_d$ and $1/\beta\tau_d$. On a logarithmic scale this means:

$$\frac{\log\left(\tau_d^{-1}\right) + \log\left(\beta^{-1}\tau_d^{-1}\right)}{2} = \log\left(\omega_{\text{peak}}\right) \approx \log\left(2\omega_b\right) \Leftrightarrow \tau_d = \frac{1}{2\omega_b\sqrt{\beta}} \tag{3.11}$$

In order to obtain the desired bandwidth ω_b, the proportional gain K is used. We obtain an expression for K by evaluating the expressions for the plant and the compensator. We will approximate the expression for the compensator for a particular frequency range. In the frequency range between $1/\tau_d$ and $1/\beta\tau_d$ (refer figure 3.5), where the bandwidth ω_b will be situated, the compensator can be approximated by:

$$C(j\omega_b) \approx K \cdot \frac{\tau_d j\omega_b + 1}{\tau_d \beta j\omega_b + 1} \tag{3.12}$$

Using this approximation together with the fact that $|1 - T(j\omega_b)| = 0$ dB, gives an expression for K:

$$K = 2\omega_b^2 m\left(\frac{\omega_b^2\tau_d^2\beta + 1}{\omega_b^2\tau_d^2 + 1}\right) \tag{3.13}$$

Low-frequency disturbances have to be suppressed up to a frequency ω_l, such that in this region $|S(j\omega_l)| < s_l$. This can be achieved by the integral action of the PID compensator, *i.e.* by finding a proper value for the parameter τ_i. In order to find an expression for τ_i, we will again approximate the expression for the compensator, but now for the low-frequency range:

$$C(s) \approx \frac{K}{\tau_i s} \tag{3.14}$$

Furthermore, the sensitivity function in the low-frequency range can be approximated by:

$$|S(s)| \approx \left|\frac{1}{P(s)C(s)}\right| \tag{3.15}$$

Remark 3.2

The approximations are justified as long as $1/\tau_{\mathrm{i}}$ *is sufficiently smaller than* $1/\tau_{\mathrm{d}}$ *and* $|P(j\omega)C(j\omega)| \gg 1$. *Rankers (1997) suggests choosing* $1/\tau_{\mathrm{d}}$ *about* 3 *times larger than* $1/\tau_{\mathrm{i}}$.

When we combine these approximations with requirement 2, we obtain the expression for τ_{i}:

$$\tau_{\mathrm{i}} \leq \frac{s_{\mathrm{l}} K}{m\omega_{\mathrm{l}}^3} \tag{3.16}$$

In order to suppress high-frequency components in the loop, *i.e. high-frequency roll-off*, an additional filter is added to the PID compensator. The extra pole should not deteriorate the stability margin, therefore it should be situated further away than the pole of the derivative action $(1/\beta\tau_{\mathrm{d}})$, but as low as possible to limit the controller bandwidth.

Evaluation of design method
Although this a useful and systematic method for the design of PID compensators:
- it is not applicable for concepts using 2 measurements;
- the disturbance is assumed to be an output disturbance.

In electromechanical systems, disturbances are often expressed conveniently in terms of force, thus input disturbances are more appropriate. In the compensator configuration, input disturbances can easily be transformed into output disturbances, when the plant is linear and time invariant. However, when two measurements are used this transformation is more complex.

Comparison of configurations
In order to address these two problems, we will first compare some characteristic closed-loop transfer functions of a second-order plant with both a PID compensator and a PID controller. By means of a subscript we indicate the input and output variable of a transfer function, *e.g.* $T_{\mathrm{rz}}(s)$ indicates the complementary sensitivity function from reference path r to the output z. Additionally we consider the transfer functions from the input disturbance w and the measurement noise n to the measured output y. For the compensator configuration we obtain the familiar expressions:

$$\begin{aligned} T_{\mathrm{rz}} &= \frac{PC}{1+PC} \\ S_{\mathrm{wz}} &= \frac{P}{1+PC} \\ T_{\mathrm{nz}} &= -\frac{PC}{1+PC} \end{aligned} \tag{3.17}$$

where we omitted the Laplace operator (s) for reasons of simplicity. For the controller configuration we obtain:

$$\begin{aligned} T_{\mathrm{rz}} &= \frac{PC_{\mathrm{h}}C_{\mathrm{pi}}}{1 + PC_{\mathrm{h}}C_{\mathrm{pi}} + PC_{\mathrm{h}}C_{\mathrm{dp}}} \\ S_{\mathrm{wz}} &= \frac{P}{1 + PC_{\mathrm{h}}C_{\mathrm{pi}} + PC_{\mathrm{h}}C_{\mathrm{dp}}} \\ T_{\mathrm{nz}} &= -\frac{PC_{\mathrm{h}}C_{\mathrm{pi}}}{1 + PC_{\mathrm{h}}C_{\mathrm{pi}} + PC_{\mathrm{h}}C_{\mathrm{dp}}} \end{aligned} \tag{3.18}$$

Other important closed-loop transfer functions, used in the design method, are the sensitivity function S and $1 - T_{\mathrm{rz}}$. For the compensator we obtain the well-known expression:

$$S = \frac{1}{1 + PC} = 1 - T_{\mathrm{rz}} \tag{3.19}$$

For the controller configuration we obtain:

$$\begin{aligned} S &= \frac{1}{1 + PC_{\mathrm{h}}C_{\mathrm{pi}} + PC_{\mathrm{h}}C_{\mathrm{dp}}} \\ 1 - T_{\mathrm{rz}} &= \frac{1 + PC_{\mathrm{h}}C_{\mathrm{dp}}}{1 + PC_{\mathrm{h}}C_{\mathrm{pi}} + PC_{\mathrm{h}}C_{\mathrm{dp}}} \end{aligned} \tag{3.20}$$

Here, we see that the sum of S and T_{rz} is not 1 anymore, as this feedback component actually has two degrees of freedom. When we assume that $C_{\mathrm{pi}} + C_{\mathrm{dp}} = C$, as $\beta \ll 1$, we can conclude that:

- S_{wz} is identical for both configurations;
- T_{nz} is identical for both configurations;
- T_{rz} is different.

Remark 3.3

With z we denote the output to be controlled. In case only position measurement at the actuator takes place, we consider the actuator position the output z to be controlled, although we are primarily interested in the position of the end-effector.

Remark 3.4

The design procedure will use more system representations than only the sensitivity function. It is wise to use these multiple views, as we have already indicated that the suppression of measurement noise is not visible in the sensitivity function.

Input disturbances
Instead of output disturbances, we will now consider input disturbances. The specification is: $|S_{wz}(j\omega)| < s_l$ for $\omega < \omega_l$, where S_{wz} is the input sensitivity function. Again, we approximate the expression for the PID compensator in the low-frequency range:

$$C \approx \frac{K}{\tau_i s} \tag{3.21}$$

Furthermore, the input sensitivity function can be approximated by:

$$|S_{wz}| \approx \left|\frac{P}{PC}\right| = \left|\frac{1}{C}\right| \tag{3.22}$$

Combining these approximations with the new specification for disturbance attenuation gives the new expression for τ_i:

$$\tau_i \leq \frac{s_l K}{\omega_l} \tag{3.23}$$

Remark 3.5

Whenever $1/\tau_i$ is smaller than ω_l, this indicates that the integral action is not necessary, i.e., the requirement is also met without integral action. In these cases PD control can be applied.

PID controller
In concepts that use two measurements, only the PID controller (figure 3.4b) can be applied. The corresponding parameters can, of course, be determined using the procedure as indicated above. However, we indicated that the performance, *i.e.* ω_b, is different when using a controller configuration. The consequence is that application of the design method will result in a different bandwidth than specified. Therefore, we will determine new expressions for the parameters of the PID controller, using a similar approach.

A disadvantage of the PID controller structure is that it cannot be described by a single loop transfer function, such that frequency analysis is not straightforward. Instead, we use the following transfer function:

$$L' = \frac{PC_h C_{pi}}{1 + PC_h C_{dp}} \tag{3.24}$$

I.e., the transfer function from the input of C_{pi} to the position z_1, with the position loop y_2 closed. The expression for the transfer function $1 - T_{rz}(s)$, including roll-off filter, is:

$$\begin{aligned} 1 - T_{\mathrm{rz}} &= \frac{1 + PC_{\mathrm{h}}C_{\mathrm{dp}}}{1 + PC_{\mathrm{h}}C_{\mathrm{pi}} + PC_{\mathrm{h}}C_{\mathrm{dp}}} \\ &= \frac{1}{L' + 1} \end{aligned} \tag{3.25}$$

As before, the function of $C_{\mathrm{dp}}(s)$ is to limit the peak of the sensitivity function. The lead coefficient β can be chosen with the aid of table 3.1, but generally 0.1 is used. The derivative time-constant τ_{d} should again be chosen such that the extra phase lead ϕ_{c} is located at the frequency where the sensitivity function peaks.

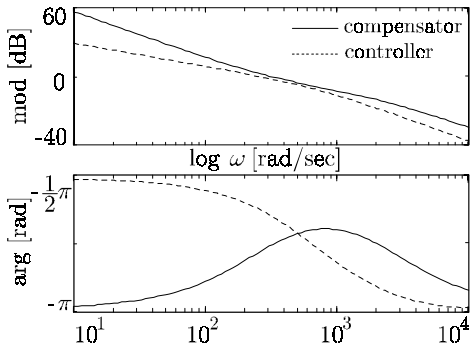

FIGURE 3.7 *Comparison of loop transfer functions with a PD compensator and a PD controller*

In figure 3.7 we compare a typical loop transfer function L of a PD compensator and a loop transfer function L' of a PD controller; the integral action is omitted for reasons of simplicity. A similar phase at the gain crossover frequency ω_{c} is approximately achieved by choosing the derivative time constant of the PD controller equal to:

$$\tau_{\mathrm{d}} = \frac{1}{4\omega_{\mathrm{b}}\sqrt{\beta}} \tag{3.26}$$

Definition 3.6 Gain crossover frequency ω_{c}

The gain crossover frequency ω_{c} is the frequency where $|L(j\omega)|$ first crosses the 0 dB-line from above.

To obtain the desired bandwidth ω_{b}, we derive an appropriate expression for the proportional gain K. Using the fact that $|1 - T_{\mathrm{rz}}(j\omega_{\mathrm{b}})| = 0$ dB and the expression for $C_{\mathrm{dp}}(j\omega_{\mathrm{b}})$ from (3.6), gives an expression for K:

$$K = 2\omega_{\mathrm{b}}^2 m\left(\frac{\omega_{\mathrm{b}}^2\tau_{\mathrm{d}}^2\beta^2 + 1}{\omega_{\mathrm{b}}^2\tau_{\mathrm{d}}^2\beta^2 + 2\omega_{\mathrm{b}}^2\tau_{\mathrm{d}}^2\beta + 1}\right) \tag{3.27}$$

The expression for the integral time constant τ_{i} is identical as for the PID compensator, as the input sensitivity functions are identical, therefore:

$$\tau_{\mathrm{i}} \leq \frac{s_{\mathrm{l}}K}{\omega_{\mathrm{l}}} \tag{3.28}$$

The high-frequency roll-off filter is also determined similarly as for the PID compensator.

Remark 3.6

Commonly, the integral action in a 2-CC control configuration is only switched on after the motion time, i.e. for $t \geq t_{\mathrm{m}}$, in order not to deteriorate the positional error.

Design procedure

We can now summarize the findings above in one design procedure.

In order to reuse the results of conceptual design, we suggest to determine the bandwidth ω_{b} of this closed-loop system and use this as the initial specification:

1. sufficiently high bandwidth ω_{b}, *i.e.* the frequency where $|1 - T_{\mathrm{rz}}(j\omega)| = 0$ dB.
2. sufficient suppression of low-frequency disturbances: $|S_{\mathrm{wz}}(j\omega)| < s_{\mathrm{l}}$ for $\omega < \omega_{\mathrm{l}}$.
3. maximum peak-value of the sensitivity magnitude: $|S(j\omega)| < M_{\mathrm{S}}$.
4. limited control energy.

Design Procedure 3.1 PID design using a second-order plant model

1. *Determine m, i.e. the total mass to be displaced.*
2. *Determine whether to use a PID compensator or a PID controller.*
3. *Determine the amount of phase lead ϕ_{c} necessary for the desired maximum peak of the sensitivity function M_S and the tameness factor β using table 3.1. Generally, the parameter β is chosen equal to* 0.1.
4. *Determine the frequency at which the extra phase lead should be located, i.e. the frequency where the sensitivity function peaks ω_{peak}.*

   $$\omega_{\mathrm{peak}} = 2\omega_{\mathrm{b}}$$

   Next, determine the value of derivative time constant τ_{d} to position the extra phase lead at this frequency. For the compensator respectively controller use:

$$\tau_{\mathrm{d}} = \frac{1}{2\omega_{\mathrm{b}}\sqrt{\beta}} \qquad\qquad \tau_{\mathrm{d}} = \frac{1}{4\omega_{\mathrm{b}}\sqrt{\beta}}$$

5. *Determine the proportional gain K to obtain the desired bandwidth ω_{b}. For the compensator respectively controller use:*

$$K = 2\omega_{\mathrm{b}}^2 m\left(\frac{\omega_{\mathrm{b}}^2\tau_{\mathrm{d}}^2\beta + 1}{\omega_{\mathrm{b}}^2\tau_{\mathrm{d}}^2 + 1}\right) \qquad K = 2\omega_{\mathrm{b}}^2 m\left(\frac{\omega_{\mathrm{b}}^2\tau_{\mathrm{d}}^2\beta^2 + 1}{\omega_{\mathrm{b}}^2\tau_{\mathrm{d}}^2\beta^2 + 2\omega_{\mathrm{b}}^2\tau_{\mathrm{d}}^2\beta + 1}\right)$$

6. *Determine the integral time constant τ_{i} in order to obtain a desired gain at low frequencies. For the compensator and controller use:*

$$\tau_{\mathrm{i}} \leq \frac{s_{\mathrm{l}}K}{\omega_{\mathrm{l}}}$$

7. *Choose the high-frequency roll-off time constant $\tau_{\mathrm{h}} < \beta\tau_{\mathrm{d}}$, but as large as possible to limit the controller bandwidth.*

Remark 3.7

So far, we have not given suggestions whether to use a compensator or a controller configuration. We come back to this issue in chapter 5.

Example
In section 3.2.2 we shortly discussed the PD controller, used during conceptual design, in the light of the design philosophy of section 3.2.1. Here, we will illustrate the differences between the compensator and the controller configuration by means of an example. We model the PM module of the FCM as a moving mass, with $m = 8.83$ [kg]. The specifications are:

1. bandwidth $\omega_{\mathrm{b}} = 266$ [rad/s].
2. suppression of low-frequency disturbances: $|S_{\mathrm{wz}}(j\omega)| < s_{\mathrm{l}} = -120$ [dB] for $\omega < \omega_{\mathrm{l}} = 10\cdot\pi$ [rad/s].
3. maximum peak-value of the sensitivity magnitude: $|S(j\omega)| < M_{\mathrm{S}} = 6$ [dB].
4. limited control energy.

The parameter values according design procedure 3.1 are given in table 3.2.

parameter	compensator configuration	controller configuration
β	0.1	0.1
τ_{d}	$5.93{\cdot}10^{-3}$	$2.97{\cdot}10^{-3}$
K	$4.50{\cdot}10^{5}$	$12.2{\cdot}10^{5}$
τ_{i}	$1.42{\cdot}10^{-2}$	$3.54{\cdot}10^{-2}$
τ_{h}	$3.0{\cdot}10^{-4}$	$1.5{\cdot}10^{-4}$

TABLE 3.2 *Parameter values of PID compensator and PID controller*

First, we omit the integral action and the roll-off filter, to illustrate the essential difference between the two structures. We consider the transfer function $1 - T_{\mathrm{rz}}(s)$, as shown in figure 3.8:

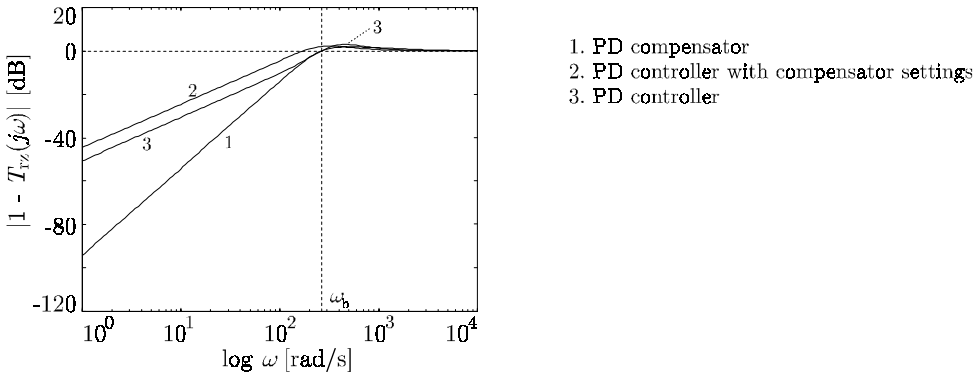

FIGURE 3.8 *Magnitude of* $1{-}T_{\mathrm{rz}}(s)$ *for different PD implementations*

We see that the compensator indeed fulfills the specifications, *i.e.* the bandwidth ω_{b} is approximately 266 [rad/s] and the peak of the sensitivity function $M_{\mathrm{S}} < 6$ [dB] (response 1). When we use the same settings (first column of table 3.2) for the PD controller, we see that the bandwidth is lower: $\omega_{\mathrm{b}} = 180$ [rad/s] (response 2). When we apply the settings that have been determined for the controller configuration (second column of table 3.2), we again obtain a bandwidth ω_{b} of approximately 266 [rad/s] (response 3).

Now, we also incorporate the integral action and we will look at three closed-loop transfer functions $1 - T_{\mathrm{rz}}(s)$, $S_{\mathrm{wz}}(s)$ and $T_{\mathrm{nz}}(\mathrm{s})$, for the same three situations as above (see figure 3.9).

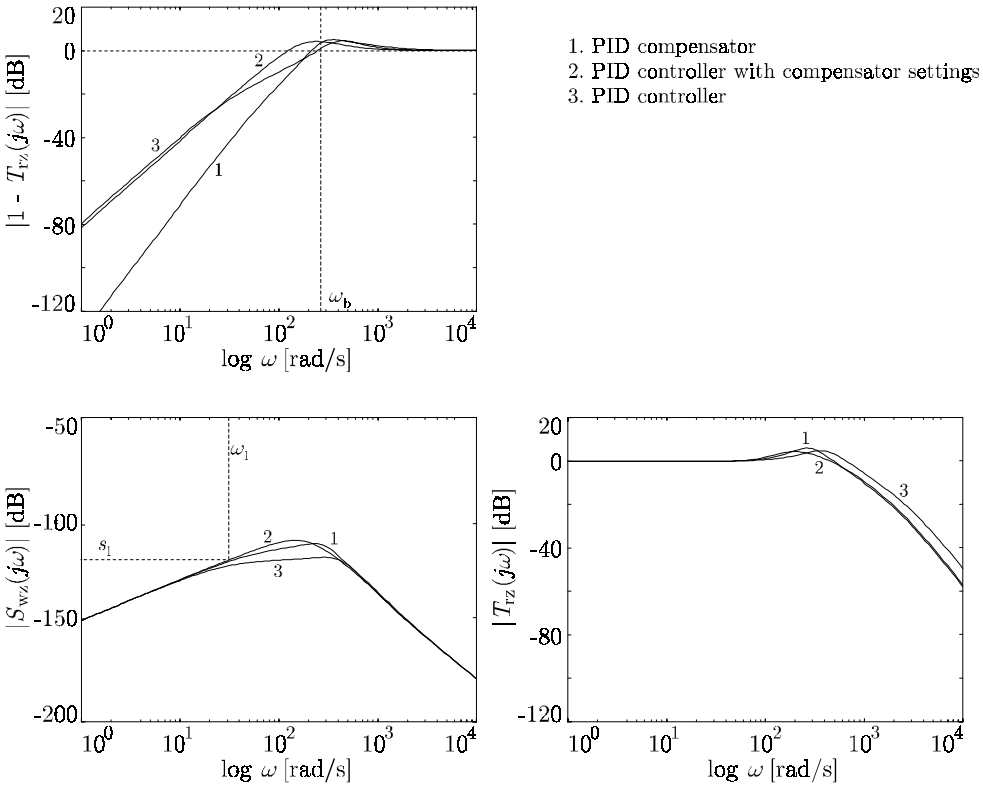

FIGURE 3.9 *Magnitude of* $1–T_{\mathrm{rz}}(s)$, $S_{\mathrm{wz}}(s)$ and $T_{\mathrm{nz}}(s)$ *for different PID implementations*

First of all we can see that the PID compensator and PID controller design according to design procedure 3.1, approximately fulfill all specifications. The PID controller configuration requires more proportional gain K in order to obtain the desired bandwidth ω_{b}. As a consequence, more low-frequency disturbance attenuation and more noise amplification occurs.

3.3.3 PID design for fourth-order plants

In this section we want to verify to what extent design procedure 3.1 is also applicable to fourth-order models (Waarsing, 1999). For fourth-order plant models with a PID controller, stability is not guaranteed *a priori*, as it is for second-order plant models. Stability depends on the type of fourth-order plant transfer function (refer section 2.2.1) and the control system, *i.e.* the concept (refer section 2.3). Therefore, we first consider the relation between the plant models $P(s)$ and PID, in

order to obtain guidelines for stability. Consecutively, we extend the design procedure such that it is applicable to all concepts that possibly yield a stable closed-loop system.

Stability analysis
In (Rankers, 1997) a stability analysis is presented for fourth-order systems, using a PID *compensator*. We will shortly summarize the results. Consider the loop transfer function $L(s)$ of a second-order plant model with a PID compensator (3.5), as shown in figure 3.10.

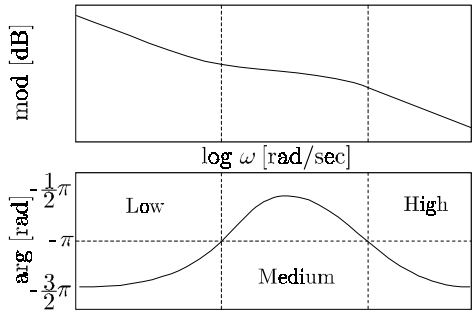

FIGURE 3.10 *Ideal open-loop frequency response without first mode of vibration for the PID compensator*

The frequency range (figure 3.10) can be divided into three regions, separated by a $-\pi$ crossing of the phase plot. In the low-frequency range the phase is below $-\pi$, due to the integral action. In the middle-frequency range the phase is above $-\pi$, due to the phase-lead of the derivative action and in the high-frequency range the phase again drops below $-\pi$. The borders of these regions can be roughly estimated by comparing figure 3.5 with figure 3.10. This comparison shows that the first $-\pi$ phase crossing of the PID compensator occurs somewhere in the middle of $1/\tau_{\mathrm{i}}$ and $1/\tau_{\mathrm{d}}$, which marks the end of the low-frequency region. The high-frequency region starts from the second $-\pi$ phase crossing of the PID compensator, somewhere in the middle of $1/\beta\tau_{\mathrm{d}}$ and $1/\tau_{\mathrm{h}}$. The medium-frequency region lies in between.

To illustrate how a vibration mode may affect the stability of the loop, (Rankers, 1997) extended the original plant model with one extra mode in each of the three frequency ranges. Three concepts with a PID compensator were considered and it was concluded that:

Concept *AR*: concept *AR* is possibly unstable when the vibration mode is located in the low- or high-frequency region, due to the extra phase lead. When located in the middle-frequency range, the extra phase lead will only add to the existing phase lead, which improves the stability.

Concept *RA*: concept *RA* has the opposite effect. If the vibration mode is located in the middle-frequency region, it will possibly be destabilizing, but if located in either the low- or high-frequency region, the system will be stable.

Concept *R*: concept *R* is never stable when the vibration mode is located in the low- or middle-frequency region. If located in the high-frequency region this concept can be dealt with.

In chapter 2 we also discussed concept *D* and concept *N* controlled systems. When a PID compensator is to be designed for a type *D* transfer function, the controlled system will always be stable, as it does not contain a vibration mode. Concept *N* will result in an unstable closed-loop system. Only when the vibration mode is in the high-frequency area, this concept can be dealt with.

When a PID *controller* is used instead of a *compensator*, this approach of stability inspection cannot be used. In the previous section we did define a loop transfer function $L'(s)$, *i.e.* the transfer function from the input of $C_{\mathrm{pi}}(s)$ to the position to be controlled z. However, a vibration mode cannot be superimposed on the loop transfer function with a second-order plant model, as the position loop of y_2 is closed (3.24). In section 3.3.2 we indicated that the closed-loop poles are located at the same position for both the controller and compensator configuration. Additionally, we will reuse the results of chapter 2 with regard to stability of different concepts. In the assessment method of chapter 2, the bandwidth ω_{b} is implicitly chosen close to the vibration mode, but always smaller, *i.e.* the medium frequency range. When the vibration mode is in the high-frequency area the plant behaves as a moving mass. However, there may be a risk of instability when the vibration mode is not located far enough into the high-frequency region.

Concept	Low	Medium	High
AR	□	+	□
D	+	+	+
RA	+	−	+
R	−	−	□
N	−	−	□
AR-D	+	+	□
AR-RA	−	□	□
AR-R	−	□	□
AR-N	−	□	□

\+ stable
□ risk of instability
− not applicable

TABLE 3.3 *Stability of concepts for vibration modes in different frequency regions*

In table 3.3 we give an indication for the risk of instability for all concepts, independent of the used configuration. It is indicated whether a concept is stable, has a risk of instability or is not applicable; this either means that the concept is unstable, or that risk of instability is such that it is not wise to use this concept in the indicated frequency region.

Remark 3.8

In table 3.3 we only discussed stability issues and not the other requirements of the PID. Generally, the vibration mode will be located in the medium or high-frequency region. When a vibration mode is located in the low-frequency region, this may have significant effects on the performance.

Design procedure
A PID is not able to control a vibration mode; it primary controls a second-order plant, *i.e.* a moving mass system. We need to consider the first mode of vibration in order to get an indication of this performance-limiting factor. The design procedure 3.1 is therefore only applicable to those concepts marked with + or □ in table 3.3. For a particular problem this table should be checked beforehand; the actual stability margin(s) also should be verified after the design.

In the situations that the vibration mode is located within the bandwidth ω_{b}, a small modification is required. The plant approximation at ω_{b} is now different:

$$P(\,j\omega_{\mathrm{b}}\,) \approx \frac{1}{m(\,j\omega_{\mathrm{b}}\,)^2} \cdot \frac{\omega_{\mathrm{r}}^2}{\omega_{\mathrm{ar}}^2} \tag{3.29}$$

This implies that the control system sees a different mass:

$$m^* = m \cdot \frac{\omega_{\mathrm{ar}}^2}{\omega_{\mathrm{r}}^2} \tag{3.30}$$

As a consequence, the expressions for the proportional gain, which contain the mass, should be adapted. The new expression for the proportional gain K for the compensator is:

$$K = 2\omega_{\mathrm{b}}^2 m^* \left(\frac{\omega_{\mathrm{b}}^2\tau_{\mathrm{d}}^2\beta + 1}{\omega_{\mathrm{b}}^2\tau_{\mathrm{d}}^2 + 1} \right) = \frac{2\omega_{\mathrm{b}}^2 m\omega_{\mathrm{ar}}^2}{\omega_{\mathrm{r}}^2} \left(\frac{\omega_{\mathrm{b}}^2\tau_{\mathrm{d}}^2\beta + 1}{\omega_{\mathrm{b}}^2\tau_{\mathrm{d}}^2 + 1} \right) \tag{3.31}$$

and similar for the proportional gain of the controller:

$$K = \frac{2\omega_{\mathrm{b}}^2 m\omega_{\mathrm{ar}}^2}{\omega_{\mathrm{r}}^2} \left(\frac{\omega_{\mathrm{b}}^2\tau_{\mathrm{d}}^2\beta^2 + 1}{\omega_{\mathrm{b}}^2\tau_{\mathrm{d}}^2\beta^2 + 2\omega_{\mathrm{b}}^2\tau_{\mathrm{d}}^2\beta + 1} \right) \tag{3.32}$$

In the situations that PID control can only be applied when the vibration mode is located in the high-frequency area, it is important that the high-frequency roll-off comes as soon as possible. In these cases we recommend choosing τ_{h} as:

$$\tau_{\mathrm{h}} = \frac{1}{\beta \tau_{\mathrm{d}}} \tag{3.33}$$

3.4 Feedforward and reference path generator

In this section we will shortly discuss the design of the feedforward component and the reference path generator. We will not present any new material, but merely indicate some design issues.

In the design philosophy we mentioned that the third degree of freedom in a 3-CC controller concerns the implementation of the reference path generator $\mathcal{R}$ and the feedforward component $\mathcal{F}$, *i.e.* in those components that generate a control signal dependent on the reference path r and independent of the measurement y. This part of the control signal is referred to as the forcing function u_{f}. De Roover (1997) gives a survey of alternative design methods for open-loop forcing functions that drive the output of a plant model along a desired trajectory, such that both the force input and the desired trajectory optimally satisfy the desires of the user. These methods are classified into input synthesis and input filtering techniques. In the first category forcing functions are designed with the desired vibration reducing properties from scratch, while in the second category the forcing function are shaped with an *a priori* control signal, such that resulting filtered input possesses the desired vibration reducing properties.

The essential task of the controlled system can be characterized as moving a mass from one location to another. In order to do so, the mass first has to be accelerated and consecutively decelerated. The corresponding forcing function is a single bang-bang function. However, the electromechanical plant will additionally contain flexible modes, which are ignored when applying this technique. These modes can (theoretically) be dealt with by introducing additional switching instances. Practical disadvantages are that modeling errors can easily result in significant residual vibrations, while the actuator will almost constantly operate in saturation mode and a large number of switching moments between extreme values may reduce the life-time of the actuator (De Roover, 1997). This can partially be overcome by the use of *e.g.* an input synthesis technique such as *limited jerk profiles*. These are smoothened forcing functions that reduce the excitation of high-frequency modes. One can also use an input filtering technique such as notch filtering or inverse plant dynamics filtering.

Early in the detailed design stage, we only have simple plant models available. The consequence is that the design of a forcing function is also relative simple. Often

the use of this simple model is also sufficient. Rankers (1997) indicated that in many industrial control systems, the model assumes that the electromechanical plant behaves as one rigid body on which Coulomb and viscous forces are applied by the guiding systems. Thus the simple design used early in the design process can partially be maintained during realization of the system. Rankers (1997) indicates that tuning of the parameters of this feedforward component is generally quite straightforward, as in most cases it only involves an estimation of the total moving mass and experimental determination of coulomb and viscous friction effects of the plant.

We will consider this relative simple design of the forcing function, *i.e.* the design of a feedforward component and a reference path generator, as generally the resulting performance is good enough. However, we will do this in the light of the design philosophy of section 3.2.1, in order to make clear how to modify and reuse the design when more advanced techniques are to be applied. An existing design can be improved upon by means of, for example, input filtering techniques, where we reuse the control signal of the existing design as the required *a priori* control signal.

The block diagram of figure 3.1, can easily be manipulated such that we obtain the more familiar configuration of figure 3.11.

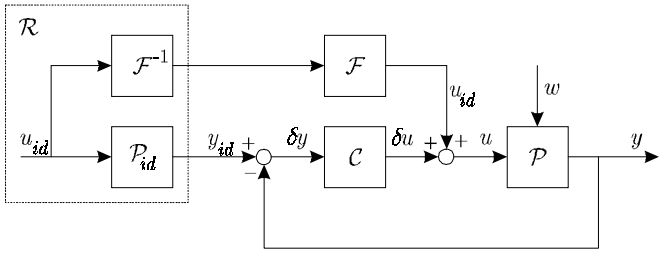

FIGURE 3.11 *Alternative implementation of ideal and uncertain part*

The variables in this figure are those used in the design philosophy. When we compare this diagram with the control configuration of figure 3.3, we see that the ideal input u_{id} corresponds to the forcing function u_{f} and the ideal output y_{id} corresponds to the reference path r. When $\mathcal{P}_{\mathrm{id}}$ is described by:

$$\mathcal{P}_{\mathrm{id}}: \quad P_{\mathrm{id}}(s) = \frac{1}{ms^2} \tag{3.34}$$

and the feedforward component $\mathcal{F}$ contains the total mass to be moved m, we obtain the well-known situation of acceleration feedforward. The reference path generator $\mathcal{R}$ contains a component $\mathcal{F}^{-1}$, which now equals m^{-1}. In practical situations $\mathcal{F}$ may be extended with additional dynamics, *e.g.* inverse dynamics

filtering, while the reference path generator is unaltered, *i.e.* $\mathcal{F}^{-1}$ still equals m^{-1} and $\mathcal{P}_{\text{id}}$ is described by (3.34).

The development of a reference path generator from the forcing function is thus easily accomplished by utilizing the rigid body mode of the plant (Meckl, 1994). Application of the bang-bang forcing function to a simple mass will result in a second-degree reference path, as the model $\mathcal{P}_{\text{id}}$ essentially is a double integrator. When a limited jerk profile is used in this situation, we obtain a third-degree reference path. Here, we see the relation with the reference paths used in the previous chapter.

The situation in figure 3.11 can thus be viewed upon as acceleration feedforward. Additionally, velocity feedforward is sometimes used to improve the performance of the system. This kind of feedforward is attractive when a PID *controller* configuration is used (refer figure 3.4). When the corresponding feedforward component is identical to the feedback component in the position loop y_2, this configuration can be rewritten as a PID compensator. In section 3.2.2 we indicated that in the controller configuration, the ideal velocity trajectory is implicitly chosen zero. When we use velocity feedforward, we actually provide a more realistic ideal trajectory that is in agreement with the ideal trajectory for the measured position. In (Groenhuis, 1991) a comparison is made of different feedforward components for a flexible mechanism, using the controller configuration in the feedback component. These simulation results indicate that when a feedforward component is used in combination with a PID controller configuration, the addition of a velocity feedforward will further improve the performance. This confirms the ideas presented in the design philosophy.

The design of the forcing function in the structured design method will depend on the amount of detail in the plant model. Initially, a simple design will suffice, which may gradually be improved upon.

- Start with a moving mass model for $\mathcal{P}_{\text{id}}$ and use a bang-bang force profile when a second-degree reference path was initially used or a limited jerk profile when a third-degree reference path was used.
- Always add velocity feedforward to acceleration feedforward in case the feedback component consists of a PID *controller* configuration.
- When suffering from residual vibrations of high-frequency modes, use a limited jerk profile instead of a bang-bang profile.
- Use notch filtering or inverse dynamics filtering in $\mathcal{F}$ to reduce residual vibrations of the lower vibration modes.
- When the design is materialized or when an indication of viscous and Coulomb friction are available, incorporate this knowledge in the $\mathcal{F}$.

When this is not sufficient, one can incorporate more extensive plant knowledge in the design of the forcing function and the generation of the reference path via $\mathcal{P}_{\text{id}}$.

This is out of the scope of this thesis and we refer to (De Roover, 1997) for these techniques. Alternatively, one can use modern techniques as Iterative Learning Control (ILC) (Bien and Xu, 1998) or Learning FeedForward Control (LFFC) (Velthuis, 2000), (Otten *et al.*, 1997). Advantages of these techniques are that only a limited amount of *a priori* plant knowledge is required to obtain high performance.

3.5 Disturbance observer design

An important reason for the use of feedback is the attenuation of disturbances. Disturbances in practical control systems can be divided in two categories. The first category contains stochastic disturbances, which are normally characterized by statistical properties, such as mean value, covariance and power spectral density. The second category contains waveform-structured signals, which show distinguishable patterns, at least over short time intervals. In this section we focus on waveform-structured signals $\mathcal{W}$, as these are appropriate to describe important disturbances in electromechanical systems and can explicitly be incorporated in the design of the control system.

The internal model principle (IMP) states that "a regulator is structurally stable only if the controller utilizes feedback of the regulated variable, and incorporates in the feedback path a suitably reduplicated model of the dynamic structure of the exogenous signals, which the regulator is required to process" (Francis and Wonham, 1976). *I.e.*, a feedback component has to include an internal model of the dynamics of the disturbance it tries to attenuate. A controller structure that includes such a model is the disturbance observer (Johnson, 1971). In this section we will derive a design procedure for a disturbance observer, as a part of the control configuration of figure 3.3. Theory on waveform-mode descriptions of realistic disturbances is given in appendix B, which describes how disturbance w, consisting of linear waveform descriptions, can be interpreted as the output of an autonomous system (figure 3.12), subject to a set of initial conditions, according to:

$$\begin{aligned} \dot{x}_w &= A_w \cdot x_w, \quad x_w(t_0) = x_{w0} \\ w &= C_w \cdot x_w \end{aligned} \tag{3.35}$$

where $x_w \in \mathbb{R}^{x_w}$ is the vector of disturbance states, $w \in \mathbb{R}^w$ is the vector of disturbances. The pair $\{A_w, C_w\}$ constitutes constant matrices with appropriate dimensions, *i.e.* $A_w \in \mathbb{R}^{x_w \times x_w}$, $C \in \mathbb{R}^{w \times x_w}$.

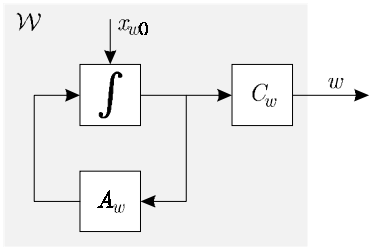

FIGURE 3.12 Disturbance model

3.5.1 Disturbance observer

The general concepts of observer theory have been described extensively in textbooks, such as (Anderson and Moore, 1971), (Kailath, 1980) and (Åström and Wittenmark, 1997). These concepts are also applicable to the disturbance observer.

We assume that the plant $\mathcal{P}$, without disturbances, is linear time-invariant, such that it can be described as:

$$\begin{aligned} \dot{x} &= Ax + Bu \\ z &= Cx + Du \end{aligned} \tag{3.36}$$

where $x \in \mathbb{R}^x$ is the vector of (physical) states, $u \in \mathbb{R}^u$ is the vector of plant inputs and $z \in \mathbb{R}^z$ is the vector of plant outputs. The quadruplet $\{A, B, C, D\}$ constitutes constant matrices with appropriate dimensions. This model can be used to estimate the states:

$$\dot{\hat{x}} = A\hat{x} + Bu \tag{3.37}$$

where $\hat{x} \in \mathbb{R}^{\hat{x}}$ is the vector of estimated states. The estimated state vector $\hat{x}$ will equal the vector of (physical) states x, when both the plant model (3.36) and the estimation (3.37) are driven by the same input. That is, when the plant model is completely correct and the initial conditions are identical. Generally, this will not be the case and an error signal is used to adjust the estimated states. The error signal is the difference between the measured output y and the estimated output and is called the *innovation signal*. This signal is multiplied by the observer gain matrix $L_\mathrm{P} \in \mathbb{R}^{\hat{x} \times y}$. This type of observer is called an asymptotic state observer. When the throughput matrix D is assumed to be zero, we obtain:

$$\dot{\hat{x}} = A\hat{x} + Bu + L_\mathrm{p}(y - C\hat{x}) \tag{3.38}$$

The observer can be augmented with a disturbance model. The state space model of this augmented observer is:

$$\begin{bmatrix} \dot{\hat{x}} \\ \dot{x}_w \end{bmatrix} = \begin{bmatrix} A & BC_w \\ 0 & A_w \end{bmatrix} \begin{bmatrix} \hat{x} \\ x_w \end{bmatrix} + \begin{bmatrix} B \\ 0 \end{bmatrix} u \tag{3.39}$$

Here, we assumed that the disturbance enters at the plant input. Now, the innovation signal is multiplied by the observer gain matrices L_P for the plant states and $L_\mathrm{D} \in \mathbb{R}^{x_w \times y}$ for the states of the disturbance model. In the augmented observer of figure 3.13 the disturbance model and plant model are indicated separately.

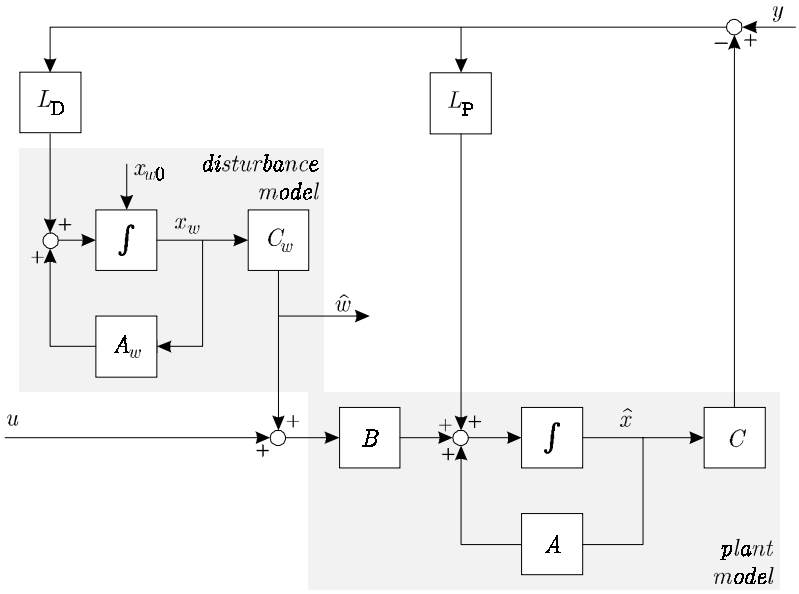

FIGURE 3.13 *Observer with disturbance model*

This observer can again be represented as an asymptotic state observer with the following matrices:

$$A_\mathrm{o} = \begin{bmatrix} A & BC_w \\ 0 & A_w \end{bmatrix},\ B_\mathrm{o} = \begin{bmatrix} B \\ 0 \end{bmatrix},\ C_\mathrm{o} = \begin{bmatrix} C & 0 \end{bmatrix},\ L = \begin{bmatrix} L_\mathrm{P} \\ L_\mathrm{D} \end{bmatrix} \text{and } \hat{x}_\mathrm{o} = \begin{bmatrix} \hat{x} \\ x_w \end{bmatrix} \tag{3.40}$$

and an estimation of the disturbance according:

$$\hat{w} = \begin{bmatrix} 0 & C_w \end{bmatrix} \begin{bmatrix} \hat{x} \\ x_w \end{bmatrix} \tag{3.41}$$

The estimated input disturbance can be used to attenuate the real input disturbance. When only the disturbance estimate, and not the complete estimated

state vector, is fed back, the observer of figure 3.13 is called a *disturbance observer*. This is shown in figure 3.14.

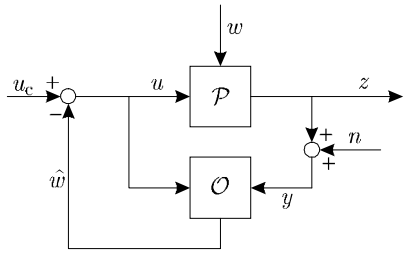

FIGURE 3.14 *Plant with disturbance observer* $\mathcal{O}$

Remark 3.9

The principle of separation also holds for the disturbance observer, therefore the poles of the closed-loop system can be placed independently from the poles of the augmented observer (Profeta et al., 1990).

Remark 3.10

Profeta et al. (1990) also prove that, provided that both $\{A, C\}$ *and* $\{A_w, C_w\}$ *are observable, a vector* $[L_P \; L_D]^T$ *can be found such that the observer poles can be placed substantially anywhere desired, subject to the physical limitations of the system and:*

1. *no pole-zero cancellation takes place (Kailath, 1980), i.e. no eigenvalue of* A_w *is a zero of the plant model the disturbance acts upon.*
2. *the zero frequency gain of the plant must not be zero*

When these conditions are fulfilled, the design of the disturbance observer reduces to a pole-placement problem. The poles have to be placed such that the desired attenuation of the disturbance is obtained.

Now, we will investigate how we can use a disturbance observer in the structured design method. Therefore, we first consider the block diagram of figure 3.14. Within this diagram we will consider four transfer matrices:

1. the transfer matrix from input u_c to output z;
2. the disturbance compensation transfer matrix from disturbance w to output z;
3. the disturbance estimation transfer matrix from disturbance w to the estimated disturbance $\hat{w}$;
4. the transfer matrix from the measurement noise n to the output z.

We will start with the first two transfer matrices. From figure 3.14 we can see that, when we neglect the measurement noise n, the Laplace transform of the output z can be expressed as:

$$Z = P \cdot \left(W + U_{\mathrm{c}} - \hat{W} \right) \tag{3.42}$$

where P is the actual plant transfer matrix. When we replace $\hat{W}$ in (3.42) by an expression in terms of U_{c}, W and Z, using (3.39) - (3.41), we obtain:

$$\begin{aligned} s\hat{X}_{\mathrm{o}} &= A_{\mathrm{o}}\hat{X}_{\mathrm{o}} + B_{\mathrm{o}}\left(U_{\mathrm{c}} - \hat{W}\right) + L\left(Z - C_{\mathrm{o}}\hat{X}_{\mathrm{o}}\right) \\ \hat{W} &= \begin{bmatrix} 0 & C_w \end{bmatrix} \hat{X}_{\mathrm{o}} = G\hat{X}_{\mathrm{o}} \end{aligned} \tag{3.43}$$

This expression can be rewritten as:

$$\begin{aligned} &\left(sI_{x_{\mathrm{o}}} - A_{\mathrm{o}} + LC_{\mathrm{o}} + B_{\mathrm{o}}G \right) \hat{X}_{\mathrm{o}} = B_{\mathrm{o}}U_{\mathrm{c}} + LZ \Leftrightarrow \\ &\hat{X}_{\mathrm{o}} = \left(sI_{x_{\mathrm{o}}} - A_{\mathrm{o}} + LC_{\mathrm{o}} + B_{\mathrm{o}}G \right)^{-1} \left(B_{\mathrm{o}}U_{\mathrm{c}} + LZ \right) \end{aligned} \tag{3.44}$$

where $I_{x_{\mathrm{o}}} \in \mathbb{R}^{x_{\mathrm{o}} \times x_{\mathrm{o}}}$ denotes the unit matrix. Combining (3.42) - (3.44) results in:

$$Z = P\left(W + U_{\mathrm{c}} - G\left(sI_{x_{\mathrm{o}}} - A_{\mathrm{o}} + LC_{\mathrm{o}} + B_{\mathrm{o}}G \right)^{-1} \left(B_{\mathrm{o}}U_{\mathrm{c}} + LZ \right) \right) \tag{3.45}$$

This expression can be written as two separate transfer matrices, *i.e.* from input U_{c} to output Z and from disturbance W to output Z. The transfer matrix that has to be inverted can be rewritten using (3.39):

$$sI_{x_o} - A_{\mathrm{o}} + LC_{\mathrm{o}} + B_{\mathrm{o}}G = \begin{bmatrix} sI_{\hat{x}} - A + L_{\mathrm{P}}C & O \\ L_{\mathrm{D}}C & sI_{x_w} - A_w \end{bmatrix} \tag{3.46}$$

The inverse of this block matrix can be determined using (Kailath, 1980):

$$\begin{bmatrix} Q & O \\ W & V \end{bmatrix}^{-1} = \begin{bmatrix} Q^{-1} & O \\ -V^{-1}WQ^{-1} & V^{-1} \end{bmatrix} \tag{3.47}$$

provided Q^{-1} and V^{-1} exist. Application to the matrix (3.46) results in:

$$\begin{bmatrix} \left(sI_{\hat{x}} - A + L_{\mathrm{P}}C \right)^{-1} & 0 \\ -\left(sI_{x_w} - A_w \right)^{-1} L_{\mathrm{D}}C \left(sI_{\hat{x}} - A + L_{\mathrm{P}}C \right)^{-1} & \left(sI_{x_w} - A_w \right)^{-1} \end{bmatrix} \tag{3.48}$$

Additionally, we use the well-known matrix identity (Kailath, 1980):

$$\left(I_y - C\left(sI_{\hat{x}} - A \right)^{-1} L_{\mathrm{P}} \right)^{-1} = I_y - C\left(sI_{\hat{x}} - A + L_{\mathrm{P}}C \right)^{-1} L_{\mathrm{P}} \tag{3.49}$$

Substitution of (3.49) and (3.48) into (3.45) leads to the first two desired transfer matrices. From input U_c to output Z:

$$Z = (I_z + PE)^{-1} P\big(I_w + EC\big(sI_{\hat{x}} - A\big)B\big)U_c \tag{3.50}$$

and from disturbance W to output Z:

$$Z = (I_z + PE)^{-1} PW \tag{3.51}$$

where

$$E = \big(C_w(sI_w - A_w)^{-1} L_D\big)\big(I_z + C\big(sI_{\hat{x}} - A\big)L_P\big)^{-1} \tag{3.52}$$

which is the transfer matrix from Z to $\hat{W}$, *i.e.* the *observer transfer matrix.*

When we compose expressions (3.50) and (3.52), we obtain the third transfer matrix, from W to $\hat{W}$:

$$\hat{W} = E(I_z + PE)^{-1} P \cdot W \tag{3.53}$$

and the fourth transfer matrix from N to Z:

$$Z = -(I_z + PE)^{-1} PE \cdot N \tag{3.54}$$

When we consider the transfer matrices above, we recognize two standard transfer matrices:

$$S_o = (I_z + PE)^{-1} \tag{3.55}$$

$$T_o = (I_z + PE)^{-1} PE \tag{3.56}$$

where S_o is called the *observer sensitivity function* and T_o the *complementary observer sensitivity function.*

Expression (3.50) shows that a disturbance observer has no influence on the transfer matrix from input U_c to output z when the plant is modeled correctly, *i.e.* when:

$$P = C\big(sI_{\hat{x}} - A\big)^{-1} B \tag{3.57}$$

The observer sensitivity function is the transfer matrix from the output disturbance w_{out} to the output z. So far, we have only considered input disturbances. However, as the system is presumed to be linear, the input disturbance w can easily be rewritten to an output disturbance w_{out}:

$$W_{out} = PW \tag{3.58}$$

Hence, we obtain a familiar expression:

$$Z = (I_z + PE)^{-1} PW = S_o W_{out} \tag{3.59}$$

We also shortly investigate the influence of modeling errors. We write the plant as:

$$P = P_0 + \Delta \tag{3.60}$$

where

$$P_0 = C\left(sI_{\hat{x}} - A\right)^{-1} B \tag{3.61}$$

P_0 stands for the nominal plant transfer matrix that is incorporated in the observer and Δ is the modeling error, *i.e.* the *unstructured uncertainty*. When we assume $w = 0$, we can write (3.50) as:

$$Z = (I_z + PE)^{-1} PU_c + (I_z + PE)^{-1} PEP_0 U_c \tag{3.62}$$

Rewriting, and using the fact that $S_o + T_o = I$ gives:

$$Z = \left(S_o P + T_o P_0\right) U_c = \left(P_0 + S_o \Delta\right) U_c \tag{3.63}$$

We know that the sensitivity function S_o is small at low frequencies and close to one at high frequencies. This means that, at low frequencies, the feedback component sees a plant with a dynamic behavior equal to the dynamic behavior of the nominal plant transfer matrix P_0. At high frequencies, the observer cannot influence the plant anymore and the original plant transfer matrix is again obtained. As always, the indefinite region is the crossover region, where the behavior of the plant, as seen by the feedback component, will be a transition from the observer model P_0 to the real plant P.

Statement 3.2

The plant with disturbance observer, seen by the feedback component, behaves as the model of the plant in the disturbance observer P_0, in the frequency range where the disturbance observer is active, i.e. where $|S_o| \ll 1$.

When we combine (3.50) and (3.59) and we disregard measurement noise, we obtain an expression for the output Z, according figure 3.14:

$$Z = (I_z + PE)^{-1} P\left(I_w + EC\left(sI_{\hat{x}} - A\right)B\right)U_c + (I_z + PE)^{-1} W_{out} \tag{3.64}$$

When we close the loop with the feedback component C, and assume $r = 0$, we obtain:

$$Z = (I_z + PE)^{-1} P\left(I_w + EC\left(sI_{\hat{x}} - A\right)B\right)(-CZ) + (I_z + PE)^{-1} W_{out} \tag{3.65}$$

When the plant is modeled correctly, *i.e.* equality (3.57) holds, this expression can be rewritten as:

$$Z = -PCZ + (I_z + PE)^{-1} W_{\text{out}} \tag{3.66}$$

Thus the sensitivity function of the overall control configuration can be written as:

$$\begin{aligned} Z &= (I_z + PC)^{-1} (I_z + PE)^{-1} W_{\text{out}} \\ &= S_{\text{c}} \cdot S_{\text{o}} \cdot W_{\text{out}} \end{aligned} \tag{3.67}$$

Thus:

$$S = S_{\text{c}} \cdot S_{\text{o}} \tag{3.68}$$

where S_{c} is the sensitivity function of the control configuration with only a feedback component, *i.e.* a 1-DOF or 1-CC controller, and S is the sensitivity function of the control configuration with both a feedback component and a disturbance compensator.

Statement 3.3 Separation of sensitivity functions

The sensitivity function S of the overall control configuration can be obtained from a multiplication of the sensitivity function S_{c}, of the closed-loop with only a feedback component, and the observer sensitivity function S_{o}, when the plant is modeled correctly.

Similarly, we can investigate the influence of the measurement noise N. When we assume the input disturbance W to be zero, we can write for the output Z:

$$Z = (I_z + PE)^{-1} P\big(I_w + EC\big(sI_{\hat{x}} - A\big)B\big)U - (I_z + PE)^{-1} PEN \tag{3.69}$$

When we again close the loop with the feedback component C and assume $r = 0$, we obtain:

$$\begin{aligned} Z = {} & (I_z + PE)^{-1} P\big(I_w + EC\big(sI_{\hat{x}} - A\big)B\big)(-CZ - CN) \\ & - (I_z + PE)^{-1} PEN \end{aligned} \tag{3.70}$$

When the plant is modeled correctly, *i.e.* equality (3.57) holds, this expression can be rewritten as:

$$Z = -PCZ - PCN - (I_z + PE)^{-1} PEN \tag{3.71}$$

The measurement noise attenuation of the overall control configuration can be written as:

$$\begin{aligned} Z &= (I_z + PC)^{-1}\left(-PC - (I_z + PE)^{-1}PE\right)N \\ &= -(T_\mathrm{c} + S_\mathrm{c}T_\mathrm{o})N \end{aligned} \tag{3.72}$$

The disturbance observer does not affect the measurement noise attenuation of the closed-loop system according $-T_\mathrm{c}$, under the condition that the product of the sensitivity function S_c and the complementary observer sensitivity function T_o is small compared to T_c.

3.5.2 Design issues

In the structured design method, the disturbance observer will only be designed when a feedback component is already available. In the PID design procedure, the specifications for disturbance attenuation were expressed in terms of the input sensitivity function $S_\mathrm{wz}(s)$. With respect to disturbance attenuation, we stated that $|S_\mathrm{wz}(j\omega)| < s_\mathrm{l}$ for $\omega < \omega_\mathrm{l}$. For the design of the disturbance observer, we will use the same specifications, thus requiring minimal information about the actual characteristics of the disturbances. The observer should sufficiently attenuate every possible disturbance, not a specific waveform, up to a certain frequency ω_l.

From (3.67), we can derive an expression for the input sensitivity function of the control configuration with disturbance observer. For SISO systems we can write:

$$Z = S_\mathrm{o}S_\mathrm{c}PW = S_\mathrm{o}S_\mathrm{c,wz}W = S_\mathrm{wz}W \tag{3.73}$$

where $S_\mathrm{c,wz}$ is the input sensitivity function of the control configuration with only a feedback component. The observer sensitivity function is:

$$S_\mathrm{o} = \frac{1}{1+PE} = \frac{1 + C\left(sI_{\hat{x}} - A\right)^{-1}L_\mathrm{P}}{1 + C\left(sI_{\hat{x}} - A\right)^{-1}L_\mathrm{P} + P(s)C_w\left(sI_{x_w} - A_w\right)^{-1}L_\mathrm{D}} \tag{3.74}$$

The feedback component, in the 1-DOF configuration, will give a certain suppression of low-frequency disturbances, expressed in the magnitude of the input sensitivity function $S_\mathrm{c,wz}$. When this is insufficient, a disturbance observer can introduce an additional attenuation factor, according (3.67):

$$|S_\mathrm{wz}(j\omega)| = \left|S_\mathrm{c,wz}(j\omega)\right| + |S_\mathrm{o}(j\omega)| \quad [\mathrm{dB}] \tag{3.75}$$

For the observer sensitivity function this means that:

$$|S_\mathrm{o}(j\omega)| < \left(s_\mathrm{l} - \left|S_\mathrm{c,wz}\left(j\omega_\mathrm{l}\right)\right|\right) = \sigma\,[\mathrm{dB}] \quad \text{for } \omega < \omega_\mathrm{l} \tag{3.76}$$

Remark 3.11

The designer should be well aware that, due to the Bode sensitivity integral, an extra suppression at low frequencies will result in extra gain at other frequencies.

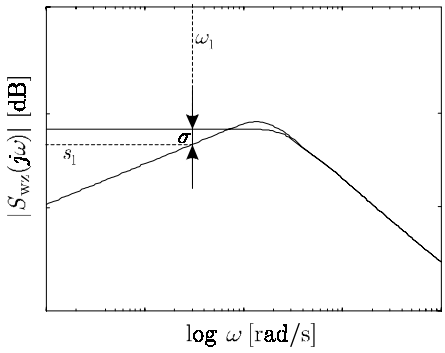

FIGURE 3.15 *Extra disturbance suppression due to disturbance observer*

In order to give the observer sensitivity function, and thus the overall input sensitivity function S_{wz}, the specified characteristics, we will place all poles of the observer sensitivity function at frequency ω_σ. The coefficients of the characteristic polynomial of S_o:

$$\chi(s) = s^n + a_{n-1}\omega_\sigma s^{n-1} + \cdots + a_1\omega_\sigma^{n-1}s + \omega_\sigma^n \tag{3.77}$$

will be chosen such that we obtain a Butterworth polynomial or that its roots are all located at $-\omega_\sigma$.

Consequently, the observer sensitivity function will peak at about this frequency. The low-frequency slope of the observer sensitivity function is determined by the order of the disturbance model; a disturbance model of order k results in a slope of $20{\cdot}k$ [dB/decade]. When a Butterworth polynomial is used, the peak of the sensitivity function at ω_σ occurs at about twice the frequency of the crossing of the 0 dB-line. When the poles are placed on the real axis this ratio c is about 3. These observations allow for an approximate frequency ω_σ for the poles of the observer:

$$\omega_\sigma \approx c \cdot \omega_1 \cdot 10^{\frac{\sigma}{20k}} \tag{3.78}$$

This expression shows a trade-off between the order k of the disturbance model and the frequency ω_σ. Experience learned that k should generally not be chosen larger than 3. The frequency ω_σ can also not be increased infinitely. When the peak of the observer sensitivity function S_o is located close to the peak of $S_{c,wz}$, the disturbance observer will interfere with the feedback component. This occurs when ω_σ approximates $2\cdot\omega_b$. When ω_σ is much smaller, the sensitivity function $S_{c,wz}$ will

damp the peak of the observer sensitivity function. As a rule of thumb we state that ω_σ should be smaller than $0.5 \cdot \omega_b$.

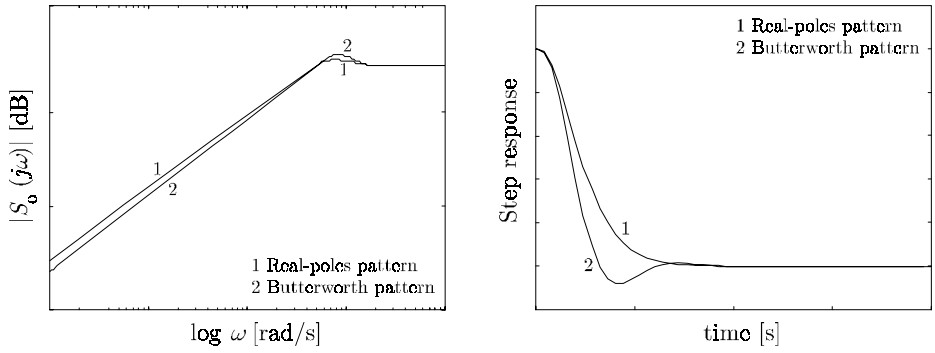

FIGURE 3.16 *Real-poles versus Butterworth pattern*

In figure 3.16 the difference between a real-poles pattern and a Butterworth pattern is illustrated. When the poles are placed on the real axis, we see a relative small peak in the observer sensitivity function and a relative well-damped step response. A Butterworth pattern gives better attenuation in the low-frequency area.

We will now derive expressions for the observer gains, in order to support the designer with well-chosen defaults (Waarsing, 1999). These expressions are determined for plant models without damping. During actual application of the disturbance observer, damping should be incorporated in the plant model. Within limits, the default observer gains can be reused. Otherwise, new values have to be determined, for example using Matlab.

3.5.3 Design of a disturbance observer

Second-order plant models

First we consider the situation that the plant is modeled as a second-order system, *i.e.* a moving mass. The observer transfer matrix (3.52) can be rewritten, using the disturbance model (refer appendix B):

$$\begin{aligned}
\begin{bmatrix} \dot{x}_{w1} \\ \dot{x}_{w2} \\ \vdots \\ \dot{x}_{wk} \end{bmatrix} &= \begin{bmatrix} 0 & 1 & & 0 \\ \vdots & & \ddots & \vdots \\ 0 & 0 & & 1 \\ 0 & 0 & \cdots & 0 \end{bmatrix} \cdot \begin{bmatrix} x_{w1} \\ x_{w2} \\ \vdots \\ x_{wk} \end{bmatrix}, \quad x_w(t_0) = x_{w0} \\
w(t) &= \begin{bmatrix} 1 & 0 & \cdots & 0 \end{bmatrix} \cdot \begin{bmatrix} x_{w1} & x_{w2} & \cdots & x_{wk} \end{bmatrix}^T
\end{aligned} \tag{3.79}$$

and a state space description of the second-order plant:

$$\begin{aligned}
\dot{x} &= Ax + Bu = \begin{bmatrix} 0 & 1 \\ 0 & 0 \end{bmatrix} x + \begin{bmatrix} 0 \\ \dfrac{1}{m} \end{bmatrix} u \\
y &= Cx + Du = \begin{bmatrix} 1 & 0 \end{bmatrix} x
\end{aligned} \tag{3.80}$$

where the states are the velocity respectively the position of the moving mass. This results in:

$$E(s) = \frac{\displaystyle\sum_{i=1}^{k} L_{\mathrm{D},i} s^{-i}}{1 + \displaystyle\sum_{j=1}^{2} L_{\mathrm{P},j} s^{-j}} = \frac{s^2 \displaystyle\sum_{i=1}^{k} L_{\mathrm{D},i} s^{-i}}{s^2 + L_{\mathrm{P},1} s + L_{\mathrm{P},2}} \tag{3.81}$$

where, k is the order of the disturbance model.

$$S_{\mathrm{o}}(s) = \frac{1}{1 + P(s)E(s)} = \frac{m s^2 \left(s^2 + L_{\mathrm{P},1} s + L_{\mathrm{P},2} \right)}{m s^2 \left(s^2 + L_{\mathrm{P},1} s + L_{\mathrm{P},2} \right) + s^2 \displaystyle\sum_{i=1}^{k} L_{\mathrm{D},i} s^{-i}} \tag{3.82}$$

Here, both the plant $\mathcal{P}$ and the plant model in the observer are modeled as a moving mass, *i.e.* equality (3.57) holds. Rewriting gives:

$$S_{\mathrm{o}}(s) = \frac{m \left(s^{k+2} + L_{\mathrm{P},1} s^{k+1} + L_{\mathrm{P},2} s^k \right)}{m \left(s^{k+2} + L_{\mathrm{P},1} s^{k+1} + L_{\mathrm{P},2} s^k \right) + \displaystyle\sum_{i=1}^{k} L_{\mathrm{D},i} s^{k-i}} \tag{3.83}$$

In order to place the poles at desired positions, we have to make the characteristic polynomial monic:

$$\chi(s) = \left(s^{k+2} + L_{\mathrm{P},1} s^{k+1} + L_{\mathrm{P},2} s^k \right) + \frac{1}{m} \sum_{i=1}^{k} L_{\mathrm{D},i} s^{k-i} \tag{3.84}$$

k	$L = [L_\mathrm{P}\ L_\mathrm{D}]^T$
1	$L = \begin{bmatrix} \chi_2 & \chi_1 & m\chi_0 \end{bmatrix}^T$
2	$L = \begin{bmatrix} \chi_3 & \chi_2 & m\chi_1 & m\chi_0 \end{bmatrix}^T$
3	$L = \begin{bmatrix} \chi_4 & \chi_3 & m\chi_2 & m\chi_1 & m\chi_0 \end{bmatrix}^T$

TABLE 3.4 *Observer gains*

We can rewrite the characteristic polynomial as:

$$\chi(s) = s^{k+2} + \chi_{k+1}s^{k+1} + \cdots + \chi_0 \tag{3.85}$$

Using the observer gain vector L, we can place the roots of $\chi(s)$ at desired locations (3.78). The coefficients of the characteristic polynomials and thus the observer gains (table 3.4) can be chosen according a real-pole pattern (table 3.5) or a Butterworth pattern (table 3.6).

$n + k$	$(\, s + \omega_\sigma \,)^{k+2}$
3	$s^3 + 3\omega_\sigma s^3 + 3\omega_\sigma^2 s + \omega_\sigma^3$
4	$s^4 + 4\omega_\sigma s^3 + 6\omega_\sigma^2 s^2 + 4\omega_\sigma^3 s + \omega_\sigma^4$
5	$s^5 + 5\omega_\sigma s^4 + 10\omega_\sigma^2 s^3 + 10\omega_\sigma^3 s^2 + 5\omega_\sigma^4 s + \omega_\sigma^5$
6	$s^6 + 6\omega_\sigma s^5 + 15\omega_\sigma^2 s^4 + 20\omega_\sigma^3 s^3 + 15\omega_\sigma^4 s^2 + 6\omega_\sigma^5 s + \omega_\sigma^6$
7	$s^7 + 7\omega_\sigma s^6 + 21\omega_\sigma^2 s^5 + 35\omega_\sigma^3 s^4 + 35\omega_\sigma^4 s^3 + 21\omega_\sigma^5 s^2 + 7\omega_\sigma^6 s + \omega_\sigma^7$

TABLE 3.5 *Real-pole polynomials*

$n+k$	Butterworth polynomial
3	$s^3 + 2\omega_\sigma s^3 + 2\omega_\sigma^2 s + \omega_\sigma^3$
4	$s^4 + 2.6\omega_\sigma s^3 + 3.4\omega_\sigma^2 s^2 + 2.6\omega_\sigma^3 s + \omega_\sigma^4$
5	$s^5 + 3.24\omega_\sigma s^4 + 5.24\omega_\sigma^2 s^3 + 5.24\omega_\sigma^3 s^2 + 3.24\omega_\sigma^4 s + \omega_\sigma^5$
6	$s^6 + 3.86\omega_\sigma s^5 + 7.46\omega_\sigma^2 s^4 + 9.14\omega_\sigma^3 s^3 + 7.46\omega_\sigma^4 s^2 + 3.86\omega_\sigma^5 s + \omega_\sigma^6$
7	$s^7 + 4.49\omega_\sigma s^6 + 10.1\omega_\sigma^2 s^5 + 14.6\omega_\sigma^3 s^4 + 14.6\omega_\sigma^4 s^3 + 10.1\omega_\sigma^5 s^2 + 4.49\omega_\sigma^6 s + \omega_\sigma^7$

TABLE 3.6 *Butterworth polynomials*

Fourth-order plant models

In deriving the observer gains in the previous section, we used a state space description of the plant model. To improve transparency, it is wise to use physical quantities as position and velocity as state variables, *e.g.* (3.80). For fourth-order models it is attractive to use the position and velocity of both the motor mass and the end-effector mass. However, this will not give a unique disturbance observer for all classes of fourth-order models, as there is no unique state space description. As an example we will describe the derivation of the observer gains for the *flexible mechanism*, with position measurement at the motor, *i.e.* concept *AR*.

The state space description of the flexible mechanism is:

$$\begin{bmatrix} \dot{x}_1 \\ \ddot{x}_1 \\ \dot{x}_2 \\ \ddot{x}_2 \end{bmatrix} = \begin{bmatrix} 0 & 1 & 0 & 0 \\ -\omega_{\mathrm{ar}}^2 & 0 & \omega_{\mathrm{ar}}^2 & 0 \\ 0 & 0 & 0 & 1 \\ \omega_{\mathrm{r}}^2 - \omega_{\mathrm{ar}}^2 & 0 & \omega_{\mathrm{ar}}^2 - \omega_{\mathrm{r}}^2 & 0 \end{bmatrix} \begin{bmatrix} x_1 \\ \dot{x}_1 \\ x_2 \\ \dot{x}_2 \end{bmatrix} + \begin{bmatrix} 0 \\ 0 \\ 0 \\ \dfrac{\omega_{\mathrm{r}}^2}{m\omega_{\mathrm{ar}}^2} \end{bmatrix} u$$
$$y_1 = \begin{bmatrix} 1 & 0 & 0 & 0 \end{bmatrix} x \tag{3.86}$$
$$y_2 = \begin{bmatrix} 0 & 0 & 1 & 0 \end{bmatrix} x$$

where x_1 is the end-effector position and x_2 the motor position. The transfer function from the measured motor position y_1 to the estimated disturbance can be written as:

$$E(s) = \frac{s^2\left(s^2 + \omega_{\mathrm{r}}^2\right)\sum_{i=1}^{k} L_{\mathrm{D},i}s^{-i}}{\sum_{j=0}^{4} c_j s^j} \tag{3.87}$$

where, k is again the order of the disturbance model and the coefficients c_j, for the flexible mechanism are given in table 3.7.

j	c_j
0	$L_{\mathrm{P},2}\left(\omega_{\mathrm{r}}^2 - \omega_{\mathrm{ar}}^2\right) + L_{\mathrm{P},4}\omega_{\mathrm{ar}}^2$
1	$L_{\mathrm{P},1}\left(\omega_{\mathrm{r}}^2 - \omega_{\mathrm{ar}}^2\right) + L_{\mathrm{P},3}\omega_{\mathrm{ar}}^2$
2	$L_{\mathrm{P},4} + \omega_{\mathrm{r}}^2$
3	$L_{\mathrm{P},3}$
4	1

TABLE 3.7 *Coefficients for flexible mechanism*

The observer sensitivity function is:

$$S_{\mathrm{o}}(s) = \frac{m\omega_{\mathrm{ar}}^2 s^2\left(s^2 + \omega_{\mathrm{r}}^2\right)\sum_{j=0}^{4} c_j s^j}{m\omega_{\mathrm{ar}}^2 s^2\left(s^2 + \omega_{\mathrm{r}}^2\right)\sum_{j=0}^{4} c_j s^j + \left(s^2 + \omega_{\mathrm{ar}}^2\right)\omega_{\mathrm{r}}^2 s^2\left(s^2 + \omega_{\mathrm{r}}^2\right)\sum_{i=1}^{k} L_{\mathrm{D},i}s^{-i}} \tag{3.88}$$

Both the plant $\mathcal{P}$ and the plant model $P_0(s)$ in the observer are modeled as a flexible mechanism, *i.e.* equality (3.57) holds. Rewriting gives:

$$S_{\mathrm{o}}(s) = \frac{m\omega_{\mathrm{ar}}^2 \sum_{j=0}^{4} c_j s^{k+j}}{m\omega_{\mathrm{ar}}^2 \sum_{j=0}^{4} c_j s^{k+j} + \left(s^2 + \omega_{\mathrm{ar}}^2\right)\omega_{\mathrm{r}}^2 \sum_{i=1}^{k} L_{\mathrm{D},i}s^{k-i}} \tag{3.89}$$

In order to place the poles at desired positions, we again make the characteristic polynomial monic:

$$\chi(s) = \sum_{j=0}^{4} c_j s^{k+j} + \frac{\omega_{\mathrm{r}}^2}{m\omega_{\mathrm{ar}}^2}\left(s^2 + \omega_{\mathrm{ar}}^2\right)\sum_{i=1}^{k} L_{\mathrm{D},i}\, s^{k-i} \tag{3.90}$$

Similar as for second-order plant models, we can place the roots of $\chi(s)$ at desired locations (table 3.5 and table 3.6) by means of the observer gain vector L. The expressions for the observer gains are more complex when fourth-order plant models are used. For a first- and second-order disturbance model we obtain, respectively:

$$L = \begin{bmatrix} \dfrac{\chi_4\omega_{\mathrm{ar}}^4 - \chi_2\omega_{\mathrm{ar}}^2 + \chi_0}{\omega_{\mathrm{ar}}^2\left(\omega_{\mathrm{ar}}^2 - \omega_{\mathrm{r}}^2\right)} \\ \dfrac{\chi_3\omega_{\mathrm{ar}}^4 - \omega_{\mathrm{r}}^2\omega_{\mathrm{ar}}^2 - \chi_1\omega_{\mathrm{ar}}^2}{\omega_{\mathrm{ar}}^2\left(\omega_{\mathrm{ar}}^2 - \omega_{\mathrm{r}}^2\right)} \\ \chi_4 \\ \chi_3 - \omega_{\mathrm{r}}^2 \\ \dfrac{\chi_0 m}{\omega_{\mathrm{r}}^2} \end{bmatrix}, \quad L = \begin{bmatrix} \dfrac{\chi_5\omega_{\mathrm{ar}}^4 - \chi_3\omega_{\mathrm{ar}}^2 + \chi_1}{\omega_{\mathrm{ar}}^2\left(\omega_{\mathrm{ar}}^2 - \omega_{\mathrm{r}}^2\right)} \\ \dfrac{\chi_4\omega_{\mathrm{ar}}^4 - \omega_{\mathrm{r}}^2\omega_{\mathrm{ar}}^4 + \chi_2\omega_{\mathrm{ar}}^2 + \chi_0}{\omega_{\mathrm{ar}}^2\left(\omega_{\mathrm{ar}}^2 - \omega_{\mathrm{r}}^2\right)} \\ \chi_5 \\ \chi_4 - \omega_{\mathrm{r}}^2 \\ \dfrac{\chi_1 m}{\omega_{\mathrm{r}}^2} \\ \dfrac{\chi_0 m}{\omega_{\mathrm{r}}^2} \end{bmatrix} \tag{3.91}$$

Design procedure

Now, we will summarize the design procedure for the disturbance observer. We assume that the procedure will be used after the design of the feedback component, *e.g.* according design procedure 3.1. It is wise to use a feedback component without integral action, as the disturbance observer will incorporate one or more integral actions. The disturbance observer is required when the disturbance attenuation of the feedback component is not sufficient. The overall specification for input disturbance attenuation is: $|S_{\mathrm{wz}}(s)| < s_{\mathrm{l}}$ for $\omega < \omega_{\mathrm{l}}$.

Design Procedure 3.2 Disturbance observer design

1. *Identify the order of the plant n and determine the appropriate state-space model of the plant.*
2. *Set the order of the disturbance observer k to* 1.
3. *Determine the suppression provided by the feedback component,* $|S_{\mathrm{c,wz}}(j\omega_{\mathrm{l}})|$.
4. *Determine the suppression required of the disturbance observer:*

   $$\sigma = s_{\mathrm{l}} - \left|S_{\mathrm{c,wz}}\left(j\omega_{\mathrm{l}}\right)\right|$$

5. *Select a real-pole polynomial or a Butterworth polynomial of order n+k from table 3.5 respectively table 3.6.*

6. *Determine the location of the observer poles in terms of the frequency* ω_σ *using:*

$$\omega_\sigma \approx c \cdot \omega_l \cdot 10^{\frac{\sigma}{20k}}$$

where c *is* 3 *for a real-pole polynomial and* 2 *for a Butterworth polynomial.*

7. *Verify whether:*

$$\omega_\sigma < 0.5 \cdot \omega_b$$

If not, increase k *and go to step* 5*. Note,* k *is usually not larger than* 3*, if this is still not sufficient, the bandwidth* ω_b *should be reconsidered.*

8. *Determine the observer gain* L*.*

3.6 Library of control systems

In the first chapter we argued that the formalized design knowledge should be incorporated in computer-based support, in order to enhance the design process. We will do so in the form of a library of control systems. As we advocate a mechatronic design approach, there will be a close relation between the design of the control system and model building. Therefore, we will apply the approach described in (De Vries *et al.*, 1993), (De Vries, 1994) and (Nilsson, 1993) for model building, *polymorphic modeling*, to the formalized design knowledge described in this chapter. The basic idea of polymorphism will first be reviewed shortly. The results of the work of De Vries have been implemented in the mechatronic design environment 20-sim (Controllab Products, 2000), which we will also use for our purpose.

3.6.1 Polymorphism

An important characteristic of both model building and control system design is that these are recursive and interactive processes. The global direction is downwards: one usually starts with decomposing the top level system into subsystems, and in the next step it is further developed by decomposing these subsystems again (De Vries, 1994). The heart of this process is formed by three aspects (De Vries and Breedveld, 1992) that are addressed simultaneously:

- the *decomposition* of the system into interrelated subsystems
- the *classification* of these subsystems and relations
- the *representation* of the resulting model

In order to enable the use of powerful decomposition, classification and representation concepts, a new concept for model building was introduced:

Definition 3.7 Polymorphic modeling

> *Polymorphic modeling is the combined application of modularization and subtyping during model building, i.e., the division of a subsystem description into a subsystems type and a subsystem specification, and the expression of a subsystem type in terms of one or more designated other types (De Vries, 1994).*

Polymorphic modeling introduces an abstraction barrier between *essential properties* and *incidental properties* of a subsystem. Essential properties are typical of a subsystem, *i.e.*, those properties that are necessary for the classification of a subsystem. Incidental properties are not typical and may take varying form. The key issue is that incidental properties are not part of the subsystem *type*, but are part of the subsystem *specification*. As a consequence, one type may have several specifications.

This polymorphic modeling approach is useful as (De Vries, 1994):
- it improves classification of subsystems by means of generic as well as specific typing;
- it completes representation of models by separately depicting essential and incidental characteristics;
- it further enhances reuse, because subsystem types and subsystem specifications can be reused separately;
- it enables a subsystem library to be organized in a kind-of-hierarchy, such that subsystems are typed (classified) incrementally downwards.

We will use polymorphism to come to a hierarchical library of control systems.

3.6.2 Hierarchical subsystem library

In this section we will propose a type hierarchy and for each type we will list some relevant specifications. De Vries (1994) suggests several rules for building a hierarchical subsystem library. An important rule states that it is preferable to first subtype according to connection characteristics and then to structural characteristics. When we apply this rule to the control configuration of figure 3.3, we obtain the hierarchy as in figure 3.17, where some specifications of $\mathcal{R}$ and $\mathcal{O}$ are already indicated. We will discuss the hierarchy per branch.

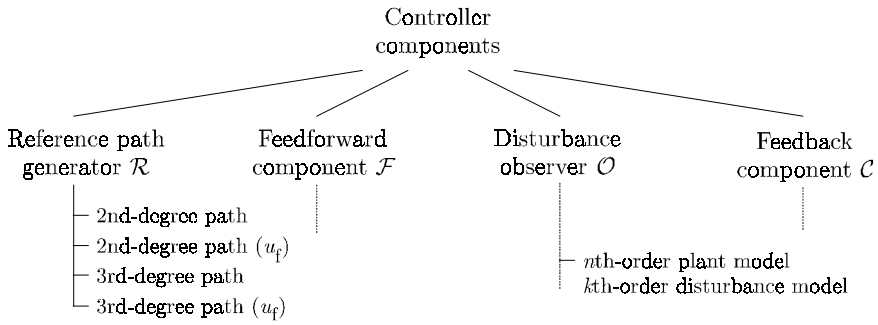

FIGURE 3.17 *Hierarchy of control system components*

Reference path generator

The type reference path generator has no input ports. The output ports are the reference path r and a vector consisting of the reference velocity, acceleration and forcing function. In figure 3.17 four specifications are indicated. These specifications are (refer section 3.4):

- *2nd-degree path.* The reference path generator contains analytical expressions for the outputs. The designer has to indicate the motion time t_m, the motion distance h_m and/or maximums for the velocity and acceleration.
- *2nd-degree path* (u_f). The reference path generator contains a desired open-loop forcing function u_f and an ideal plant model $\mathcal{P}_{id}$ (figure 3.11), *i.e.* a bang-bang force profile and a moving mass model $\mathcal{P}_{id}$.
- *3rd-degree path.* Similar as 2nd-degree path, except additionally a maximum jerk has to be specified.
- *3rd-degree path* (u_f). Similar as 2nd-degree path (u_f), except a limited jerk profile is used instead of a bang-bang profile.

Feedforward component

In figure 3.18 the hierarchy of feedforward components is shown.The overall feedforward component $\mathcal{F}$ can be a composition of several of its subtypes, as indicated by the four specifications of $\mathcal{F}$. The subtypes are force, velocity and acceleration feedforward. The input port is a vector consisting of the reference velocity, acceleration and forcing function. The output is a control signal u_f. In section 3.4, we already discussed some design aspect of the feedforward component.

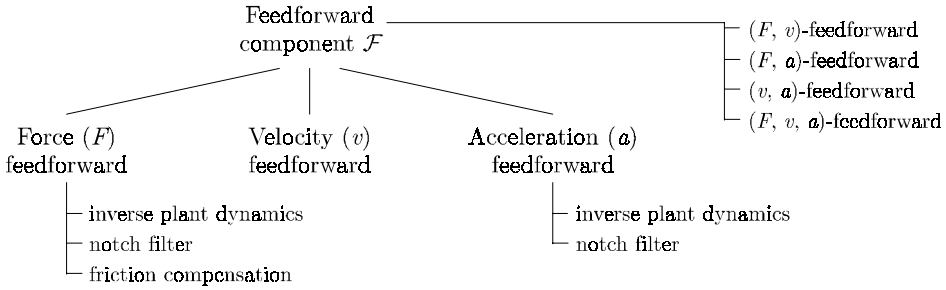

FIGURE 3.18 *Hierarchy of feedforward components*

We will shortly discuss the subtypes:

- *Velocity feedforward.* This subtype is only used in combination with a feedback component that contains a *controller* configuration. The input of this component is the reference velocity. The specifications correspond to the components in the velocity-loop of the feedback component (refer section 3.4).
- *Force feedforward.* The input is a forcing function u_{f}. In section 3.4, we mentioned the use of inverse dynamics, notch filtering or friction compensation. These are specifications of this subtype.
- *Acceleration feedforward.* The acceleration of the reference path is the input of this subtype. Two specifications are considered: inverse dynamics and notch filtering.

Feedback component

In the hierarchy of feedback components we consider two subtypes, *i.e.* the compensator and the controller.

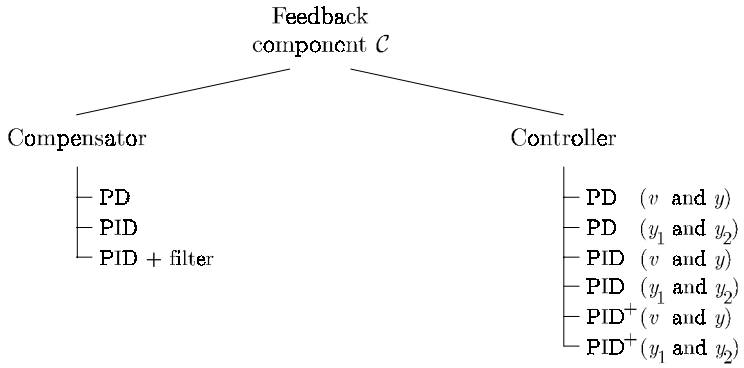

FIGURE 3.19 *Hierarchy of feedback components*

The difference between these subtypes has been discussed in section 3.3. The input ports of the feedback component are the reference path r and the measurement y. The measurement y of the controller consists of two components: *i.e.* two position measurements y_1 and y_2 or a position measurement y and a velocity measurement v. The first has been discussed in this chapter and the latter in the previous chapter. Figure 3.19 shows that for each subtype, PD and PID specifications are supplied. The design procedures for the feedback component have been incorporated in the component descriptions. That is, the designer can indicate the specifications for the controlled system in order to obtain an appropriate control system.

Disturbance observer
The disturbance observer type is characterized by two input ports, *i.e.* the control signal u and the measurement y, and an output port, *i.e.* the estimation of the disturbance. In figure 3.17 a specifications is shown in terms of the plant model order n and disturbance model order k. The library will contain disturbance models of maximally order three and second- or fourth-order plant models. Expressions for the default values of the observer gains derived in section 3.5.3, are incorporated.

For the overall control configuration we consider four specifications. Each specification is composed of a different combination of components, as indicated in figure 3.20.

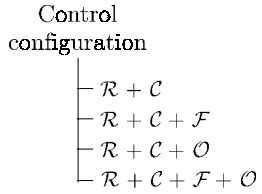

FIGURE 3.20 *Specifications of control configuration*

The library of control systems thus supplies standard configurations, which can be considered *templates* for the design of motion control systems.

The library of control systems presented here enhances computer-supported design of electromechanical motion systems, conform the evolutionary nature of design. The designer can start with simple plant models and a simple control configuration. When more detail is incorporated in the plant model, the control system can be extended gradually changing the type and/or specification of the configuration and/or of the components, with the help of the library structure.

3.7 Evaluation and conclusions

In order to meet the more or less conflicting requirements for a controlled system, in terms of performance, stability, disturbance attenuation and robustness for model uncertainties, a transparent and structured design method is proposed. Starting from a successful conceptual design, this method supports the (evolutionary) design of motion control systems.

The overall control system consists of several components that, within limits, have their specific functionality. The decomposition proposed here uses a reference path generator, a feedback component, a feedforward component and a disturbance observer. For two components in this configuration, *i.e.* the feedback component and the disturbance observer, design procedures are given.

For the feedback component, we suggest to use PID *controller* and PID *compensator* configurations. The essential difference being that the derivative action does not operate on the reference path, in case of the *controller* configuration, but only on the measured output. The design procedure for both of these relies on a second- or fourth-order plant model. By means of quantitative specifications, in the form of bounds on appropriate frequency responses, expressions for the design parameters have been derived. Performance-related specifications naturally follow from the conceptual design; disturbance-related specs enter the overall design in this stage. By stepwise calculation of the design parameters, a feedback component is designed that meets the specified frequency responses of the closed-loop system (if possible).

When the specifications of the disturbance attenuation cannot be met by a feedback component only, the control configuration can be extended with a disturbance observer. For this component, also a design procedure is given, as a natural extension of the design procedure of the feedback component. The underlying idea is that the sensitivity function of the overall control configuration is the product of the observer sensitivity function and the sensitivity function of the control configuration without disturbance observer.

The structured design of the control configuration starts with a conceptual design of a controlled system, with only a feedback component. It is recommended to bring this design into the frequency domain, by determining its bandwidth ω_b. Next, a PD *controller* should be designed, using the bandwidth ω_b in the design procedure for the feedback component. This controller configuration should be maintained when a concept with 2 measurements is used or when no additional components are used. In other cases, a *compensator* should be designed. The plant model will gradually become more complex during this design stage. Whenever the controlled system does not work as desired, the control configuration can be

modified or extended with appropriate means. For each component, an indication is given on how the control configuration can be improved.

The structured design method does not prescribe a single recipe for all problems, but merely gives a number of solutions that can be used whenever required. These solutions are incorporated in a library of control systems. The result is a computer-supported design method that, with fairly simple means, allows the design of a good-enough control system in relative short time.

4 Physical parameter uncertainty

4.1 Introduction

Controller design for electromechanical motion systems generally uses physically motivated plant models. However, the behavior of any real system is never known completely. The real-world system may change with time (components may age or their parameters may vary with temperature) or operating conditions may vary (load changes, disturbances). As the ultimate goal of mechatronic design is to build a system that will work in the real world, the control system must be able to withstand internal perturbations as well as external disturbances. Assuming that the environment does not change, the problem is model uncertainty; a mathematical representation of a system often involves simplifying and sometimes wishful assumptions (Stefani *et al.*, 1994). Therefore, in designing control systems, one has to deal with model uncertainty. Horowitz (1982) states the same in a powerful one-liner: the true importance of feedback is in achieving *desired performance* despite *uncertainty*. In this chapter we will focus on these aspects for electromechanical motion systems, in a more specific sense than in chapter 3.

The desired performance of controlled electromechanical motion systems concerns the motion of an end-effector. Similar as in previous chapters, we consider point-to-point motions where the end-effector has to move over a distance h_{m} within the motion time t_{m} (figure 4.1). The positional error, *i.e.* the maximum absolute error after the motion time, should be smaller than a specified maximum positional error e_0. Most controller design methods cannot deal with these task specifications directly and a conversion to controller design specifications is necessary. The result of the conversion should be such that violations of the task specifications, due to uncertainties, are transparent during design.

Uncertainties are often represented such that they lend themselves well for mathematical analysis. Whenever possible, it is more appropriate to use a *physically motivated* uncertainty representation. During the design process as well as during operation, the *physical parameters* in the model are not known exactly. Lower and upper bounds for these parameters can often be indicated, resulting in so-called

parametric uncertainty. In physical models of electromechanical plants, typical uncertain physical parameters are stiffness, mass and damping.

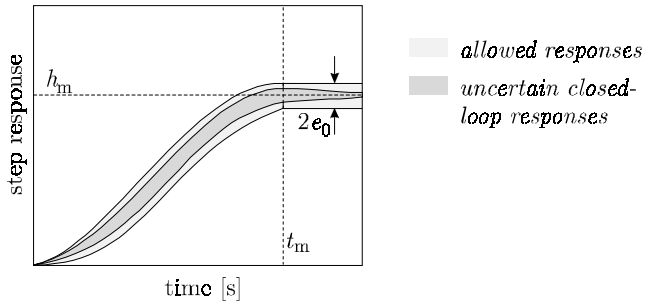

FIGURE 4.1 *Matching problem of specifications and uncertain closed-loop responses*

In figure 4.1 the essential problem addressed in this chapter is indicated: the task and the allowed uncertainty are specified *quantitatively* and these have to be fulfilled by the closed-loop system, despite *quantitatively* specified physical parameter uncertainty. We formally define this problem as:

Definition 4.1 Matching problem

Given the motion and uncertainty specifications (figure 4.1) and a physical model of the electromechanical plant with physical parameter uncertainty, design a control system that meets the specifications despite the uncertainty.

This can be considered a particular problem that may arise in the detailed design stage of chapter 3. In this chapter we will develop a (computer-supported) tool in order to deal with the matching problem.

Remark 4.1

We will consider uncertain linear time-invariant continuous-time SISO systems, where the notion of transfer functions can be used freely.

Section 4.2 gives a motivation for using Quantitative Feedback Theory for controlling electromechanical motion systems with uncertain physical parameters. The philosophy and design procedure of QFT are described in section 4.3. This section is concluded with a discussion of problems encountered during application of QFT design to electromechanical motion systems. The two major problems are addressed next. Section 4.4 describes the theoretical background on systems with uncertain physical parameters and reviews possibilities for converting these into uncertainty regions in the Nichols chart. Section 4.5 deals with the problem of the

conversion of time-domain specifications into frequency-domain specifications. A new conversion algorithm is presented. Based on the theory from sections 4.4 and 4.5, computer-based support has been developed using the 20-sim environment (Controllab Products, 2000) that can be used in combination with the Matlab QFT toolbox (Borghesani *et al.*, 1994). In section 4.6 the computer-based support is discussed. Section 4.7 presents the conclusions.

4.2 Motivation for Quantitative Feedback Theory

The particular property that a controlled system must possess in order to work properly in uncertain situations is called *robustness*. Mathematically, this means that the controller must perform satisfactorily not just for one plant, but for a family (or set) of plants. The problem of designing controllers that satisfy robust stability and robust performance specifications is called *robust control*. Often, plant uncertainties are considered to be norm-bounded variations of a frequency response function or of matrices in a state-space description. These uncertainty representations are mathematically motivated; they lend themselves well for mathematical analysis. Nevertheless, whenever possible we will use a *physically motivated* uncertainty representation. To emphasize the importance of this insight, Ackermann postulates the "first basic rule of robust control":

Statement 4.1 Basic rule of robust control

> *Require robustness of a control system only for physically motivated parameter values and not with respect to arbitrarily assumed uncertainties of the mathematical model (Ackermann, 1993).*

A robust controller design method that does not ignore Ackermanns rule in advance is known as *Quantitative Feedback Theory* (Horowitz, 1991; Houpis and Rasmussen, 1999). QFT has been developed for linear and nonlinear, time-invariant and time-varying, continuous and sampled-data, uncertain SISO and MIMO plants, and for both output and internal variable feedback (D'Azzo and Houpis, 1995). Several successful applications of QFT to electromechanical motion systems have been reported, *e.g.* (Landau *et al.*, 1995) and (Park *et al.*, 1997).

As early as in 1959 Isaac Horowitz was the first to recognize the importance of uncertainty in feedback design (Jayasuriya, 1993). This insight led Horowitz to the development of the design methodology now known as QFT. The reason for the term "quantitative" can best be explained by quoting Horowitz:

Statement 4.2 Quantitative feedback

The true importance of feedback is in "achieving desired performance despite uncertainty". If so, then obviously the actual design and the cost of feedback should be closely related to the extent of the uncertainty and to the narrowness of the performance tolerances. In short, it should be ***quantitative*** *(Horowitz, 1982).*

QFT aims at satisfying quantitative bounds that are imposed on the variations in the closed-loop transfer function or command response $H(s)$ as a result of specified variations of the open-loop transfer function $L(s)$. The control configuration used in QFT is shown in figure 4.2.

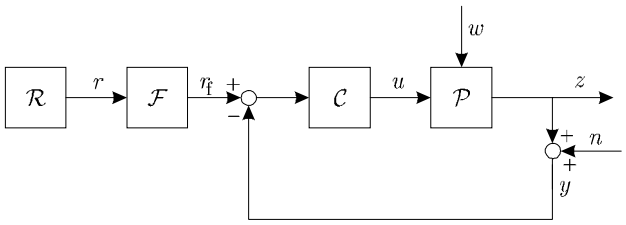

FIGURE 4.2 *Control configuration used in Quantitative Feedback Theory*

The command response $H(s)$ and loop transfer function in this configuration are:

$$H(s) = F(s) \cdot \frac{L(s)}{1 + L(s)} = F(s) \cdot T(s) \tag{4.1}$$

$$L(s) = P(s)C(s) \tag{4.2}$$

where $F(s)$ is the prefilter, $C(s)$ the compensator, $P(s)$ the plant transfer function and $T(s)$ the complementary sensitivity function. The QFT design method relies on the graphical representation of the open-loop transfer function in the Nichols chart. In this chart, the effects of open-loop variations on the closed-loop transfer function can be seen easily.

Remark 4.2

The control configuration of figure 4.2 is different from the configuration considered in chapter 3. In section 4.5.7 we will therefore shortly discuss the relation between the design methods described here and in the previous chapter.

Ackermann distinguishes two categories of approaches for the design of robust control systems. The first category contains "one-shot" procedures that lead to controllers that guarantee robust stability for a plant family and that do not require further robustness analysis. Examples are μ-optimization and H_∞-optimal

control (Doyle *et al.*, 1989; Kwakernaak, 1993; Zhou *et al.*, 1996). The second category contains tools that help the designer to understand the design conflicts between operating conditions and different specifications and support an interactive design process involving trail and error procedures and robustness analysis of the resulting closed-loop system, *e.g.* QFT. At first sight only the first category looks appealing. However, these methods generally violate the basic rule of robust control and often lead to controllers of unnecessary high order and with insufficient flexibility for trade-offs with other design requirements. If the evaluation of the resulting closed-loop system is done by other criteria than those used directly in the design (for example by step responses or simulations with a nonlinear plant model), then the design procedure becomes a trail and error procedure anyway (Ackermann, 1993).

Jayasuriya separates QFT from other frequency domain robust control methods, such as LQG/LTR, H_∞-optimal control and μ-synthesis for (Jayasuriya, 1993):

- it emphasizes cost of feedback as measured in terms of controller bandwidth;
- its ability to deal nonconservatively with parametric, nonparametric and mixed uncertainty models;
- its utilization of both amplitude and phase of the loop transfer function, pointwise in frequency, for the quantification of performance.

Although QFT has also been subject to criticism for its pragmatism (Doyle, 1986; Yaniv and Horowitz, 1987) and H_∞-optimal control can also be successfully applied to electromechanical motion systems (Steinbuch and Norg, 1998), we will use QFT to deal with systems with uncertain physical parameters. The main reason is the ability of QFT to deal non-conservatively with the uncertainty models (Jayasuriya, 1993). In contrast, H_∞-optimal control and μ-synthesis will generally yield conservative estimates of the plant uncertainty and hence, Ackermann's basic rule of robust control will be violated. Secondly, it appears that QFT gives the best designs for hard SISO control problems, see *e.g.* (Landau *et al.*, 1995) and (De Roover, 1997).

4.3 Quantitative Feedback Theory

4.3.1 QFT design problem

The purpose of robust control is to obtain good performance even though the behavior of the plant is not completely known. “Good performance” can be described as a closed-loop transfer function gain $|H(j\omega)|$ lying in a certain tolerance band, shown as a shaded area in the Bode diagram of figure 4.3.

$$0 \leq \alpha(\omega) \leq |H(j\omega)| \leq \beta(\omega) \tag{4.3}$$

The magnitude of this *desired* closed-loop transfer function is equal to 0 dB up to a certain frequency and decreases rapidly above this frequency (high-frequency roll-off). Usually, the bounds $\alpha(\omega)$ and $\beta(\omega)$ are specified in such a way that the variation $|\beta(\omega)-\alpha(\omega)|$ is sufficiently small in a significant frequency range $\omega < \omega_h$ over which benefits of feedback are desirable. In choosing the limits $\alpha(\omega)$ and $\beta(\omega)$, it is unrealistic to specify tight variations beyond a frequency ω_h, because it is inevitable that the system sensitivity increases in the high-frequency range. So for $\omega \gg \omega_h$ it is generally assumed that $|\beta(\omega)/\alpha(\omega)|$ can be very large while the actual values $|\alpha(\omega)|$ and $|\beta(\omega)|$ are small.

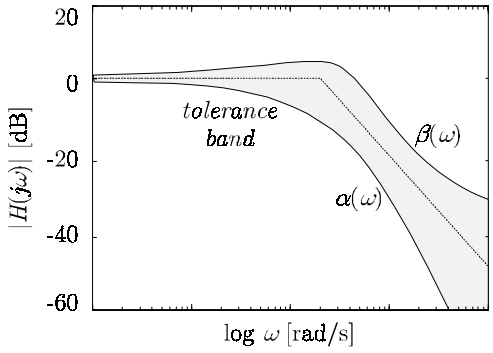

FIGURE 4.3 *Design specifications; tolerance band for the closed-loop gain* $|H(j\omega)|$

If the plant is *minimum-phase*, *i.e.*, the plant has no open-loop zeros in the right half s-plane, the magnitude of the closed-loop transfer function completely characterizes the closed-loop performance. In that case only the specifications in (4.3) have to be met in order to obtain robust performance. If the plant is non-minimum phase, additional tolerance bounds should be defined for the phase of the closed-loop transfer function (Jayasuriya, 1993; D'Azzo and Houpis, 1995).

The system to be controlled, *i.e.* the electromechanical plant, can be represented by a model that contains both structured and unstructured uncertainty, *i.e. mixed uncertainty*. The way in which unstructured uncertainty enters QFT design is via a constraint on the closed-loop magnitude. This closed-loop magnitude constraint guarantees a certain stability margin for each member of the family of plants with structured uncertainty. Preliminaries and notation of uncertain systems will be explained in section 4.4.1.

The goal of the QFT design problem, for the family of plants with mixed uncertainty, is to determine an admissible pair of strictly proper, rational, and stable transfer functions $C(s)$ and $F(s)$ in the 2-DOF configuration of figure 4.2, such that they achieve:

- *robust stability*: the closed-loop system is stable for all members of the plant family with *mixed uncertainty*;

- *robust performance*: the given frequency-domain specifications are satisfied for all members of the plant family with *structured uncertainty*.

During the QFT design procedure, it is tried to keep the gain of the compensator $C(s)$ as small as possible. Of all compensators fulfilling the requirements, the one having the minimum high-frequency gain is the *optimal* compensator (Thompson and Nwokah, 1994).

4.3.2 QFT design procedure

A short overview of the QFT design procedure will now be presented. For mathematical details we refer to (Horowitz, 1991; Jayasuriya, 1993) and for a more elaborate description of the design procedure refer to (D'Azzo and Houpis, 1995). In the textbook of Houpis and Rasmussen (1999) both fundamentals and applications are discussed. The design steps are summarized hereafter and are illustrated with an example of a flexible mechanism with a small amount of mechanical damping:

$$\begin{aligned} P_0(s) &= \frac{b_0}{a_4 s^4 + a_3 s^3 + a_2 s^2 + a_1 s} \\ b_0 &= Ac \\ a_4 &= m_1 m_2 \\ a_3 &= (d_{10} m_2 + d_{20} m_1) \\ a_2 &= (c m_2 + c m_1 + d_{10} d_{20}) \\ a_1 &= c(d_{10} + d_{20}) \end{aligned} \tag{4.4}$$

The values of the physical parameters are: gain $A = 3.57 \cdot 10^{-5}$, load mass $m_1 = 2$ [kg], motor mass $m_2 = 0.54$ [kg], dominant stiffness $c = 1512$ [Nm], damping on the load $d_1 = 0.11$ [Ns/m] and the damping on the motor $d_2 = 0.76$ [Ns/m]. The roots of the denominator polynomial of this nominal plant transfer function are: $s_1 = 0$, $s_2 = -0.34$, $s_{3,4} = -0.12 \pm 59.6i$. The nominal numerator equals: $b_0 = 5.4 \cdot 10^{-2}$. For purposes of illustration, we assume a mathematically motivated uncertainty of the numerator b_0 and the real pole s_2, described by:

$$\begin{aligned} b_0 &\in \left[2.8 \cdot 10^{-2};\ \ 7.9 \cdot 10^{-2}\right] \\ s_2 &\in \left[-0.17;\ \ -0.34\right] \end{aligned} \tag{4.5}$$

Initially we choose unit feedback, such that the nominal loop gain $L_0(s)$ equals:

$$L_0(s) = P_0(s)C(s) = P_0(s) \tag{4.6}$$

The QFT design procedure contains the following steps:

1. Choose the *nominal plant transfer function* $P_0(s)$. In the example, the nominal version of (4.4) can be obtained by choosing a nominal value for the uncertain physical parameters. A restriction on this choice is that the nominal loop $L_0(s)$ must satisfy the zero exclusion condition (Ackermann, 1993).

2. Choose a set of *critical frequencies*. During the design procedure, satisfaction of robust stability and robust performance boundaries is not obtained for all frequencies. A set of critical frequencies should be selected, such that satisfaction of the boundaries for these frequencies will guarantee satisfaction of the boundaries for all frequencies in the range of interest. Five critical frequencies are indicated with a small circle in the Nichols chart of figure 4.4. The selected critical frequencies are: 0.2, 2, 5, 20 and 60 [rad/s].

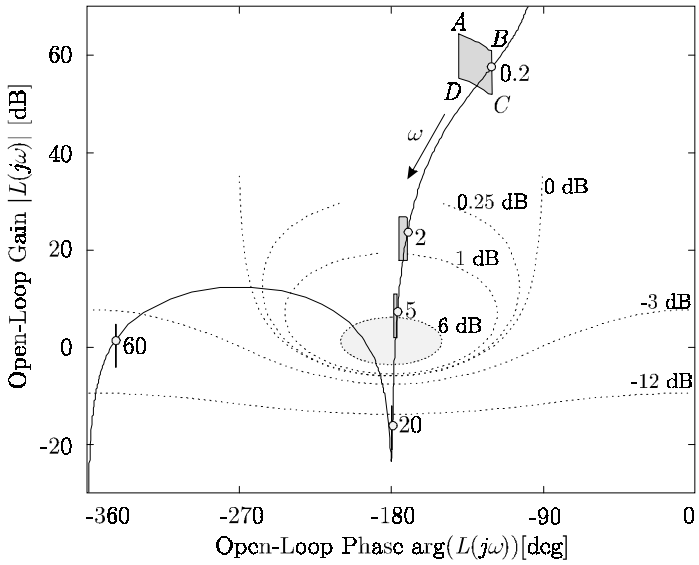

FIGURE 4.4 *Open-loop response in Nichols chart including templates for critical frequencies*

3. Determine the *templates* that indicate the effect of parameter uncertainties on the gain and phase of the nominal loop at a critical frequency. In figure 4.4 these templates are the gray areas that decrease in size for higher critical frequencies. The effects of parameter uncertainties are the largest for the critical frequency 0.2 [rad/s]. For mathematically motivated uncertainty the extreme values of the uncertainties (4.5) correspond with the vertices of the templates (figure 4.4):

A:	$a_0 = 0.079,\ s_2 = -0.17$	*C*:	$a_0 = 0.028,\ s_2 = -0.34$
B:	$a_0 = 0.079,\ s_2 = -0.17$	*D*:	$a_0 = 0.028,\ s_2 = -0.34$

4. Determine the *stability boundaries*, which serve as a guide during design of the compensator $C(s)$, for a number of critical frequencies. For each of the critical frequencies, the stability boundary consists of the *nominal* points in the Nichols chart for which the template touches the 6 dB-locus (*i.e.* the stability margin). For the construction of these boundaries, one can think of fixing a pencil at the nominal point in the template for a certain critical frequency. Next, the entire template is moved around the 6 dB-locus, meanwhile keeping the pencil at the nominal point of the template. In figure 4.5a, the template for the critical frequency 0.2 [rad/s] is moved anti-clockwise around the 6 dB-locus, in four steps. The contour that is found figure 4.5b, *i.e.* the line the pencil has drawn, after having moved the template, is the stability boundary for the corresponding critical frequency.

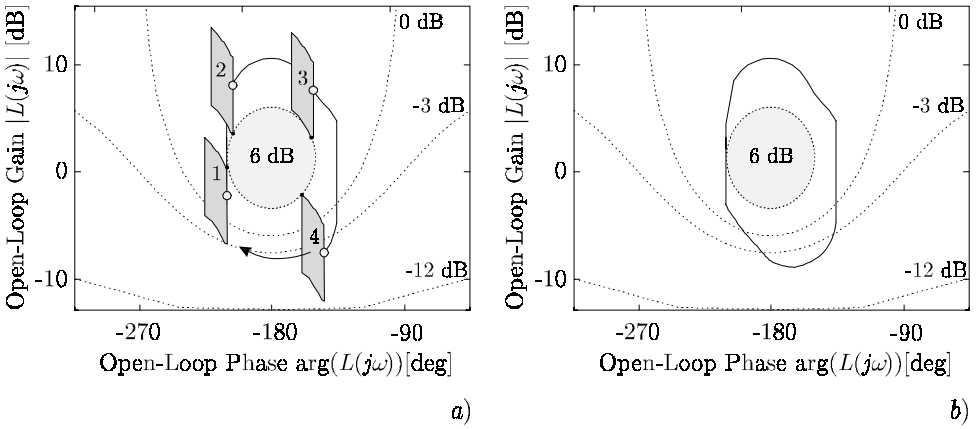

FIGURE 4.5 *Stability bound for critical frequency* 0.2 [rad/s]
a) construction process
b) final result

5. Determine the *performance boundary* per critical frequency. A point on the performance boundary may for instance be obtained by fixing the nominal point of a template at a certain open-loop phase, and shifting the template up or down until the *lowest* position is found where the actual variation in the closed-loop gain equals the allowed variation, as specified by the tolerance band. The closed-loop magnitude can be read from the closed-loop grid (or M-lines) in the Nichols chart. In figure 4.6a this procedure is shown for the critical frequency 5 [rad/s]. At an open-loop phase of $-130°$ the template has been shifted down and at location 2, the variation in the closed-loop gain equals the allowed variation in closed-loop gain at 5 [rad/s] in the frequency tolerance band of figure 4.6b. For phases smaller than $-260°$ (location 3) the locus already has been determined.

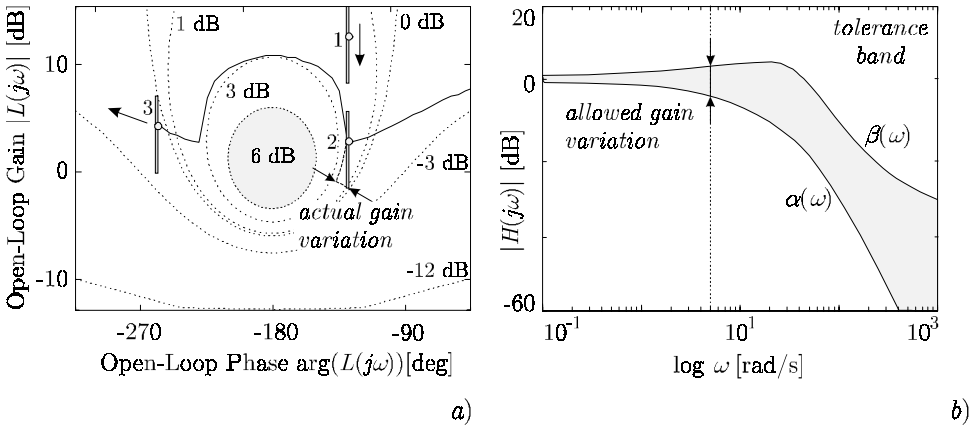

FIGURE 4.6 *Performance bound for critical frequency* [5 rad/s]
a) actual closed-loop gain variation in Nichols chart
b) allowed closed-loop gain variation in Bode diagram

6. Design a compensator through *loop shaping*, such that it achieves:
   - *robust stability*: at each critical frequency, the corresponding open-loop response is on or to the right of the corresponding stability boundary;
   - *robust performance*: at each critical frequency, the corresponding open-loop response is on or above the corresponding performance boundary.

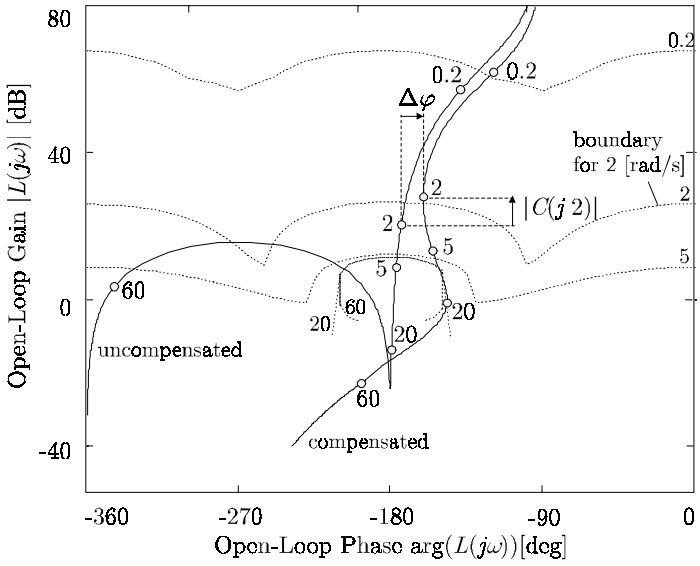

FIGURE 4.7 *Loop shaping in the Nichols chart*

This goal should be achieved with a compensator of low complexity and without over-design (*i.e.*, the loop characteristic should be *on* the boundaries rather than outside or above). In figure 4.7 it is shown how gain and phase are added to the open-loop $L(s)$ (*i.e.* insertion of a lead filter in the compensator) at frequency 2 [rad/s], such that the combined stability and performance boundaries are satisfied.

7. Design a *prefilter* $F(s)$ such that the tolerance bounds of figure 4.3 are satisfied. In figure 4.8 the complementary sensitivity function $T(s)$ resulting after loop shaping is shown in the Bode diagram as response band A. Correct loop shaping guarantees that the width of this response band is smaller than or equal to the width of the tolerance band. The prefilter is designed such that the response is manipulated into the tolerance band of figure 4.3. A possible result is given as frequency response band B.

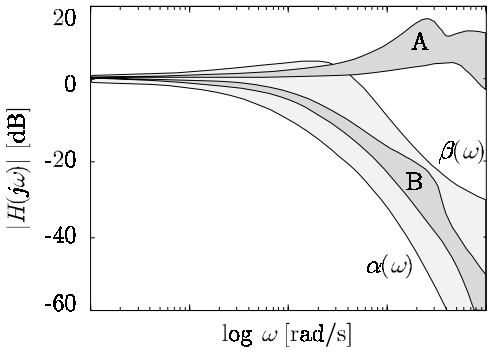

FIGURE 4.8 Prefilter design in a Bode diagram

4.3.3 Problems in QFT design

As the QFT design procedure heavily relies on calculations and graphics, computers are well suited to support large parts of the design procedure. The Matlab QFT toolbox (Borghesani *et al.*, 1994) does support several design steps. However, there remain some problems in the design of controllers for electromechanical motion systems with uncertain physical parameters:

- The first major problem is the difference in the performance specifications for electromechanical motion systems and the starting point of QFT design. Performance specifications of electromechanical systems are typically stated in terms of space and time, such that they have to be converted into the frequency domain. Since there is no known way of exactly converting time-domain specifications into a frequency-domain format, this conversion is

considered to be an art (Jayasuriya, 1993). Note that this a general problem for controller design and not specific for QFT.

- Structured uncertainty of electromechanical systems is expressed in uncertain physical parameters. The second major problem in applying QFT to these systems is that this structured uncertainty has to be expressed in terms of templates. For physically motivated uncertainty, it is difficult to determine the shape of the templates. It is not always obvious which combinations of parameter values contribute to the contour of the templates. This is caused by the fact that physical parameters can affect a transfer function in many different ways.

Statement 4.3 Problems in QFT design

Two major problems arise during the application of QFT to electromechanical motion systems with uncertain physical parameters. Uncertain physical parameters have to be transformed into templates in the Nichols chart and time-domain performance specifications have to be converted into the frequency domain.

4.4 Template construction

In this section we will discuss the problem that QFT requires uncertain physical parameters in a physical plant model to be mapped onto templates in the Nichols chart, as depicted in figure 4.9.

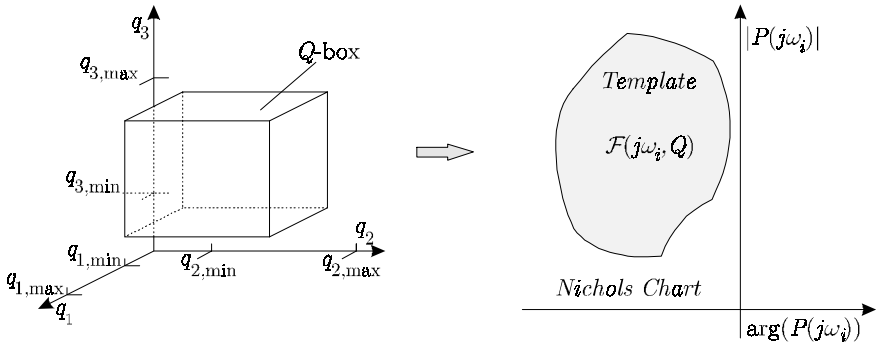

FIGURE 4.9 *Mapping a hyperrectangle Q onto a template $\mathcal{F}(j\omega_i,Q)$ in the Nichols chart*

In literature the similar problem of constructing value sets (*i.e.* uncertainty regions in the complex plane) has received considerable attention. In this section we will discuss some methods for template construction and select those that are useful for models of electromechanical motion systems. For these methods we will develop computer support that automatically generates the input for the Matlab QFT toolbox (Borghesani *et al.*, 1994), as discussed in section 4.4. Parts of the material described in this section is also described in (Coelingh *et al.*, 1998) and (Holterman, 1997).

We distinguish two classes of methods to obtain the contour of a template:
- *Analytical methods* determine the physical parameter combinations that yield points at the contour of the template by symbolic analysis of the model structure.
- *Numerical methods* determine the physical parameter combinations that yield points at the contour of the template by numerical analysis of the model structure.

4.4.1 Preliminaries on plant uncertainty models

First we will give some preliminaries on and the notation of uncertain plant models. The physical parameters appearing in the plant model are all gathered in the physical parameter vector q:

$$q = \begin{bmatrix} q_1 & q_2 & \cdots & q_k \end{bmatrix}^T \tag{4.7}$$

The elements of q are assumed to lie between mutually independent bounds:

$$q_i \in \begin{bmatrix} q_{i,\min}; & q_{i,\max} \end{bmatrix} \tag{4.8}$$

where

$$q_{i,\min} \leq q_{i,\max} \tag{4.9}$$

In case of inequality the parameter q_i is said to be *uncertain*. The set of possible uncertain parameter vectors is given by the hyperrectangle Q.

Definition 4.2 Q-box

The Q-box is an hyperrectangle defined by the set

$$Q = \left\{ q = \begin{bmatrix} q_1 & q_2 & \ldots & q_l \end{bmatrix}^T \;\middle|\; q_i \in \begin{bmatrix} q_{i,\min}; & q_{i,\max} \end{bmatrix}, \;\; i = 1, 2, \ldots, l \right\} \tag{4.10}$$

A polynomial p of order n in s, containing real coefficients $a_i(q)$ that are a function of the uncertain physical parameters q, is denoted as:

$$p(s,q) = \sum_{i=0}^{n} a_i(q)s^i \tag{4.11}$$

A plant transfer function with uncertain physical parameters will be denoted as:

$$P(s,q) = \frac{N(s,q)}{D(s,q)} \tag{4.12}$$

where $N(s,q)$ and $D(s,q)$ are polynomials as defined in (4.11) of respectively order m and n. The definition of a *family* allows us to describe different functions, such as polynomials and transfer functions expressed in terms of s or $j\omega$ in a general way.

Definition 4.3 Family

An uncertain function f with its corresponding Q-box is defined as a family

$$\mathcal{F}(\cdot,Q) = \left\{ f(\cdot,q) \;\middle|\; q \in Q \right\} \tag{4.13}$$

A plant with structured uncertainty can now be defined as a parametric plant family:

Definition 4.4 Parametric plant family

The parametric plant is defined as a family denoted by:

$$\mathcal{P}_{\mathrm{p}}(s,Q) = \left\{ P(s,q) = \frac{a_m(q)s^m + \ldots + a_0(q)}{b_n(q)s^n + \ldots + b_0(q)} \;\middle|\; q \in Q \right\} \tag{4.14}$$

For a certain nominal parameter vector q_0, $P(s,q_0)$ is called the *nominal plant*, denoted as $P_0(s)$.

Since one also has to cope with *unstructured* uncertainty, the parametric plant family is extended with an additional term. The plant to be controlled $P(s,q)$ is now assumed to be a member of the family of plants $\mathcal{P}_{\mathrm{m}}(s,Q)$, which is formally described by the following *mixed* uncertainty model:

Definition 4.5 Mixed uncertainty model

The mixed uncertainty model is defined as

$$\mathcal{P}_{\mathrm{m}}(s,Q) = \mathcal{P}_{\mathrm{p}}(s,Q)(1 + \Delta(s)) \tag{4.15}$$

The unstructured uncertainty is accounted for by means of the term $\Delta(s)$, which satisfies:

$$|\Delta(j\omega)| \leq r(\omega) \ . \tag{4.16}$$

Here:

$$r(\omega) = \begin{cases} \varepsilon(\omega), & 0 < \omega \leq \omega_{\mathrm{h}} \\ r_{\mathrm{l}}(\omega), & \omega > \omega_{\mathrm{h}} \end{cases} \tag{4.17}$$

is a typical description in which the low- to middle-frequency (up to ω_{h}) model has primarily parametric uncertainty (*i.e.*, $\varepsilon(\omega) \approx 0$), whereas in the higher frequencies (larger than ω_{h}) the model has also significant unstructured uncertainty characterized by $r_{\mathrm{l}}(\omega)$. This provides a band around the parametric plant subset $\mathcal{P}_{\mathrm{p}}(s,Q)$ (Jayasuriya, 1993). The reason for this distinction between low and high frequencies is that usually the higher order modes of the plant are disregarded. However, it should be noticed that it is possible for the plant to have significant unstructured uncertainty even for frequencies smaller than ω_{h}.

The plant to be controlled $P(s,q)$ is a member of the parametric plant family $\mathcal{P}_{\mathrm{p}}(s,Q)$. When we evaluate this plant at a particular frequency ω_i and a particular point in the Q-box we obtain a point in the complex plane $\mathbb{C}$. When we evaluate this plant for the entire Q-box at frequency ω_i we obtain an uncertainty region called a *value set*.

Definition 4.6 Value set

A value set $\mathcal{F}_{\mathbb{C}}(j\omega_i,Q)$ is defined as the set of complex numbers obtained by evaluating a family $\mathcal{F}(s,Q)$ at a particular frequency ω_i:

$$\mathcal{F}_{\mathbb{C}}\left(j\omega_i,Q\right) = \left\{ f\left(j\omega_i,q\right) \in \mathbb{C} \,|\, q \in Q \right\} \tag{4.18}$$

where $\mathbb{C}$ is the complex plane.

When the plant $P(s,q)$ is evaluated at a particular frequency ω_i and a particular point in the Q-box we obtain a point in the Nichols chart N. When we evaluate this plant for the entire Q-box at frequency ω_i we obtain an uncertainty region called a *template*.

Definition 4.7 Template

A template $\mathcal{F}_{\mathrm{N}}(j\omega_i,Q)$ is defined as the set of points in the Nichols chart N *obtained by evaluating a family $\mathcal{F}(s,Q)$ at a particular frequency ω_i:*

$$\mathcal{F}_{\mathrm{N}}\left(j\omega_i,Q\right) = \left\{ f\left(j\omega_i,q\right) \in N \;\middle|\; q \in Q \right\} \tag{4.19}$$

where N *is the Nichols chart.*

A value set can easily be transformed into an uncertainty region in the Nichols plane, which is required for QFT. The point $(\Re(f), \Im(f))$ in a value set corresponds to the following point:

$$\left(\arctan\left(\frac{\Im(f)}{\Re(f)} \right) , \;\; 20\log\left(\sqrt{\Re^2(f) + \Im^2(f)} \right) \right) \tag{4.20}$$

in the Nichols chart. The contour of a value set is mapped onto the contour of the corresponding template in the Nichols chart.

4.4.2 Analytical template construction

An uncertain parametric plant family can be written as the division of two uncertain polynomial families :

$$\mathcal{P}_{\mathrm{p}}(\cdot, Q) = \frac{\mathcal{N}(\cdot, Q)}{\mathcal{D}(\cdot, Q)} \tag{4.21}$$

Depending on the structure of (4.21) different techniques can be applied for constructing templates. We distinguish template addition and tree-structured decomposition.

Template addition

The template $\mathcal{F}_{\mathrm{N}}(j\omega, Q)$ can be determined *a priori* if the numerator and the denominator of the transfer function of the plant depend on different parameters. In that case, the uncertain physical parameter vector q can be split into $q_{\mathrm{N}} \in Q_{\mathrm{N}}$ for the numerator and $q_{\mathrm{D}} \in Q_{\mathrm{D}}$ for the denominator:

$$\mathcal{P}_{\mathrm{p}}(\cdot, Q) = \frac{\mathcal{N}(\cdot, Q_{\mathrm{N}})}{\mathcal{D}(\cdot, Q_{\mathrm{D}})} \tag{4.22}$$

The uncertain numerator and denominator families can both be represented in the Nichols chart or s-plane for a particular frequency ω_i:

$$\begin{aligned} \mathcal{N}(j\omega_i, Q_{\mathrm{N}}) &= \left\{ N(j\omega_i, q_{\mathrm{N}}) \,\middle|\, q_{\mathrm{N}} \in Q_{\mathrm{N}} \right\} \\ \mathcal{D}(j\omega_i, Q_{\mathrm{D}}) &= \left\{ D(j\omega_i, q_{\mathrm{D}}) \,\middle|\, q_{\mathrm{D}} \in Q_{\mathrm{D}} \right\} \end{aligned} \tag{4.23}$$

The theory of constructing value sets from uncertain polynomials (Ackermann, 1993) can be used to construct a value set for both the numerator and denominator. These can be converted to templates in the Nichols chart (4.20), which can be added to construct a template of the plant transfer function. This procedure is shown in figure 4.10. Each step will be discussed hereafter.

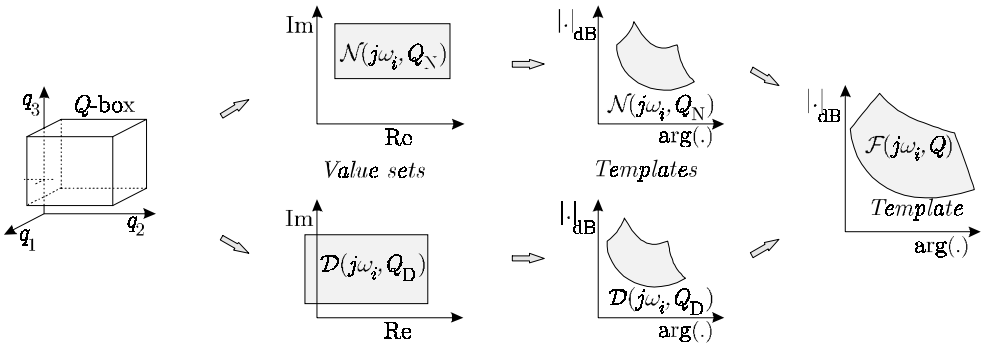

FIGURE 4.10 *Procedure for template addition*

First we consider the problem of constructing templates for uncertain polynomials, *i.e.* the first two steps in figure 4.10. Depending on the type of polynomial, the contour of a value set can be calculated. For the determination of a value set, it is important that the polynomial is classified in the simplest category.

Some well-known categories of polynomials are described hereafter in order of increasing complexity.

Definition 4.8 Interval polynomial

An interval polynomial is a polynomial (4.11) for which the uncertain coefficients vector a ranges over the box:

$$\mathcal{A} = \left\{ \; a \; \middle| \quad a_i \in \left[a_{i,-}; \;\; a_{i,+} \right], \; i = 0, \quad 1, \quad ..., \quad n \; \right\} \tag{4.24}$$

For an interval polynomial the coefficients a_i are considered not to be a function of other parameters. The contour of a value set is the rectangle between the complex points corresponding to the Kharitonov polynomials ((Kharitonov, 1978) and (Minnichelli *et al.*, 1989)):

$$\begin{aligned}
p_{+-}(s) &= a_{0,+} + a_{1,-}s + a_{2,-}s^2 + a_{3,+}s^3 + a_{4,+}s^4... \\
p_{++}(s) &= a_{0,+} + a_{1,+}s + a_{2,-}s^2 + a_{3,-}s^3 + a_{4,+}s^4... \\
p_{-+}(s) &= a_{0,-} + a_{1,+}s + a_{2,+}s^2 + a_{3,-}s^3 + a_{4,-}s^4... \\
p_{--}(s) &= a_{0,-} + a_{1,-}s + a_{2,+}s^2 + a_{3,+}s^3 + a_{4,-}s^4...
\end{aligned} \tag{4.25}$$

This rectangle can be transformed to a template in the Nichols chart using (4.20), as shown in figure 4.11.

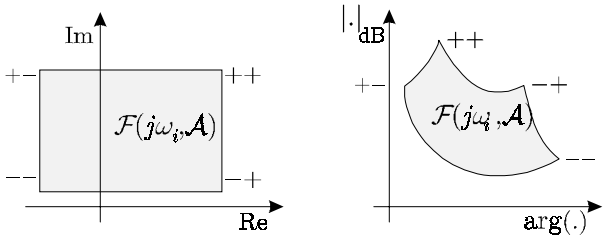

FIGURE 4.11 *Value set and template for interval polynomial.*

Definition 4.9 Affine polynomials

An affine polynomial is a polynomial (4.11) for which all coefficients $a_i(q)$ *are affine functions of the uncertain parameter vector q:*

$$a_i(q_u) = c_i + d_i^T q_u \tag{4.26}$$

According to the Edge theorem of (Bartlett *et al.*, 1988) a polynomial family $\mathcal{P}(s,Q)$ with affine coefficients $a_i(q)$ and hyperrectangle Q is stable if and only if the edges of Q are stable. The Q-box is mapped onto a closed convex polygon $P(\omega,q)$. All edges of the polygon P correspond to edges of Q (Ackermann, 1993). The contour of the value set is obtained by calculating the polynomial value for all vertices of the parameter space Q and next determining the convex hull of these points in the complex plane.

Consider the following polynomial with uncertain parameters q_1, q_2, $q_3 \in$ [-1; 1]:

$$p = q_1 + 2q_2 + (q_2 + 2q_3)s + (q_3 + 2q_1)s^2 + s^3 \tag{4.27}$$

The value set for $\omega = 1$ is given in figure 4.12. The points marked with +++, -++ etc. correspond to vertices of Q. The edges of Q are mapped onto the straight lines between these points. The contour of the value set is the convex hull of these straight lines.

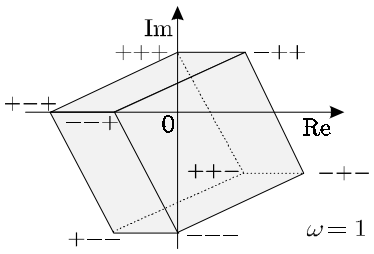

FIGURE 4.12 *Values set for affine polynomial.*

Definition 4.10 Multilinear polynomials

A multilinear polynomial is a polynomial (4.11) with coefficients $a_i(q)$ that are a multilinear function of the uncertain parameter vector q, i.e. when all but one uncertain parameter in q is kept constant, then $a_i(q)$ is affine in the remaining parameters in q.

Multilinear polynomials contain coefficients containing terms like q_1q_2, q_2q_3, $q_1q_2q_3$ etc, but no terms like ${q_1}^2$ or $q_1{q_2}^2$.

For multilinear polynomials, the contour of the value set may correspond to extreme values of one of the physical parameters, but interior points of Q may also contribute to the contour. An illustration of this fact is given in figure 4.13. The edges of Q are mapped onto the four straight lines A, B, C, D, creating the lighter shaded area. However, an interior line in the Q-box is mapped onto the curve *outside* this polygon, thus creating the darker shaded area.

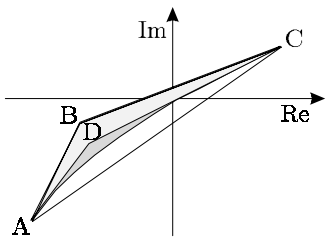

FIGURE 4.13 *Value set for multilinear polynomial.*

For multilinear polynomial families, a rough approximation of the value set may be obtained with the use of the mapping theorem of Desoer (Zadeh and Desoer, 1963): The convex hull of the value set $\mathcal{P}(j\omega,Q)$ of a polynomial with multilinear coefficient functions is the convex hull of the images of the vertices of Q. Thus creating the triangle ABC in figure 4.13, which is somewhat conservative.

Once the templates of the numerator and denominator polynomials are known, the template $\mathcal{F}_{\mathrm{N}}(j\omega_i, Q)$ can be constructed by subtracting any denominator vector from any numerator vector (figure 4.14a), *i.e.* the last step in figure 4.10:

$$\arg\left(P\left(j\omega_i, q\right)\right) = \arg\left(N\left(j\omega_i, q_N\right)\right) - \arg\left(D\left(j\omega_i, q_D\right)\right) \tag{4.28}$$

$$\left|P\left(j\omega_i, q\right)\right|_{\mathrm{dB}} = \left|\mathrm{num}\left(j\omega_i, q_N\right)\right|_{\mathrm{dB}} - \left|\mathrm{den}\left(j\omega_i, q_D\right)\right|_{\mathrm{dB}} \tag{4.29}$$

For simplicity of notation, we will further omit the arguments of the templates. Subtraction of a set of vectors, forming a template $\mathcal{D}$ in the Nichols chart, corresponds to the addition of the mirror image $\mathcal{D}_{\mathrm{mirror}}$ of this template. Here, the mirror image $\mathcal{D}_{\mathrm{mirror}}$ of template $\mathcal{D}$ is the result of rotation of around the origin $\mathcal{D}$ over 180°.

Let n_0 be the nominal numerator in $\mathcal{N}$ and d_0 the nominal denominator in $\mathcal{D}$ (figure 4.14a). If the denominator would be certain, the mirrored template $\mathcal{D}_{\mathrm{mirror}}$ would degenerate to the nominal mirrored denominator $-d_0$. Template $\mathcal{F}$ would equal the shifted template $\mathcal{N}^* = \mathcal{N} - d_0$, and the nominal plant P_0 would correspond to the shifted nominal numerator $n_0 - d_0$ (figure 4.14b). In case the denominator is *uncertain*, the uncertainty in the entire plant increases. The shifted template $\mathcal{N}^*$ must be extended with those points that can be reached within $\mathcal{D}_{\mathrm{mirror}}$, when the nominal point $-d_0$ lies within $\mathcal{N}^*$. $\mathcal{F}$ thus can be constructed by shifting $\mathcal{D}_{\mathrm{mirror}}$ around $\mathcal{N}^*$, keeping the nominal point $\mathcal{D}_{\mathrm{mirror}}$ on the contour of $\mathcal{N}^*$ (figure 4.14c). Template $\mathcal{F}$ (figure 4.14d) can be regarded the result of the addition of the templates $\mathcal{N}$ and $\mathcal{D}_{\mathrm{mirror}}$.

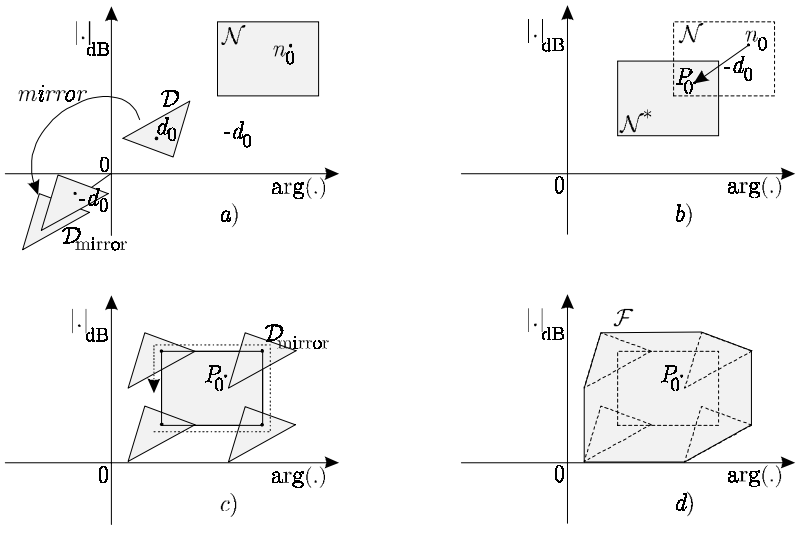

FIGURE 4.14 *Template addition*

The results above have been generalized for robust analysis and design in (Barmish, 1989), (Chapellat and Bhattacharyya, 1989) and (Siljak, 1989).

Tree structured decomposition (TSD)

In some cases a transfer function can be decomposed into a tree structure of simpler terms with disjoint subsets of the uncertain parameters (Ackermann, 1993). The value sets of these disjoint subsets can be constructed independently, using the techniques summarized above. Consecutively, the value set of the transfer function can be constructed from the independent value sets, using operations as described by Ackermann (1993).

The difficulty of this approach is that a decomposition has to be found that results in disjoint subsets of uncertain parameters, *i.e.* determination of the tree structure. Algorithms for TSD have been described in (Sienel, 1992) and (Ackermann, 1993). These algorithms can be applied to polynomials, transfer functions or block diagrams, requiring (extensive) symbolic manipulations, but they are not always successful.

Sienel (1992) also shows that the tree structure can already be determined while forming the model of a plant if one follows the rule to keep uncertain parameters at their place and not to expand expressions unnecessarily. Wilson and Eryilmaz (1999) use bond graphs to obtain a tree-structured transfer function from a model, with as few algebraic manipulations as possible. In Wilson and Eryilmaz, 1998) the same authors give rules that describe when a given input-output pair of a physical plant model will lead to a tree-structured transfer function with disjoint parameters. This property can be guaranteed for collocated input-output pairs, but Wilson and Eryilmaz (1998) extend this property to a broader class of systems, and provide a means to determine by inspection whether a given input-output pair will result in a transfer function with disjoint parameters.

4.4.3 Numerical template construction

Gridding

If it is not possible or difficult to determine which physical parameter combinations contribute to the contour of a template beforehand (*a priori*), the contour can be determined *a posteriori*. In order to be certain about the contour of a template, one should calculate the mapping $(\arg(P(j\omega,q)),\ |P(j\omega,q)|_{\mathrm{dB}})$ for the entire Q-box. The response should thus be calculated for an infinite set of parameter vectors, which of course is impossible. One can however approximate this infinite set with arbitrary accuracy by a finite subset of parameter vectors in the Q-box. This subset is referred to as the *grid* and the approximation technique is referred to as *gridding*. The problem in gridding is to determine the density of the grid beforehand. Visual

inspection of the template however yields an immediate answer to the question whether an applied grid was dense enough or not. Therefore it is advisable to start with a relatively low grid density that can be iteratively increased (figure 4.15 and figure 4.16). Once the gridding result is dense enough, one has to determine the points of the template that contribute to the contour.

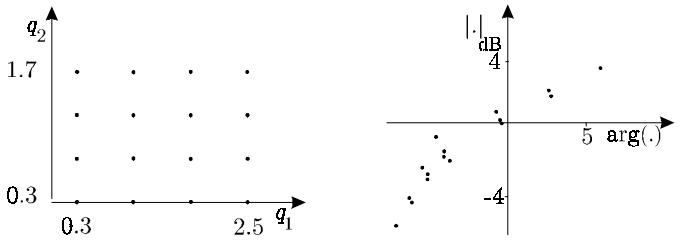

FIGURE 4.15 *Gridded Q-box and gridding result*

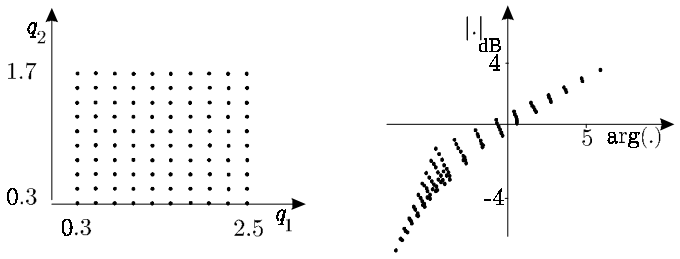

FIGURE 4.16 *A denser grid, a better gridding result*

The major drawback of gridding is the required computational effort. For m uncertain parameters with each n grid points, a total of n^m responses have to be determined. This method is only useful in situations with a small number ($n \leq 4$) of uncertain parameters.

Convex Hull Algorithm

To overcome the combinatorial explosion caused by gridding Wilson *et al.* (1996) developed an alternative algorithm to determine the convex hull of a value set or template. Similarly as in the Generalized Mapping Theorem of Barmish and Tempo (1996), the image set of an uncertain transfer function is obtained by a technique that involves minimizing a scalar dot product and using the design parameters that achieve this minimization to obtain a boundary point on the image set.

To obtain a value set, the mapping from the frequency space Ω and the hyperrectangle Q into the complex plane is considered:

$$V_{\mathbb{C}} : \Omega \times Q \mapsto \Re(\,) \times \Im(\,) \subset \mathbb{C} \tag{4.30}$$

where

$$V_{\mathbb{C}}(\,\omega, q\,) = \Big(\Re(P(\,j\omega, q\,)), \Im(P(\,j\omega, q\,))\Big) \tag{4.31}$$

$V_{\mathbb{C}}(\omega,q)$ is projected onto a unit vector at angle θ from the horizontal axis, and consecutively minimized (figure 4.17). The magnitude of the projection of $V_{\mathbb{C}}(\omega,q)$ onto this unit vector is obtained using the following dot product

$$H(\,\omega, \theta, q\,) = e^{j\theta} \cdot P(\,j\omega, q\,) = \cos\theta\, \Re(P(\,j\omega, q\,)) + j \sin\theta\, \Im(P(\,j\omega, q\,)) \tag{4.32}$$

Next, the point $q \in Q$ is determined that minimizes (4.32):

$$H\left(\omega, \theta, q_\theta^*\right) = \min_{q \in Q}(H(\,\omega, \theta, q\,)) \tag{4.33}$$

When the point q_θ is substituted in the mapping function (4.31), a boundary point of $P(j\omega,q)$ in the complex plane results. This optimization is repeated over a series of angles, θ=$\{0,\ \Delta\theta,\ \ldots,\ 2\pi\text{-}\theta\}$ and the collection of $\{q_\theta\}$ is substituted in (4.31). The result is a collection of points that define the convex hull boundary of the image set of the uncertain transfer function, denoted by $\partial P(j\omega)$. This boundary and its interior points are referred to as the minimized frequency response template (Wilson *et al.*, 1996).

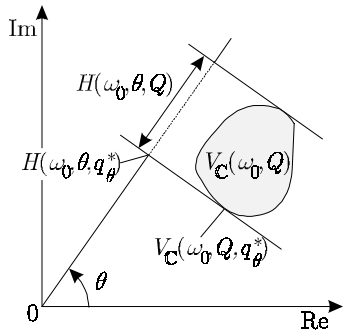

FIGURE 4.17 *Projection of uncertainty template onto unit vector*

Adaptive Angular Sweep Algorithm

Both the Generalized Mapping Theorem (Barmish and Tempo, 1996) and the Convex Hull Algorithm (Wilson *et al.*, 1996) require gridding of the angle θ. Wilson *et al.* (1999) recognized that a uniform grid makes no allowance for the location, size or shape of a convex hull. Consequently, it introduces more computations than typically necessary. Therefore, Wilson *et al.* (1999) developed an adaptive angular sweep approach to grid the angle θ nonuniformly such that the maximum normal

distance between the boundary of the actual convex hull and its approximation with a set of angles Θ is less than an arbitrary error bound.

4.4.4 Templates for electromechanical motion systems

Several techniques for template construction have now been discussed. Our aim is to develop design support that automatically generates templates from a physical model of electromechanical motion systems and a set of critical frequencies. Therefore, we will select methods suitable for this class of systems and suitable for automation.

Over-bounding

Before selecting suitable methods, we consider what may happen when template addition is applied to a transfer function that shares dependency on some uncertain physical parameters between the numerator and the denominator. We illustrate this with the transfer function from input force to actuator position of the flexible mechanism (4.4):

$$
\begin{aligned}
P_0(s,q) &= \frac{b_2 s^2 + b_1 s + b_0}{a_4 s^4 + a_3 s^3 + a_2 s^2 + a_1 s} \\
b_2 &= A m_1 \\
b_1 &= A d_{10} \\
b_0 &= A c \\
a_4 &= m_1 m_2 \\
a_3 &= (d_{10} m_2 + d_{20} m_1) \\
a_2 &= (c m_2 + c m_1 + d_{10} d_{20}) \\
a_1 &= c(d_{10} + d_{20})
\end{aligned}
\tag{4.34}
$$

We assume that the mass of the end-effector m_1 is unknown but bounded; it may vary between 100% and 200% of its nominal value. The damping d_{10} may vary between 50% and 200% of its nominal value and other physical parameters are assumed to be certain.

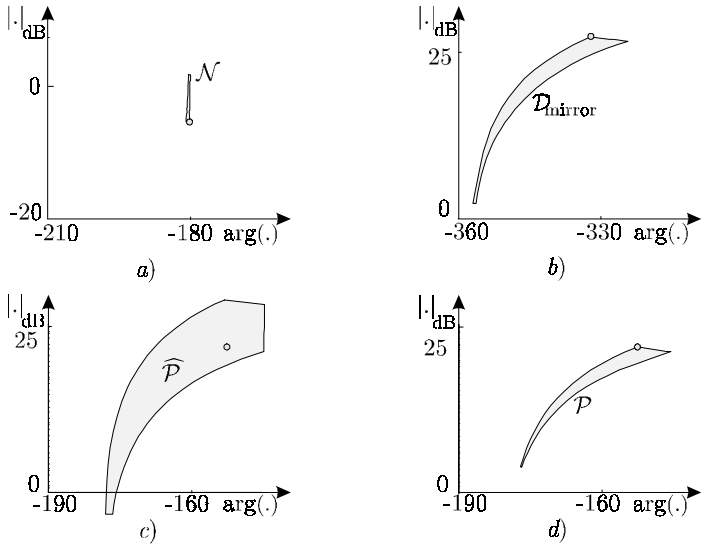

FIGURE 4.18 *a) shifted numerator sub-template*
b) denominator sub-template
c) overbounded template
d) actual template

When we apply template addition, we obtain the results as shown in figure 4.10 and figure 4.14. In figure 4.18a the template $\mathcal{N}$ of the numerator is shown. The mirrored template $\mathcal{D}_{\text{mirror}}$ of the denominator is shown in figure 4.18b. Addition of the templates results in the over-bounded template of figure 4.18c. The actual template $\mathcal{P}$ is much smaller, as can be seen from figure 4.18d. Thus, in this case application of template addition results in significant over-bounding. In (Wilson *et al.*, 1996) possible consequences are shown by means of an example in which a constant coefficient compensator fails to meet the design specifications when analyzed using an interval plant such as above, while the specifications are actually met when analyzed with more accurate plant models, *i.e.* a so-called minimized plant and a gridded plant model. When using the interval plant, the designer has to make the system robust for non-existing uncertainties and an unnecessary increase of the cost of feedback is likely.

Analytical template construction

Analytical template construction methods, *i.e.* template addition and tree structured decomposition, are only applicable to a limited group of plant models. In the relatively simple problem of figure 4.18, the drawback of template addition is already illustrated. The application of tree structured decomposition may be difficult or impossible. The use of bond graph models (Wilson and Eryilmaz, 1998; Wilson and Eryilmaz, 1999) does certainly simplify the problem of finding a

decomposition, but it does not overcome the fact that a significant number of plant models cannot be decomposed into a tree structure, for example the transfer function from actuator force to end-effector position of the flexible mechanism (Wilson and Eryilmaz, 1998). An attractive solution would be to decompose the model in a tree structure as far as possible and apply a numerical technique to those parts of the structure that contain repeated parameters.

Numerical template construction

For up to about four uncertain parameters, gridding is a straightforward, maybe time-consuming, but nearly errorless method that can easily be automated. Its applicability is not limited to a particular class of models. Ackermann (1993) states that "in most practical cases gridding the whole Q-box is more effective than solving the system of equations". The Adaptive Angular Sweep Algorithm (Wilson *et al.*, 1999) is also not restricted to certain classes of models and it can handle a relative large amount of uncertain parameters.

Two numerical template construction methods are selected as suitable for enhancing automated design of QFT-controllers for electromechanical motion systems with uncertain physical parameters. For a small amount of uncertain parameters *gridding* is attractive, because an interesting feature of automated gridding is that the designer can select predefined grid-points (on the contour) of a template and investigate which combination of parameter values corresponds to that particular point. In this way, the designer is given the opportunity to signal physical parameter uncertainties that unnecessarily complicate controller design. The designer could reconsider the plant design in order to avoid undesired situations. For a large amount of uncertain parameters, the Adaptive Angular Sweep Algorithm is attractive, as this method is computationally less expensive. However, only a limited number of points on the contour of a template can be investigated on the underlying values of the physical parameters.

4.5 Performance specifications

4.5.1 Introduction

Quantitative Feedback Theory is a frequency-domain design method. However, performance specifications for electromechanical motion systems are typically stated in terms of space and time. Therefore, these specifications have to be converted into the frequency domain. We will consider transient systems that perform *point-to-point motions*, where the end-effector of an electromechanical motion system must respond to a (smoothened) step input. *I.e.*, the reference path r indicates a motion distance h_{m} and a motion time t_{m}. The positional error, *i.e.* the maximum

absolute error after the motion time, should be smaller than a specified maximum positional error e_0. We define the conversion problem as:

Definition 4.11 Specification conversion problem

Given the dominant plant behavior and point-to-point motion specifications in terms of the motion distance h_m, the motion time t_m and the maximum positional error e_0, construct a frequency tolerance band $\mathcal{H}_{spec}$ for the command response $H(s)$, such that fulfillment of the tolerance band indicates fulfillment of the point-to-point motion specifications.

The frequency-domain specification $\mathcal{H}_{spec}$ for QFT implicitly consists of two parts that are both achieved when the actual frequency-response band $\mathcal{H}$ fits in the specified frequency-response band $\mathcal{H}_{spec}$. These two parts are:
- a specification for the desired performance of the controlled system.
- a specification for the admissible uncertainty for the controlled system.

In (Horowitz and Sidi, 1972) the synthesis of feedback systems using QFT is described. The first principle step in the described design procedure is the translation of time domain bounds on $z(t)$ into bounds on the command response $|H(j\omega)|$. The set of acceptable command response transfer functions $\mathcal{T}_{spec}$, which is also referred to as the *thumbprint specification*, has to contain the closed-loop responses of all plants that are member of the parametric plant family $\mathcal{P}_p$. In (Horowitz and Sidi, 1972) the proposition is to start with assuming a simple second- or third-order model for the command response $H(s)$ and finding the bounds on the model parameters which correspond to the bounds on the time response. From the model parameter bounds the resulting bounds on $|H(j\omega)|$ can be determined. Or, stated differently, the acceptable command responses $\mathcal{T}_{spec}$ are to be converted into acceptable frequency responses $\mathcal{H}_{spec}$. This approach has been described more extensively in (D'Azzo and Houpis, 1995). However, because of the trail-and-error nature of this approach (Krishnan and Cruickshanks, 1977), alternative approaches have been developed.

4.5.2 Alternative approaches

Time-domain analogue of QFT

Instead of applying a frequency-domain technique like QFT, one can design a controller in the time-domain. Barnard and Beydoun (1993) claim to have developed the time-domain analogue of QFT. In this method the tracking error $e(t)$ is defined as the difference between the output of the prefilter and the output $z(t)$ of the 2-DOF feedback system, *i.e.* servo behavior is considered. The first step in the design method is to develop a relatively simple controller for the uncertain plant. Next, the parameters of this controller are optimized according to a criterion, such that the maximum error is minimized. Though this method seems promising,

it turns out to be difficult to determine conditions under which the controller parameters will converge (Barnard and Beydoun, 1993).

Another, more important problem is the fact that, once the optimal parameters have been found, the performance of the corresponding optimal controller may be unsatisfactory, *i.e.* the actual minimized maximum error may be larger than the specified maximum error. In that case the next step would be to design an initial controller of a higher order, and to optimize over the parameters of this new controller. This is in contrast to QFT, in which all effort during the design procedure is aimed at satisfaction of the *original objectives*. If application of traditional, frequency-domain QFT to a control problem does not provide the desired controller, this will become clear *during* instead of *after* the design procedure. The design engineer can see at any time during controller design whether or not the objectives, stated in the frequency-domain, will be met. In the proposed time-domain QFT analogue all effort is aimed at the optimal controller of a fixed order. Whether this optimal controller performs satisfactory, can not be determined until *after* the design procedure. If so, the design engineer does not know whether it is the minimum bandwidth controller. If not, the design engineer has no indication on how to modify the design. For these reasons (traditional) frequency-domain QFT is preferable, thus the time- to frequency-domain conversion problem remains to exist.

Conversion of sensitivity specifications

Krishnan and Cruickshanks (1977) proposed a "simple and rational method of converting time-domain sensitivity specifications into frequency-domain criteria", which has been build upon by East (1981). There are some problems in applying this method: before, during and after conversion.

Before conversion

The first problem is the specification of appropriate time-domain requirements. Krishnan and Cruickshanks (1977) assume the response $z(t,q)$ to an input $r(t)$ to lie between two extreme responses:

$$a(t) \leq z(t,q) \leq b(t) \text{ for all } t. \tag{4.35}$$

Given these two extremes, one can define the mean desired response

$$m(t) = \tfrac{1}{2}(b(t) + a(t)) \tag{4.36}$$

and the maximum variation on this mean response

$$v(t) = \tfrac{1}{2}(b(t) - a(t)) \ . \tag{4.37}$$

Both $m(t)$ and $v(t)$ are assumed to be known functions of time t, such that their Laplace transforms $M(s)$ and $V(s)$ can be determined. However, in examples discussed by Krishnan and Cruickshanks (1977) they specify $m(t)$ and $v(t)$ as the

sum of exponentially decreasing functions. In doing this, they implicitly choose the Laplace transform. This means that the requirements are not purely in the time-domain.

During conversion
The second problem is in the conversion procedure itself. Instead of fulfilling the time-domain requirement

$$(z(t,q) - m(t))^2 \leq v^2(t) \text{ for all } t, \tag{4.38}$$

which is equivalent to (4.35), it is tried to satisfy the *weaker* requirement

$$\int_0^t (z(\tau,q) - m(\tau))d\tau \leq \int_0^t v^2(\tau)d\tau \text{ for all } t > 0 \tag{4.39}$$

A *sufficient* condition in the frequency-domain corresponding to (4.39) is given by

$$\max_q \left| \frac{R(j\omega)F(j\omega)}{M(j\omega)} \frac{L(j\omega,q)}{1 + L(j\omega,q)} - 1 \right| \leq \left| \frac{V(j\omega)}{M(j\omega)} \right| \text{ for all } \omega \tag{4.40}$$

where $R(s)$, $F(s)$ and $L(s)$ represent reference input, prefilter and open-loop transfer function respectively. Krishnan and Cruickshanks (1977) consider (4.40) as the starting-point for a frequency-domain design method. However, it should be noted that several concessions have been made during the derivation of this condition: the original time-domain requirement (4.35) is first weakened (4.39) and next tightened (4.40). Therefore, the frequency-domain requirement is not the *exact* equivalent of the original time-domain requirement.

After conversion
The third and last problem is the conversion result (4.40). QFT can not cope with this frequency-domain requirement directly. Krishnan and Cruickshanks (1977) therefore propose a special choice of the prefilter

$$F(s) = \frac{M(s)}{R(s)}, \tag{4.41}$$

thus simplifying (4.40) to

$$\max_q |S(j\omega,q)| \leq \left| \frac{V(j\omega)}{M(j\omega)} \right| \text{ for all } \omega, \tag{4.42}$$

with S the sensitivity function. The sensitivity conversion method does not yield the closed-loop response tolerance band required by QFT, but an upper bound on the sensitivity function. However, Horowitz (1991) emphasized that "... the sensitivity function is very insensitive to a major cost of feedback", *i.e.*, sensor or measurement noise. It is for this reason that Horowitz prefers shaping the open-loop frequency response $L(s)$ rather than shaping the sensitivity $S(s)$.

4.5.3 Original conversion method

Despite these alternative solutions, we believe that the most direct and useful form of the specifications on the response would be in the time domain, *e.g.* bounds on the step response. Therefore, we will describe the approach of (Horowitz and Sidi, 1972) and (D'Azzo and Houpis, 1995) in more detail. First, we formulate what an ideal conversion method should do:

Statement 4.4 Ideal conversion method

An ideal conversion method has to assure that:
- *all frequency responses that fit in the frequency tolerance band* $\mathcal{H}_{\text{spec}}$*, correspond to time responses that fit in the thumbprint specification* $\mathcal{T}_{\text{spec}}$*,*
- *all time responses that fit in the thumbprint specification* $\mathcal{T}_{\text{spec}}$*, correspond to frequency responses that fit in the frequency tolerance band* $\mathcal{H}_{\text{spec}}$*,*

under the condition that the assumed system model $H(s)$ *is correct.*

We begin by assuming a second-order system model for $H(s)$, as in (D'Azzo and Houpis, 1995) and (Houpis and Rasmussen, 1999):

$$H(s) = \frac{\omega_{\text{n}}^2}{s^2 + 2\zeta\omega_{\text{n}}s + \omega_{\text{n}}^2} \tag{4.43}$$

with ω_{n} the eigenfrequency and ζ the relative damping. The thumbprint specification $\mathcal{T}_{\text{spec}}$ for this system is constructed from two step responses. Characteristics of these responses are shown in figure 4.19. The time responses $z(t)_{\text{L}}$ and $z(t)_{\text{U}}$ represent the upper and lower bound of $\mathcal{T}_{\text{spec}}$, *i.e.* an acceptable response must lie between these bounds. We determined these responses such that at $t = t_{\text{m}}$ the overshoot equals e_0 respectively the lag error equals, $-e_0$.

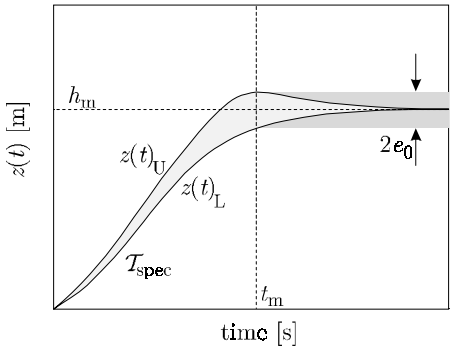

FIGURE 4.19 *Characteristic of thumbprint specification*

As an example, we choose a motion distance h_m of 1 [m], a motion time t_m of 1 [s] and a maximal positional error e_0 of 0.01 [m]. The two extreme responses can be described as:

- *upper:* The overshoot of $z(t)_U$ has the size e_0 and occurs at t_m. The parameters corresponding to this response are $\omega_n = 5.57$ [rad/s] and $\zeta_{min} = 0.83$, giving the system model $H(s)_U$.
- *lower:* The lag error of $z(t)_L$ has the size $-e_0$ at t_m. The parameters corresponding to this response are $\omega_n = 5.57$ [rad/s] and $\zeta_{max} = 0.93$, giving the system model $H(s)_L$.

The magnitudes of the frequency responses of $H(s)_U$ and $H(s)_L$ form the upper bound B_U and lower bound B_L, which constitute the frequency tolerance band $\mathcal{H}_{spec}$. Characteristics of this tolerance band are shown in figure 4.20a. In a minimum-phase system, the magnitude of the frequency response $|H(j\omega)|$ completely specifies the transfer function $H(s)$, therefore only a tolerance on the magnitude of the frequency response is determined.

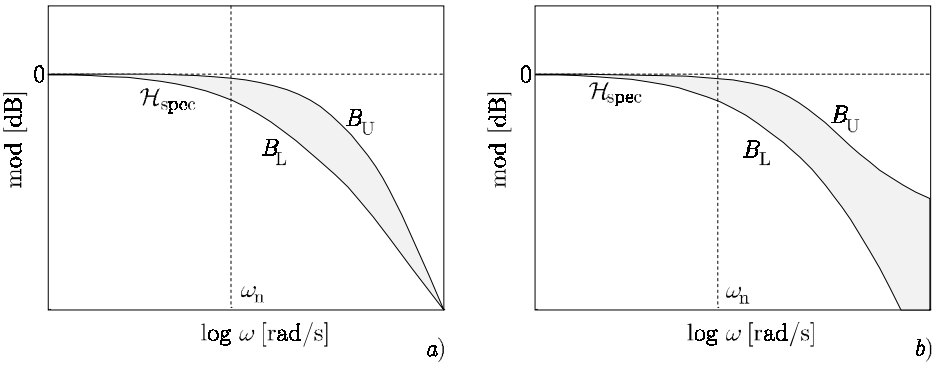

FIGURE 4.20 *a) Characteristic tolerance band of original conversion method*
b) Characteristic tolerance band with additional pole and zero

Because the models $H(s)_U$ and $H(s)_L$ are both second-order with identical eigenfrequency ω_n, the asymptotes are identical for $\omega \to \infty$. However, it is desirable to increase the spread between B_U and B_L for increasing ω. This can be achieved by changing B_U and B_L, without violating $\mathcal{T}_{spec}$. Firstly, $H(s)_U$ is augmented with a negative real pole that is as close to the origin as possible but far enough away not to affect the time response significantly. Secondly, the spread is further increased by augmenting $H(s)_L$ with a negative real zero without significantly affecting the time response. The additional pole and zero raise B_U respectively lower B_L in the high-frequency range, such that we obtain a new tolerance band $\mathcal{H}_{spec}$. The characteristics are shown figure 4.20b.

This method is a useful approach, however there are two problems:

1. In the second-order model $H(s)$ only uncertainty in ζ is considered and not in ω_n. However, physical parameter uncertainty in $\mathcal{P}$ will often affect the eigenfrequency ω_n as well as the relative damping ζ.
2. The thumbprint specification of figure 4.19 is not ideal for describing point-to-point motion specifications. It will be shown that there are second-order step responses that meet the motion specifications, but do not fit within the thumbprint specification.

4.5.4 Modified conversion method

Second-order dominant behavior
In order to overcome the problems indicated above, we modify the approach of Horowitz and Sidi (1972) by extending $\mathcal{T}_{spec}$. The new thumbprint specification is constructed from three responses, which are characterized by:

1. an overshoot of $z(t)$ that has size e_0 and occurs at t_m. The parameters corresponding to this response are, similar as for $z(t)_U$, ω_{max} and ζ_{min}.
2. a lag error of $z(t)$ that has size $-e_0$ at t_m. The parameters corresponding to this response are, similar as in $z(t)_L$, ω_{max} and ζ_{max}.
3. an overshoot of $z(t)$ that has size e_0 and occurs at $t > t_m$, with $h(t_m) = h_m - e_0$. The parameters corresponding to this response are ω_{min} and ζ_{min}.

We allow variations [ω_{min} - ω_{max}] in the eigenfrequency for a relative damping ζ_{min}. Therefore, the proposed modification also solves problem 1, as formulated at the end of section 4.3.3. Characteristics of the newly obtained thumbprint specification $\mathcal{T}_{spec}$ are shown in figure 4.21.

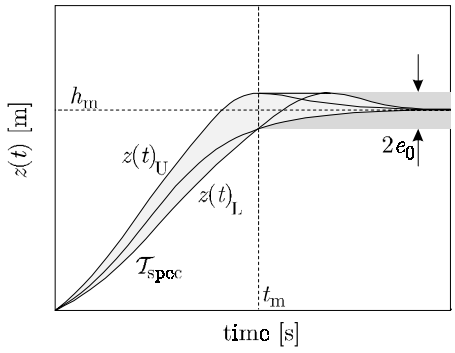

FIGURE 4.21 *Characteristics of the modified thumbprint specification*

The values of the parameter bounds for the example are:

$\omega_{min} = 4.19$ [rad/s] $\quad \zeta_{min} = 0.83$
$\omega_{max} = 5.57$ [rad/s] $\quad \zeta_{max} = 0.93$

The parameter bounds span a triangle in the ω_n-ζ plane that contains all second-order time responses that fit within $\mathcal{T}_{spec}$.

Remark 4.3

There are other second-order responses that meet the point-to-point motion specifications. These are fast responses with a high eigenfrequency, for which the overshoot occurs before t_m. In a controller design problem solutions with a high eigenfrequency may unnecessarily increase the cost of feedback, therefore we focus on the solutions with a peak time at $t \geq t_m$.

Remark 4.4

The parameter bounds do not span a rectangle in the ω_n-ζ plane, as the response with ω_{min} and ζ_{max} is too slow to meet the point-to-point motion specifications.

Next, we draw the frequency responses $|H(j\omega)|$ corresponding to the three time responses and determine the frequency tolerance band $\mathcal{H}_{spec}$ (figure 4.22). It can be seen that the upper and lower bound do not have the same high-frequency asymptote, as they have different eigenfrequencies.

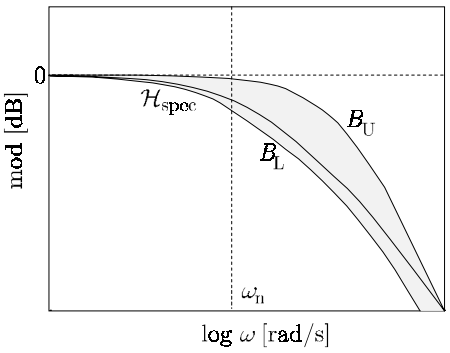

FIGURE 4.22 *Modified frequency tolerance band*

By means of simulation we will verify whether the modified conversion method is an ideal conversion method, according statement 4.4. In the simulations we use the example presented above. In figure 4.23 the results of the conversion are shown for different grid points in the ω_n-ζ plane. For each grid point we indicated whether the corresponding frequency response fits within the frequency tolerance band $\mathcal{H}_{spec}$ and/or whether the step response fits within the thumbprint specification $\mathcal{T}_{spec}$.

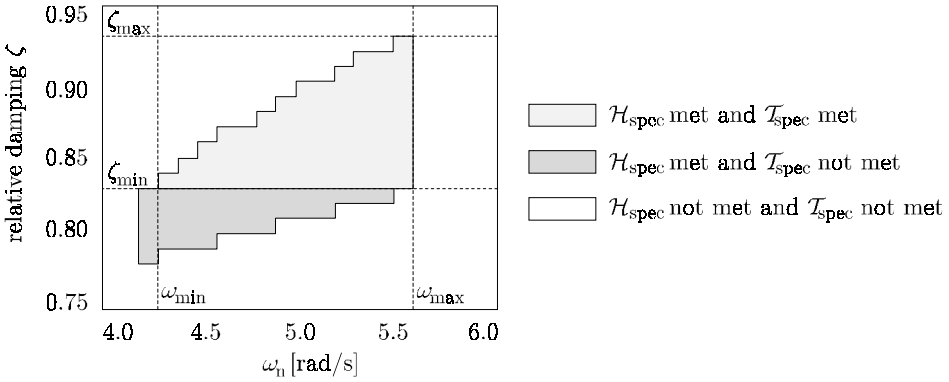

FIGURE 4.23 *Results of modified conversion method*

It can be seen that there are several responses fitting in the frequency band $\mathcal{H}_{\text{spec}}$ but not in the thumbprint $\mathcal{T}_{\text{spec}}$. Obviously, this is not ideal, as the designer has access to responses that unjustly seem valid in the frequency domain.

The cause of this problem is the following. We initially stated that in a minimum-phase system the magnitude of the frequency response $|H(j\omega)|$ completely specifies the transfer function $H(s)$, which in turn uniquely determines the step response. However, the magnitude of a *response band* $\mathcal{H}$ does *not* completely specify the intended *set* of transfer functions, as there are also undesired frequency responses fitting in the tolerance band. It is wise to simultaneously consider the phase as well as the gain of the response band.

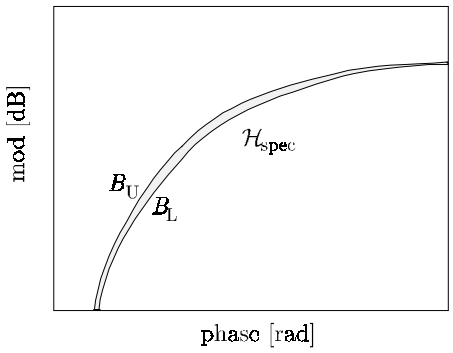

FIGURE 4.24 *Characteristic frequency tolerance band in Nichols chart*

Therefore, we propose to convert the tumbprint $\mathcal{T}_{\text{spec}}$ into a frequency response band $\mathcal{H}_{\text{spec}}$ in the Nichols chart, instead of into a band in the Bode diagram. The

frequency tolerance band in the Nichols chart, which corresponds to the band in figure 4.22, is shown in figure 4.24.

Again, we use the example to verify the conversion method by performing simulations of different grid points in the ω_n-ζ plane.

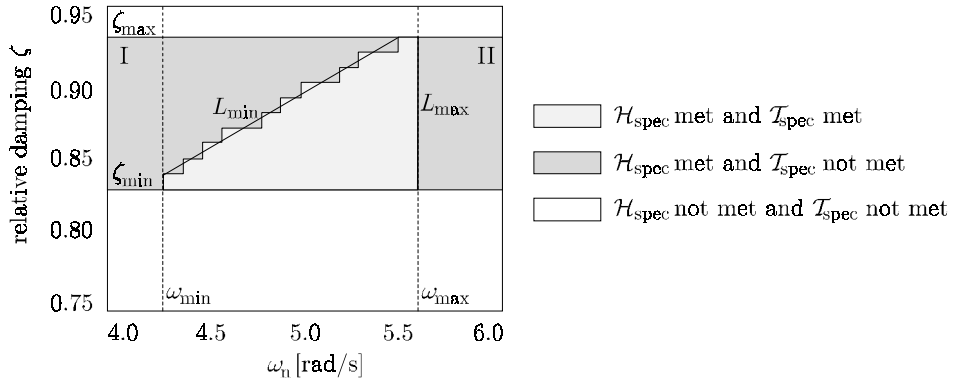

FIGURE 4.25 *Results of modified conversion method using Nichols chart*

In figure 4.25 it can be seen that for the same combinations of values of ω_n and ζ as before, both time and frequency specifications are met. But similar as in using a Bode diagram, several responses exist where only the frequency tolerance band is met. Two different areas are distinguished, as indicated in figure 4.25:

- Area I, where $\zeta_{min} \leq \zeta \leq \zeta_{max}$ and ω_n is located left from L_{min}, *i.e.* the line constituted by the points $(\omega_{min,}\ \zeta_{min})$ and $(\omega_{max,}\ \zeta_{max})$.
- Area II, where $\zeta_{min} \leq \zeta \leq \zeta_{max}$ and $\omega_n > \omega_{max}$, *i.e.* right from the line L_{max}.

To isolate the area where ideal conversion takes place, we introduce frequency limits in the Nichols chart. Once the actual response $\mathcal{H}$ is shaped such that it fits within the frequency tolerance band $\mathcal{H}_{spec}$, the dominant pole-pair has a valid relative damping (figure 4.25). However, in order to avoid the response being in area I and II, the eigenfrequency of this pole-pair has to be located to the right of L_{min} and to the left of L_{max}. In order to verify this condition, we will project the frequency limits L_{min} and L_{max} onto the Nichols chart. First, we calculate the frequency responses of the corner points of the triangle of figure 4.25 where ideal conversion takes place. The responses are located on the boundaries of $\mathcal{H}_{spec}$ and equal:

$$H\left(j\omega_i\right) = \frac{\omega_i^2}{-\omega_i^2 + 2\zeta_i\omega_i j\omega_i + \omega_i^2} = \frac{1}{2j\zeta_i} \tag{4.44}$$

where i stands for either min or max. It turns out that these responses are independent of the frequency ω_n. As a consequence, the projections of the lines L_{min}

and $L_{\max}$ in the Nichols chart are identical. In figure 4.26 these are denoted as one vertical line B_ω, constituted by the points:

$$B_{\omega,\mathrm{U}} = \frac{1}{2j\zeta_{\min}} \quad \text{and} \quad B_{\omega,\mathrm{L}} = \frac{1}{2j\zeta_{\max}} \tag{4.45}$$

which is obtained by varying ζ from $\zeta_{\min}$ to $\zeta_{\max}$. When we want to evaluate the eigenfrequency of the dominant pole-pair of an actual response $H(j\omega)$, which fits in $\mathcal{H}_{\mathrm{spec}}$, we have to consider the response for the frequency on the line $L_{\min}$ that corresponds to the actual relative damping ζ of $H(s)$:

$$\omega_{\mathrm{low}} = \omega_{\min} + \frac{\omega_{\max} - \omega_{\min}}{\zeta_{\max} - \zeta_{\min}} \cdot (\zeta - \zeta_{\min}) \tag{4.46}$$

Similarly, we have to consider the response for the frequency on the line $L_{\max}$ that corresponds to the actual relative damping ζ of $H(s)$, *i.e.* $\omega_{\max}$. When the response $H(j\omega_{\mathrm{low}})$ is located to the right of the line B_ω than ω_{n} of the dominant pole-pair of $H(s)$ is located to the right of the line $L_{\min}$ in the ω_{n}-ζ plane. Similarly, when the response $H(j\omega_{\max})$ is located to the left of the line B_ω than ω_{n} of the dominant pole-pair of $H(s)$ is located to the left of the line $L_{\max}$ in the ω_{n}-ζ plane.

In figure 4.26 we indicated $H(j\omega_{\mathrm{low}})$ and $H(j\omega_{\max})$ for a single response, as well as the frequency limit B_ω. In this figure both points meet the frequency limit, thus both the frequency-domain and time-domain specifications are met.

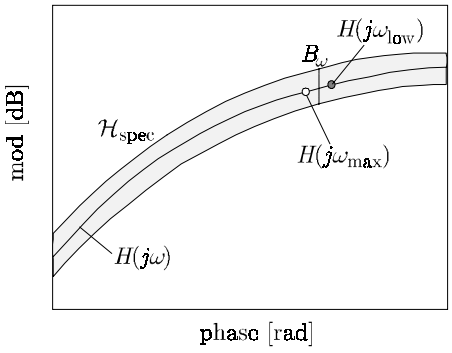

FIGURE 4.26 *Frequency limit within Nichols chart*

Statement 4.5 Conversion using second-order system models

When the uncertain response band $\mathcal{H}$ is fitted in the specified frequency response band $\mathcal{H}_{\mathrm{spec}}$ and the frequency limits are met (figure 4.26), then the time responses will fit in the thumbprint $\mathcal{T}_{\mathrm{spec}}$ and the point-to-point motion specifications are met.

Remark 4.5

When $H(j\omega_{\max})$ is on the right side of B_ω then the time response does not fit within the thumbprint specification, but the point-to-point motion specifications are still met, however, probably with an unnecessary high cost of feedback. In this situation the positional error is already smaller than e_0 before the specified motion time t_m is passed.

Higher-order dominant behavior
When a higher-order dominant behavior for $H(s)$ is considered, we need to introduce additional assumptions. When, for example, a third-order dominant behavior is assumed, three independent parameters can be identified: the eigenfrequency ω_n, the relative damping ζ of the complex pole-pair and the location of the real pole a. The additional assumption concerns the ratio of a and ω_n. When this ratio is fixed, still only two parameter values have to be determined for which the time-domain specifications are met: the eigenfrequency ω_n and the relative damping ζ. Similarly as for second-order systems, a triangular region in the ω_n-ζ plane (figure 4.25) exists for which ideal conversion takes places, which can be isolated by means of a frequency limit (figure 4.26). When we introduce a real pole to the example above, with a $= -\omega_n$, then the triangle in the ω_n-ζ plane is described by:

$$\omega_{\min} = 5.25 \text{ [rad/s]} \qquad \zeta_{\min} = 0.73$$
$$\omega_{\max} = 6.89 \text{ [rad/s]} \qquad \zeta_{\max} = 0.88$$

For higher-order poles and zeros a similar approach can be used, *i.e.* fix the relation between the magnitudes and determine the values of the eigenfrequency and the relative damping of the pole-pair. This approach is attractive, as only (independent) bounds on the parameters of the dominant pole-pair have to be searched, instead of multiple, possibly dependent, parameter bounds for all poles and zeros of the dominant behavior. The location of the dominant pole-pair in the s-plane is of most importance, as this is closely related to the speed and overshoot of the response.

4.5.5 Example

As an example we will consider the placement module of the FCM. We describe this plant as an uncertain moving mass:

$$P(s) = \frac{1}{ms^2} \tag{4.47}$$

with

$$m \in \left[6.85;\ \ 7.35\right] \quad \text{[kg]}$$

We define 5 equidistant grid points in this range en select the nominal value of the mass m_0 as 7.10. For the specification we reuse the (fictitious) values used so far, *i.e.* $h_{\mathrm{m}} = 1$ [m], $t_{\mathrm{m}} = 1$ [s] and $e_0 = 0.01$ [m]. We assume a dominant second-order system behavior for $H(s)$, such that we can also reuse the frequency response band $\mathcal{H}_{\mathrm{spec}}$ described above.

First we design a compensator using QFT that satisfies performance and stability bounds. We obtain a PD compensator, described by:

$$C(s) = \frac{K\left(s\tau_{\mathrm{d}} + 1\right)}{\left(s\beta\tau_{\mathrm{d}} + 1\right)} = \frac{107\,(0.41 \cdot s + 1)}{(0.41 \cdot 0.1 \cdot s + 1)} = \frac{10.7\,(s + 2.43)}{(s + 24.3)} \tag{4.48}$$

We will compare prefilter design in the Bode diagram with design in the Nichols chart. A prefilter that meets the tolerance band $\mathcal{H}_{\mathrm{spec}}$ in the Bode diagram is:

$$F(s) = \frac{0.15\,(s + 15.79)}{(s + 2.43)} \tag{4.49}$$

The corresponding command response is shown in figure 4.27. The frequency tolerance band $\mathcal{H}_{\mathrm{spec}}$ in the Bode diagram is indeed met, but it can also be seen that the thumbprint specification $\mathcal{T}_{\mathrm{spec}}$ is not met.

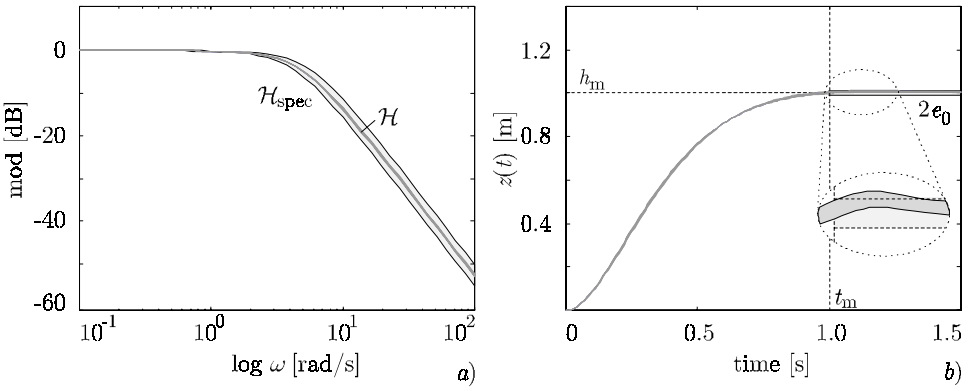

FIGURE 4.27 *Example: prefilter design in Bode diagram*

When the prefilter (4.49) is considered in the Nichols chart, it appears that the responses indeed do not fit in the frequency tolerance band. When the prefilter is modified such that the response does fit in the Nichols tolerance band, we obtain:

$$F(s) = \frac{0.15\,(s + 16.03)}{(s + 2.43)} \cdot \frac{25\left(s^2 + 2 \cdot 0.82 \cdot 4.7s + 22.1\right)}{22.1\left(s^2 + 2 \cdot 0.86 \cdot 5s + 25\right)} \tag{4.50}$$

The result is shown in figure 4.28. The responses fit in the frequency tolerance band and the step responses meet the point-to-point motion specification.

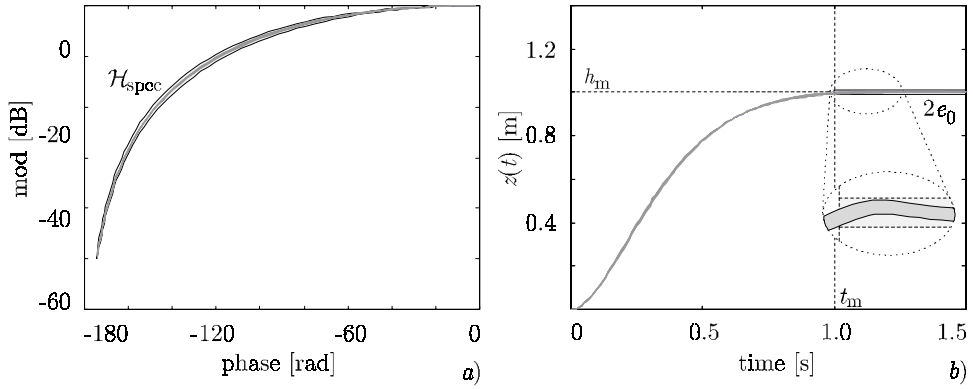

FIGURE 4.28 *Example: prefilter design in Nichols chart*

When we take a closer look at the prefilter (4.49), we see that the real pole compensates the zero of the compensator, such that we obtain dominant second-order behavior. This is also holds for the prefilter (4.50), but additionally there is a zero-pair that approximately cancels the poles of the complementary transfer functions and a complex pole-pair that introduces the desired dominant behavior. This corresponds to what one would obtain using the polynomial approach to pole placement, as discussed in (Wolovich, 1974) and (Åström and Wittenmark, 1997). Hence, the proposed method naturally leads the designer to sensible choices. A main advantage of the conversion procedure proposed here is that, unlike in the polynomial approach, *the uncertainty is incorporated explicitly.*

4.5.6 The conversion procedure

The overall design procedure becomes as follows. At the start of the conversion procedure, we have to assume a particular dominant system behavior. After completion of the QFT design, the validity of this assumption has to be evaluated. Whenever required, iterations may take place, as indicated in figure 4.29.

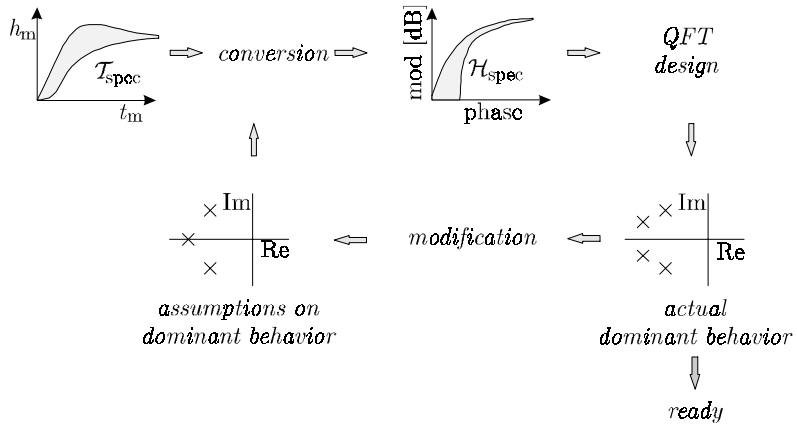

FIGURE 4.29 *Iterative conversion procedure*

The need for iterations originates from the fact that assumptions have to be made *before* the compensator $C(s)$ and the prefilter $F(s)$ are actually designed. The question whether the initial assumptions are correct, can only be answered *after* completion of the controller design procedure. To support the designer, well-chosen defaults for the dominant behavior are to be supplied.

Default assumption
The default assumption should be chosen as simple as possible. Within the dominant system behavior, we distinguish a *desired* component, as well as an *expected* component. The desired component is generally a complex pole pair with such an eigenfrequency and relative damping that it meets the time-domain performance. However, other poles and zeros may be located close to this pole pair, such that these also contribute to the dominant behavior. These may be predicted or may be known from previous iterations. We refer to these poles and zeros as the expected component, as their contribution is only known exactly after completion of the design procedure.

Remark 4.6

By means of prefilter design, the dominant behavior of $H(s)$ can be manipulated, as poles and zeroes of the expected component can be compensated for in $F(s)$. However, as these poles and zeroes may be uncertain, cancellation is not always possible or desirable.

The simplest assumption is to consider only the desired component; by default we use a second-order model. When a higher-order model is assumed, we will use additional assumptions, as explained in section 4.3.4.

Remark 4.7

The assumption on the dominant system behavior does not cause a loss of transparency during QFT design of the control system.

Unstructured uncertainty
In QFT, unstructured uncertainty enters the design at higher frequencies in the frequency tolerance band. As discussed in section 4.3.3, the frequency tolerance band should therefore have an increasing spread at higher frequencies (figure 4.30a).

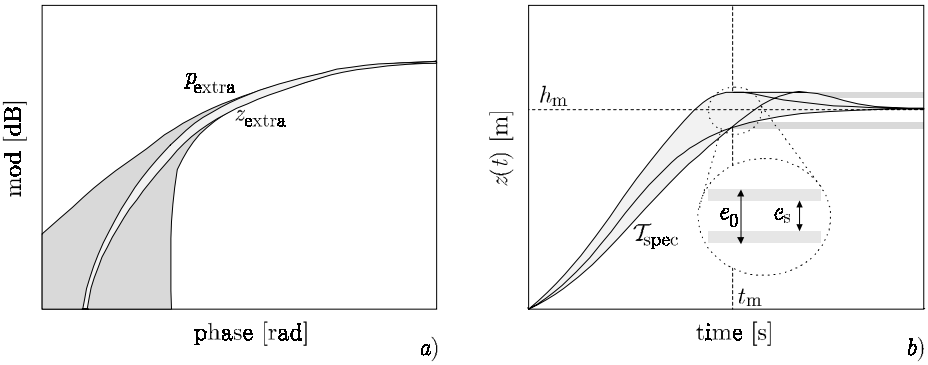

FIGURE 4.30 *Increased error due to unstructured uncertainty*

To obtain the increasing spread, a non-dominant zero z_{extra} is introduced in the upper tolerance bound and the lower tolerance bound is extended with a non-dominant pole p_{extra} (D'Azzo and Houpis, 1995). These additional dynamics will become noticeable in the time domain by a slight increase of the positional error. Hence, the unstructured uncertainty can be accounted for in the time-domain specification by dividing the maximum allowable positional error e_0 into a fraction e_{s} and e_{u}, as in figure 4.30b, where e_{u} is the shaded horizontal band. Loop shaping is done such that the frequency response is within the non-shaded tolerance bound determined by e_{s}. High-frequency uncertainty at worst will enlarge the positional error with e_{u}. By default it is assumed that $e_{\text{s}} = 0.9 \cdot e_0$.

Design procedure 4.1 Conversion algorithm (part I)

The conversion algorithm from the point-to-point motion specifications via the thumbprint specification $\mathcal{T}_{\text{spec}}$ to a frequency tolerance band $\mathcal{H}_{\text{spec}}$ is:

1. *Determine the overshoot of the step response of a system with the specified dominant behavior, with normalized eigenfrequency ($\omega_{\text{n}} = 1$) and relative damping $\zeta = 0.5$. If the overshoot is smaller than e_{s}, decrease ζ; increase ζ*

otherwise. Repeat the adjustment of the relative damping until $\zeta_{\min}$ *is found for which the overshoot equals the maximum allowed overshoot* e_s.

2. *Determine the maximum value of the eigenfrequency* $\omega_{\max}$ *from the ratio between the normalized peak-time* τ_p *(the time at which the overshoot occurs for normalized natural frequency* ω_n*) and the desired motion time* t_m*:* $\omega_{\max} = \tau_p / t_m$.
3. *Determine the lag error (at* $t = t_m$*) of the step response of a system with the specified dominant behavior, with eigenfrequency* $\omega_{\max}$ *and relative damping* $\zeta_{\min}$*. Increase the relative damping until* $\zeta_{\max}$ *is found where the lag error at* t_m *equals the maximum allowed error* e_s.
4. *Determine the lag error for a system with the specified dominant behavior, with eigenfrequency* $\omega_{\max}$ *and relative damping* $\zeta_{\min}$*. Decrease the eigenfrequency until* $\omega_{\min}$ *is found where the lag error at* t_m *equals the maximum allowed error* u_s.
5. *Construct the thumbprint specification* $\mathcal{T}_{spec}$ *from three responses of the assumed system model* $H(s)$ *with:*
   a. $\omega_{\max}$ *and* $\zeta_{\min}$
   b. $\omega_{\max}$ *and* $\zeta_{\max}$
   c. $\omega_{\min}$ *and* $\zeta_{\min}$.

   Include the region between the maximum values of step response a. and b., such that variations $\omega_n \in [\omega_{\min} ; \omega_{\max}]$ *are allowed for a relative damping* $\zeta_{\min}$.

Now the initial frequency tolerance band $\mathcal{H}_{spec}$ *has been constructed from the frequency response of system model* $H(s)$*. To allow for unstructured uncertainty, this band is expanded using the remaining part of the maximum relative positional error (*$e_u = e_0 - e_s$*):*

6. *Add a zero to the upper bound* $H(s)_U$ *at* $z_{extra} = -\omega_{\max}$*. Increase the magnitude of this zero until the overshoot at* t_m *equals* e_0.
7. *Add a pole to the lower bound* $H(s)_L$ *at* $p_{extra} = -\omega_{\max}$*. Increase the magnitude of this pole until the lag error at* t_m *equals* $-e_0$.

In the presented conversion procedure, the bounds of the model parameters are determined by means of a search. For low-order system models, these bounds could also be determined analytically, when using step responses. However, for second- or third-degree reference paths (refer chapter 2) this is not straightforward. With a small modification, procedure 4.1 can be applied to these reference paths as well (Holterman, 1997).

When the conversion has been completed, a compensator $C(s)$ can be designed using QFT. Consecutively, a prefilter $F(s)$ is to be designed, using the following procedure.

Design procedure 4.2 Prefilter design

1. *Draw the expanded tolerance band $\mathcal{H}_{\text{spec}}$ and the actual response band $\mathcal{H}$ in the Nichols chart.*
2. *Determine the frequency limit $B_{\omega,}$, by calculating the frequency response on the boundaries of $\mathcal{H}_{\text{spec}}$ for ω_{min} and ω_{max}.*
3. *Incorporate the desired components of the dominant system behavior in the prefilter.*
4. *Continue prefilter design such that $\mathcal{H}$ fits in $\mathcal{H}_{\text{spec}}$ and the frequency responses for ω_{low} and ω_{max} are on the left respectively the right of B_{ω}.*

When the initial assumptions on the dominant system behavior were correct, the controlled system will meet the point-to-point specifications. In case the actual dominant behavior differs significantly from the assumed dominant behavior, the assumptions need to be modified.

Design procedure 4.3 Conversion procedure (part II)

Iterations for assumed dominant system behavior:

8. *Determine the pole-zero map of the controlled system H(s).*
9. *Fix the ratio between the magnitude of the dominant complex pole-pair and the other poles and zeros.*
10. *Determine the minimum and the maximum value of the relative damping of the dominant pole-pair at ω_{n}, using the search algorithm of steps 1-4 of this design procedure.*

During design of the prefilter, the controlled system $H(s)$ is designed such that the response fits in the frequency tolerance band. Or stated differently, the frequency response is shaped such that the assumptions are met. Therefore, the conversion procedure is likely to converge, which is confirmed by several applications.

As an alternative to adjusting the assumptions, it may be advantageous to adjust the structured error fraction e_{s}/e_0. This is desirable if the width of the frequency response tolerance band does not continuously increase for high frequencies. It indicates that the influence of the extra pole and zero is rather small. Decreasing the structural error fraction e_{s}/e_0 can increase their influence.

Remark 4.8

Applying the conversion procedure manually is rather laborious; proper application requires computer-based support.

4.5.7 Relation with structured design method

We will now shortly discuss how the conversion method, including QFT design, fits within the structured design method of chapter 3. Uncertain physical parameters are a particular problem that may occur in the detailed design stage. In order to *quantitatively* deal with this uncertainty, one has to specify the desired performance of the controlled system, including the *allowed* uncertainty. The task specifications, in terms of space and time, were handled by the assessment method of chapter 2. Reusing the bandwidth of the conceptual design, a frequency-domain design of the feedback component can be made, using the structured design method of chapter 3. However, the allowed uncertainty was not specified quantitatively in the frequency domain. This has been addressed by the conversion procedure presented above.

The feedback component, that was designed according to the design procedure of chapter 3, can serve as an initial compensator for QFT design. Previously, we considered three combinations of position sensors, where the position was measured with respect to the fixed world or another reference:

1. position measurement at the end-effector. In this situation it is straightforward to apply the conversion method and QFT design.
2. position measurement at the actuator. In this case (indirect control) the task specification for the end-effector has to be translated into a desired motion for the actuator position. This not straightforward, when dynamic effects are to be incorporated.
3. position measurement at the actuator and at the end-effector. In this case the inner loop can be closed with an initial feedback component. Conversion of specifications and QFT compensator design can be performed with an alternative "plant", consisting of the original plant and the closed inner loop.

In order to deal with the disturbance observer during QFT design, one can again construct an alternative plant, which now consists of the original plant and the disturbance observer. The feedforward component can be converted into an initial prefilter.

4.6 Computer-based support

Computer-based support has been developed for the design of QFT controllers for electromechanical motion systems with physical parameter uncertainty, using the mechatronic design environment 20-sim (Controllab Products, 2000) and the Matlab QFT toolbox (Borghesani *et al.*, 1994). The conversion of specifications and prefilter design are only supported when using the Bode diagram. As explained in the previous section, the use of the Nichols chart is preferable, but this has not yet

been incorporated in the computer-based support. However, the use of the design procedure 4.1 is almost identical and here we will give a flavor of the application of the computer-based support (Holterman, 1997). For automatic construction of templates we will only discuss gridding. Computer-support for the Adaptive Angular Sweep Algorithm (Wilson *et al.*, 1999) is available, but not discussed here.

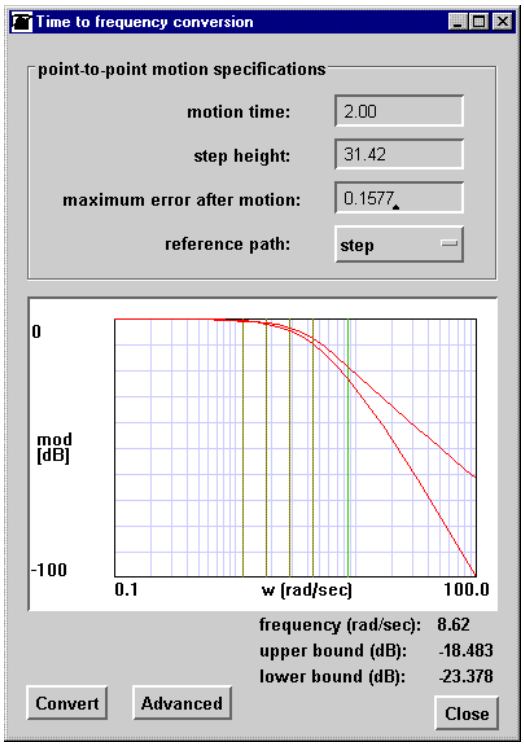

FIGURE 4.31 *Performance specifications*

The motion specification can be entered in a graphical user interface (figure 4.31), where a step function is selected as the reference path and the motion time t_{m} and step height (or motion distance) h_{m} are entered. Using the default assumptions, as motivated in the previous section, the time-domain specifications are automatically converted into a frequency tolerance band in the Bode diagram. In a menu the default assumptions can be modified. The Bode diagram can be used to select a set of critical frequencies for QFT design, by clicking on the appropriate frequency. In figure 4.31 five critical frequencies are indicated, by means of solid vertical lines.

From the physical model of the electromechanical plant, a transfer function can be derived. The coefficients of this transfer function are expressed as a function of the *physical* parameters. In a special editor (figure 4.32), the designer can indicate

whether a physical parameter is certain or uncertain. For uncertain parameters a nominal value and a lower and upper bound have to be indicated. When gridding is used to construct the templates, the number of grid points for an uncertain parameter also has to be indicated.

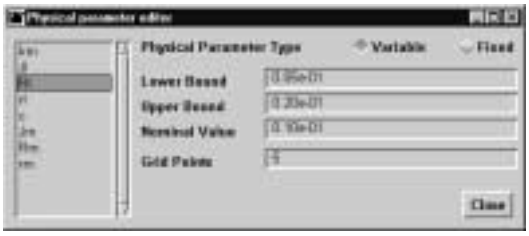

FIGURE 4.32 *The physical parameter editor*

Next, the uncertain plant will be represented by a set of plants, as required by the Matlab QFT toolbox. The templates are automatically generated by evaluating the response of the set of certain plants for the selected critical frequencies. For QFT design only the contours of the templates are needed. In a template editor (figure 4.33), the user has to indicate which grid points contribute to the contour of the template. Points in the template can be selected by clicking the Nichols chart. The relation between the points in a template and the underlying physical parameter values is preserved. Therefore, it is possible to determine which values for the physical parameters lead to a point on the contour, such that the designer can determine which uncertain parameters are critical in the design.

FIGURE 4.33 *The template editor*

Performance and stability boundaries, as well as the templates in the Nichols chart are automatically drawn, using the Matlab QFT toolbox. The same toolbox is used to design a compensator and a prefilter. The computer support will finally evaluate the performance of the controlled system in both the frequency domain and in the time domain. For each selected grid point the frequency response is shown together with the frequency tolerance band. Additionally, the time responses of the closed-loop system are compared with the motion specifications.

4.7 Evaluation and conclusions

The dynamic behavior of electromechanical motion systems is generally described by physically motivated plants. The physical parameters in these models are often only known within bounds. The controller has to assure that the motion specifications are met, despite this uncertainty. It is attractive to use Quantitative Feedback Theory to design these controllers, as this controller design method can deal nonconservatively with uncertain physical parameters. Additionally, QFT is attractive because of the transparency of the cost of feedback.

QFT requires uncertain physical parameters to be mapped onto templates in the Nichols chart. A review of several methods for template construction has been made, where we distinguished analytical and numerical template construction. Whether analytical methods can be applied, depends on the structure of the plant model. Template addition can only be used when uncertain physical parameters do not occur in both the numerator and denominator. Tree structured decomposition is also limited to certain model structures. An attractive solution to this problem would be to decompose the model in a tree structure as far as possible and apply a numerical technique to those parts of the structure that contain repeated parameters. Two numerical template construction methods are selected as suitable, *i.e.* gridding and the Adaptive Angular Sweep Algorithm (Wilson *et al.*, 1999). For a small amount of uncertain parameters gridding is attractive, because an interesting feature of automated gridding is that the designer can select predefined grid-points (on the contour) of a template and investigate which combination of parameter values corresponds to that particular point. In this way, the designer is given the opportunity to signal physical parameter uncertainties that unnecessarily complicate controller design. For a large amount of uncertain parameters the Adaptive Angular Sweep Algorithm is attractive, as this method is computationally less expensive. Here, only a limited number of points on the contour of a template can be investigated on the underlying values of the physical parameters.

Performance specifications for electromechanical motion systems are usually given in terms of space and time. However, QFT requires the specifications to be

expressed in the form of a frequency tolerance band. The approach of Horowitz and Sidi (1972), D'Azzo and Houpis (1995) and Houpis and Rasmussen (1999) as the most direct and useful form of converting the specifications, as here the time-domain specifications can be specified as bounds on the time response. By assuming a dominant behavior of the closed loop system, the time-domain specifications can be converted into bounds of the parameters of the assumed system model. Consecutively, this can be converted into a frequency tolerance band. The original conversion method used the Bode diagram to determine this tolerance band. However, we have shown that fulfillment of the Bode tolerance band does not mean fulfillment of the time-domain specifications. The designer has access to responses that unjustly seem valid in the frequency domain. We propose to use the Nichols chart for the frequency tolerance band. When the frequency response of an uncertain closed-loop system fits within this tolerance band and an additional frequency limit is met, ideal conversion takes place. *I.e.*, when the frequency specifications are met, the motion specifications are also met. We have formulated an iterative conversion procedure for the specifications. When the actual closed-loop system does not match the assumed behavior, iteration takes place. The procedure is based on a number of default assumptions that enable straightforward application. Only at the moment that iteration appears to be necessary, the designer may decide to revise the default assumptions.

Computer-based support, incorporating gridding and the iterative time to frequency conversion procedure, has been developed. The newly developed QFT design support is easily accessible and user-friendly. It provides useful means to support QFT-based controller design for SISO LTI systems with physical parameter uncertainty in combination with point-to-point motion specifications.

5 Application

5.1 Introduction

The design support described in chapter 2 and 3 will now be applied to the Placement Module (PM module) of the Fast Component Mounter. We have developed this support for application in a mechatronic design process, where a realization of the complete electromechanical subsystem is not existing during the design of the control system. However, the actual design of other subsystems than the control system is out of the scope of this thesis. Therefore, we will use an existing PM module, as an example of an industrial electromechanical motion system, to evaluate and to illustrate the design support. It is not an objective to maximize the performance of this specific PM module, using detailed knowledge of the plant dynamics obtained from system identification. Rather our aim is to *satisfy* the requirements in a short design cycle. We will only use that plant knowledge that generally would have been available at a particular design stage. The designed control systems will be applied without additional tuning, in order to get a fair impression of their practical relevance. The only modification made to the control systems is conversion to discrete-time algorithms.

In section 5.2, we will build a simple model of the PM module, in the style of a conceptual design, and apply the model simplification and reduction algorithm of chapter 2. Consecutively, we apply the assessment method presented in the same chapter. In section 5.3, we will extend the plant model with additional dynamic effects and we will stepwise apply the structured design method of chapter 3. Firstly, the conceptual design is reused for frequency-domain design of a feedback component. Secondly, an appropriate feedforward component is added to the control configuration and finally a disturbance observer. Section 5.4 discusses the practical application of the different control systems. We will consider some design issues for implementation of the control algorithms and we will show experimental results. In section 5.5 we present the conclusions.

5.2 Conceptual design

The conceptual design stage is crucial in a mechatronic design process. Here, the functional interaction between domain specific subsystems is determined. By means of the assessment method of chapter 2, we will try to obtain a feasible design for the PM module. We will indicate the available trade-off between the design of the reference path generator, control system, electromechanical subsystem and the attainable performance.

5.2.1 Characterization of the task

The task of the PM module is to place a component with an accuracy of 100 [μm] at 30 [ms] after the motion time. The maximum velocity and acceleration of the system are specified as 1 [ms^{-1}], respectively 10 [ms^{-2}] (Philips, 1998). We consider a 1-dimensional motion along the spindle, *i.e.* in y-direction. The relation between the motion distance h_{m}, the motion time t_{m}, maximum acceleration $a_{\max}$ and maximum velocity $v_{\max}$ for the prescribed second-degree path is (Koster *et al.*, 1999).

$$\left.\begin{aligned} a_{\max} &= 4\frac{h_{\mathrm{m}}}{t_{\mathrm{m}}^2} = 10 \ \left[\mathrm{ms}^{-2}\right] \\ v_{\max} &= 2\frac{h_{\mathrm{m}}}{t_{\mathrm{m}}} = 1.0 \ \left[\mathrm{ms}^{-1}\right] \end{aligned}\right\} \Rightarrow h_{\mathrm{m}} = 0.1 \ [\mathrm{m}], t_{\mathrm{m}} = 0.2 \ [\mathrm{s}] \tag{5.1}$$

This is the *characteristic task* of the controlled system, *i.e.* the performance obtained for this task is characteristic for the controlled system. The task we will use in simulations and experiments will also include a period of 0.05 [s] with constant maximum velocity. We will use the task specified in table 5.1.

quantity		value
maximum error (after t_{s})	e_0	100 [μm]
motion time	t_{m}	250 [ms]
motion distance	h_{m}	0.15 [m]
settling time	t_{s}	30 [ms]
maximum acceleration	$a_{\max}$	10 [m/s^2]
maximum velocity	$v_{\max}$	1 [m/s]

TABLE 5.1 *Specifications for the PM module*

5.2.2 Characterization of the plant dynamics

As indicated in chapter 2, we start with a simple model of the PM module that is built from several component models. In figure 5.1, the initial bond graph model of the PM module is shown.

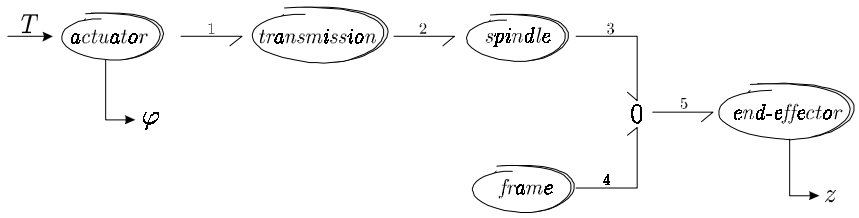

FIGURE 5.1 *Initial bond graph model of the PM module*

The component models are relatively simple and are depicted in figure 5.2.

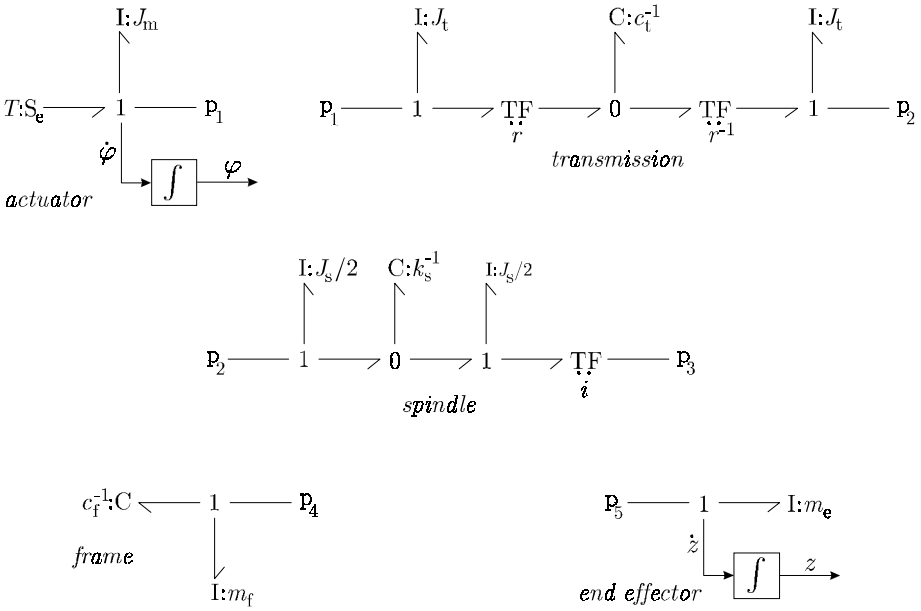

FIGURE 5.2 *Initial component models*

The values of the parameters in this model are given in table 5.2.

quantity		value
motor inertia	J_{m}	$3.25 \cdot 10^{-5}$ [kg·m^2]
pulley inertia	J_{t}	$1.20 \cdot 10^{-6}$ [kg·m^2]
pulley radius	r	$1.43 \cdot 10^{-2}$ [m]
belt stiffness	c_{t}	$2.3 \cdot 10^{6}$ [N·m^{-1}]
spindle inertia	J_{s}	$3.12 \cdot 10^{-5}$ [kg·m^2]
spindle stiffness	k_{s}	$4.10 \cdot 10^{2}$ [N·m·rad^{-1}]
pitch of spindle	p	$2.0 \cdot 10^{-2}$ [m]
frame stiffness	c_{f}	$4.3 \cdot 10^{6}$ [N·m^{-1}]
frame mass	m_{f}	11.5 + 5 [kg]
end-effector mass	m_{e}	2.3 [kg]

TABLE 5.2 *Parameter values for the component models of figure 5.2.*

The frame mass is a summation of the actual mass of the frame (11.5 kg) and the mass of the electronics and its container (5.0 kg) that is connected to the frame. The transmission ratio of the spindle with pitch p equals:

$$i = \frac{p}{2\pi} = 3.18 \cdot 10^{-3} \quad [\mathrm{m} \cdot \mathrm{rad}^{-1}] \tag{5.2}$$

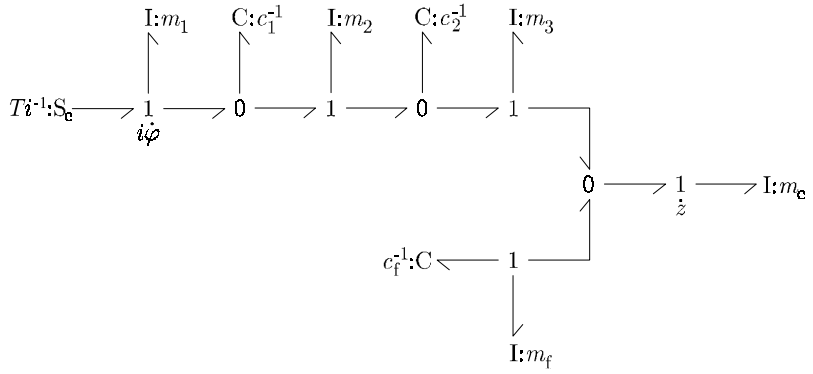

FIGURE 5.3 *Simplified bond graph model of the PM module*

In order to be able to apply the assessment method of chapter 2, we have to transform the plant model into a standard form. Therefore, we first apply the simplification algorithm (design procedure 2.2), to remove transformation ratio's

and dependent elements from the initial bond graph model. The result is depicted in figure 5.3. The expressions for the parameters are:

$$m_1 = \frac{J_\mathrm{m} + J_\mathrm{t}}{i^2} = 3.33 \quad [\mathrm{kg}] \tag{5.3}$$

$$c_1 = \frac{c_\mathrm{t} \cdot r^2}{i^2} = 4.6 \cdot 10^7 \quad [\mathrm{N \cdot m^{-1}}] \tag{5.4}$$

$$m_2 = \frac{2 \cdot J_\mathrm{t} + J_\mathrm{s}}{2 \cdot i^2} = 1.66 \quad [\mathrm{kg}] \tag{5.5}$$

$$c_2 = \frac{k_\mathrm{s}}{i^2} = 4.0 \cdot 10^7 \quad [\mathrm{N \cdot m^{-1}}] \tag{5.6}$$

$$m_3 = \frac{J_\mathrm{s}}{2 \cdot i^2} = 1.54 \quad [\mathrm{kg}] \tag{5.7}$$

Finally, the model reduction algorithm (design procedure 2.3) is applied, such that we obtain a standard model that only incorporates the rigid body mode and the lowest mode of vibration.

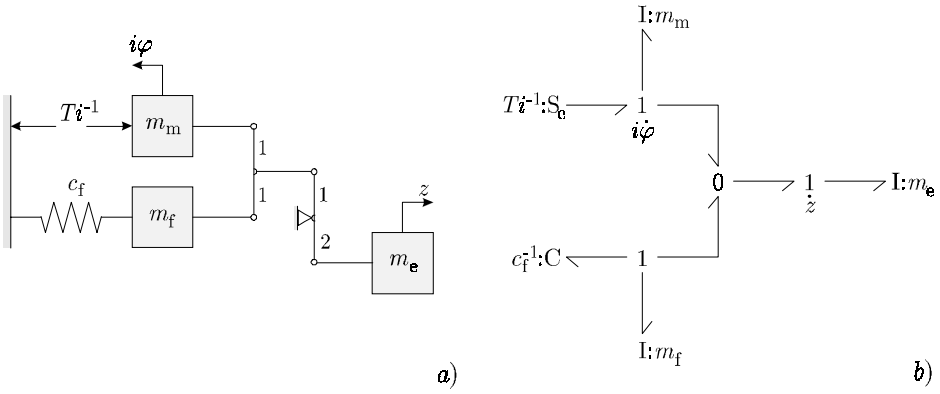

FIGURE 5.4 *Reduced or standard model of the PM module*
a) iconic diagram
b) bond graph

The resulting model is depicted in figure 5.4, where

$$m_\mathrm{m} = m_1 + m_2 + m_3 = 6.53 \quad [\mathrm{kg}] \tag{5.8}$$

Whether the standard model (flexible actuator suspension) of figure 5.4 is a good approximation of the initial bond graph model (figure 5.1), can be verified by comparing the open-loop frequency characteristics in the magnitude plot of Bode diagram. In figure 5.5a the frequency responses from input force to motor position are shown, for both the initial and the standard model. In figure 5.5b the frequency responses from input force to end-effector position are shown. Note that the response of the initial model has been transformed with the transmission ratio of the spindle, in order to make comparison possible. These figures show a good approximation in the low-frequency range, which includes the lowest mode of vibration, *i.e.* they are almost equal up to a frequency of 10^3 [rad/s].

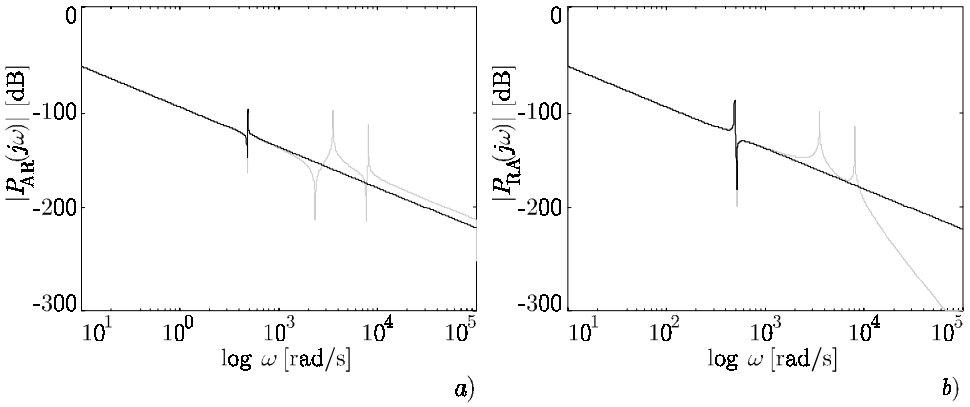

FIGURE 5.5 *Bode magnitude plots of the open-loop transfer functions from input force to a) actuator position and b) end-effector position, for both the initial (gray curve) and reduced-order plant model (black curve)*

A numerical indication of the approximation is indicated in table 5.3. The simplification and the reduction algorithm work according expectation.

	initial model		standard model	
ω_{ar} (AR)	477	[rad/s]	478	[rad/s]
ω_r	486	[rad/s]	486	[rad/s]
ω_{ar} (RA)	510	[rad/s]	510	[rad/s]

TABLE 5.3 *Lowest mode of vibration of the initial and the standard model*

5.2.3 Assessment

Once the plant model is in the standard form, we apply the assessment method of design procedure 2.1.

1. *Determine the class of electromechanical motion system that is at hand.*
   In figure 5.4 we recognize the flexible actuator suspension (refer section 2.2.2). We will consider the transfer functions from the input force to both the actuator position and end-effector position.

   Actuator position
   The transfer function from the input force Ti^{-1} to the actuator position $i\varphi$ is of type AR and is described by:

   $$P(s) = \frac{s^2 + \omega_{\mathrm{ar}}^2}{ms^2\left(s^2 + \omega_{\mathrm{r}}\right)^2} \cdot \frac{\omega_{\mathrm{r}}^2}{\omega_{\mathrm{ar}}^2} \tag{5.9}$$

   where $\omega_{\mathrm{ar}} < \omega_{\mathrm{r}}$; m denotes the total mass to be moved:

   $$m = m_{\mathrm{m}} + m_{\mathrm{e}} = 8.83 \quad [\mathrm{kg}] \tag{5.10}$$

   The anti-resonance frequency ω_{ar} respectively resonance frequency ω_{r} of the lowest mode of vibration is:

   $$\omega_{\mathrm{ar}} = \sqrt{\frac{c}{m_{\mathrm{f}} + m_{\mathrm{e}}}} = 478 \quad [\mathrm{rad/s}] \tag{5.11}$$

   $$\omega_{\mathrm{r}} = \sqrt{\frac{c\left(m_{\mathrm{m}} + m_{\mathrm{e}}\right)}{m_{\mathrm{m}}\left(m_{\mathrm{f}} + m_{\mathrm{e}}\right) + m_{\mathrm{f}}m_{\mathrm{e}}}} = 486 \quad [\mathrm{rad/s}] \tag{5.12}$$

   End-effector position

   The transfer function from the input force to the position of the end-effector x_1 is of type RA, which is described by (5.9) with $\omega_{\mathrm{ar}} > \omega_{\mathrm{r}}$. The total mass and the resonance frequency are again given by expression (5.10) respectively (5.12). The anti-resonance frequency of the type RA transfer function is:

   $$\omega_{\mathrm{ar}} = \sqrt{\frac{c_{\mathrm{f}}}{m_{\mathrm{f}}}} = 510 \quad [\mathrm{rad/s}] \tag{5.13}$$

2. *Determine the concept that is at hand, by looking at the location of the position and velocity sensor. Refer to table 2.5 to verify whether optimal dimensionless controller settings can validly be applied.*

The concept refers to the closed-loop transfer function from the reference path r to the measured position y. In case of the PM there are three possible concepts:

- concept AR position and velocity measurement at the actuator
- concept RA position and velocity measurement at the end-effector
- concept AR-RA position measurement at the end-effector and velocity at the actuator

The actual PM module only contains a position sensor on the motor axis, therefore we will consider concept AR. Whether the optimal dimensionless controller settings can validly be applied depends on the value of the frequency ratio ρ:

$$\rho = \left(\frac{\omega_{\text{ar}}}{\omega_{\text{r}}} \right)^2 \tag{5.14}$$

For concept AR, the frequency ratio must have a value between 0.1 and 0.8. The actual value of the frequency ratio is:

$$\rho = 0.97 \tag{5.15}$$

which is larger than the permitted 0.8. Despite this fact, we will continue application of the assessment method, but we have to reconsider the violation of the bounds on ρ afterwards.

3. *Depending on the situation, perform one of three alternatives:*
   Note that for the assessment we have to use the characteristic task of (5.1).
   a. When we assume the reference path and the desired performance, in terms of the maximum positional error e_0, to be fixed, we calculate the periodic ratio τ according:

$$\tau = \sqrt{\frac{e_0}{\varepsilon \cdot h_{\text{m}}}} = \sqrt{\frac{1.0 \cdot 10^{-4}}{0.09 \cdot 0.1}} = 0.11 \tag{5.16}$$

   Here, we selected the value for ε from table 2.6, *i.e.* concept AR gives $\varepsilon = 0.09$. The minimum required anti-resonance frequency of the plant is:

$$\omega_{\text{ar,req}} = \frac{2\pi}{\tau t_{\text{m}}} = \frac{2\pi}{0.11 \cdot 0.2} = 298 \text{ [rad/s]} \tag{5.17}$$

   which is smaller than the actual anti-resonance frequency, thus the lowest mode of vibration is not a limitation for the *desired* performance.
   b. When we assume the reference path and the anti-resonance frequency to be fixed, we calculate the periodic ratio τ according to:

$$\tau = \frac{2\pi}{\omega_{\text{ar}} t_{\text{m}}} = 0.066 \tag{5.18}$$

The attainable performance in this situation is predicted as:

$$e_0 = E_0 \cdot h_{\mathrm{m}} = \varepsilon \cdot \tau^2 \cdot h_{\mathrm{m}} = 39 \quad [\mu\mathrm{m}] \tag{5.19}$$

which is smaller than the *desired* accuracy of 100 [μm].

c. When we assume the desired performance and the anti-resonance frequency to be fixed, we can propose a characteristic reference path. This requires a trade-off between the motion time and the motion distance:

$$\begin{aligned} &\frac{2\pi}{\omega_{\mathrm{ar}} t_{\mathrm{m}}} = \sqrt{\frac{e_0}{\varepsilon \cdot h_{\mathrm{m}}}} \\ &\Rightarrow t_{\mathrm{m}}^2 = 0.16 \cdot h_{\mathrm{m}} \end{aligned} \tag{5.20}$$

4. Determine the control system for a particular problem setting.
The dimensionless optimal controller settings for concept AR are $\Omega_{\mathrm{p}} = 0.8$ and $\Omega_{\mathrm{d}} = 0.9$ (refer table 2.5). For the particular problem setting of the PM module, with $\omega_{\mathrm{ar}} = 478$ [rad/s], we obtain:

$$\begin{aligned} k_{\mathrm{p}} &= m \cdot \left(\Omega_{\mathrm{p}} \cdot \omega_{\mathrm{ar}}\right)^2 = 1.29 \cdot 10^6 \\ k_{\mathrm{d}} &= m \cdot \Omega_{\mathrm{d}} \cdot \omega_{\mathrm{ar}} = 3.80 \cdot 10^3 \end{aligned} \tag{5.21}$$

From application of the assessment method we learn that the specifications can be met with the given electromechanical subsystem. The specification given for the PM module requires the positional error to be attained only after a settling time of 30 [ms]. After this settling time the maximum positional error will only be further decreased. As the frequency ratio (5.15) of the PM module is not within the bounds specified by the assessment method, the stability margin may be smaller than guaranteed. The guaranteed margin is such that the closed-loop poles are located sufficiently far, *i.e.* a distance $-g$, into the left-half plane:

$$g = G \cdot \omega_{\mathrm{ar}} \tag{5.22}$$

where G was chosen 0.2 (refer section 2.3.2). For the PM module the required margin is:

$$g = G \cdot \omega_{\mathrm{ar}} = 96 \tag{5.23}$$

The actual margin, with damping as used in the assessment method, is significantly smaller: only 41. However, a type AR transfer function with a PD-type controller is always stable, therefore we will proceed with the design, with the knowledge that the stability margin may require extra attention in the remainder of the design process.

5.2.4 Evaluation

The closed-loop system with the PD-type controller used in the assessment method is shown in figure 5.6.

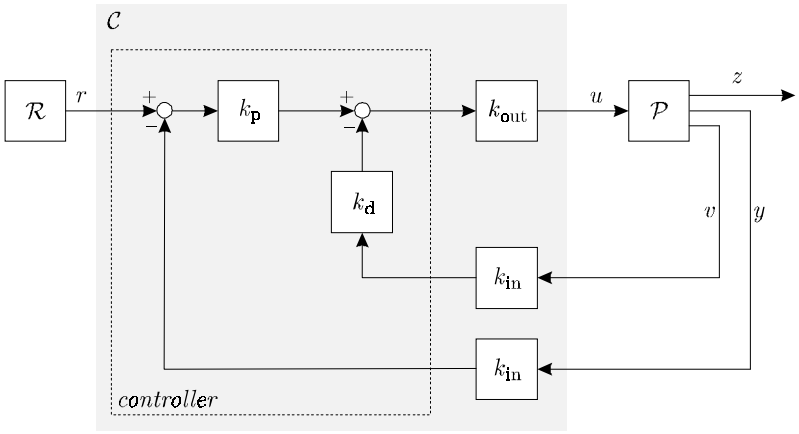

FIGURE 5.6 *Closed-loop system with PD-type controller of assessment method*

The measured output y, *i.e.* the motor position of the PM module, is multiplied with k_in and the output signal of the controller is multiplied with k_out, in order to obtain the control signal u. The controller has been designed using the standard model of figure 5.4, with input $T{\cdot}i^{-1}$ and output $i{\cdot}\varphi$. However, the initial model requires input T and output φ. Therefore, extra gains are introduced:

$$\begin{aligned} k_\mathrm{in} &= i = 3.18 \cdot 10^{-3} \quad [\mathrm{m \cdot rad^{-1}}] \\ k_\mathrm{out} &= i = 3.18 \cdot 10^{-3} \quad [\mathrm{m \cdot rad^{-1}}] \end{aligned} \tag{5.24}$$

By means of simulations in 20-sim we will evaluate the conceptual design. We will use the initial bond graph model, to verify the performance. In figure 5.7 we see that the end-effector follows the reference trajectory well. The error *during* the point-to-point motion rises up to 3 [mm] and the required torque of the actuator is about 0.3 [Nm].

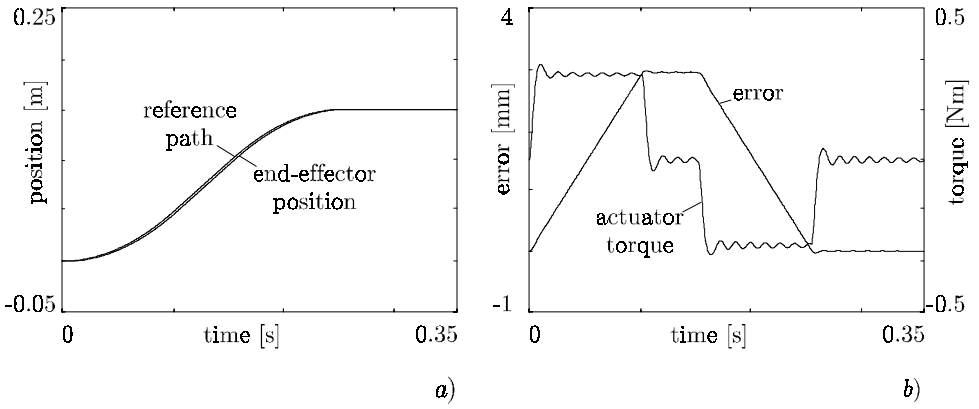

FIGURE 5.7 *Simulation of the controlled initial bond graph model of the PM module, performing the task of table 5.1*

To get a better idea of the positional error after the motion time t_m, we zoom in on the error plot. The error of interest is shown in figure 5.8.

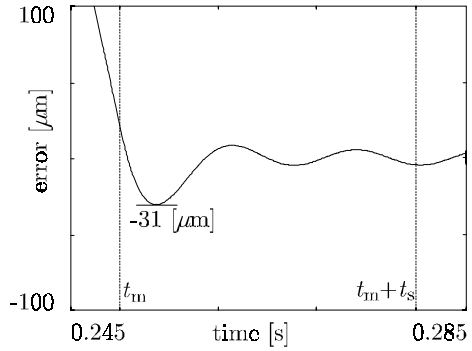

FIGURE 5.8 *The positional error of the conceptual design, with the initial plant model*

The simulations show that the positional error after the motion time t_m is 31 [μm], which is indeed smaller than the predicted maximum positional error of 39 [μm]. After the settling time t_s of 30 [ms], we see that the error is decreased even further. Therefore, we conclude that we obtained a feasible design for the controlled system and we will proceed the design process, keeping in mind the relatively small stability margin.

5.3 Detailed design

We will continue the design process with the structured design method as described in chapter 3. We describe an evolutionary design process, starting with the reuse of the conceptual design, and extending the design with appropriate components. However, first we will incorporate additional knowledge about the electromechanical subsystem in the plant model, which usually becomes available during detailed design.

5.3.1 Modeling the plant

The structure of the plant model, as indicated in figure 5.1, is still valid during detailed design. The subsystem types can be reused, but we will use different specifications for the actuator and the end-effector, *i.e.* the *polymorphic modeling* approach of De Vries (1994) that was also discussed in section 3.6. The subsystem specifications used during conceptual design only described those dynamic effects that influence the dominant behavior of the plant. During detailed design, more information comes available and the specifications will describe the dynamic behavior in more detail, such that it better resembles the real-world plant. We will incorporate the available knowledge in the plant model, in order verify the performance of the control system.

Actuator
In figure 5.9 a more detailed model of the DC servomotor is depicted. This is a model of the servomotor (PARVEX RS240B) that has been selected for this application.

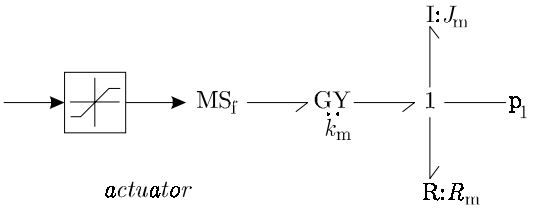

FIGURE 5.9 *Detailed model of the DC servomotor*

When we compare this model to the actuator model in figure 5.2, we see the addition of a gyrator with motor constant k_m. The control system should now calculate input current instead of input force, thus an MSf-source is used. On the mechanical side we added some viscous friction R_m to the motor inertia J_m. The

maximum current of the motor amplifier is limited to 5.0 [A]. The values of all parameters are indicated in table 5.4.

quantity		value
motor constant	k_m	$6.8 \cdot 10^{-2}$ [N·m·A^{-1}]
motor inertia	J_m	$3.25 \cdot 10^{-5}$ [kg·m^2]
viscous friction	R_m	$2.48 \cdot 10^{-5}$ [N·m·s·rad^{-1}]
maximum current	i_{max}	5.0 [A]

TABLE 5.4 *Parameter values for the actuator model of figure 5.9*

End-effector
The end-effector is a carriage that contains the pipette, which picks up and places the components. The guidance of the carriage will have a finite stiffness, thus allowing for a small displacement of the tip of the pipette (figure 5.10). Here, we see an example of the flexible guidance model that was introduced in section 2.2.2.

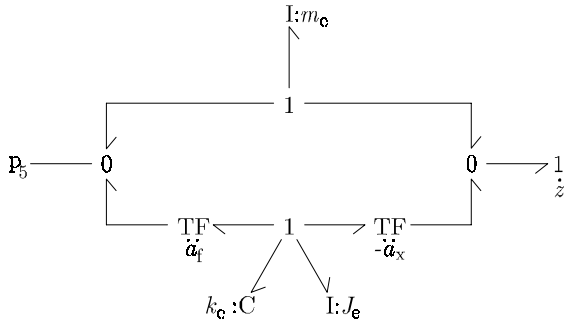

FIGURE 5.10 *Extended model of the end-effector*

The carriage has a mass m_e and an inertia J_e. The stiffness c_e of the guidance is represented as a rotational stiffness k_e, according to:

$$k_e = 2 \cdot c_e \cdot b^2 \tag{5.25}$$

where b is the distance between the two contact points of the guidance system (refer figure 3.12a). The location of the force a_f and the location of interest a_x, are defined as the vertical distances along the carriage, from the center of mass to the location where the force excites the carriage, respectively to the location of the tip of the pipette.

quantity		value
carriage inertia	J_e	$8 \cdot 10^{-3}$ [kg·m^2]
carriage mass	m_e	2.3 [kg·m^2]
guidance stiffness	c_e	$5.6 \cdot 10^{7}$ [N·m^{-1}]
distance	b	0.05 [m]
location force	a_f	$5.5 \cdot 10^{-2}$ [m]
location of interest	a_x	-0.12 [m]

TABLE 5.5 *Parameter values for the end-effector model of figure 5.10.*

Remark 5.1

We do not incorporate the MIMO behavior of the PM module. Motions of the pipette in e.g. the x-direction or motions of other PM modules in the FCM will probably have influence on the motion in y-direction. However, in order to estimate the exact influence, further analysis is required.

5.3.2 Design of a feedback component

Before we can design a feedback compensator we have to formulate appropriate design specifications. Design procedure 3.1 requires the specifications to be expressed in terms of the bandwidth and the low-frequency behavior of the input sensitivity function. An indication for performance has already been obtained during conceptual design; therefore, it is desirable to reuse this result. We will determine the bandwidth ω_b of the conceptual design with the standard plant model:

$$\omega_b = 266 \quad \text{[rad/s]} \tag{5.26}$$

We will therefore state the specification as:

1. sufficiently high bandwidth:
   $\omega_b = 266$ [rad/s].
2. sufficient suppression of low-frequency vibrations:
   $|S_{wz}(j\omega)| < $ -120 [dB] for $\omega < 10\pi$ [rad/s].
3. maximum peak-value of the sensitivity magnitude
   $M_S = 6$ [dB]
4. limited control energy.

where $S_{wz}(j\omega)$ is the input sensitivity function. The specification for the suppression of the low-frequency vibrations is chosen rather arbitrarily: disturbance forces up to

10π [rad/s], acting on the input of the plant, have to be suppressed with at least – 120 [dB]. This means that a forces with a frequency smaller than 10π [rad/s] and an amplitude of 10 [N], may result in a displacement of 10 [μm].

We apply design procedure 3.1 for PID controllers in two steps. Firstly, we design a PD controller in order to illustrate the reuse of the conceptual design and secondly we add the integral action.

1. *Determine m, i.e. the total mass to be displaced.*
   In the previous section we determined:

   $$m = 8.83 \quad [\text{kg}] \tag{5.27}$$

2. *Determine whether to use a PID compensator or a PID controller.*
   We start with the design of a PID controller, as this configuration was used during conceptual design.

3. *Select the parameter β, i.e. the tameness factor.*
   It is chosen equal to the default value 0.1.

4. *Determine the value of the derivative time constant τ_{d} to obtain extra phase lead.*
   For the controller we use.

   $$\tau_{\mathrm{d}} = \frac{1}{4\omega_{\mathrm{b}}\sqrt{\beta}} = 2.97 \cdot 10^{-3} \tag{5.28}$$

5. *Determine the proportional gain K to obtain the desired bandwidth ω_{b}.*
   For the controller we use:

   $$K = 2\omega_{\mathrm{b}}^2 m \left(\frac{\omega_{\mathrm{b}}^2 \tau_{\mathrm{d}}^2 \beta^2 + 1}{\omega_{\mathrm{b}}^2 \tau_{\mathrm{d}}^2 \beta^2 + 2\omega_{\mathrm{b}}^2 \tau_{\mathrm{d}}^2 \beta + 1} \right) = 1.12 \cdot 10^6 \tag{5.29}$$

We can compare the newly obtained PD controller with the controller settings of the assessment method (5.21). The proportional gain of the conceptual design is a little larger and the derivative action can be rewritten as:

$$\frac{k_{\mathrm{d}}}{k_{\mathrm{p}}} = 2.94 \cdot 10^{-3} \tag{5.30}$$

which almost equals the value for τ_{d}. The frequency responses and the bandwidth ω_{b} of both designs are indeed the same, although they are obtained from different starting points. We obtained a smooth transition from conceptual design to detailed

design, *i.e.* a design in the frequency domain, by reusing the bandwidth ω_b. Now, we add the integral action by continuing the design procedure:

6. *Determine the integral time constant τ_i in order to obtain a desired gain at low frequencies.*

$$\tau_\mathrm{i} \leq \frac{s_\mathrm{l} K}{\omega_\mathrm{l}'} = 3.5 \cdot 10^{-2} \tag{5.31}$$

7. *Choose the time constant of the roll-off filter $\tau_\mathrm{h} < \beta\tau_\mathrm{d}$, but as large as possible to limit the controller bandwidth.*
We choose:

$$\tau_\mathrm{h} = 1.5 \cdot 10^{-4} \tag{5.32}$$

Similarly, we can design a PID compensator, starting with step 3 of the design procedure.

3. *Select the parameter β, i.e. the tameness factor.*
It is chosen equal to the default value 0.1.

4. *Determine the value of the derivative time constant τ_d to obtain extra phase lead.*
For the compensator we use:

$$\tau_\mathrm{d} = \frac{1}{2\omega_\mathrm{b}'\sqrt{\beta}} = 5.93 \cdot 10^{-3} \tag{5.33}$$

5. *Determine the proportional gain K to obtain the desired bandwidth ω_b.*
For the compensator we use:

$$K = 2\omega_\mathrm{b}^2 m \left(\frac{\omega_\mathrm{b}^2 \tau_\mathrm{d}^2 \beta + 1}{\omega_\mathrm{b}^2 \tau_\mathrm{d}^2 + 1} \right) = 4.5 \cdot 10^5 \tag{5.34}$$

6. *Determine the integral time constant τ_i in order to obtain a desired gain at low frequencies.*

$$\tau_\mathrm{i} \leq \frac{s_\mathrm{l} K}{\omega_\mathrm{l}'} = 1.4 \cdot 10^{-2} \tag{5.35}$$

7. *Choose the time constant of the roll-off filter $\tau_\mathrm{h} < \beta\tau_\mathrm{d}$, but as large as possible to limit the controller bandwidth.*
We choose:

$$\tau_{\mathrm{h}} = \beta\tau_{\mathrm{d}} = 3.0 \cdot 10^{-4} \tag{5.36}$$

In figure 5.11, the frequency responses of the PID controller and PID compensator are shown, with the standard fourth-order plant model. Due to the addition of an integral action, the bandwidth is a little lower than specified for both configurations.

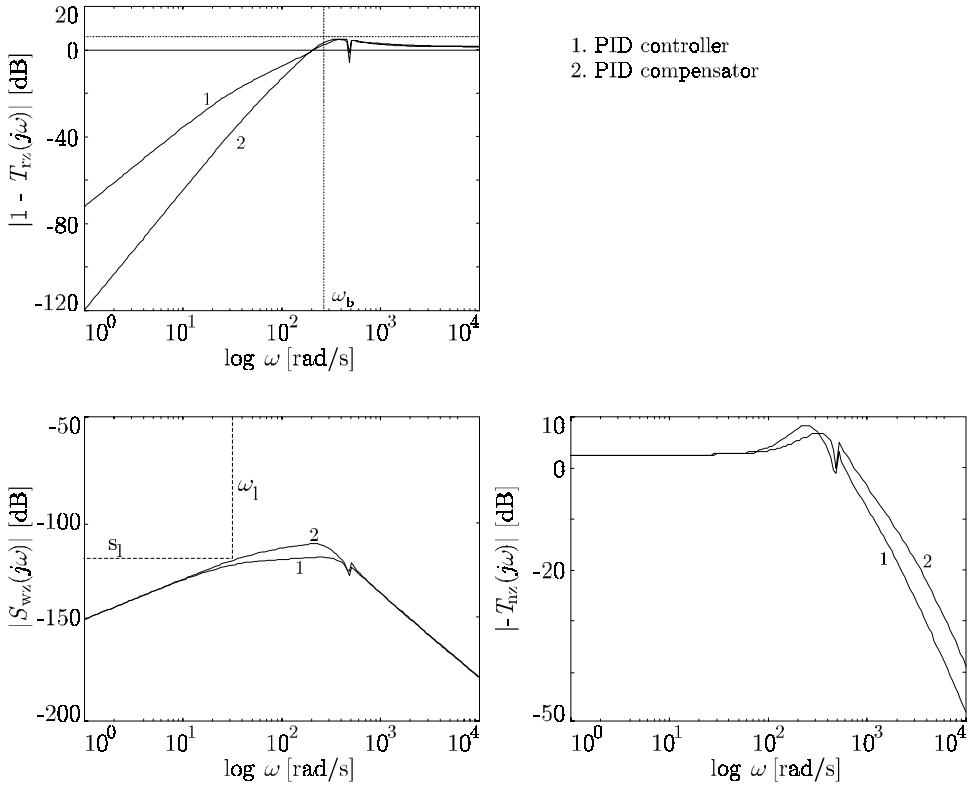

FIGURE 5.11 *Frequency responses of the PID controller and PID compensator, using standard plant model*

Application of the assessment method indicated that the stability margin requires extra attention. Here, we see that the peak of $|1 - T(j\omega)|$ is smaller than 6 [dB], thus providing a sufficient stability margin. The desired low-frequency disturbance attenuation can be achieved with both designs. The controller configuration does not require an integral action to meet this requirement, as the suppression of the PD controller is already –120 [dB], but we maintain the integral action as it does provide infinite gain at zero frequency. The proportional gain of the compensator is much lower than the proportional gain of the controller, which results in a lower

cost of feedback. The roll-off can start at a lower frequency, thus the amplification of measurement noise, is much smaller for the compensator configuration.

We will also compare the two control configurations by means of simulations, using the extended plant model, presented in section 5.3.1. The controller configuration allows a large error during the motion time. Therefore, the integral action will only be switched on, once the end-effector is near the end position. The specifications of the PM module indicate that the switching moment is 8 [ms] after the motion time. The same switching moment is used here.

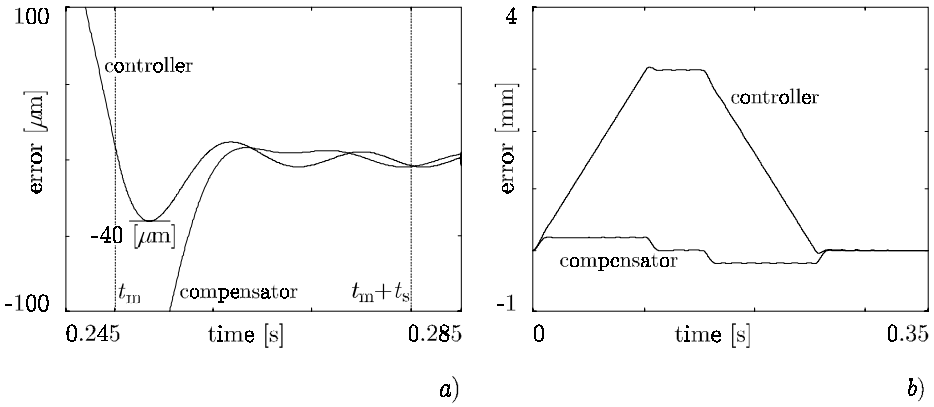

FIGURE 5.12 *Positional error of closed-loop systems with PID controller and PID compensator*

In figure 5.12, it can be seen that both designs fulfill the specification after the settling time. The maximal error after the motion time t_m is much smaller for the PID controller (40 [μm]) than for the compensator (210 [μm] at $t = t_m$). This illustrates why a PID controller is attractive in point-to-point motion systems with only a feedback component.

Remark 5.2

Also in the situation that the proportional gain of the compensator equals the proportional gain of the controller, the controller configuration results in a smaller maximum positional error.

5.3.3 Design of a feedforward component

To investigate the possibilities of performance improvement, we extend the control configuration with a feedforward component. The PID controller is extended with velocity and acceleration feedforward and the PID compensator with only acceleration feedforward:

$$K_{\text{vel}} = K \cdot \tau_{\text{d}} = 3.3 \cdot 10^2 \tag{5.37}$$

$$K_{\text{acc}} = m = 8.83 \tag{5.38}$$

The simulation results are shown in figure 5.13.

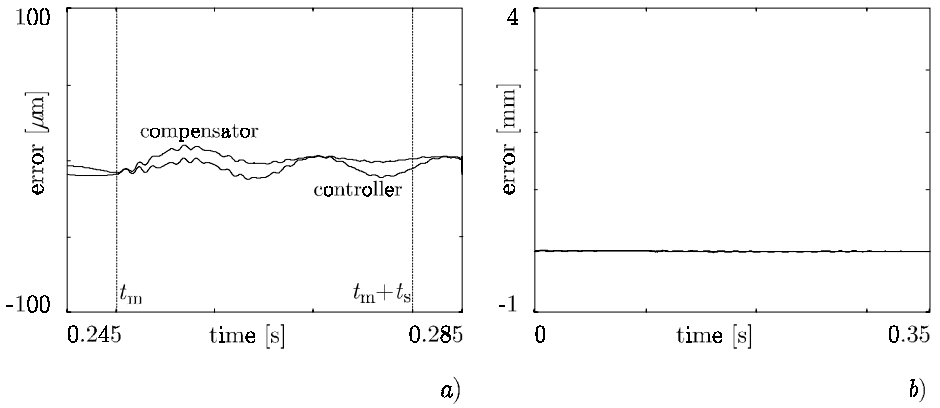

FIGURE 5.13 *Positional error of closed-loop systems with PID controller and PID compensator, including a feedforward component*

In these simulations, the integral action is continuously active, as there are no large errors during the motion time, due to addition of velocity feedforward to the PID controller. Both designs result in similar performance. When we compare the error plots of figure 5.13 with figure 5.12, we see a significant decrease of the error during, as well as after the motion time t_{m}. However, it should be noted that the compensator configuration achieves this performance with a lower proportional gain, thus at a lower cost of feedback. Therefore, a compensator is most attractive in a control configuration that includes a feedforward component. Note that this is only possible for concepts requiring one sensor (refer chapter 2).

5.3.4 Design of a disturbance observer

Instead of an integral action in the feedback component, we will now try to obtain the low-frequency disturbance suppression by means of a disturbance observer: $|S_{\text{wz}}(j\omega)| < -120$ [dB] for $\omega < 10\pi$ [rad/s]. For the feedback component, we will use a PD compensator, as it provides a lower cost of feedback than the PD controller does. We apply design procedure 3.2.

1. *Identify the order of the plant n and determine the appropriate state-space model of the plant.*
   We will model the PM module as a second-order system ($n = 2$), *i.e.* a moving mass, according:

$$\begin{aligned} \dot{x} &= Ax + Bu = \begin{bmatrix} 0 & 1 \\ 0 & 0 \end{bmatrix} x + \begin{bmatrix} 0 \\ \frac{1}{m} \end{bmatrix} u \\ y &= Cx + Du = \begin{bmatrix} 1 & 0 \end{bmatrix} x \end{aligned} \tag{5.39}$$

2. *Set the order of the disturbance observer k to* 1.

3. *Determine the suppression provided by the feedback component:*

$$\left| S_{\text{c,wz}}\left(j\omega_{\text{l}} \right) \right| = -113 \quad [\text{dB}] \tag{5.40}$$

where $S_{\text{c,wz}}(j\omega_{\text{l}})$ is the input sensitivity function of the plant with only a PD compensator.

4. *Determine the suppression σ required of the disturbance observer:*

$$\sigma = s_{\text{l}} - \left| S_{\text{c.wz}}\left(j\omega_{\text{l}} \right) \right| = -7 \quad [\text{dB}] \tag{5.41}$$

5. *Select a real-pole polynomial or a Butterworth polynomial of order n+k* = 3. We use a third-order Butterworth polynomial:

$$s^3 + 2\omega_\sigma s^3 + 2\omega_\sigma^2 s + \omega_\sigma^3 \tag{5.42}$$

6. *Determine the location of the observer poles in terms of the frequency* ω_σ *using:*

$$\omega_\sigma \approx c \cdot \omega_{\text{l}} \cdot 10^{\frac{\sigma}{20k}} = 141 \quad [\text{rad/s}] \tag{5.43}$$

where c is chosen 2 for a Butterworth polynomial.

7. *Verify whether:*

$$\omega_\sigma < 0.5 \cdot \omega_{\text{b}}$$

This inequality is not fulfilled, as $0.5 \cdot \omega_{\text{b}}$ equals 133 [rad/s]. However, as this difference is small, we will continue the design.

8. *Determine the observer gain L.*
From table 3.4 and (5.42) we obtain:

$$\begin{aligned} L &= \begin{bmatrix} \chi_2 & \chi_1 & m\chi_0 \end{bmatrix}^T = \begin{bmatrix} 2\omega_\sigma & 2\omega_\sigma^2 & m\omega_\sigma^3 \end{bmatrix}^T \\ &= \begin{bmatrix} 2.82 \cdot 10^2 & 3.98 \cdot 10^4 & 2.38 \cdot 10^7 \end{bmatrix} \end{aligned} \tag{5.44}$$

In figure 5.14, the frequency responses of the PD compensator with and without disturbance observer are shown, using the standard plant model.

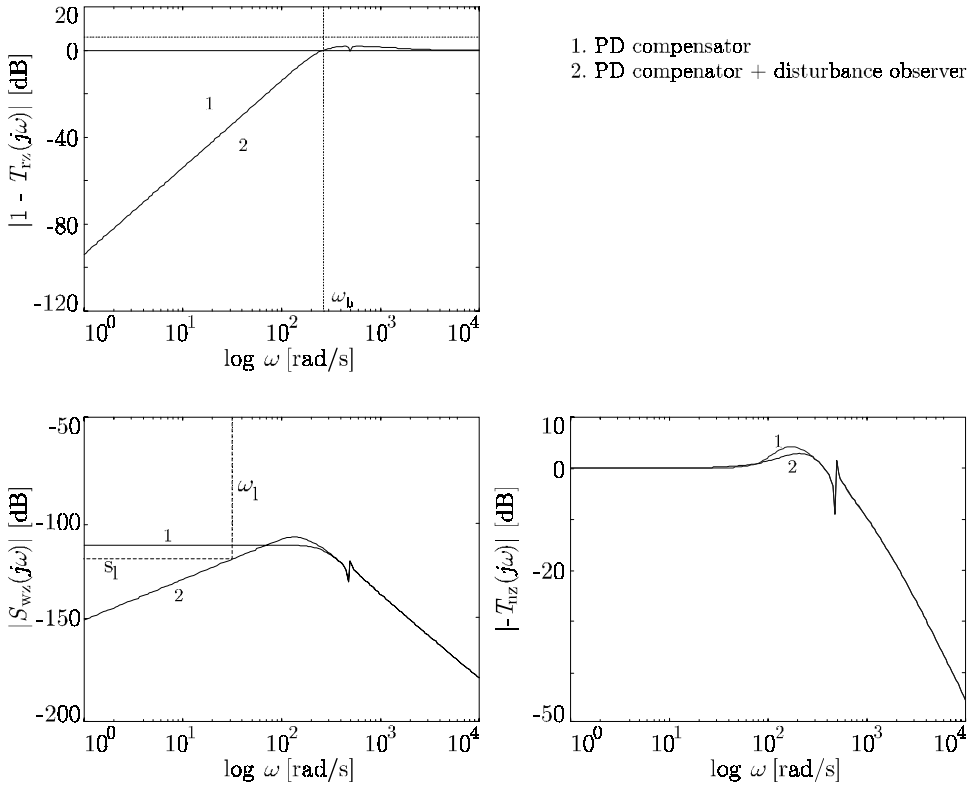

FIGURE 5.14 *Frequency responses of the PD compensator with and without disturbance observer, using standard plant model*

The frequency response from reference path to end-effector position is unaffected by the addition of the disturbance observer. The disturbance observer provides the desired low-frequency disturbance suppression. We see that, due to Bode sensitivity integral, some extra gain is introduced for frequencies just lager than ω_1. The suppression of measurement noise at high frequencies is also unaffected by the disturbance observer.

We will also investigate the influence of the disturbance observer in the simulations. We compare the errors for a control configuration with a PID compensator and a control configuration with PD compensator and disturbance observer. The results are shown in figure 5.15.

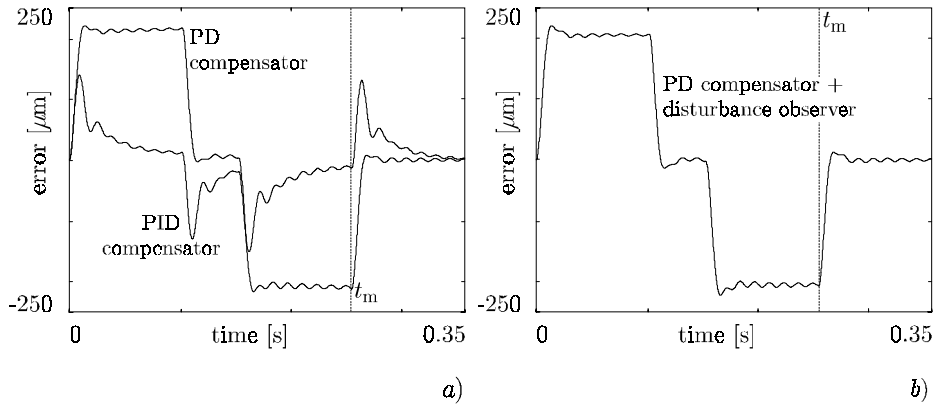

FIGURE 5.15 *Comparison of errors of closed-loop system with PID/PD compensator respectively PD compensator with disturbance observer*

Simulations confirm that the disturbance observer does not affect the response from reference path to end-effector position, while low-frequency disturbance attenuation can be achieved. The PID compensator affects the positional error ($t > t_m$) severely.

Remark 5.3

Note that the difference with the PID compensator of figure 5.12 is that in figure 5.15 the integral action is continuously active and not only 8 [ms] *after the motion time.*

In order to illustrate the suppression of input disturbances in simulation, we applied a step disturbance of 10 [N] at the plant input.

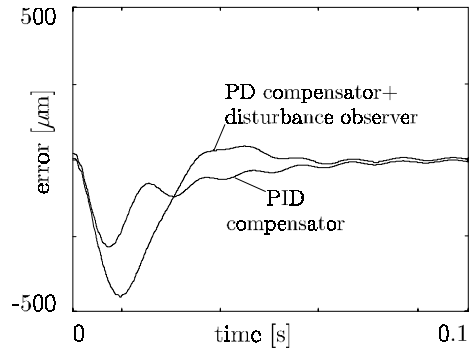

FIGURE 5.16 *Response on a step disturbance of* 10 [N] *at the plant input for closed-loop system with PID compensator respectively PD compensator with disturbance observer*

Both the PID compensator and the PD compensator with disturbance observer, suppress this disturbance well. The disturbance observer reduces the error relatively fast, but it leads to a larger maximum error.

5.4 Practical application

We will apply and test the different control configurations to the real PM module. The motor position is measured by an encoder that can measure 2000 steps per revolution, which corresponds to a resolution of 10 [μm] at the end-effector. The position of the end-effector is measured over a small range by means of a Position Sensitive Detector (PSD), such that we can verify the behavior of the variable of interest. The PSD output is not used for feedback.

We start with the PD-type controller of section 5.2.3 that has been designed with the assessment method of chapter 2. In figure 5.17, the experimental error plots are shown that correspond to the simulations of figure 5.7 and figure 5.8.

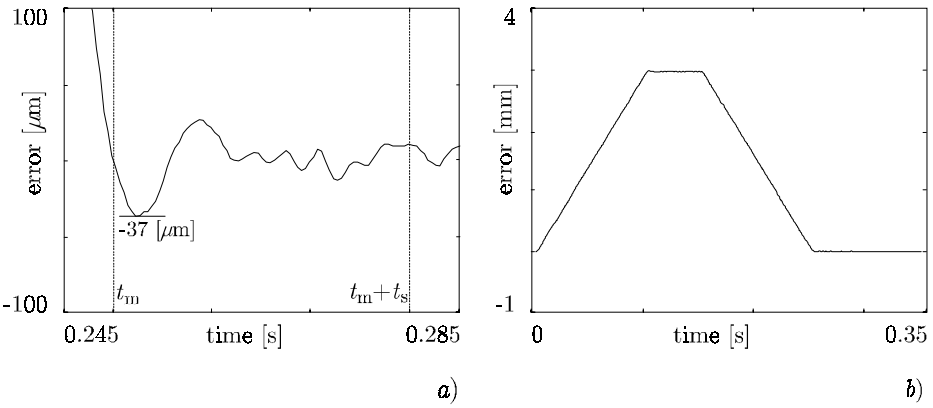

FIGURE 5.17 *Error plots of PM module with the PD-type controller from the assessment method*

The error during motion time ($t < t_m$) is, similarly as in simulation, approximately 3 [mm]. The maximal positional error after the motion time is 37 [μm], which is 6 [μm] larger than in simulation, but corresponding well with the positional error of 39 [μm] predicted by the assessment method.

Next, we consider the PID controller and PID compensator designed in section 5.3.2, where the integral action is switched on 8 [ms] after the motion time. In

figure 5.18, the experimental error plots are shown that correspond to the simulations of figure 5.12.

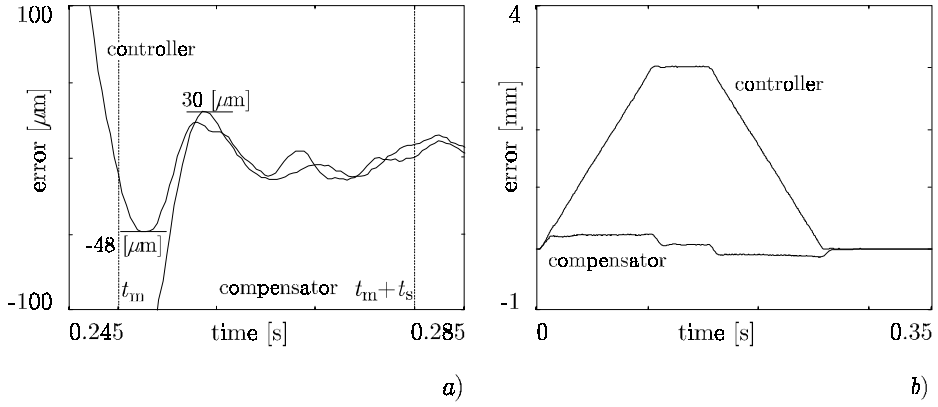

FIGURE 5.18 *Error plots of PM module with PID controller and PID compensator (switched integral action)*

The characteristics of the error plots are similar to those in simulation, although the actual values of the positional errors are again a little larger.

In figure 5.19, the errors of the experiment with the PID compensator and acceleration feedforward are shown, which correspond to the simulations of figure 5.13.

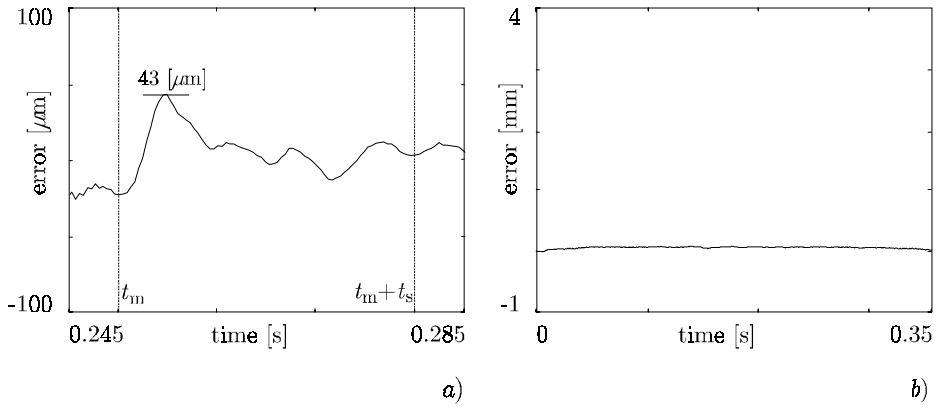

FIGURE 5.19 *Experiments with feedback and feedforward components*

The characteristics of the experiments and simulations are similar, however, the maximum positional error of the experiment is significantly larger than in simulation. The reasons are:

- *nonlinear friction.* The integral action is now also active for $t < t_m$. Due to nonlinear friction, the error during motion is strictly positive and the integral action will get a relatively large value, which deteriorates the error after the motion time ($t > t_m$).
- *limited encoder resolution.* The encoder on the actuator has a resolution of 10 [μm]. When errors of a few quantization levels occur, the discrete-time derivative action of the feedback component will already give relative large outputs. This signal consecutively excites the PM module such that vibrations as shown in figure 5.19 occur.

The PD compensator is also used in combination with the disturbance observer of section 5.3.4. Experimental results, corresponding to the simulations of figure 5.15, are shown in figure 5.20. The results confirm the observations done on basis of simulations.

Remark 5.4

The augmented plant model in the disturbance observer has first been converted to a discrete-time model.

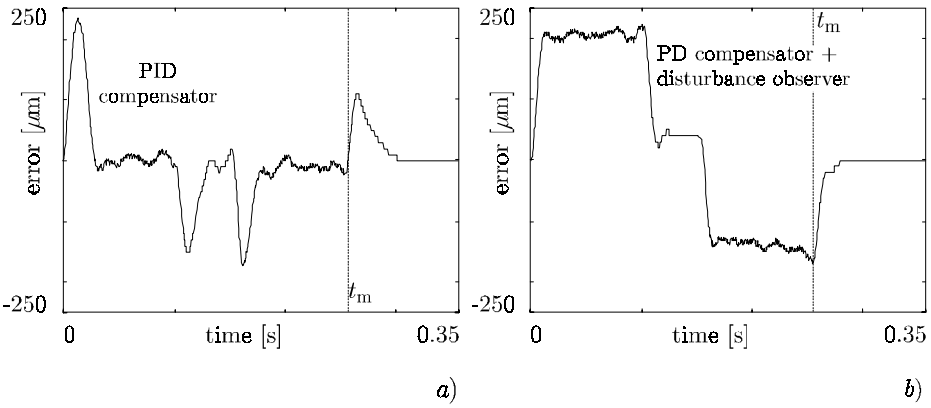

FIGURE 5.20 *Experiments with PID compensator and disturbance observer (non-switched integral action)*

When we compare the responses of the PD compensator with and without a disturbance observer shortly after t_m (figure 5.21), we see that the disturbance observer hardly affects the positional error.

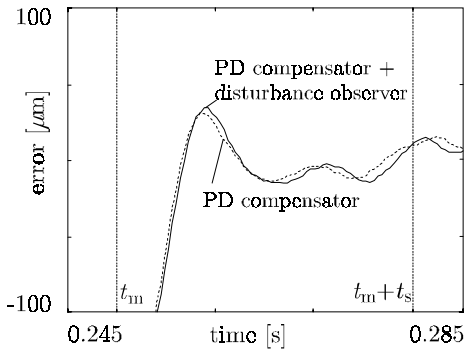

FIGURE 5.21 *Experimental positional errors of PD compensator with and without disturbance observer*

5.5 Conclusions

By means of application to an industrial motion system, we have illustrated the design enhancement presented in this thesis. We mainly focussed on evaluation of the design enhancement and not on maximization of the performance of the controlled system.

Application of the assessment method indicates that the limited stiffness of the frame is the principal performance-limiting factor. Assessment learned that the specification of a maximal positional error of 100 [μm] can be met; a maximum error of 39 [μm] was indicated as feasible. Simulations with an initial plant model, as well as practical experiments, confirm these results. This illustrates that, using minimal plant knowledge, the assessment method provides the designer with relevant knowledge about the design problem, early in the design process.

During detailed design, the conceptual design is reused relatively easy and useful. This is achieved, by using the bandwidth of the conceptual design as the initial specification for the design of the feedback component. This component now also has to provide low-frequency disturbance suppression. Simulations and frequency analysis confirm that the specifications are feasible. In a 1-DOF (or 2-CC) configuration, the PID *controller* is more attractive as it leads to a smaller positional error. When an additional feedforward component is used, both configurations will give similar performance. In this situation, it is more attractive to use a PID *compensator*, as it has a lower cost of feedback. Experiments on the real system confirm these results. The performance obtained in simulation could

not be reproduced in experiments, due to nonlinear friction and the limited resolution of the position encoder. Simulations and frequency analysis show that a disturbance observer can provide low-frequency disturbance attenuation, without severely affecting the performance. Measurements confirm that a PD compensator with a disturbance observer gives similar performance as using only a PD compensator, while a PID compensator causes larger errors, especially in the time interval of interest. The main benefit of the structured design method is that it leads to a short design process, especially when the library of control systems is used, while providing insight in the design problem. The recommended controller settings proved to be relevant in practical evaluations, that is, as long as the parameters of the initial model are about correct.

6 Discussion

6.1 Synopsis

We have discussed the development of design support for controllers for electromechanical motion systems, using a mechatronic design approach. We focussed on transient systems that typically have to perform pick-and-place movements. The placement module of the Philips Fast Component Mounter has been used as a running example. Our aim has been to:

- make it easier to obtain insight in the design problem
- decrease the control engineering skills required of the designer
- improve the performance and robustness properties of the final design.

As an overall result, the required development time should decrease.

Two distinct stages of mechatronic control system design have been addressed: conceptual design and detailed design.

Conceptual design
The aim of conceptual design is to obtain a feasible design for the path generator, control system and electromechanical plant with appropriate sensor locations, in an integrated way. We described standard problem *classes*, which differ in terms of the location of the *dominant stiffness* in the physical plant model. In order to transform plant models into standard form, we have developed (automated) model simplification and model reduction algorithms that preserve the relations between the parameters of the transformed model and the (physically motivated) parameters of the original model. A set of standard fourth-order *plant transfer functions*, referred to as *types*, resulted by considering all optional output variables (*i.e.* all positions that may be of interest). Based on this, several standard *closed-loop transfer functions* have been defined, referred to as *concepts*.

Dimensionless quantities have been used to characterize design parameters that are relevant for the closed-loop behavior, *i.e.*, parameters of the reference path generator, PD-type controller and plant. For all concepts, relations between the dimensionless quantities of the reference path, controller and plant have been obtained heuristically by means of numerous simulations. These relations can now be used in an *assessment method*. The assessment method can be applied in several ways, depending on the available knowledge about the design problem. Interactive computer-based support incorporating all this has been developed.

Detailed design
In order to meet the more or less conflicting requirements for a controlled system, in terms of performance, stability, disturbance attenuation and robustness for model uncertainties, a transparent and structured design method is proposed. Starting from a successful conceptual design, this method supports the (evolutionary) design of motion control systems. The overall control system that is considered in the method consists of several components that, within limits, have their specific functionality. The decomposition proposed here uses a reference path generator, a feedback component, a feedforward component and a disturbance observer. For two components in this configuration, *i.e.* the feedback component and the disturbance observer, design procedures are given.

For the feedback component, we suggest to use PID controller and PID compensator configurations. The essential difference being that the derivative action does not operate on the reference path, in case of the controller configuration, but only on the measured output. The design procedure for both configurations relies on a second- or fourth-order plant model. By means of quantitative specifications, in the form of bounds on appropriate frequency responses, expressions for the design parameters have been derived. Performance-related specifications naturally follow from the conceptual design; disturbance-related specs enter the overall design in this stage. By stepwise calculation of the design parameters, a feedback component is designed that meets the specified frequency responses of the closed-loop system (if possible).

When the specifications of the disturbance attenuation cannot be met by a feedback component only, the control configuration can be extended with a disturbance observer. For this component, a design procedure is given, as a natural extension of the design procedure of the feedback component. For standard plant models (classes), default expressions for the design parameters of the disturbance observer are provided.

The structured design method does not prescribe a single recipe for all problems, but merely gives a number of solutions that can be used whenever required. These solutions are incorporated in a library of control systems, that contains:

- templates for standard control configurations;
- component models;
- relations between specification parameters and design parameters.

Physical parameter uncertainty
A physically motivated plant model generally describes the dynamic behavior of electromechanical motion systems. The physical parameters in such a model are often only known within bounds. The controller has to assure that the motion specifications are met, despite this uncertainty. The above-mentioned design method cannot deal with this structured uncertainty quantitatively. To that end, Quantitative Feedback Theory can be used to (re)design the control system, as this design method can deal nonconservatively with uncertain physical parameters. Additionally, QFT is attractive because of the transparency of the cost of feedback.

QFT requires uncertain physical parameters to be mapped onto templates in the Nichols chart. A review of several methods for template construction has been made, where we distinguished analytical and numerical template construction methods. Whether analytical methods can be applied, depends on the structure of the plant model. Template addition can only be used when uncertain physical parameters do not occur in both the numerator and denominator. Tree structured decomposition is also limited to certain model structures, but an attractive solution to this problem would be to decompose the model in a tree structure as far as possible and apply a numerical technique to those parts of the structure that remain. Three numerical known methods for template construction have been considered: gridding, the Convex Hull Algorithm and the Adaptive Angular Sweep Algorithm, which can be applied independently of the model structure.

Performance specifications for electromechanical motion systems are usually given in terms of space and time. However, QFT requires that specifications are expressed in the form of a frequency tolerance band. Time-domain specifications can be specified as bounds on the time response. By assuming a dominant behavior of the closed loop system, these can be converted into bounds of the parameters of the assumed system model. Consecutively, these bounds can be converted into a frequency tolerance band in the Nichols chart. We have formulated an iterative conversion procedure for the specifications. When the actual closed-loop system does not match the assumed behavior, iteration takes place. The procedure is based on a number of default assumptions that enable straightforward application. Only at the moment that iteration appears to be necessary, the designer may decide to revise the default assumptions.

Computer-based support, incorporating gridding and the iterative time to frequency conversion procedure, has been developed.

Application
By means of application to an industrial motion system, we have illustrated the design enhancement presented in this thesis. We mainly focussed on evaluation of the design enhancement and not on maximization of the performance of the controlled system.

For the PM module of the FCM assessment of the conceptual design learned that the specification of a maximal positional error of 100 [μm] can be met; a maximal error of 39 [μm] was indicated as feasible. The limited stiffness of the frame proved to be the principal performance-limiting factor. Simulations with an initial plant model, as well as practical experiments, confirmed these results. Using the structured design method of chapter 3, the feedback component was extended with an integral action in order to provide low-frequency disturbance suppression. Simulations and frequency analysis confirm that the formulated detailed design specifications are feasible. Experiments on the real system confirm these results. Simulations and frequency analysis show that a disturbance observer can provide low-frequency disturbance attenuation, without severely affecting the performance. Measurements confirm that a PD compensator with a disturbance observer gives similar performance as using only a PD compensator, while this combination with a PID compensator causes larger errors, especially in the time interval of interest.

6.2 Conclusions

In mechatronic control system design, one should distinguish a conceptual design stage and a detailed design stage, as:
- these stages concern design problems with different characteristics;
- designers work in different ways;
- different kinds of design support are required.

For conceptual design, fourth-order plant models are most suited, as they are simple and of low order, have a small number of parameters, and yet competently describe the performance-limiting factor. Therefore, they are a good basis to provide reliable estimates of the dominant dynamic behavior and the attainable closed-loop bandwidth. When the proposed model simplification and reduction methods are used, individual component characteristics can still be related to the dominant plant behavior and *vice versa*.

The assessment method proposed here considers functional interaction between domain specific subsystems and considers consequences of solutions and alternative solutions in other domains. Hence it advocates a truly mechatronic approach. The method cannot be applied in all cases, as some concepts cannot be made robustly

stable by PD-type control. However, in a mechatronic design process a designer should avoid these situations whenever possible. When, for example, measurement of the end-effector position of the PM module is considered, concept *RA* is at hand, which cannot be made robustly stable using PD-type control. Rather than applying a more complex control system, the designer should consider velocity feedback from the actuator, thus obtaining concept *AR-RA*, which can be validly handled by the assessment method.

The computer support that is now available for conceptual design is such that it:
- supports the complete conceptual design stage;
- supplies design automatons for fast and correct model simplification and order reduction, while maintaining plant parameter interpretations;
- provides transparency in the relations between different design parameters;
- supports application of the assessment method in an explorational design mode, as local design goals can easily be changed, while information after a change is preserved;
- puts emphasis on the interpretation of the results instead of the application of procedures.

The principal benefits of the assessment method and the computer support are that they quickly provide insight in the design problem and that feasible goals and required design efforts can be estimated at an early stage.

The structured design of the control configuration in the detailed design stage should start with a conceptual design of a controlled system, with only a feedback component. Next, this design should be brought into the frequency domain, by determining the bandwidth ω_b of $1–T(s)$. A PD *controller* should be designed on basis of ω_b. This controller configuration should be maintained when a concept with two measurements is used or when no feedforward component is used. In all other cases, the PD controller should be converted into a PD *compensator*. As the plant model will gradually become more complex, the control configuration can be modified or extended with appropriate means whenever the controlled system does not behave as desired.

A disturbance observer can be designed as a natural extension to the feedback component, as similar frequency-domain specifications can be used. The main underlying idea here is that the sensitivity function of the overall control configuration is the product of the observer sensitivity function and the sensitivity function of the control configuration without disturbance observer.

The combination of the structured design method and the library of control systems allows the design of a good-enough control system:
- with fairly simple means, thus without requiring advanced control engineering skills of the designer;

- with a well-structured result; functionality of components in the control system are transparent;
- in an evolutionary, yet procedural way;
- in relative short time.

With respect to physical parameter uncertainty, it can be concluded that two template construction methods are suitable for electromechanical motion systems, *i.e.* gridding and the Adaptive Angular Sweep Algorithm. For a small amount of uncertain parameters gridding is attractive, because the designer can investigate predefined grid-points (on the contour) of a template, in order to signal physical parameter uncertainties that unnecessarily complicate controller design. For a large amount of uncertain parameters the Adaptive Angular Sweep Algorithm is attractive, as this method is computationally less expensive. However, only a limited number of points on the contour of a template can be investigated.

When time-domain specifications are to be converted to a frequency tolerance band for QFT design, it is better to determine the tolerance band in the Nichols chart than in the Bode diagram. The reason is that the phase of the assumed dominant behavior is also incorporated then. Fulfillment of the Bode tolerance band does not mean fulfillment of the time-domain specifications, as the designer has access to responses that unjustly seem valid in the frequency domain. When the frequency response of an uncertain closed-loop system fits within the Nichols tolerance band and an additional frequency limit is met, ideal conversion takes place.

The newly developed QFT design support provides useful means to support QFT-based controller design for SISO LTI systems with physical parameter uncertainty in combination with point-to-point motion specifications. It provides a clear view upon the influence of physical parameter uncertainty on the design of the closed-loop system and hence is useful during a mechatronic design approach.

The application illustrates that, using minimum plant knowledge, the assessment method provides the designer with relevant knowledge about the design problem, early in the design process. The structured design method, in short time, provides insight in the design problem and leads to a control system that is relevant in practice, that is, as long as the (few) parameters of the initial model are about correct.

All in all, we conclude the following. To fully exploit the advantages of the mechatronic control system design one has to obtain a deep understanding of the design problem. This generally implies that an elaborate and complex design trajectory has to be followed. The complexity in this trajectory is due to fact that the designer has to apply the abstract design methods of control theory to practical design problems that involve several engineering disciplines. In order to enhance

the design process for electromechanical motion systems and shorten the time needed for this, we have:

1. *formalized design knowledge*. That is, sets of standard classes, types and concepts are available that help the designer to quickly recognize the situation at hand. Insight is given in how to deal with low-frequency disturbances, physical parameter uncertainty and, during all design stages, with time-domain performance specifications. Finally, a modular control system configuration has been formulated that can be realized gradually so as to accommodate increasing knowledge about the proposed system design.
2. *automated activities*. On the basis of the formalized design knowledge a number of design procedures are available. For the class of electromechanical motion systems the procedures can be applied consecutively and together cover the conceptual design stage and the first part of detailed design stage. No procedures have been given for MIMO control aspects.
3. *incorporated formalized knowledge and automated activities in computer-based systems*. The knowledge acquired in the previous points is incorporated in a library of models and control systems for the mechatronic design environment 20-sim. Procedures have either been incorporated in the form of parametric relations in the 20-sim models or as a toolbox.

The design support presented in this thesis helps the designer to more easily gain insight in the design problem, without requiring advanced control engineering skills, while indicating whether performance and robustness demands of the final design are being satisfied. An important consequence is that the required overall development time decreases.

A Fast Component Mounter

The Fast Component Mounter (FCM) is a multirobot chip/IC shooter of the Philips EMT Powerline™. Typical application sectors are consumer electronics, telecommunications and computers, which require high-volume production. Advantages claimed over competitive systems are the compact dimensions, low cost per placement and a high output (Philips, 2000).

The FCM comprises a series of up to 16 servo-controlled pick-and-place robots, the so-called placement modules (PM modules), as shown in figure A.1.

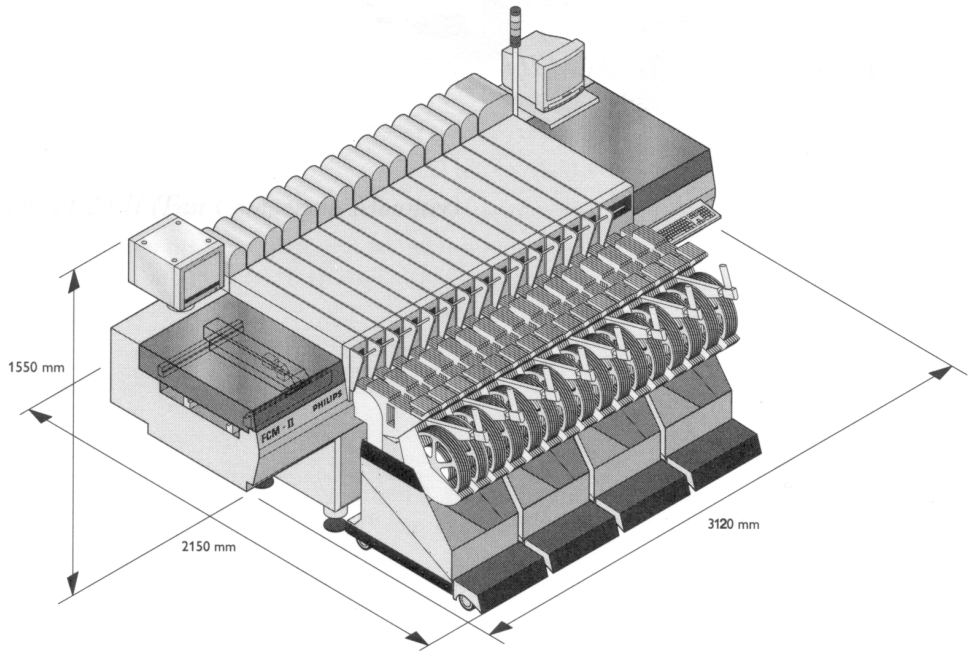

FIGURE A.1 *The Fast Component Mounter (Philips, 1998)*

The PM modules are mounted on the FCM base, which consists of a casting and all necessary supplies. During operation the PCB is first aligned with the FCM base and consecutively transported along the PM modules. Simultaneous operation of the PM modules, including in-flight component centering and fault detection by means of a laser alignment system, save throughput time; a new board can enter the FCM, while placement continues. The FCM is capable of placing 60,000 components per hour under nominal conditions.

A PM module (figure A.2) can collect electronic components from up to six feeders, enabling the complete FCM to mount 96 different components. Each module operates on a narrow strip of the PCB's surface, thus reducing time-consuming movements. Hence, a high overall output is obtained, while the individual PM modules operate at relative low speed, to minimize wear and to assure positioning accuracy. In this thesis the motion of the pipette in the y-direction is considered.

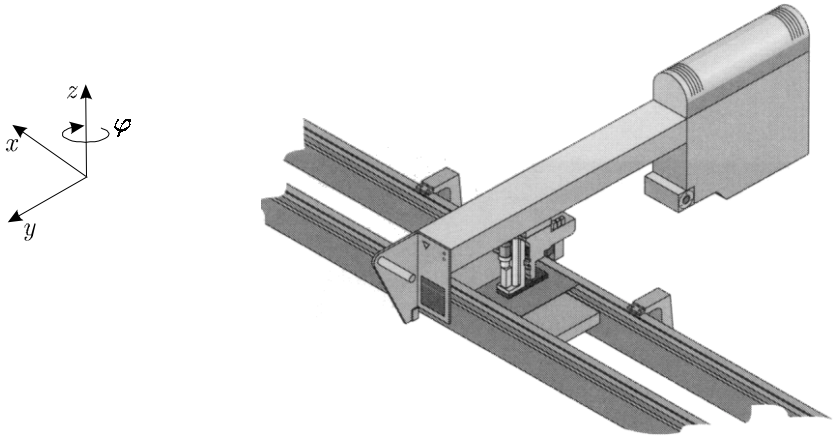

FIGURE A.2 *A placement module (Philips, 1998)*

B Waveform-mode descriptions

In this appendix, we will consider waveform-structured disturbances, especially in terms of the *linear waveform description* (Johnson, 1976). Waveform-structured signals can be mathematically modeled by a semideterministic analytical expression:

$$w(t) = \mathcal{W}\Big(\upsilon_1(t), \upsilon_2(t), \cdots, \upsilon_M(t); w_1, \cdots, w_L\Big) \tag{B.1}$$

where $\upsilon_i(t)$, $i = 1, 2, \ldots, M$ are known elementary waveform functions and w_k, $k = 1, \ldots, L$ are unknown piecewise constant parameters. In the linear case, this expression has the special form:

$$w(t) = w_1\upsilon_1(t) + w_2\upsilon_2(t) + \cdots + w_M\upsilon_M(t) \tag{B.2}$$

The *unknown* disturbance $w(t)$ is built up at any given time t by a summation of *known* basis-functions υ_i with *unknown* weighing-coefficients. In figure B.1 an example is shown (Johnson, 1976), where it is clear that $w(t)$ can be considered as a linear combination of step and ramp functions:

$$w(t) = w_1\upsilon_1(t) + w_2\upsilon_2(t), \text{ with } \upsilon_1(t) = 1, \upsilon_2(t) = t \tag{B.3}$$

Additionally, figure B.1 shows how the weighting coefficients w_1 and w_2 can be calculated. However, these calculations do not predict how the coefficients will change in the future. The basis-functions of the disturbance $w(t)$ only indicate the underlying waveform, but they do not predict the actual behavior of the disturbance.

Identification of an appropriate set of basis functions is the first step in utilizing the waveform mode characterization (B.2) for control system design. The second step consists of determining an associated state model. One could think of (B.2) as a known general solution of some unknown (sought after) differential equation (Johnson, 1976).

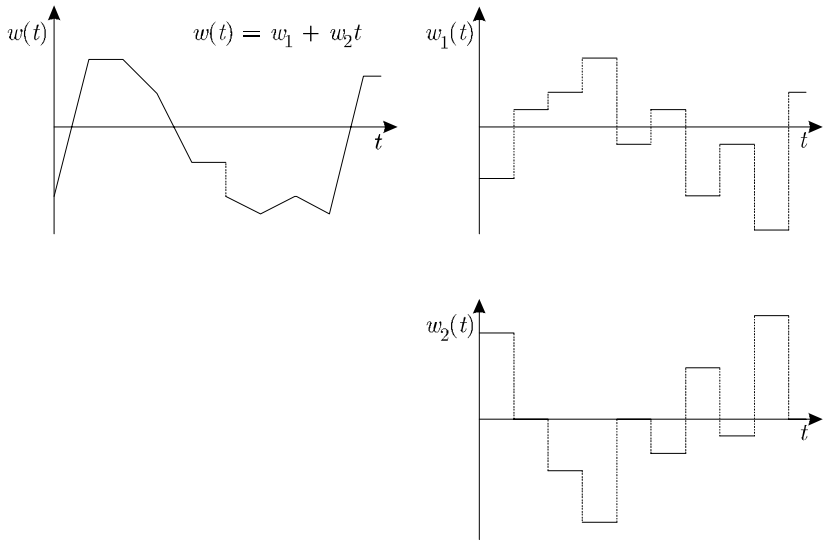

FIGURE B.1 *Typical disturbance w(t) having waveform structure*

Suppose every basis function $v_i(t)$ is Laplace transformable to $\Upsilon_i(s)$ and additionally suppose that $\Upsilon_i(s)$ has the familiar rational form:

$$\Upsilon_i(s) = \frac{\Psi_{m_i}(s)}{\Phi_{n_i}(s)} \tag{B.4}$$

where $\Psi_{m_i}(s)$ is a polynomial in s of degree m_i and $\Phi_{n_i}(s)$ is a polynomial in s of degree n_i, where $0 \leq m_i \leq n_i \leq \infty$. If the coefficients w_i are temporarily treated as constants, the Laplace transform of (B.2) is:

$$\begin{aligned} W(s) &= \mathcal{L}[\,w(t)\,] \\ &= w_1\Upsilon_1(s) + w_2\Upsilon_2(s) + \cdots + w_M\Upsilon_M(s) \\ &= \sum_1^M w_i \frac{\Psi_{m_i}}{\Phi_{n_i}} \end{aligned} \tag{B.5}$$

This can be rewritten as a single ratio of polynomials:

$$W(s) = \frac{\Psi(s)}{\Phi(s)} \tag{B.6}$$

Notice that the unknown weighting coefficients w_i only appear in the numerator polynomial $\Psi(s)$. The denominator polynomial $\Phi(s)$ is the monic least common

denominator among the set of denominators $\left\{\Phi_{n_1}(s),\Phi_{n_2}(s),\cdots,\Phi_{n_M}(s)\right\}$. The denominator polynomial $\Phi(s)$ can now be written as:

$$\Phi(s) = s^{\rho} + \phi_{\rho-1}s^{\rho-1} + ... + \phi_1 s + \phi_0 \tag{B.7}$$

where

$$\rho \leq \sum_{1}^{M} n_i \tag{B.8}$$

From (B.6), it follows that $w(s)$ can be seen as the output of a fictitious linear dynamical system subject to a set of initial conditions, which, under the Laplace transform, will give the numerator polynomial $\Psi(s)$. The coefficients ϕ_i are completely known, because they only depend on the chosen basis-functions $\Upsilon_i(t)$. In other words, the disturbance $w(t)$ can be interpreted as the output of an autonomous system (figure B.2), subject to a set initial conditions, according to:

$$\mathcal{W}: \quad \begin{bmatrix} \dot{x}_w \\ w \end{bmatrix} = \begin{bmatrix} A_w \\ C_w \end{bmatrix} \cdot x_w, \quad x_w(t_0) = x_{w0} \tag{B.9}$$

where $x_w \in \mathbb{R}^{x_w}$ is the vector of disturbance states, $w \in \mathbb{R}^{w}$ is the vector of disturbances. The pair $\{A_w,\ C_w\}$ constitutes constant matrices with appropriate dimensions, *i.e.* $A_w \in \mathbb{R}^{x_w \times x_w}$, $C \in \mathbb{R}^{w \times x_w}$.

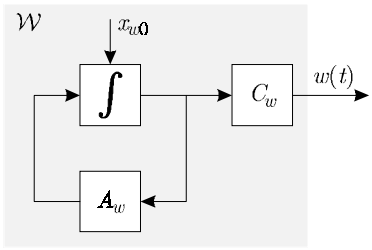

FIGURE B.2 *Disturbance model*

A state space description of this concept, in the controllable canonical form, is:

$$\begin{aligned} \mathcal{W}: \quad \begin{bmatrix} \dot{x}_{w1} \\ \dot{x}_{w2} \\ \vdots \\ \dot{x}_{w\rho} \end{bmatrix} &= \begin{bmatrix} 0 & 1 & & 0 \\ \vdots & & \ddots & \vdots \\ 0 & 0 & & 1 \\ -\phi_0 & -\phi_1 & \cdots & -\phi_{\rho-1} \end{bmatrix} \cdot \begin{bmatrix} x_{w1} \\ x_{w2} \\ \vdots \\ x_{w\rho} \end{bmatrix}, \quad x_w(t_0) = x_{w0} \\ w(t) &= \begin{bmatrix} 1 & 0 & \cdots & 0 \end{bmatrix} \cdot \begin{bmatrix} x_{w1} & x_{w2} & \cdots & x_{w\rho} \end{bmatrix}^T \end{aligned} \tag{B.10}$$

A change of the weighting coefficients w_i corresponds with a new set of initial conditions imposed to the system (B.9). These initial conditions equal the coefficients of the numerator polynomial $\Psi(s)$ of (B.6).

C Design procedures

FIGURE C.1 *Conceptual design*

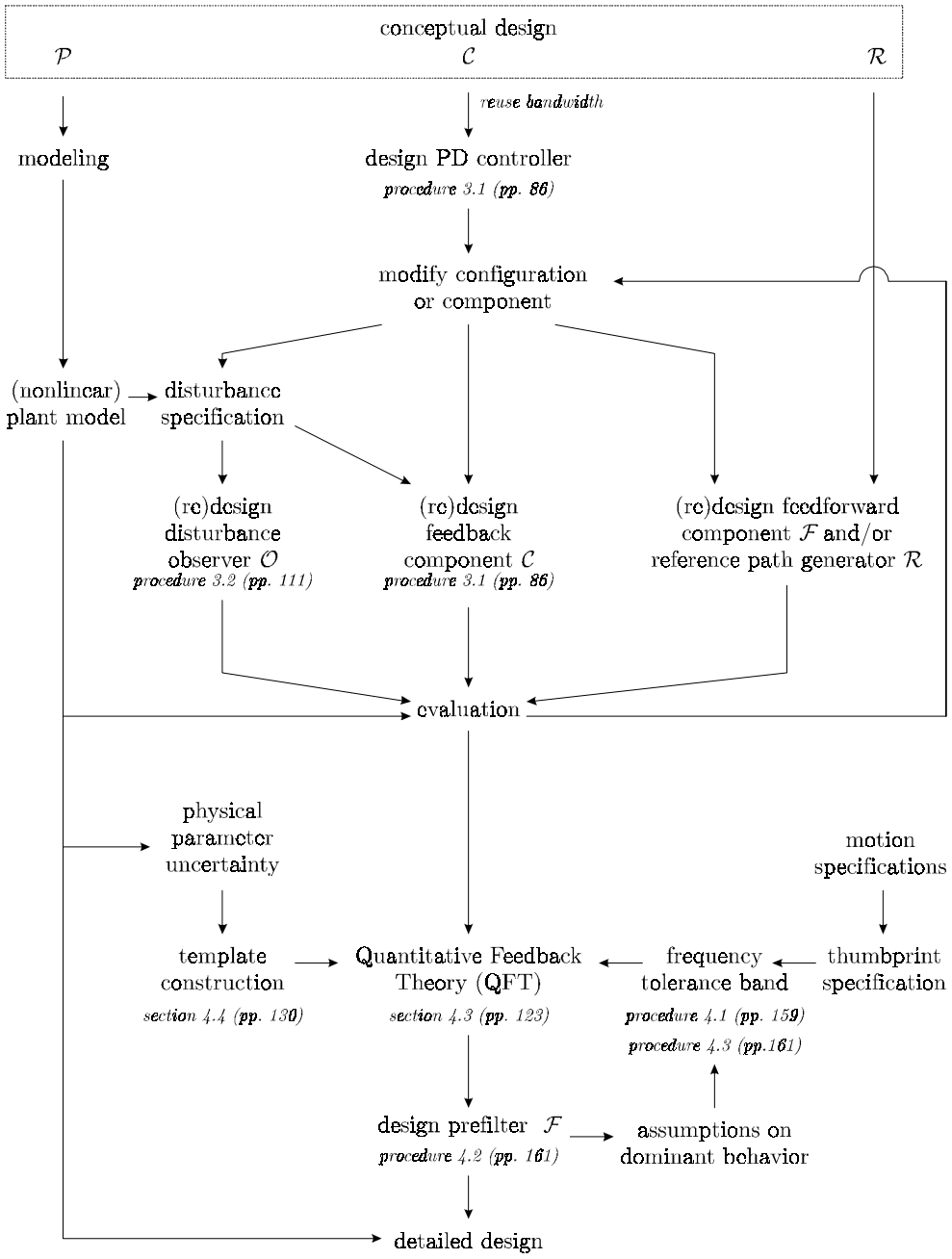

FIGURE C.2 *Detailed design*

References

Anderson, B.D.O. and J.B. Moore (1971), *Linear Optimal Control,* Prentice-Hall Inc., Englewood Cliffs, NJ, USA.

Ackermann, J. (1993), *Robust Control - Systems with uncertain physical parameters,* Springer-Verlag, London, UK.

Armstrong-Hélouvry, B., P. Dupont and C. Canudas de Wit (1994), A Survey of Models, Analysis Tools and Compensation Methods for Control of Machines with Friction, *Automatica*, **30** (7), 1083-1138.

Åström, K.J., C.C. Hang, P. Persson and W.K. Ho (1992), Towards Intelligent PID Control, *Automatica*, **28** (1), 1-9.

Åström, K.J. and T. Hägglund (1995), *PID Controllers: Theory, Design and Tuning,* Instrument Society of America, Research Triangle Park, NC, USA.

Åström, K.J. and B. Wittenmark (1997), *Computer-Controlled Systems - Theory and Design,* Prentice-Hall, Upper Saddle River, NJ, USA.

Athans, M. (1971), The Role and Use of the Stochastic Linear-Quatratic-Gaussian Problem in Control System Design, *IEEE Trans. Automatic Control*, **AC-16** (6), 529-552.

Bartlett, A.C., C.V. Hollot and L. Huang (1988), Root Locations of an Entire Polytope of Polynomials: It Suffices to Check the Edges, *Mathematics of Control, Signals and Systems*, **1** , 61-71.

Barmish, B.R. (1989), A Generalization of Kharitonov's Four-Polynomial Concept for Robust Stability Problems with Linearly Dependent Coefficient Perturbations, *IEEE Trans. Automatic Control*, **AC-34** (2), 157-165.

Barmish, B.R. and R. Tempo (1996), On Mappable Nonlinearities in Robustness Analysis, *IEEE Trans. Automatic Control*, **AC-41** (6), 895-899.

Barnard, R. and S. Beydoun (1993), Optimal Feedback Design for Uncertain Systems: A Time-Domain Fixed-Point Approach in L-infinity, *Trans. ASME J. Dynamic Systems, Measurement and Control*, **115** , 319-324.

Bien, Z. and J.-X. Xu (1998), *Iterative Learning Control - Analysis, Design, Integration and Applications,* Kluwer Academic Publishers, Norwell, MA, USA.

Blanchard, B.S. and W.J. Fabrycky (1990), *Systems Engineering and Analysis,* Prentice-Hall, Englewood Cliffs, NJ, USA.

Borghesani, C., Y. Chait and O. Yaniv (1994), *Quantitative Feedback Theory,* The MathWorks, Inc., Natick, MA, USA.

Breedveld, P.C. (1984a), Essential Gyrators and Equivalence Rules for 3-port Junction Structures, *J. Franklin Institute*, **318** (2), 77-89.

Breedveld, P.C. (1984b), Decomposition of Multiport Elements in a Revised Multibond Graph Notation, *J. Franklin Institute*, **318** (4), 253-273.

Breedveld, P.C. and J. van Amerongen (1994), Dynamische Systemen (Dynamic Systems), in Dutch, course material, Open Unversity, Heerlen, The Netherlands.

Breunese, A.P.J. (1996), *Automated support in mechatronic systems modeling,* PhD thesis, University of Twente, Enschede, The Netherlands.

Breunese, A.P.J., J.L. Top, J.F. Broenink and J.M. Akkermans (1998), Libraries of Reusable Models: Theory and Application, *Simulation*, **71** (1), 7-22.

Buur, J. (1990), *A theoretical approach to mechatronics system design,* PhD thesis, Technical University of Denmark, Lyngby, Denmark.

Cellier, F.E. (1991), *Continuous Systems Modeling,* Springer-Verlag, New York, USA.

Chapellat, H. and S.P. Bhattacharyya (1989), A Generalization of Kharitonov's Theorem: Robust Stability of Interval Plants, *IEEE Trans. Automatic Control*, **AC-34** (3), 306-311.

Coelingh, H.J., T.J.A. de Vries, P.B.T. van Lochem and J. van Amerongen (1997a), *Automated optimal controller design in mechatronics,* Proc. 7th IFAC Symp. Computer Aided Control Systems Design (CACSD'97), Gent, Belgium, 157-162.

Coelingh, H.J., T.J.A. de Vries and J. van Amerongen (1997b), *Automated Conceptual Design of Controllers for Mechatronic Systems,* Proc. Lancaster Int. Workshop on Engineering Design (CACD'97), Lancaster, UK, 27-45.

Coelingh, H.J., T.J.A. de Vries and J. van Amerongen (1997c), Automated Conceptual Design of Mechatronic Systems, *Journal A*, **38** (3), 26-29.

Coelingh, H.J., T.J.A. de Vries and J. van Amerongen (1998), *Automated Performance Assessment of Mechatronic Motion Systems during the Conceptual Design Stage,* Proc. 3rd Int. Conf. Advanced Mechatronics (ICAM'98), Okayama, Japan, 472-477.

Coelingh, H.J., T.J.A. de Vries, J. Holterman and J. van Amerongen (1998), *Mechatronic Systems with Uncertain Physical Parameters,* Proc. 6th. UK Mechatronics Forum Int. Conf. Mechatronics'98, Skövde, Sweden, 187-192.

Controllab Products (2000), *20-sim*, www.20sim.com.

Cook, R.D. (1974), *Concepts and Applications of Finite Element Analysis,* John Wiley & Sons, New York, USA.

D'Azzo, D.D. and C.H. Houpis (1995), *Linear Control System Analysis and Design - Conventional and Modern,* McGraw-Hill, New York, USA.

De Roover, D. (1997), *Motion control of a wafer stage - A design approach for speeding up IC production,* PhD thesis, Delft University of Technology, Delft, The Netherlands.

De Vries, T.J.A. and P.C. Breedveld (1992), A model of the modelling process, *Bond graphs for engineers,* P. C. Breedveld and G. Dauphin-Tanguy, Elsevier, Amsterdam, The Netherlands, 291-302.

De Vries, T.J.A., P.C. Breedveld and P. Meindertsma (1993), *Polymorphic Modelling of Engineering Systems,* Proc. Int. Conf. on Bond Graph Modeling and Simulation , Western Simulation MultiConference, SCS, San Diego, California, USA, 17-22.

De Vries, T.J.A. (1994), *Conceptual design of controlled electro-mechanical systems - a modeling perspective,* PhD thesis, University of Twente, Enschede, The Netherlands.

De Vries, T.J.A., P.B.T. Weustink and J.A. Cremer (1997), *Improving Dynamic System Model Building through Constraints,* Proc. Lancaster Int. Workshop on Engineering Design (CACD'97), Lancaster, UK, 83-95.

Decoster, M. and A.R. van Cauwenberghe (1976a), A comparative study of different reduction methods (part 1), *Journal A*, **17** (2), 68-74.

Decoster, M. and A.R. van Cauwenberghe (1976b), A comparative study of different reduction methods (part 2), *Journal A*, **17** (3), 125-134.

Doyle, J.C. (1986), *Quantitative Feedback Theory (QFT) and Robust Control,* Proc. 1986 American Control Conf., Seatlle, WA, USA, 1691-1698.

Doyle, J., K. Glover, P.P. Khargonekar and B.A. Francis (1989), State-Space Solutions to Standard H-2 and H-infinity Control Problems, *IEEE Trans. Automatic Control*, **AC-34** (8), 831-847.

East, D.J. (1981), A new approach to optimum loop synthesis, *Int. J. Control*, **34** (4), 731-748.

Francis, B.A. and W.M. Wonham (1976), The Internal Model Principle of Control Theory, *Automatica*, **12** , 457-465.

Graebe, S.F. (1999), Guest Editorial Special Section on 'Robust Control Benchmark - New Results', *Eur. J. Control*, **5** , 183-184.

Groenhuis, H. (1991), *A design tool for electromechanical servo systems,* PhD thesis, University of Twente, Enschede, The Netherlands.

Hewit, J.R. and K. Bouazza-Marouf (1996), Practical Control Enhancement via Mechatronic Design, *IEEE Trans. on Industrial Electronics*, **43** (2), 16-22.

Holterman, J. (1997), *Robust controller design in the presence of physical parameter uncertainty,* MSc thesis, University of Twente, Enschede, The Netherlands.

Horowitz, I.M. and M. Sidi (1972), Synthesis of feedback systems with large plant ignorance for prescribed time-domain tolerances, *Int. J. Control*, **16** (2), 287-309.

Horowitz, I. (1982), Quantitative feedback theory, *IEE Proc. Pt. D*, **129** , 215-226.

Horowitz, I. (1991), Survey of quantitative feedback theory (QFT), *Int. J. Control*, **53** (2), 255-291.

Houpis, C.H. and S.J. Rasmussen (1999), *Quantitative Feedback Theory - Fundamentals and Applications,* Marcel Dekker, Inc., New York, USA.

IRDAC (1986), Opinion on R&D needs in the field of mechatronics, Industry R&D Advisory Committee of the Comm. of the EC, Brussels, Belgium.

Isaksson, A.J. and S.F. Graebe (1993), *Model Reduction for PID Design,* Proc. 12th IFAC World Congress, Sydney, Australia, 257-262.

Isermann, R. (1996), On the Design and Control of Mechatronic Systems - a Survey, *IEEE Trans. on Industrial Electronics*, **43** (1), 4-15.

Jayasuriya (1993), Frequency Domain Design for Robust Performance under Parametric, Unstructured, or Mixed Uncertainties, *Trans. ASME J. Dynamic Systems, Measurement and Control*, **115** , 439-451.

Johnson, C.D. (1971), Accommodation of External Disturbances in Linear Regulator Servomechanism Problems, *IEEE Trans. Automatic Control*, **AC-16** (6), 635-644.

Johnson, C.D. (1976), Theory of Disturbance-Accomodating Controllers, *Control and Dynamic Systems,* **12**, C. T. Leondes, Academic Press, New York, U.S.A., 223-315.

Jonker, B. (1988), *A finite element dynamic analysis of flexible spatial mechanisms and manipulators,* PhD thesis, Delft University of Technology, Delft, The Netherlands.

Kailath, T. (1980), *Linear Systems,* Prentice-Hall, Englewood Cliffs, NJ, USA.

Kane, T.R. and D.A. Levinson (1985), *Dynamics: Theory and Applications,* McGraw-Hill, New York, USA.

Kharitonov, V.L. (1978), Asymptotic stability of an equilibrium position of a family of systems of linear differential equations, *Differentsial'nye Uravneniya*, **14** (11), 2086-2088.

Konda, S., I. Monarch, P. Sargent and E. Subrahmanian (1992), Shared Memory in Engineering Design: A Unifying Theme for Research and Practice, *Research in Engineering Design*, **4** , 23-42.

Koster, M.P., W.T.C. van Luenen and T.J.A. de Vries (1999), Mechatronica (Mechatronics), in Dutch, course material, University of Twente, Enschede, The Netherlands.

Krishnan, K.R. and A. Cruickshanks (1977), Frequency-domain design of feedback systems for specified insensitivity of time-domain response to parameter variations, *Int. J. Control*, **25** (4), 609-620.

Kwakernaak, H. and R. Sivan (1972), *Linear Optimal Control Systems,* Wiley, New York, USA.

Kwakernaak, H. (1993), Robust control and H-infinity optimization - Tutorial paper, *Automatica*, **29** (2), 255-273.

Landau, I.D., D. Rey, A. Karami, A. Voda and A. Franco (1995), A Flexible Transmission System as a Benchmark for Robust Digital Control, *Eur. J. Control*, **1** (2), 77-96.

Levine, W.S. (1996), *The Control Handbook,* CRC Press, Inc., Boca Raton, Florida, USA.

Ljung, L. (1999), *System Identification - Theory for the User,* Prentice Hall PTR, Upper Saddle River, NJ, USA.

MathWorks (2000), *The MathWorks: Developers of MATLAB and Simulink*, www.mathworks.com.

McClamroch, N.H. (1998), Presidents message, *IEEE Control Systems Magazine*, **18** (4), 4-6.

Meckl, P.H. (1994), Robust Motion Control of Flexible Systems using Feedforward Forcing Functions, *IEEE trans. Control Systems Technology*, **2** (3), 245-254.

Minnichelli, R.J., J.J. Anagost and C.A. Desoer (1989), An Elementary Proof of Kharotonov's Stability Theorem with Extensions, *IEEE Trans. Automatic Control*, **AC-34** (9), 995-998.

Miu, D.K. (1991), Physical Interpretation of Transfer Function Zeros for Simple Control Systems with Mechanical Flexibilities, *Trans. ASME J. Dynamic Systems, Measurement and Control*, **113** , 419-424.

Miu, D.K. (1993), *Mechatronics - Electromechanics and Contromechanics,* Springer-Verlag, New York, USA.

Nilsson, B. (1993), *Object-oriented modeling of chemical processes,* PhD thesis, Lund Institute of Technology, Lund, Sweden.

Oelen, W. (1995), *Modeling as a tool for design of mechatronic systems,* PhD thesis, University of Twente, Enschede, The Netherlands.

Otten, G., T.J.A. de Vries, J. van Amerongen, A.M. Rankers and E.W. Gaal (1997), Linear Motor Motion Control using a Learning Feedforward Controller, *IEEE/ASME Trans. Mechatronics*, **2** (3), 179-187.

Park, M.S., Y. Chait and M. Steinbuch (1997), Inversion-Free Design Algorithms for Multivariable Quantitatve Feedback Theory: An Application to Robust Control of a CD-ROM, *Automatica*, **33** (5), 915-920.

Paynter, H.M. (1975), *Analysis and Design of Engineering Systems,* MIT Press, Cambridge, MA, USA.

Philips (1998), *Fast Component Mounter - II Specifications,* Eindhoven, The Netherlands.

Philips (2000), *PowerLine Fast Component Mounter*, Philips Electronic Manufacturing Technology, www.emt.ie.philips.com/fcm_mounter.html.

Profeta, J.A., W.G. Vogt and M.H. Mickle (1990), Disturbance Estimation and Compensation in Linear Systems, *IEEE Trans. Aerospace and Electronic Systems*, **26** (2), 225-231.

Profeta, J.A., W.G. Vogt and M.H. Mickle (1990), Torque Disturbance Rejection in High Accuracy Tracking Systems, *IEEE Trans. Aerospace and Electronic Systems*, **26** (2), 232-237.

Rankers, A.M. (1997), *Machine dynamics in mechatronic systems - an engineering approach,* PhD thesis, University of Twente, Enschede, The Netherlands.

Rinderle, J.R. and B.L. Subramaniam (Ed.) (1991), *Automated bond graph modeling and simplification to support design*, *in* Automated Modeling, ASME,

Rumbaugh, J., M. Blaha, W. Premerlani, F. Eddy and W. Lorensen (1991), *Object-Oriented Modeling and Design,* Prentice-Hall, Englewood Cliffs, NJ, USA.

Sienel, W. (1992), *Algorithms for Tree Structured Decomposition,* Proc. 31st IEEE Conf. Decision and Control, Tucson, Arizona, USA, 739-740.

Siljak, D.D. (1989), Parameter Space Methods for Robust Control Design: A Guided Tour, *IEEE Trans. Automatic Control*, **AC-34** (7), 674-688.

Simon, H.A. (1973), The structure of ill-structured problems, *Artificial Intelligence*, **4** , 181-201.

Skelton, R.E. and P.C. Hughes (1980), Modal Cost Analysis for Linear Matrix-Second-Order Systems, *Trans. ASME J. Dynamic Systems, Measurement and Control*, **102** , 151-158.

Skogestad, S. and I. Postlethwaite (1996), *Multivariable Feedback Control,* John Wiley & Sons, Chichester, UK.

Söderström, T. and P. Stoica (1989), *System Identification,* Prentice-Hall, New York, USA.

Stefani, R.T., C.J. Savant, B. Shahion and G.H. Hostetter (1994), *Design of Feedback Control Systems,* Saunders College Publishing, Boston, MA, USA.

Steinbuch, M. and M.L. Norg (1998), Advanced Motion Control: An Industrial Perspective, *Eur. J. Control*, **4** , 278-293.

Thompson, D.F. and O.D.I. Nwokah (1994), Analytic Loop Shaping Methods in Quanititative Feedback Theory, *Trans. ASME J. Dynamic Systems, Measurement and Control*, **116** , 169-177.

Ullman, D.G. (1997), *The Mechanical Design Process,* McGraw-Hill, New York, USA.

Van Amerongen, J. (1998), *The Role of Control in Mechatronics,* Mini Symposium - Mechatronics in Control System Design, IEE Control'98 Conference, University of Wales, Swansea, U.K., 6.

Van Amerongen, J., E. Coelingh and T.J.A. de Vries (2000), Computer Support for Mechatronic Control System Design, *J. Robotics and Autonomous Systems*, *(accepted for publication).*

Van Brussel, H.M.J. (1996), Mechatronics - A Powerful Concurrent Engineering Framework, *IEEE/ASME Trans. Mechatronics*, **1** (2), 127-136.

Van Dijk, J. (1999), Personal communication.

Van Lochem, P.B.A. (1997), *Towards automated mechatronic system design,* MSc thesis, University of Twente, Enschede, The Netherlands.

Velthuis, W.J.R. (2000), *Learning feed-forward control,* PhD thesis, University of Twente, Enschede, The Netherlands.

Waarsing, R. (1999), *Enhancement of controller design for mechatronic motion systems,* MSc thesis, University of Twente, Enschede, The Netherlands.

Wilson, B.H., B. Eryilmaz and B. Shafai (1996), Improving control design for nonlinear parametric uncertainty, *Int. J. Control*, **66** (6), 863-883.

Wilson, B.H. and B. Eryilmaz (1998), Using Bond Graphs to Synthesize Tree-structured Transfer Functions: Improved Frequency-Domain Analysis of Uncertain Systems, *J. Franklin Inst.*, **335B** (8), 1443-1465.

Wilson, B.H., B. Eryilmaz and B. Shafai (1999), An Andaptive Angular Sweep Algorithm for Value Set Construction, *IEEE Trans. Automatic Control*, **AC-44** (3), 551-555.

Wilson, B.H. and B. Eryilmaz (1999), Simplified Tree-Structured Decomposition using Bond Graphs, *Automatica*, **35** (4), 755-760.

Wittenburg, J. (1977), *Dynamics of Systems of Ridgid Bodies,* B.G. Teubner, Stuttgart, Germany.

Wolovich, W.A. (1974), *Linear Multivariable Systems,* Springer-Verlag, New York, USA.

Wortelboer, P.M.R. (1994), *Frequency-weighted balanced reduction of closed-loop mechanical servo systems: Theory and tools,* PhD thesis, Delft University of Technology, Delft, The Netherlands.

Yaniv, O. and I.M. Horowitz (1987), Quantitative feedback theory - Reply to criticisms, *Int. J. Control*, **46** (3), 945-962.

Zadeh, L. and C. Desoer (1963), *Linear Systems Theory: the state space approach,* McGraw-Hill, New York, USA.

Zhou, K., J.C. Doyle and K. Glover (1996), *Robust and Optimal Control,* Prentice-Hall, Upper Saddle River, NJ, USA.

Zienkiewicz, O.C. (1971), *The Finite Element Method in Engineering Science,* McGraw-Hill, London, UK.

Naschrift

Als afsluiting van dit proefschrift wil ik een aantal mensen bedanken die een bijdrage hebben geleverd aan dit werk en die ervoor gezorgd hebben dat ik iedere ochtend fluitend op m'n fietsje stapte, op weg naar de UT.

Met Theo de Vries en Wubbe Jan Velthuis heb ik dagelijks samengewerkt, zij hebben er in belangrijke mate voor gezorgd dat ik met veel plezier kan terugkijken op de tijd waarin dit proefschrift tot stand is gekomen. Theo, jouw begeleiding en bijdragen heb ik altijd als zeer waardevol en prettig ervaren. Wubbe, meer dan 4 jaren zin en onzin in 8236 zijn fantastisch geweest, nu op naar 5895.

Job van Amerongen ben ik dank verschuldigd voor zijn kritische op- en aanmerkingen op mijn proefschrift en voor de prettige samenwerking binnen Drebbel. Rien Koster heeft met zijn enthousiasme en zijn visie op mechatronica een belangrijke invloed op mijn werk gehad en hiervoor ben ik hem zeer erkentelijk. Johannes van Dijk bedank ik voor af en toe een duw in de goede richting.

Een aantal mensen hebben tijdens hun afstudeeropdracht een belangrijke bijdrage geleverd aan dit werk: Patrick van Lochem, Jan Holterman, René Waarsing en Willem Buys. Jan bedank ik niet alleen voor het prakkiseer'n over QFT, maar ook voor het zeer nauwkeurig doorlezen en corrigeren van het concept proefschrift.

Philips CFT heeft de PM module beschikbaar gesteld en Bastiaan Jansen, Dirk-Jan van Lubek en Nathan van Seters hebben er vervolgens beweging in gekregen.

Voor de goede werksfeer, tussen de eerste kop koffie op maandagochtend en het allerlaatste Hopfenperlchen op vrijdagmiddag zorgden: Paul, Frank, Chris, Maaike, Dick, Gerrit, Erik, Marcel, Roger en alle andere (oud-) medewerkers.

Tenslotte bedank ik Moniek, omdat ik ook elke avond weer fluitend naar huis fiets, en mijn ouders (niet alleen voor de fiets).

Erik